Exploring the inter-relationship between vasculopathy, inflammation and fibrosis in Systemic Sclerosis

Flower, Victoria

Award date:
2020

Awarding institution:
University of Bath

Exploring the inter-relationship between vasculopathy, inflammation and fibrosis in systemic sclerosis

Submitted by

Victoria A Flower

A thesis submitted for the degree of Doctor of Philosophy

University of Bath

Department of Pharmacy and Pharmacology

January 2020

Abstract

Systemic sclerosis (SSc) is a rare but potentially devastating multisystem disease with unknown aetiology. The pathological hallmarks constitute a triad of autoimmunity, unique disease specific patterns of vasculopathy and tissue fibrosis. LeRoy's vascular hypothesis links these features through early endothelial injury resulting in tissue hypoxia and subsequent aberrant tissue remodelling by over-active fibroblasts, most readily manifesting as Raynaud's phenomenon and cutaneous fibrosis respectively. Existing evidence supports a vascular-fibrotic link, but current therapeutic options are few and strategies tend to target each one individually, in part due to a lack of comprehensive understanding of the complex and evolving pathogenesis. Vascular biomarkers such as vascular endothelial growth factor-A (VEGF-A) and associated angiopoietins are potential drivers of both vasculopathy and fibrosis and have been implicated in SSc pathogenesis. We hypothesize that differential VEGF-A isoform expression (through conventional and alternative VEGF-A splicing), may dictate the relevant burden of vasculopathy and fibrosis thus explaining disease heterogeneity and disease progression. Associated antiangiogenic angiopoietin-2 may also play role. Furthermore, VEGF-A isoform expression may be directed by hypoxia inducible factor-α (HIF1α/2α) paralog expression driven by the unique hypoxic stimulus that results from SSc vasculopathy. The advancement of medicinal products for SSc is limited on a second front, namely the shortcomings of current subjective outcome measures for both vasculopathy and cutaneous fibrosis used in clinical trials. This research therefore aimed to investigate the use of non-invasive imaging techniques as potential future outcome measures in SSc. Secondly, we aimed to use these objective measures to further explore the inter-relationship between vasculopathy, inflammation and fibrosis and the role of vascular biomarkers in driving disease. Herein, we report on the potential for laser speckle contrast imaging (LSCI) to demonstrate vascular dysfunction in SSc and for novel applications of high frequency ultrasound (HFUS) to document reduced vascularity in the fingers even at ambient temperatures. We have provided evidence that HFUS is a reproducible method of objectively assessing skin pathology through the combination of three HFUS applications and for the first time we provide histological validation for its use. We report on the over-expression of VEGF-A_{165}b in plasma and skin and its negative relationships with finger perfusion and skin fibrosis demonstrating inhibitory associations with both features. We additionally report of the association between increased angiopoietin-2 expression and both vasculopathy and increased skin fibrosis. We report for the first time that HIF2α is over-expressed in SSc skin demonstrating the hypoxic stimuli in fibrotic skin and its associations with VEGF-A_{165}b isoform expression. In summary, this thesis presents evidence for the translational potential of non-invasive imaging techniques in SSc as well as advancing the understanding of its pathogenesis through the inter-relationship of the pathogenic triad with vascular biomarkers and implicating such as potential future therapeutic targets.

Declaration of work undertaken in this thesis

All work for this thesis was undertaken by Dr Victoria Flower unless otherwise stated.

Skin biopsy samples (used for Masson's trichrome and immunofluorescence, chapter 6 and 9 respectively)) were taken by V Flower and then paraffin embedded and sectioned by Kasiya Wellington, Pathology department, Royal United Hospital, Bath, U.K.

ELISAs for panVEGF-A, VEGF-A_{165}b, TGFβ, Pro-Col I and Biorad protein assay for fibroblast cell cultures were performed by Masters students Millie Swanston and Tom Wells (chapter 10). All other ELISAs were performed by V Flower.

Acknowledgements

I would like to thank Dr John Pauling, colleague, supervisor and friend, without whose help this project would never have begun. I would also like to thank Professor Stephen Ward and Dr Amanda Mackenzie for their support and supervision at the University of Bath and Dr Shaney Barratt for her invaluable VEGF knowledge and training. I also thank Dr Helen Knowles and Dr Giordano Pula for their collaboration in initial project design.

I am repeatedly indebted to the team at the RNHRD research department and Dr Jacqueline Shipley and Darren Hart who have never tired of my questions and are always willing to provide immediate help with equipment failure.

Lastly and most importantly, I would like to thank my husband, Nick, and my children, Ayla and Sam for your limitless patience and support.

Abbreviations

ANA	Anti-nuclear antibody
Ang	Angiopoietin
ACA	Anti-centromere antibody
ACEi	Angiotensin converting enzyme inhibitor
AIIRB	Angiotensin II receptor blocker
ARNT	Aryl hydrocarbon nuclear translocator
AUC	Area under the curve
cAMP	Cyclic adenosine monophosphate
CAV	Caveolin
CCB	Calcium channel blocker
CDI/CDU	Colour doppler imaging/ultrasound
cSMI	Superb microvascular imaging with colour overlay
CCH	Chronic continuous hypoxia
CI	Confidence interval
CIH	Chronic intermittent hypoxia
CTGF	Connective tissue growth factor
dcSSc	Diffuse cutaneous systemic sclerosis
DDD	Distal-dorsal difference
DMARD	Disease modifying anti-rheumatic drug
DU	Digital ulceration
DVVi	Dorsovolar vascularity index
ELISA	Enzyme linked immunosorbent assay
Endo-MT	Endothelial to mesenchymal transition
ERA	Endothelin receptor antagonist
FFPE	Formalin fixed paraffin embedded
FVi	Fingertip vascularity index
GAVE	Gastric antral vascular ectasia
GORD	Gastro-oesophageal reflux disease
HAQ-DI	Health assessment questionnaire disability index
HC	Healthy control
HFUS	High frequency ultrasound
HIF	Hypoxia inducible factor
HIF1α	Hypoxia inducible factor 1α
HIF2α	Hypoxia inducible factor 2α
HIF1β	Hypoxia inducible factor 1β
HRE	Hypoxia response elemnet
HSCT	Haemopoietic stem cell transplant
ICC	Inter-class correlation coefficient
Id-1	Inhibitor of DNA-binding protein -1
IHC	Immunohistochemistry
IF	Immunofluorescence
ILD	Interstitial lung disease
IL-1β, -6	Interleukin-1β, -6
IPF	Idiopathic pulmonary fibrosis
IRT	Infrared thermography
IQR	Interquartile range
K-W	Kruskal-Wallis
lcSSc	Limited cutaneous systemic sclerosis
LDF	Laser doppler flowmetry
LDI	Laser doppler imaging

LSCI	Laser speckle contrast imaging
MWU	Mann-Whitney U
mRSS	Modified Rodnan skin score
MVEC	Microvascular endothelial cells
NC	Nailfold capillaroscopy
NFκB	Nuclear factor κB
NO	Nitric oxide
NP-1	Neuropilin-1
NP-2	Neuropilin-2
NVi	Nailfold vascularity index
OCT	Optical coherence tomography
PAH	Pulmonary arterial hypertension
PDE-5	Phosphodiesterase-5 inhibitor
PDGF	Platelet derived growth factor
PDGFR	Platelet derived growth factor receptor
PORH	Post occlusive reactive hyperaemia
P-PP	Platelet poor plasma
PROM	Patient-reported outcome measure
P-RP	Platelet rich plasma
PRP	Primary Raynaud's phenomenon
PU	Perfusion units
RCS	Raynaud's condition score
RCT	Randomised control trial
RNAPIII	Anti-RNA polymerase III antibody
ROI	Region of interest
RP	Raynaud's phenomenon
Scl-70	Anti-Topoisomerase antibody
S.D.	Standard deviation
SHAQ	Scleroderma health assessment questionnaire
SRC	Scleroderma renal crisis
SRP	Secondary Raynaud's phenomenon
SSc	Systemic sclerosis
SSc-RP	Systemic sclerosis related RP
SSRI	Selective serotonin reuptake inhibitor
ST	Skin thickness
SWE	Shear wave elastography
TGFβ	Transforming growth factor β
Tie-2	Tie-2 receptor
TNF	Tumour necrosis factor
U1RNP	U1 Ribonucleoprotein (& U3, U11, U12)
uPAR	Urokinase-type plasminogen activator receptor
VAS	Visual analogue score
VEDOSS	Very early diagnosis of systemic sclerosis
VEGF-A-D	Vascular endothelial growth factor-A to -D
VEGFR1/flt1)	Vascular endothelial growth factor receptor 1
VEGFR2/KDR/flk1	Vascular endothelial growth factor receptor 2
VEGFR3/flt4	Vascular endothelial growth factor receptor 3

Contents

Index of tables

Chapter 5

Chapter 6

Chapter 7

Chapter 8

Chapter 9

Index of figures

Chapter 4

Chapter 5

Chapter 6

Chapter 8

Chapter 9

Chapter 10

Chapter 11

Appendix A2

Appendix A3

Appendix A4

Publications arising from this thesis

Original research articles

Flower. VA, Barratt. SL, Hart. D, Mackenzie. A, Shipley. J, Ward. S, Pauling. JD. Convergent validity of high frequency ultrasound with clinical assessment and dermal collagen in systemic sclerosis related skin disease. *Submitted for peer review.*

Review articles

Flower. VA, Barratt. SL, Ward. S, Pauling. JD. The role of vascular endothelial growth factor in systemic sclerosis. *Curr Rheum Rev*. 2019;15(2):99-109. (1)

Barratt. SL, **Flower. VA**, Pauling. JD, Millar. AB. VEGF (Vascular Endothelial Growth Factor) and fibrotic lung disease. *Int J Mol Sci,* 2018;19(5):1268 (2).

Conference proceedings

Flower. VA, Barratt. SL, Hart. D, Mackenzie. A, Shipley. J, Ward. S, Pauling. JD. Assessment of the repeatability and convergent validity with dermal collagen of high frequency ultrasound in systemic sclerosis. *American College of Rheumatology, Atlanta USA November 2019,* ***Poster abstract*** *& 16th International Workshop on Scleroderma research, Cambridge UK July 2019,* ***oral abstract.***

Flower. VA, Barratt. SL, Hart. D, Mackenzie. A, Shipley. J, Ward. S, Pauling. JD. Anti-angiogenic VEGF-A_{165}b is associated with systemic sclerosis Peripheral Vasculopathy. *American College of Rheumatology, Atlanta USA November 2019,* ***poster abstract*** *& 16th International Workshop on Scleroderma research, Cambridge UK July 2019,* ***poster abstract****.*

Flower VA, Barratt. SL, Hart. D, Mackenzie. A, Shipley. J, Ward. S, Pauling. JD. Increased plasma angiopoietin-2 in systemic sclerosis: Potential for use as a biomarker of vasculopathy and fibrosis. *American College of Rheumatology, Chicago USA, October 2018,* ***poster abstract****.*

Flower VA, Barratt. SL, Hart. D, Mackenzie. A, Shipley. J, Ward. S, Pauling. JD. High Frequency Ultrasound as a novel approach to Quantifying the Digital Microangiopathy of systemic sclerosis. *American College of Rheumatology, Chicago USA, October 2018,* ***poster abstract****.*

Chapter 1. Introduction

Systemic sclerosis (SSc) is a rare multisystem autoimmune disease whose pathological hallmarks constitute a triad of vasculopathy, autoimmunity and aberrant tissue remodelling, manifesting as Raynaud's phenomenon (RP), circulating autoantibodies and cutaneous fibrosis (scleroderma) respectively. These hallmark features manifest as a combination of multisystem sequelae (Figure 1.1), resulting in widely heterogeneous disease phenotypes, some with potentially devastating consequences. The incidence is approximately 20 per million people per year (3), with a peak age of onset between 55-64 years (4). There is a preponderance for females with a gender ratio of 7:1 (3, 5) as well as for African, Asian and Caribbean populations who are also more likely to suffer the most severe phenotypes (6, 7).

1.1 Aetiology

The foundations of SSc aetiology remain unknown but are likely to be based on a genetic predisposition compounded by environmental precipitants. The precise environmental trigger of SSc for the individual patient is rarely identified. However, organic solvents, chlorine, welding vapour (8) and silica (9) have been implicated as allergenic triggers.

A number of studies have positively identified genetic susceptibilities including single nucleotide polymorphisms in HLA loci, some of which associate with particular autoantibody profiles (10, 11). Specific genetic loci have also been identified in populations who experience a high prevalence of SSc such as the Choctaw American Indians (12). Single cell sequencing has demonstrated changes in gene expression in macrophages, pericytes and fibroblasts in favour of collagen production and fibrosis (13). Additionally,

over-expression of EZH2 gene in SSc fibroblasts and endothelial cells appears to drive both pro-fibrotic and anti-angiogenic pathways.

Whilst the familial risk ratio is increased at 13 for first-degree relatives (14), concordance in twins studies conform only 4-5% incidence (15) suggesting that factors other than gene expression must influence disease emergence. Recent study has focused on epigenetic influences in SSc (16). Studies have demonstrated increased DNA methylation (17) as well as increased expression of methyl cap binding protein 2 resulting in augmented Wnt signalling (18), both in favour of collagen and extracellular matrix production in SSc. Non-coding RNA expression in skin, serum and fibroblasts is also altered in SSc (11, 19). Additionally, CD4+ cells demonstrate reduced DNA methylation enzymes (10).

1.2 Clinical manifestations and autoantibody profiling

Analogous to the well-recognised association of rheumatoid factor with rheumatoid arthritis, SSc pertains to its own autoantibody profiles. Anti-nuclear autoantibodies (ANA) are positively identified in >93% (5), reflecting one of the SSc specific autoantibodies in the majority of cases (5, 20). Principally, anti-centromere autoantibody (ACA, ~30%), anti-topoisomerase (Scl-70, ~20%) and anti-RNA polymerase III autoantibody (RNAPIII, ~15%) are represented more commonly than anti-U3 ribonucleoprotein (U3RNP, ~5%), anti-Th/To (~5%) and rare SSc-specific antibodies such as anti-U11/12 ribonucleoprotein (U11/U12RNP), anti-RuvBL1/2 and anti-EIF2B (~1% each). SSc *associated* antibodies may be alternatively expressed including anti-Ku, anti-U1 ribonucleoprotein (U1RNP), anti-Nor-90 and anti-B23. These SSc associated antibodies may also be associated with SSc overlap syndromes with myositis, sjogrens or SLE (20).

Whilst SSc is a notoriously heterogeneous disease, SSc specific and associated autoantibodies have strong associations with particular clinical phenotypes (21) (Table 1.1), thus transcribing a degree of predictive value for clinicians at the point of clinical care. Regarding the principle SSc autoantibodies, ACA+ SSc exhibits a dominant vascular phenotype over fibrotic pathways with increased risk of digital ulcers (DU), telangiectasia and pulmonary arterial hypertension (PAH), but minimal cutaneous or pulmonary fibrosis. In contrast, Scl-70+ or RNAPIII+ SSc typically develop both significant vasculopathy and fibrosis (but demonstrate organ specific predilection depending on autoantibody profile)(21).

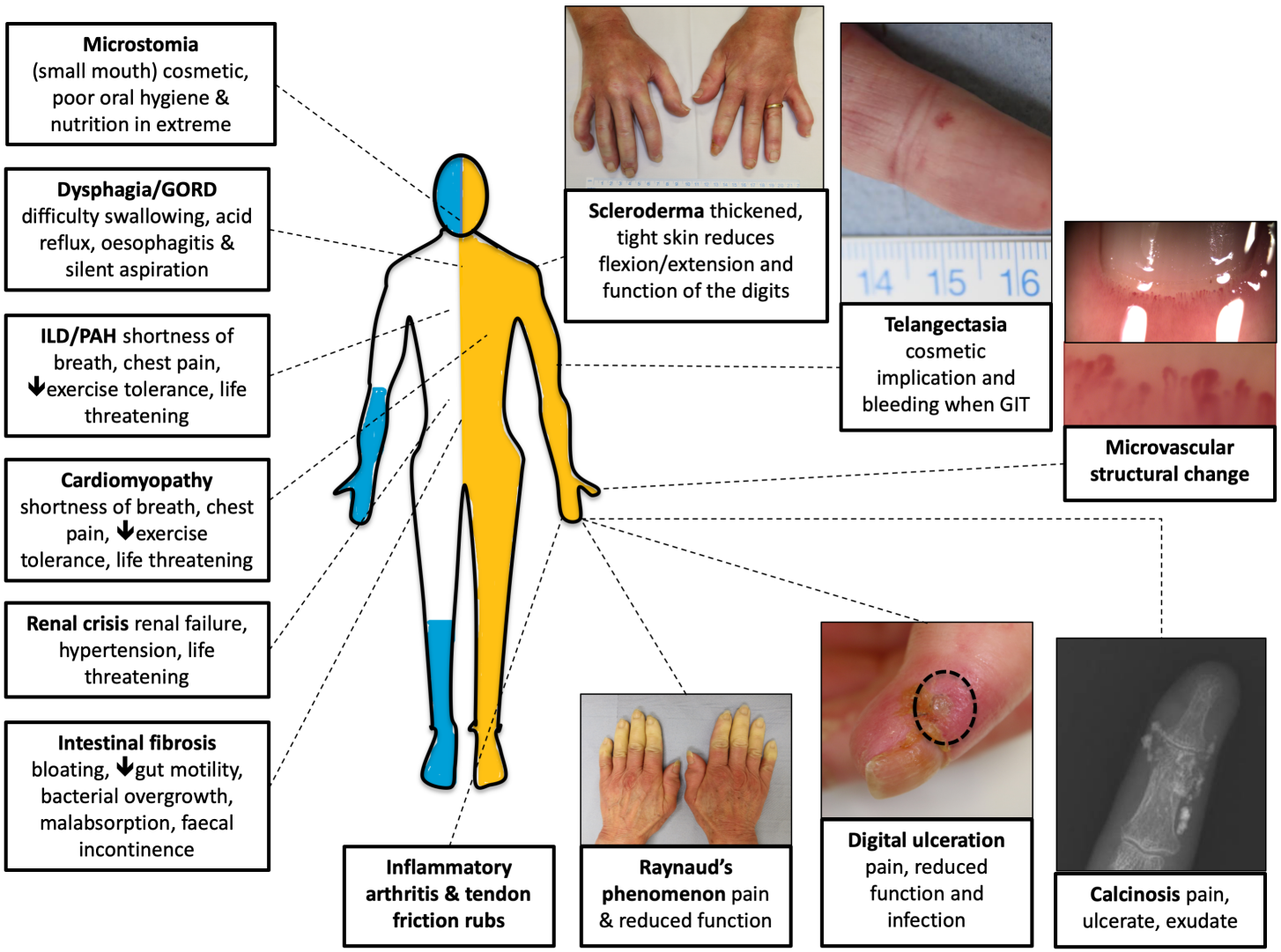

Figure 1. 1 Clinical features of systemic sclerosis.

The potential clinical features (bold) of systemic sclerosis (SSc) and the resultant symptoms experienced by the patient are illustrated. Vascular and fibrotic manifestations across all organs demonstrates the systemic nature of the disease. SSc may be sub-classified as limited cutaneous (lcSSc) where scleroderma is limited to the peripheries (blue); namely involving the face and distal to the elbows and knees. Alternatively, where scleroderma has extended to more proximal distributions (orange), the patient is classified as having diffuse cutaneous SSc (dcSSc). Abbreviations: GORD, gastroesophageal reflux disease; ILD, interstitial lung disease; PAH, pulmonary arterial hypertension; GIT, gastrointestinal.
Figure created by VF using study images with patient consent.

Table 1. 1 Clinical associations of SSc subgroups and autoantibody profiles.

The typical phenotypes associated with SSc subgroups, SSc-specific and SSc-associated autoantibodies are illustrated by the strength of the association with each manifestation (+/++/+++/++++) (5, 20, 22-28). No autoantibody is exclusively associated with either disease subtype, however, ACA+ is rarely observed in the context of diffuse skin disease. Scleroderma renal crisis occurs in only 3% of the SSc population but 15% of dcSSc with particular association with U3RNP and RNAPIII. *Abbreviations:* ACA, anti-centromere antibody; dcSSc, diffuse cutaneous SSc; DU, digital ulcers; GAVE, gastric antral vascular ectasia (watermelon stomach); ILD, interstitial lung disease; lcSSc, limited cutaneous SSc; PAH, pulmonary arterial hypertension; RP, Raynaud's phenomenon; RNAPIII, RNA-polymerase III antibody; Scl-70, anti-Topoisomerase antibody; U1RNP, anti-U1 ribonucleoprotein; U3RNP, anti-U3 ribonucleoprotein; U11/12RNP, anti-U11/12 ribonucleoprotein.

	Subgroup		**SSc-specific antibodies**							**SSc-associated antibodies**		
Clinical manifestation	lcSSc	dcSSc	ACA	Scl-70	RNAPIII	U3RNP	Th/To	U11/12RNP	RuvBL1/2	Pm-Scl	U1RNP	Ku
% of SSc	60%	40%	20-30%	20-30%	5-25%	4-10%	2-5%	1-3%	1-2%	2%	7-8%	2%
RP	+++	+++	+++	+++	+++	+++	+++	+++	+++	+++	+++	+++
Scleroderma												
lcSSc			+++	+		+	+	+		+	++	+
dcSSc				++	+++	+		+	+	++		
DU	++	+++	+	+++							+++	
Telangectasia	++	++	++									
ILD	+	+++		++++	+	+++	+++	+++		++	+	
PAH	+	+	++	+		+++	++				++	
Cardiomyopathy	+	++		+++		+++			+			
Gastrointestinal												
upper	++	+++										
lower			++	++	++	+++						
Renal crisis		++	-		+++	+++						
GAVE					+++							
Inflammatory arthritis	+	++									+++	+++
Tendon friction rubs	+	+++										
Myositis	+	++				++			+++	+++	+++	+++

1.3 Disease classification

1.3.1 Classification criteria

There have been recent strides to improve the classification of SSc. An initial attempt at classification favoured dcSSc and risked overlooking early and limited disease phenotypes (29). LeRoy and Medsger proposed criteria for early disease in 2001 to address this issue (30). Most recently in 2013, the ACR/EULAR joint committee created classification criteria that have largely superseded these approaches and require an aggregate score of at least 9 points across known clinical features (31) (Table 1.2). The modern criteria demonstrate clear improvement with improved sensitivity for classifying definite SSc (79.6% versus 53.3%) (32). This is achieved in part by assigning merit to the presence of puffy fingers, an early inflammatory phase of skin disease that precedes established skin fibrosis.

Table 1. 2 ACR/EULAR 2013 classification criteria for systemic sclerosis.

A minimum total of 9 points from the criteria is required for classification as definite systemic sclerosis in accordance with ACR/EULAR 2013 consensus (31). [1]sclerodactyly, the typical appearance of shiny skin and tapering of the digits occurring due to skin tightening.

Criterion	Score
Bilateral skin thickening of the hands extending proximal to the metacarpophalangeal joints	9
Skin thickening of the fingers:	*Highest score of:*
Puffy fingers	2
Sclerodactyly[1] of the fingers distal to the metacarpophalangeal joints but proximal to the proximal interphalangeal joints	4
Finger tip lesions:	*Highest score of:*
Digital tip ulcers	2
Fingertip pitting scars	3
Telangectasia	2
Abnormal nailfold capillaries	2
Pulmonary arterial hypertension and/or interstitial lung disease	2
Raynaud's phenomenon	3
Presence of one or more systemic sclerosis specific autoantibodies: Anti-centromere Anti-topoisomerase I Anti-RNA Polymerase	3

1.3.2 Disease subsets by distribution of skin disease

Despite the likely phenotype associated with SSc specific autoantibodies, the unescapable heterogeneity limits the use of autoantibodies as a definitive classification strategy in clinical trials. Historically, SSc has been divided into two subtypes based on the extent of skin fibrosis (23, 33), lcSSc or dcSSc (Figure 1.1). A third group with features of SSc but without any detectable skin changes may be denoted systemic sclerosis sine scleroderma (SSc sine scleroderma).

1.3.3 Classification by stage of disease

For the purposes of research studies more so than clinical practice, patients are typically considered as early in the disease course (early SSc) during the period within 3 years of onset of the first non-RP symptom (34). Alternatively, those beyond that 3-year window are classified as late SSc.

The international expert opinion of the EULAR Scleroderma Trials and Research Group (EUSTAR) assigns a 'very early diagnosis of SSc' (VEDOSS) disease classification (essentially 'pre-SSc') (35, 36) to patients with RP, a positive ANA and a history of puffy fingers who also have NC changes and/or SSc specific autoantibodies, but not meeting ACR/EULAR criteria for definite SSc (36, 37).

An important differentiation between patients classified as VEDOSS versus early SSc exists, such that the latter meet the ACR/EULAR criteria (31) at the point of entry to a clinical study (i.e. they have definite SSc). However, the 3-year window attributable as early SSc is assigned from the first non-RP symptom which may retrospectively include puffy fingers during the

VEDOSS phase. As such, there is a narrow window during which early but definite SSc patients can be recruited to clinical studies before they are classified as late SSc disease. This poses a challenge for the clinicians and limits the power of some studies.

1.4 Pathogenesis

1.4.1 The vascular hypothesis

LeRoy originally described the vascular hypothesis (38) linking the three hallmark pathological features through a process of a primary autoimmune insult on the vasculature, resultant progressive obliterative microangiopathy causing tissue hypoxia, and subsequent excessive collagen deposition by overactive fibroblasts in an attempt at tissue healing. The cycle is perpetuated as the increased oxygen demand of an inflammatory milieu coupled with the increased diffusion distance caused by inflammatory cell influx and accumulation of fibrotic tissue, exacerbate hypoxia. Indeed, oxygen saturations in fibrotic skin of SSc patients are notably low (pO_2 23.7+/-2.1mmHg compared to 33.6+/-4.1mmHg in healthy controls ($p<0.05$)) (39). There is increased oxidative stress and production of $O_2\bullet^-$ reactive oxygen species in SSc dermal fibroblasts (40). Despite the significant hypoxic drive, attempts at adequate neoangiogenesis in SSc fail resulting in a phenotypically avascular disease.

In line with the vascular hypothesis, endothelial injury is noted as an important initiating event in SSc and vasculopathy occurs early in the disease process. Endothelial activation, dysfunction and apoptosis, increased vascular permeability, vessel wall remodelling, platelet aggregation, and a perivascular inflammatory cell infiltrate are present early and in the absence of established tissue fibrosis (41-43). Clinically, vasculopathy manifests as

RP and morphological capillary changes at the nailfold (Figure 1.2), which precede the onset of overt cutaneous fibrosis (44, 45) by an average of four years (46). Additionally, there is evidence of impaired skin oxygen recovery in non-lesional skin after an ischaemic attack demonstrating that functional vasculopathy precedes tissue fibrosis (47).

SSc-specific autoantibodies have traditionally been considered as a clinical feature and biomarker of SSc disease. However, some evidence suggests they may have a pathogenic role through stimulation of fibroblast populations (48). Anti-endothelial cell antibodies have also been identified in some SSc cohorts and potentially convey a pathogenic role causing vascular destruction and inflammation (49, 50).

1.5 Vasculopathy in systemic sclerosis

1.5.1 Pathogenesis of Raynaud's phenomenon

Raynaud's phenomenon describes vascular dysfunction and reversible vasospasm occurring as a hypersensitivity reaction to cold or emotional stress (51).

Primary RP (PRP) occurs in the absence of other causative pathology and is common amongst the general population (~10%), particularly in women and within communities exposed to colder weather. Indeed, a study of young females in Scandinavia indicated a prevalence of RP of ~22% (52) compared to warmer Italian climates reporting a prevalence of only 2.1% (53). Sufferers may experience symptoms of episodic digital colour change, a white and blue (ischaemic phase) and red (hyperaemic reperfusion phase) affecting extremities (digits, nose, nipples and ears) (51). All three phases may be

associated with pain, numbness, impaired hand function and health-related quality of life.

Physiologically, the ischaemic phase is driven by muscular contraction in the vessel wall stimulated by alterations in neurogenic excitation, partly mediated by increased cold induced α2c adrenoreceptor activity in the vasculature (54) as well as changes in signalling mediators from a dysfunctional endothelium. Increased levels of asymmetric dimethylarginine (a nitric oxide synthase inhibitor) (55), alterations in nitric oxide levels itself (55), increased protein tyrosine kinase activity (54) and endothelin-1 (55) have been implicated in RP pathogenesis. There has also been an observed reduction in calcitonin-gene related peptide secreting neurons in the skin of RP sufferers (55).

Reactive hyperaemia is a physiological response following a period of ischaemia and is initially driven by neurogenic responses from predominantly sympathetic cholinergic signalling causing vasodilatation to improve tissue reperfusion following ischaemic injury (56). Vasodilation is then further potentiated by nitric oxide (56). Reactive hyperaemia that occurs as part of RP symptomatology demonstrates impaired responses in comparison to physiological normal. This is observed in PRP (57, 58), RP in hand-arm-vibration syndrome (59) and RP associated with other secondary pathologies.

1.5.2 Secondary Raynaud's phenomenon

Secondary RP (SRP) is reported as a symptom in over 95% of patients with SSc (SSc-RP) (5). Histologically, SSc-RP differs from its PRP counterpart by additional structural vascular abnormalities occurring in the former. Endothelial and intimal proliferation of small and medium sized arteries (54)

and smooth muscle cell migration and differentiation in the intima lead to collagen formation and vessel fibrosis (54). Coupled with intravascular platelet activation (11, 55), this causes a persistent narrowing of the vessel lumen and chronic tissue hypoperfusion even at baseline (51, 60). Persistent structural macrovascular changes present in SSc-RP result in reduced finger perfusion compared to both healthy controls (61-64) and PRP even at ambient temperatures (61, 65). In addition to the vascular stenosis, vessels remain hypersensitive to cold such that they experience acute superimposed RP attacks. As such, SSc-RP demonstrates reduced finger perfusion during induced vasoconstriction compared to healthy controls (64), as well as impaired reperfusion response compared to both healthy controls and PRP (61). The result of the structural and functional vascular impairment in SSc is ischaemia and hypoxic stress on the tissues. Whether cause or effect, SSc demonstrate increased markers of oxidative stress compared to PRP and HC (40). In SSc this is inversely associated with the maximal vasodilatory capacity suggesting a link between the ability of the vascular to re-perfuse the tissues and the degree of oxidative stress. Increased levels of asymmetric dimethylargininge is observed in RP, and to a greater extent in SSc-RP than PRP (66-68). SSc-RP also demonstrates increase adhesion molecules compared to PRP (66).

The implications of severe SSc-RP for patients is a combination of pain, functional impairment and even social isolation (69, 70). SSc-RP may result in DU, tissue necrosis and auto-reabsorption of digits (5, 71), which further increases morbidity (72).

1.5.3 Patient-reported outcome measures for Raynaud's phenomenon

Following data collected from patients with moderate-severe SSc-RP, it has previously been suggested that the impact of SSc related vasculopathy can be adequately reflected on a selection of patient and physician outcome measures including the Raynaud's diary (a 14 day diary documenting the frequency of attacks and perceived severity of their RP) and a patient visual analogue scale for RP severity (Raynaud's condition score, RCS) (73). The RCS diary is currently the preferred outcome measure for clinical trials for potential SSc-RP therapies (74).

1.5.4 Non-invasive imaging techniques to assess Raynaud's phenomenon

1.5.4.1 Assessment of microvascular dysfunction

Infrared thermography (IRT) (75), laser doppler imaging (LDI) (76), laser doppler flowmetry (LDF) (77) and laser speckle contrast imaging (LSCI) (75) are non-invasive methods of indirectly assessing peripheral blood perfusion. Functional vascular assessment can be made with addition of either warm or cold thermal challenge or extra-corporeal arterial occlusion to stimulate cold induced vasospasm and endothelial-dependent vasodilation. Hyperaemia can be stimulated using thermal exposure as part of a cold challenge protocol (78) to induce the RP ischaemic phase followed by observation of the hyperaemic response, or with direct localised skin warming (77, 79, 80) to induce vasodilation. Alternatively, application of an occlusive cuff around the examined limb can be used to induce an ischaemic phase of an RP-like attack. The resultant post occlusive reactive hyperaemic (PORH) response can be used to non-invasively determine endothelial function. Practically

speaking, PORH (a variant of flow-mediated dilation tests) is a logistically more straightforward provocation test than the cold challenge, as the latter requires submerging the hands in cool water whilst simultaneously avoiding water coming into contact with skin and impeding imaging acquisition. The peak PORH response has been shown to be highly reproducible (80).

To date, the majority of studies applying PORH methodology to investigate SSc vascular dysfunction have used LDF (Table 1.3). The overriding conclusions from these studies demonstrate that SSc have impaired microvascular perfusion at baseline as well as impaired vascular kinetics during post ischaemic reperfusion compared to controls. Similar results of impaired PORH response are reported in just 4 studies that utilised LSCI and PORH for functional vascular assessment (Table 1.4). LSCI has been validated in a large multicentre UK study for the use as a potential outcome measure in SSc-RP (75). Good spatial and temporal resolution as well as capacity for a wider field assessment marks LSCI as a potentially superior imaging modality than other laser-derived methods (81). The utility of LSCI and PORH in SSc therefore requires further study.

Table 1. 3 Summative results of studies using laser doppler flowmetry and PORH in SSc.

Abbreviations: DDD, distal-dorsal difference; HC, healthy controls; NC, nailfold capillaroscopy; n.s., non-significant; PORH, post occlusive reactive hyperaemia; PRP, primary Raynaud's phenomenon; SRP, secondary Raynaud's phenomenon.

Study & purpose	Sample size (n)	Concurrent medication use & exclusions	Methodology	Main findings
Wollersheim et al., 1989 (82) Comparing PORH between PRP, SRP and HC (abstract only)	n = 91 24 HC 29 PRP 38 SRP incl. SSc	-	LDF	• Altered baseline flow between PRP and HC • Notable overlap between PRP and SRP at baseline. • PORH differentiated PRP and SRP. • PORH differentiated SSc-RP from other SRP.
Wigley et al., 1990 (77) Cross-sectional study comparing PORH between PRP, SSc and HC	n = 63 29 HC 13 PRP 21 SSc 10 lcSSc 11 dcSSc	Withdrawal of vasodilators and aspirin for 2 weeks	Laserflow BPM 403 LDF • Baseline 5 mins • Cuff inflation to 200mmHg 5 mins • 5 mins of PORH recording • Distal pad of left ring finger ROI	• Baseline flow significantly lower in SSc vs PRP and HC. • Peak PORH significantly lower in SSc vs PRP or HC. • Significantly longer time to peak PORH in SSc vs PRP or HC. • Older age in SSc cohort did not affect results.
Rajagopalan et al., 2003 (66) Cross-sectional study comparing PORH in PRP and SRP (mixed cohort)	n = 40 20 PRP 20 SRP • 35% SSc • 65% other CTDs	Exclusion criteria included current use of: • >2 anti-hypertensive medications, • statins, • recent initiation of ACEI/ARB, • current smokers	Lisca PIM II system LDF • 2 mins baseline • 4 mins cuff inflation to non-dominant forearm 50mmHg above systolic BP • 6 mins PORH recording • Proximal dorsal middle finger ROI	• No significant difference in baseline finger perfusion between PRP vs SRP. • SRP had significantly reduced AUC for hyperaemic response to ischaemia, reduced peak PORH (n.s.). • No difference in time to peak PORH compared to PRP.
Boignard et al., 2005 (80) Cohort study investigating hyperaemic responses of PRP, SSc & HC and correlation of PORH with thermal hyperaemia	n = 60 20 HC 20 PRP 20 SSc 6 dcSSc 14 lcSSc	Withdrawal of vasodilators for 1 week Exclusion criteria included smoking, statins, nitrate, NSAIDs	PeriFlux 5000 LDF • Baseline 10 mins • Cuff inflation 5 mins at 50mmHg above resting systolic • Thermal hyperaemic response also studied • Distal pad of 3rd left finger ROI • Reproducibility o Peak PORH ICC 0.94 o Time to peak PORH 0.56	• SSc had significantly lower baseline perfusion than HC, but not PRP. • Trend for lower peak PORH in SSc than PRP and HC (SSc<PRP<HC). • SSc had significantly longer time to reach peak PORH vs PRP and HC. • Time to peak PORH correlated with time to peak thermal hyperaemic response. • Time to peak PORH was longer in dcSSc compared to lcSSc, but not the amplitude of peak PORH.
Cracowski et al., 2006 (40) Cross-sectional study investigating the relationship between peak PORH and urinary F2 isoprostane	n = 101 25 HC 33 PRP 43 SSc	Withdrawal of vasodialtors for 1 week Exclusion criteria included smoking, statins, nitrate, NSAIDs, any major confounding cardiac disease, smoking and diabetes.	PeriFlux 5000 LDF • Baseline 10 mins • Cuff inflation 5 mins at 50mmHg above resting systolic • Distal pad of 3rd left finger ROI	• Trend for increased baseline perfusion in HC vs PRP & SSc (n.s.) • Peak PORH significantly reduced in SSc & PRP versus controls. • SSc had a significantly longer time to peak PORH than PRP and HC.

Salvat-Melis et al., 2006 (83) Cohort study investigating the relationship between hyperaemia, skin fibrosis & vasculopathy in lcSSc versus PRP and HC	n = 63 21 HC 21 PRP 21 lcSSc	Withdrawal of vasodialtors for 1 week Exclusion criteria included smoking, statins, nitrates, NSAIDs	PeriFlux 5000 LDF • Baseline 10 mins • Cuff inflation 50mmHg above resting systolic for 5 mins • PORH 30 mins recording • Distal pad of 3rd finger, face, forearm ROI	• Trend for reduced peak PORH (HC > PRP > SSc) and increased time to peak PORH at the finger pad, HC < PRP < SSc (n.s.). • No difference in vascular PORH kinetics at the forearm between groups.
Roustit et al., 2008 (84) Cross-sectional study comparing microvascular and macrovascular PORH in PRP, SSc vs HC	n = 111 33 HC 36 PRP 42 SSc	Withdrawal of vasodilators 1 week prior Exclusion criteria included current smoking	PeriFlux 5000 LDF • Cuff inflation 50mmHg above resting BP 5 mins • Distal palmar index finger ROI	• Reduction in baseline flux in PRP & SSc vs HC (n.s.). • Peak PORH significantly reduced in PRP and SSc vs HC. • Time to peak PORH significantly increased in SSc vs PRP and vs HC.
Grattagliano et al., 2010 (85) Cross-sectional study investigating dynamic perfusion after cold and PORH testing in SSc & PRP vs HC	n = 111 31 HC 25 PRP 59 SSc 49 lcSSc 10 dcSSc	Withdrawal of vasodilators 1 months prior Exclusion criteria – active digital ulcers.	LDF PeriFlux 5000 • Baseline 20 mins • Cuff inflation 200mmHg 5 mins to left arm • PORH recording 15 mins • Distal ring finger left hand ROI	• Time to return to baseline flux after occlusion was significantly longer in dcSSc than lcSSc, PRP or HC (dcSSc > lcSSc > HC > PRP), but not between other groups. • Reduction in peak PORH for PRP, SSc, lcSSc and dcSSc vs HC (n.s.). • PORH AUC was significantly greater in lcSSc than HC.
Rossi et al., 2012 (86) Open label study investigating the effect of statin therapy on microvascular function in SSc and HC	n = 28 15 HC 13 SSc 3 DcSSc 10 LcSSc	Smokers excluded	Periflux PF4001 LDF • 10 mins baseline • Cuff inflation 200mmHg for 3 mins. • Peak PORH measured before and after 10 weeks of statin therapy. • Dorsal 3rd right finger ROI	• Before statin therapy SSc had significantly lower baseline perfusion, lower peak PORH and longer time to peak PORH vs HC. • After stain therapy SSc had significantly increased baseline, increased peak PORH and reduced time to peak PORH compared to before therapy. After statin therapy no difference in kinetics were noted between SSc vs HC.
Waszczykowska et al., 2014 (87). Cross-sectional study to assess the suitability of LDF to assess microvascular dysfunction in SSc and HC	n = 54 27 HC 27 SSc 17 LcSSc 10 DcSSc	Vasodilators permitted	PeriFlux 5000 LDF • 5 min baseline • 1 min cuff inflation 200mmHg • Dorsal distal phalanx of non-dominant index finger examined	• Non-significant increase in SSc baseline Flux • Significantly reduced Flux during ischaemic challenge and peak PORH compared to HC. • Significantly reduced baseline Flux was associated with reduced hyperaemia
Broz et al., 2015 (47) Cross-sectional study investigating PORH in non-lesional SSc skin vs HC	n = 24 12 HC 12 SSc 3 DcSSc 5 LcSSc 4 other	Vasodilators permitted (none of the HC were taking regular medications)	PeriScan PIM II LDF • 1 min baseline • 3 min cuff inflation around left thigh 50mmHg above resting systolic • 6 mins PORH recording • Left calf ROI	• Baseline non-lesional skin perfusion comparable in SSc versus controls. • No significant difference in peak or time to peak PORH, but a non-significant trend for lower peak PORH in SSc.

Table 1. 4 Summative results of studies using laser speckle contrast imaging and PORH in SSc.

Study & purpose	Sample size (n)	Concurrent medication use & exclusions	Methodology	Main findings
Della Rossa et al., 2013 (88) Cross-sectional study o investigate microvascular function by cold challenge and PORH in PRP, SSc and HC	n = 76 HC 20 PRP 20 SSc 36 VEDOSS 8 Established SSc 28	Stable dose of vasodilators permitted.	Pericam PSI LSCI • 5 mins baseline • 4 mins cuff inflation 30mmHg above resting systolic BP on left arm	• SSc had significantly increased baseline flux vs PRP and HC • SSc had significantly reduced peak PORH and AUC vs PRP. • SSc had a longer time to peak flux (n.s.). • Proportionally fewer RP sufferers had a DDD, SSc < PRP < HC. • Established SSc had lower peak PORH vs early SSc. • Peak PORH and AUC correlated with capillary density in RP overall. • SSc demonstrated a heterogeneity of finger flux. • No difference in baseline perfusion or PORH kinetics for lcSSc vs dcSSc or vasodilator use or NC pattern
Domsic et al., 2014 (89) A cross-sectional study to investigate vascular dysfunction in micro- and microvasculature of Early dcSSc vs HC	n = 30 HC 15 Early dcSSc 15	Early SSc (<2 years since non-RP symptom) Vasodilator use permitted	PeriCam LSCI • 5 mins baseline • Cuff inflation to 260mmHg or 60mmHg above systolic for 5 minutes • 2nd proximal metacarpophalangeal joint ROI	• Baseline not directly compared • Significantly reduced peak PORH in SSc vs HC • Significantly prolonged time to peak PORH in SSc
Gaillard-Bigot et al., 2014 (61) Cross-sectional study to investigate variable microvascular response to PORH at different anatomical hand locations in SSc and PRP vs HC	n = 45 HC 15 PRP 15 SSc 15	Withdrawal of Calcium channel blockers 1 week prior Exclusion criteria: • Smoking • Active digital ulcers	Pericam PSI LSCI • 10 mins baseline • 5 mins cuff inflation 50mmHg • 6 mins of PORH recording • Dorsal hand and fingers ROI	• Significantly reduced baseline flux in distal fingers of PRP and SSc vs HC (and thumb in SSc). • Peak PORH and AUC were significantly reduced in PRP and SSc versus HC. • SSc had significantly longer time to peak PORH at the index, middle and ring fingers versus PRP and HC. • DDD at baseline and peak PORH were significantly reduced in PRP and SSc. Reduced DDD peak PORH was more pronounced in SSc (n.s.). • No significant difference noted at the dorsum of the hand in PRP or SSc. • SSc demonstrated a heterogeneity of finger flux.
Della Rossa et al., 2016 (90) To investigate the value of PORH test in VEDOSS vs established SSc	n = 60 VEDOSS 10 Established SSc 50	Vasodialtors and smoking history permitted	Pericam PSI LSCI • 4 mins of cuff inflation 30mmHg above resting systolic BP, right arm • Dorsal hand ROI	• Peak PORH significantly increased in VEDOSS versus established SSc. • Peak PORH significantly reduced with progressive Nailfold capillaroscopic changes. • Peak PORH correlated with nailfold capillary density.

1.5.5 Structural microvascular changes in systemic sclerosis

In addition to peripheral vascular dysfunction manifesting as RP, SSc also exhibits changes in the size, morphology and architectural array of microvasculature. These structural microvascular changes are notable in the skin, scalp (91) and bone marrow (92). Nailfold capillaroscopy (NC) uses a simple non-invasive microscope technique (93) to directly visualise capillaries at the nail cuticle, where the capillaries are superficial and lie perpendicular to the skin surface. Cutolo et al. described the progressive phases of SSc NC evolution (94) (Figure 1.2) from normal through 'early', 'active' and 'late' phases with progressive loss of capillary number occurring over an average of 6 years (95). Whilst NC changes also occur in other connective tissue diseases (96, 97), the vascular pathology in SSc appears unique such that the patterns described by Cutolo et al., demonstrate 71-89.5% sensitivity and 80-95% specificity for SSc (35, 98). Indeed, just two features may be used to determine the presence of a SSc NC pattern with good reliability, the number of capillaries per millimetre and the presence of giant capillaries (99). Capillary morphology changes early in the disease course (100) before skin fibrosis is apparent. NC therefore provides an effective non-invasive and reproducible (101) clinical tool used in specialist Rheumatology centres to facilitate early diagnosis. Indeed, NC changes form part of the current ACR/EULAR classification criteria for SSc (31, 102).

The chronology of vasculopathy preceding fibrosis by some years, means that some patients with very early disease (VEDOSS) may present with features of autoimmune RP before definite SSc is established. NC also forms part of the VEDOSS criteria (35, 36), and can further aid early recognition of

those patients who are at risk of evolving to definite SSc and require close clinical follow up (45).

Figure 1. 2 Systemic sclerosis specific nailfold capillaroscopy patterns.

Figure illustrates the evolution of nailfold capillaroscopy (NC) changes in SSc, from normal through early, active and late patterns (94). Normal NC pattern as seen in healthy individuals, is recognized by 7-9 regular hairpin shaped capillaries per millimeter. The early pattern demonstrates maintained capillary number but enlarged* (>20μm limb diameter) and occasionally giant** (>50 μm) capillaries are present. Active pattern shows frequent giant capillaries**, microhaemorrhages∞ with some reduction in capillary number. The late pattern is classified primarily by severe capillary loss and evidence of neoangiogenesis⌘ with few/absent giant capillaries/microhaemorrhages. Figure created by VF using study images with participant consent.

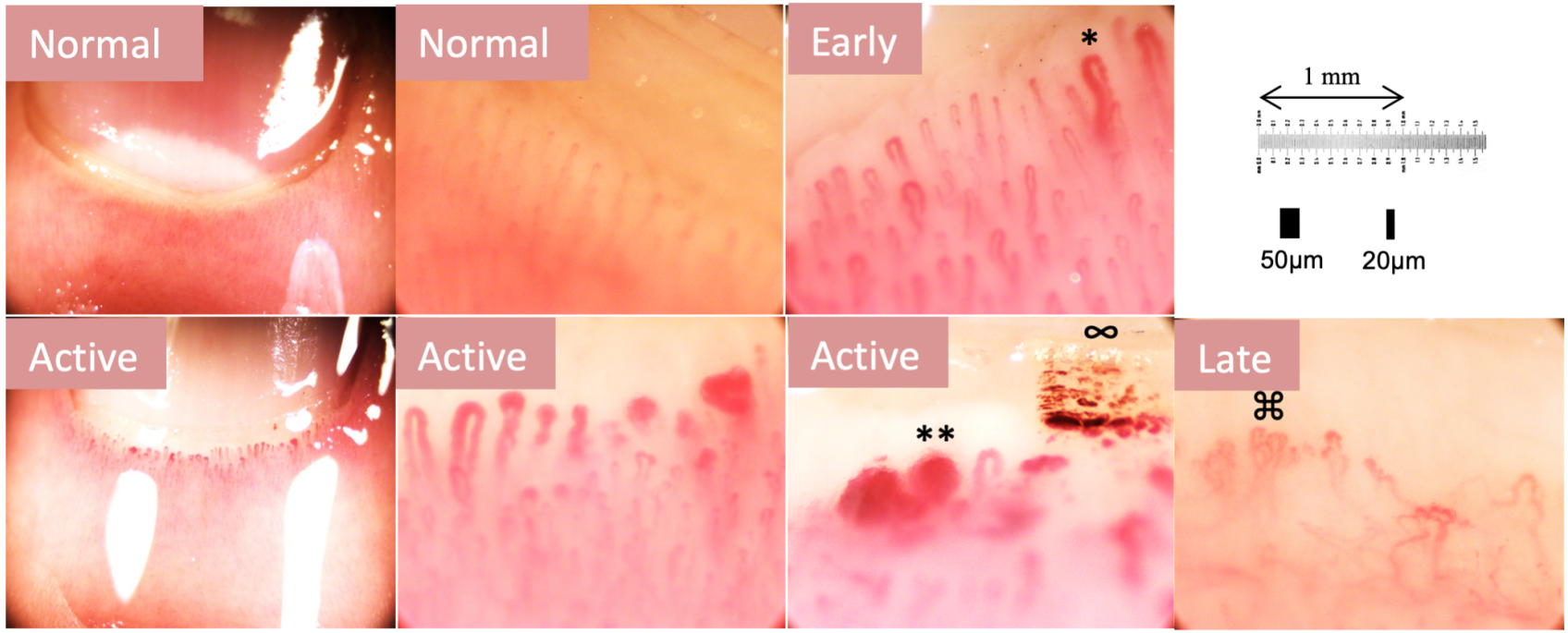

1.5.6 The relationship between structural microvascular changes and digital perfusion

In addition to the episodic vasospasm from discrete RP attacks, capillary loss contributes to persistent tissue hypoxia in SSc. Increased oxidative stress occurs in association with worse NC changes (103). Perfusion at the nailfold is reduced across all NC patterns, but most severely in the presence of capillary loss (104, 105). Similarly, tissue reperfusion and recovery after RP attacks are progressively delayed with increasing inter-capillary distance (88, 106) and advancing NC pattern (90). Disorganised angiogenesis is a potential contributor to impaired tissue perfusion. Enlarged capillaries typically associated with the active NC phase are dysfunctional, demonstrated by the negative relationship between nailfold capillary width and baseline hand temperature on infrared thermography (106).

The clinical implication of the impaired tissue perfusion associated with NC changes is an increased risk of developing new DU in the presence of capillary loss (107-109). NC provides clinically meaningful predictive value such that patient progression across NC patterns (110, 111) and larger capillary loop diameter (112) predict the risk of future DU occurrence. More advanced NC patterns also associate with increased frequency of cardiopulmonary disease including PAH (108, 110, 111, 113-116) and resultant mortality (117, 118). There is growing interest in the potential prognostic value of NC in predicting disease progression in SSc (119, 120). There is also emerging evidence that progression of the microangiopathy of SSc may be associated with evolution of RP symptoms in SSc, with late disease being associated with more persistent symptoms of digital ischaemia (121).

1.5.7 The relationship between microvascular changes at the nailfold and fibrosis

Evidence that vasculopathy predates other overt features of SSc (including fibrotic features) in support of LeRoy's vascular hypothesis (38), is illustrated in the 20-year prospective study following the evolution of NC changes in patients with RP. Koenig et al., (46) noted transition on NC from giant capillaries to capillary loss occurring in close temporal relationship to the onset of definite SSc (usually defined by the emergence of cutaneous fibrosis). A number of studies have also identified a positive and progressive association between the severity of microangiopathy on NC and extent of skin fibrosis (108, 113, 118, 122-124). As a reflection of this, early NC changes are more frequently identified in lcSSc (23, 108) and late changes highly prevalent in dcSSc (5, 113). Similarly, DU are also more common in dcSSc than lcSSc (125), but significantly less commonly encountered in SSc sine scleroderma (ssSSc, defined by the absence of cutaneous fibrosis), a subset not associated with a specific NC pattern (although reports perhaps limited by low study numbers) (125).

The expression and rate of progression of NC features also varies according to autoantibody specificities. SSc patients carrying RNAPIII (typically associated with dcSSc) have been noted to develop enlarged capillaries significantly earlier (4 vs. 15 years) than patients with ACA (typically associated with lcSSc) with a similar disparity reported for capillary loss (46). Similarly, Scl-70 positive SSc are more likely to exhibit SSc-specific NC patterns (113) with an OR 6.4 for late NC pattern (95). ANA negative patients who are typically considered to have milder phenotypes appear to progress through NC patterns more slowly (95).

Patients with SSc-specific NC changes also have an increased frequency of pulmonary fibrosis compared to those with normal or non-specific NC changes (126). Similar findings are reported for ILD with more advanced NC patterns (108, 113, 114). Although there is mixed reporting on the association of individual NC parameters such as capillary loss with ILD (123, 127, 128).

Taken together, these in vivo observations suggest the extent and severity of vasculopathy may be an important factor dictating not only vascular sequelae but also fibrosis and therefore SSc clinical phenotype. However, despite the numerous references to the potential predictive value of NC in SSc, it should be noted that the varied nature and quality of some studies with lack of adequate consideration of confounding, limits the detailed interpretation and translational potential (119).

1.5.8 Application of ultrasound to assess peripheral blood perfusion

Ultrasound is a readily available clinical tool that is utilised to evaluate larger vessels in a number of common vascular diseases (129). The obliterative vasculopathy in SSc affects medium and large arteries and has been illustrated using ultrasonography to contribute to poor peripheral blood flow, RP symptoms and subsequent vascular sequelae (130-133).

Ultrasound has also been used to assess the impaired peripheral microvascular perfusion in SSc (65, 131), which is distinguishable from both PRP and healthy controls (65). Ultrasound assessment of microvasculopathy in SSc is limited to data from just these two studies.

There are some practical disadvantages to the use of both NC and LSCI including their limited accessibility outside of specialised Rheumatology centres. In contrast, ultrasound is a readily available apparatus in every hospital. The few studies that have examined impaired microvascular perfusion by ultrasound show promise for its application. However, further study to validate its use in SSc vasculopathy is needed.

1.6 Skin pathology in systemic sclerosis

The Greek derivative Scleroderma, literally meaning 'hard skin', is perhaps the most recognisable feature of SSc and as such is oft synonymous with the formal disease designation. It is not however, a manifestation that is specific to this disease and a number of SSc mimics exist including graft versus host disease (134), nephrogenic fibrosis (135, 136), stiff skin syndrome (137) and scleromyxoedema (136, 138).

The pathology of SSc related skin disease is not simply one of fibrous stiffening of the skin, but a complex and evolving pathological process consisting of three phases (139, 140). The initial 'oedematous' phase demonstrates increased skin thickness predominantly due to inflammation and resultant interstitial oedema (141, 142). It is this phase that is responsible for the early 'puffy fingers' observed by patients and clinicians prior to the onset of definite skin fibrosis. Depending on the rapidity of systemic onset, the oedematous phase may last for weeks to years (139). This is followed by a more prolonged 'indurative' phase with the potential to span several years (139). Here, increased dermal collagen is laid down resulting in thickened fibrotic skin (143) and reduce normal skin suppleness. There is abnormal maturation of epidermal keratinocytes with over expression of keratin resulting in both thickening (144) and eventual thinning of the epidermis

(145). Additional loss of the stratum corneum ridging (145, 146) and atrophy of adnexal structures (147) creates a shiny appearance of the skin. With concurrent loss of peri-adnexal fat there is tapering of digits and the classical feature of sclerodactyly ensues. During the indurative fibrotic phase there is typically a clinical plateau with little discernible change in the severity of skin fibrosis. Finally, the skin enters an 'atrophic' stage where there is natural regression of fibrosis (142). The skin thins towards, or even beyond depths of healthy skin such that lesional skin may be in fact thinner than healthy controls. Towards the terminal phase of SSc skin evolution, there are variable degrees of tethering to the underlying subcutis, such that skin may become completely immobile over underlying tissues (139).

Typically, the evolution of skin fibrosis is different for those with lcSSc and dcSSc. Those with dcSSc tend to have a more rapid onset with skin scores typically peaking around 18 months after disease onset in patients with RNAPIII antibodies (34, 139) followed by some natural improvement reflecting both the resolution of oedema and skin thinning during the atrophic stage. LcSSc tend to display a more indolent rate of progression with lower peak scores occurring around 3-5 years followed by a plateau in total skin score (34).

1.6.1 Clinical Implications of systemic sclerosis skin disease

Whilst scleroderma is not a direct cause of patient mortality in SSc, it does carry significant patient morbidity. Afflicted patients experience tight restrictive skin that can be intensely dry and itchy (148) which impacts on local skin microbiome (149). Reduced function measured on HAQ-DI correlates with higher skin scores (72, 150) and mirrors changes in total skin score (72). Skin thickening affecting the digits reduces fingertip sensation for

fine motor tasks, reduces both flexion to form a grip and full extension resulting in a clawed posture and significantly reduces hand function measured on HAQ-DI (150). Hand contractures and skin fibrosis affecting the face also have significant impact on personal dissatisfaction with body image (151). Thickening around the mouth tightens and purses the lips (microstomia) restricting both mouth opening and effective closure. In severe cases microstomia can limit nutritional intake and contribute to the dental complications. Skin dryness can lead to fissuring particularly on the hands, which is both painful and a potential portal for infection. Skin fibrosis can also compound systemic disease by impeding chest expansion and worsens shortness of breath secondary to pulmonary disease.

There are several key points that can be derived from the simple clinical assessment of skin disease for an individual patient with SSc. Firstly, the anatomical distribution (and thus the sub-classification according to limited or diffuse SSc), is associated with systemic disease manifestations. DcSSc tend to experience more systemic organ manifestations including ILD, gastrointestinal, cardiovascular, renal and digital ulceration (5). Secondly, the severity of scleroderma is inversely associated with survival rates, such that with both higher peak and rate of progression of skin disease there is worse survival (152, 153). However, the absolute number of major organ events does not correlate with mortality in those with a high burden of skin disease at baseline (154). Thirdly, an improvement in skin disease occurring early in dcSSc appears to be an indicator for favourable prognosis. Data from the Pittsburgh database in 2001 (155) demonstrated that early dcSSc patients (<3 years from onset) who showed an improvement of more than 25% two years after peak mRSS, have significantly better survival rates than non-improvers such that at 5 and 10 years ‘improvers’ have 90/80% survival

respectively versus 77/60% in 'non-improvers' ($p < 0.0001$). This data has subsequently been supported by more recent data from the Royal Free cohort (154). Functional patient-reported outcome measures might contribute to this prognostic information as HAQ-DI correlates with temporal changes in mRSS and predicts survival (72). Establishing both the anatomical distribution (thus classifying the patient's disease), as well as monitoring for clinically relevant skin changes is therefore of great clinical importance.

1.6.2 Clinical assessment of systemic sclerosis related skin disease

The fundamental examination technique of palpation forms the basis of the modified Rodnan skin score (mRSS). Rodnan initially described a semi-quantitative method of measuring skin thickening through manual palpation of skin at 26 anatomical areas scoring severity on 0-4 scale (140, 156). This method was later modified such that fewer anatomical areas were examined and the scale narrowed to 0-3 (mRSS, 0 = normal up to 3 = severely thickened) (157). It is a quick, non-invasive and provides an economical single point outcome measure that correlates well with histological grading of fibrosis on skin biopsy (158). It is therefore considered as a surrogate of skin biopsy by SSc experts and is the gold standard for clinical assessment of SSc related skin disease. It has an acceptable 12% variance in intra-observer variability (159). However, the mRSS is limited by its subjective nature and inadvertently influenced by the degree of subcutis tethering, often masking clinical regression towards the atrophic phase (139). The mRSS also lacks the sensitivity to make qualitative assessment of the skin, specifically differentiating the reversible inflammatory phase from established fibrosis (139). As such, inter-observer variability is high with variations in scores of up to 25% even with didactic teaching of methodology

(159). The standard deviation of inter-observer assessment of skin thickness for both original and modified methods is approximately 4-5 skin thickness score points (160), which is notable when considering the potential error in evaluating therapeutic response in clinical trials. Indeed, a number of recent trials have failed to achieve statistical significance for their primary end point of an improvement in mRSS (161-163) (tocilizumab Phase III NCT02453256, RISE-SSc riociugat NCT02283762, ASSET trial abatacept NCT02161406) despite firm scientific rationale for their therapeutic potential. This begs the question as to whether this is due to limitations of the outcome measure rather than drug inefficacy (164). Certainly, Kaloudi et al., demonstrated a notable lack of correlation between local skin thickness judged by palpation and objective dermal thickness on ultrasound (165).

Hinchcliff et al., demonstrated that intrinsic gene expression in SSc skin biopsies distinguished those who responded to immunosuppressant therapy as being in the inflammatory phase compared to non-responders in the fibrotic phase (166). Further research is required to fully understand the implications of intervention at different pathological stages. However, this data suggests that accurate identification of different skin phases may help provide an individual and targeted approach to treatment, which currently cannot be provided by the mRSS alone.

Other more objective quantifiable methods exist including the use of a durometer (167), vesmeter (168) or cutometer (169) to measure skin hardness but still lack evaluation of skin thickness, tethering or oedema. Non-invasive Optical coherence tomography (OCT) utilises the birefringent properties of skin to evaluate collagen content reflected as an optical density. It has been proposed as providing a virtual biopsy in SSc (146, 170).

However, the ability of OCT to assess inflammation and oedema is not clear and limit its clinical and research application. To date there are a small number of studies demonstrating positive results for the potential use of ultrasound to examine both quantitative and qualitative SSc skin changes covering skin thickness, stiffness and oedema (122, 141, 171-176).

1.6.2.1 Assessment of skin disease by ultrasound

The use of ultrasound was first suggested as a method of assessing skin thickness in 1979 using wavelengths of 15 MHz (177). Advances in modern machinery now allow application of frequencies above this level, so called high frequency ultrasound (HFUS, >15MHz) (172). HFUS assessment of healthy skin identifies the dermis as a highly echogenic structure compared to the hypoechoic or echolucent subcutaneous fat layer (178, 179). The marked difference in echogenicity (skin brightness or darkness) between the skin layers provides a clear interface and allows the assessor to distinguish between layers of the skin and as such allows an accurate and reproducible measure of skin thickness (172). HFUS has previously been demonstrated as a useful tool for assessing a variety of skin conditions. It has been successfully applied in pre-operative and post-operative assessment of malignant skin lesions, particularly melanoma where the pre-operative depth and margins of the hypoechoic lesion can guide the extent of surgical management (180). The depth of melanoma on HFUS correlates well with actual thickness found on histology (181). It can also detail qualitative features of chronic skin diseases such as dermatitis, hypersensitivity reactions and psoriasis (182).

Comparatively few studies have assessed HFUS in SSc. Those that have suggest that average skin thickness in SSc is detectably greater than healthy

controls (171) and diminishes with disease duration reflecting ‘atrophic’ progression (171). Skin thickness on HFUS correlates well with local and total mRSS scores (141, 165, 171, 172) with the best correlation occurring at the hand, forearm and sternum (171). Furthermore, the echogenicity on HFUS negatively reflects the degree of inflammatory oedema such that darker tissue (low echogenicity) contains more oedema. Considering this, Hesselstrand et al., (141) used echogenicity to demonstrate the contribution of inflammation on skin thickness in the early phase of SSc pathology. Similarly, echogenicity has been used to map the progression of SSc skin disease from early ‘inflammatory’ thickening through to ‘atrophic’ stages in a longitudinal study (172).

Interestingly, it has been suggested HFUS can identify subclinical skin thickening before it is clinically detectable both in patients already classified as dcSSc and those with lcSSc who’s disease later evolved (141). Combining HFUS measurement of increased skin thickness and reduced echogenicity (more cutaneous oedema) in early disease can also distinguish between lcSSc and dcSSc by the severity observed in the latter (141). HFUS is therefore an attractive tool that has the potential to aid early diagnosis of SSc, correctly classify patients with dcSSc at higher risk of major organ involvement and aid earlier identification of disease progression that may benefit from systemic immunosuppression.

Few studies have utilized elastography to assess skin stiffness in SSc, but as expected have demonstrated increased skin stiffness at lesional sites (175, 176). Furthermore, it has been proposed that detectable pathology can be observed in apparently non-lesional skin (175). Elastography may also be complementary to other ultrasound parameters by confirming the dermal

interfaces and improving the accuracy and reproducibility of skin thickness measurement (174).

Further work is needed to confirm the utility of ultrasound in SSc skin disease, but it shows promise to overcome some of the limitations of the mRSS and improve objective assessment in clinical trials.

1.7 Morbidity and mortality associated with SSc

Beyond the physical symptoms resulting from systemic vascular and fibrotic SSc pathology, there is a major psychological impact of an SSc diagnosis. The burden of physical symptoms and the body dissatisfaction that can be associated with it is notable and depression affects up to 65% of patients (183). Disease specific factors such as pain and overall disease activity contribute to low mood (183). Depression, pain and functionality all impede sleep quality (184) compounding the physical and emotional impact of this devastating disease. Appreciably, therefore, SSc also results in a significant impact on work disability (185).

SSc has the highest disease-specific mortality rate of all the autoimmune rheumatic diseases. A review of deaths among the EUSTAR SSc registry demonstrated that 55% were directly attributable to SSc, including to pulmonary (PAH and ILD, 60-70.9%), cardiac (5-9%) and renal disease (6-7%) (186, 187). A further 25% of the remainder of deaths may also been indirectly related to an SSc diagnosis (188).

1.8 Pharmacotherapies for vasculopathy and fibrosis in systemic sclerosis

Despite the hypothesised inter-relationship between the three pathological features of SSc (vasculopathy, inflammation and fibrosis), current medicinal treatment options tend to approach management of each as distinct entities (189, 190). The need for multifaceted approach to therapy reflects both the complexity of the disease and the lack of detailed understanding of the inter-relationships uniting the pathological triad.

1.8.1 Vasculopathy

1.8.1.1 Raynaud's phenomenon and digital ulceration

Therapy for SSc-RP is aimed at increasing tissue perfusion by vasodilation. First-line therapy with calcium channel blockers (CCB) (191, 192) improves the frequency and severity of RP attacks (193), but there is no evidence to demonstrate improvement in DU. Other vasodilators including angiotensin II receptor blockers (AIIRB) and angiotensin converting enzyme inhibitors (ACEi) as well as vasoactive medications such as fluoxetine (a selective serotonin reuptake inhibitor, SSRI) may also be considered for SSc-RP (189, 190). Patients with recurrent SSc-DU may benefit from escalation to Sildenafil (a phosphodiesterase-5 inhibitor, PDE-5). Availability of generic forms makes it an affordable therapy which both improves healing and prevents occurrence of new DU (193). Bosentan (an Endothelin receptor antagonist, ERA), is a third-line option for refractory SSc-DU (189, 190). However, it is a high cost medicinal product that has been demonstrated to prevent new DU but failed to demonstrate efficacy for DU healing in 2 randomised control trials (193). Intermittent iloprost infusion (a prostacyclin analogue that stimulates vasodilation through cyclic adenosine

monophosphate (cAMP)) may also be used to improve healing of severe DU (189, 190, 193) particularly when associated with localised infection.

One study has shown that administration of oestrogen improves endothelium dependent vasodilation in SSc-RP (194). Indeed, in healthy women there is attenuated cold tolerance during menstruation when oestrogen is lowest (195). Hormone therapy is however not advocated as a specific treatment for SSc-RP, in part due to associated risk of oestrogen sensitive malignancy.

1.8.1.2 Pulmonary arterial hypertension

The obliterative SSc vasculopathy affecting the peripheral circulation resulting in RP is mirrored centrally in the pulmonary vasculature resulting in PAH. Medicinal products for PAH are unsurprisingly similar to RP therapies. Vasodilators such as PDE-5 inhibitors, ERA and continuous prostacyclin infusions have strongly favourable data for both symptomatic and haemodynamic improvement in SSc-PAH (196).

Two further drugs are proposed for the management of SSc-PAH. Riociguat (a stimulator of soluble guanylate cyclase, a downstream mediator of NO) is available for SSc-PAH management (190, 197). Early data suggests it may also improve peripheral perfusion in SSc-RP (198), improve healing of DU (199) and reduce DU recurrence (200). Further evidence is needed to support its clinical application for peripheral vascular indications.

Selexipag (a prostacyclin receptor agonist that stimulates vasodilation through cAMP on vascular smooth muscle and platelets) reduces PAH related complications and improves survival (196). It too has been assessed for SSc-RP. However, based on data from the RP diary and RCS, selexipag

showed a surprising inferiority to placebo (201) and therefore is not included in national guidelines for SSc-RP management. The results of studies like this raise concerns over the validity of such outcome measures for use in clinical trials.

1.8.2 Fibrosis

1.8.2.1 Cutaneous and pulmonary fibrosis

The majority of current therapeutic options for cutaneous and pulmonary involvement are immunomodulatory.

Whilst the immunosuppressive benefits of glucocorticoids are widely used as adjunct therapy in most rheumatological conditions, they are less favoured in systemic sclerosis largely due to the association with precipitating scleroderma renal crisis, particularly in early diffuse disease (191). Short duration and modest doses of prednisolone are however advocated for the benefit of musculoskeletal manifestations in particular (189) and may be used in the short term for severe skin or pulmonary disease.

Available evidence for disease modifying antirheumatic drugs (DMARDs) in severe SSc skin disease is surprisingly limited but supports the use of cyclophosphamide (202-204) as an induction agent followed by longer-term maintenance therapy with methotrexate or mycophenolate mofetil (191, 205). Of these, methotrexate holds the strongest body of evidence for skin fibrosis supported by two randomized placebo-controlled trials (RCT) (206, 207) compared to observational data only for mycophenolate (208-211). The benefits of combining high dose cyclophosphamide with autologous haemopoietic stem cell transplantation (HSCT) have been examined in Europe and the United States of America. Reports of phase I/II trials

demonstrated clinical improvement and reduction in disease related mortality have been encouraging (212-214), however, relapse in disease has occurred in up to 35% of patients within ten months of treatment (215).

Whilst the available data does support the use of traditional DMARD regimes to manage SSc skin disease, the effects are considered modest (216) and more aggressive intervention with HSCT has high risk of treatment related mortality (212, 213, 217). More effective therapeutic options are therefore greatly needed.

Conflicting study results and a high number of adverse events in clinical trials has prevented the progression of imatinib (a tyrosine kinase inhibitor) (191, 218-221) and TNF inhibitors (222, 223) to clinical use. Observational data for the use of intravenous immunoglobulin for refractory skin disease has been promising (224), but its use is limited by lack of RCT evidence.

There is more favourable emerging evidence for targeted depletion of regulatory T cells by abatacept to improve skin disease (163). Similarly, janus kinase inhibition may also have anti-fibrotic effect on skin disease (NCT 03274076) (225), but both are still under evaluation in clinical trials. rituximab (an anti-CD20 monoclonal antibody that depletes peripheral B cells population) has also been shown to significantly reduces the mRSS (226-228) as well as improve lung function (227). The effects of rituximab on SSc-ILD are currently being assessed in a large RCT (RECITAL study, NCT 01862926) (229).

Interleukin-6 (IL-6) inhibition by tocilizumab reduces skin scores (161, 230, 231) and stabilizes lung function (161, 230). However, mRSS improvement

failed to achieve significance (230, 231). A larger phase III study has also identified favourable responses in the skin and lungs of patients with early dcSSc (232).

The current and potential therapeutic options discussed have thus far targeted immune pathways. Some recent clinical trials have focussed their therapeutic targets on vascular pathways with the aim of eliciting anti-fibrotic potential. Indeed, there is promising evidence of anti-fibrotic effect from stimulation of soluble guanylate cyclase in skin of mouse models of SSc (233). A subsequent RCT investigating the efficacy of riociguat in SSc skin disease (RISE-SSc study, NCT 02283762) (162) has encouraging preliminary reports for a strong trend towards clinical improvement in mRSS (234).

Following successful application in idiopathic pulmonary fibrosis, nintedanib (a blanket tyrosine kinase inhibitor including VEGFR1-3, PDGFR and fibroblast growth factor receptor) has been studied for its potential anti-fibrotic effect in SSc including positive in vitro effects on lung fibroblasts (235, 236). Very recent results of a phase III trial for SSc-ILD (SENSCIS trial, NCT 02597933) have been reported demonstrating successful therapeutic stabilization and even improvement in pulmonary function (237). As such, nintedanib has received marketing approval for use in SSc-ILD in the United States of America. However, despite data demonstrating reduction of skin fibrosis in bleomycin rodent models with nintedanib (238), no significant therapeutic effect was noted on mRSS in the SENSCIS trial (237). Furthermore, as nintedanib antagonises VEGF-A pathways it has the potential to worsen vascular complications and patients with significant DU were excluded from trials. As such, this disease still lacks a single effective

and acceptable agent to treat multiple manifestations from pathogenic mechanisms of disease.

1.8.3 The limitations of outcome measures in advancing systemic sclerosis management

A number of the recent aforementioned clinical trials have failed to achieve statistical significance for their respective outcomes (201, 220, 221, 230, 231, 234, 237) despite theoretical promise for their application. The majority of these studies utilised the mRSS. Whilst the mRSS remains the gold standard for skin scoring, the SSc clinical community widely agree that it has significant limitations in its failure to differentiate stage of skin pathogenesis and has poor inter-observer variability with subsequent negative impact on clinical trial success. There have been similar challenges in establishing treatment efficacy in clinical trials of RP and DU (201). In order to further the treatment options for this disease we must first develop and validate robust objective outcome measures to assess SSc disease severity.

1.9 The role of vascular biomarkers in systemic sclerosis pathogenesis

A number of different signalling molecules have been implicated in SSc pathogenesis, but a clearer understanding of the pathogenic drivers is still required. In view of the vascular hypothesis indicating that vasculopathy is an early clinical feature, there is particular interest in hypoxia induced vascular biomarkers.

1.9.1 Hypoxia inducible factor

HIF is a family of transcription factors within the PER ARNT SIM (PAS) transcription group (239). HIF is a heterodimer consisting of an α subunit

(HIF1α, 2α, 3α, whose level is largely dependent on hypoxic stimulus and thus determines HIF transcriptional activity (240)) and a β subunit (a constitutively expressed nuclear protein also known as aryl hydrocarbon nuclear translocator, ARNT) (239). Under normoxic conditions HIFα is rapidly degraded by proteasomes and therefore is only detected at significant levels under hypoxic conditions (239). As HIFα accumulates, the HIFα/β dimer binds to hypoxia response elements (HRE) to up-regulate gene transcription (240), stimulating a number of physiological responses designed to enhance tissue perfusion and protect cells from oxidative stress (including angiogenesis, glycolytic metabolism, erythropoiesis, cell proliferation, tissue remodelling and apoptosis) (241). HIF1α is expressed widely throughout almost all tissues whereas HIF2α paralog is differentially expressed in endothelium, renal, hepatic, pulmonary and brain tissue (242). HIF1α has been implicated in a number of diseases characterized by altered angiogenesis, inflammation and fibrosis (240, 243). Both HIF1α (244) and HIF2α (245) are associated with PAH (a potential manifestation of SSc vasculopathy), actions of which may be mediated through VEGF-A and IL-6 (246). There is some evidence that HIF1α and HIF2α have differential actions (247) such that HIF1α primarily regulates metabolic targets whereas HIF2α has a more prominent role in angiogenesis (248).

1.9.2 Vascular endothelial growth factor family

The Vascular endothelial growth factor (VEGF) family comprises placental growth factor (PlGF) and four mammalian VEGF subgroups (VEGF A-D). Downstream effects of VEGF are communicated through three tyrosine kinase receptors (VEGFR1 (flt1), VEGFR2 (KDR/flk1), VEGFR3 (flt4)), supported by co-receptors (neuropilin-1 (NP-1) and neuropilin-2 (NP-2))

(249). Figure 1.3 illustrates the biological actions of VEGF family receptors and associated co-receptors.

VEGF-A was initially described as a vascular permeability factor (250) and subsequently shown to exhibit both mitogenic and angiogenic properties (251, 252). Levels are precisely controlled such that a single allele deletion results in embryonic failure (253) and VEGFR1 gene mutation causes disorganized endothelial cell lining and failed angiogenesis (254). However, its biological actions now appear wider, including inflammatory chemo-attraction (255) and fibrosis (256). Hypoxia is a major up-regulator of VEGF-A both as a downstream signalling molecule of HIF (240) and via hypoxic mRNA stabilization (249).

Variable splicing of the 6th and 7th exons of VEGF-A results in different isoforms (hereafter referred to as VEGF-A$_{xxx}$a), named according to their respective number of amino acids (e.g. VEGF-A$_{165}$a) (257). VEGF-A$_{165}$a is the dominant pro-angiogenic factor amongst the VEGF-A family acting through the principle tyrosine kinase receptor (VEGFR2) (258), to stimulate neoangiogenesis through proliferation and migration of endothelial cells to form new tubular vessel structures (259).

Until relatively recent scientific history all VEGF isoforms had been considered pro-angiogenic factors. However, since 2002 a number of alternative splice variants of VEGF-A (VEGF-A$_{xxx}$b and VEGF-Ax) have been identified, some of which inhibit angiogenesis through competitive binding of VEGFR2 (260-262) and absence of NP-1 co-receptor binding (Figure 1.3) (263). The latter also directs alternative intracellular trafficking in favour of VEGFR2 degradation (264). However, VEGF-A$_{xxx}$b isoforms may have

physiologically beneficial roles such as inhibiting placental neoangiogenesis and pre-eclampsia during pregnancy (265) and inhibition of tumour growth and metastatic progression in many cancers (260). Excessive VEGF-A_{165}b expression has been implicated in the pathology of peripheral arterial disease (266) and is down-regulated in some colorectal cancers (267).

Figure 1. 3 Biological actions of VEGF and its receptors.

Figure created by VF and adapted from collective reports from (258, 261, 268, 269) (249). Illustrates vasculogenic actions of VEGF family through their respective signaling receptors including three tyrosine kinase receptors (VEGF receptor-1 (VEGFR1/flt1), VEGF receptor-2 (VEGFR2/KDR/flk1), VEGF receptor-3 (VEGFR3/flt4), supported by co-receptors (neuropilin-1 (NP-1), neuropilin-2 (NP-2) and heparin sulphate proteoglycan [HSP]). VEGFR2 is the principal receptor for VEGF-A signaling including VEGF-A_{xxx}b isoforms with additional low affinity binding for VEGF-C and VEGF–D following proteolysis. VEGFR1 and VEGFR3 impose regulatory function on VEGFR2. VEGF-A binding to NP and HSP is isoform specific dependent upon exon splicing (249, 262, 268). Data reporting the affinity of VEGF-A_{121}a for NP1 is mixed and therefore inconclusive (261). Abbreviations: TK, tyrosine kinase; BM, basement membrane; HSC, haemopoietic stem cells; ECM, extracellular matrix; EC, endothelial cell; PlGF, placental growth factor.

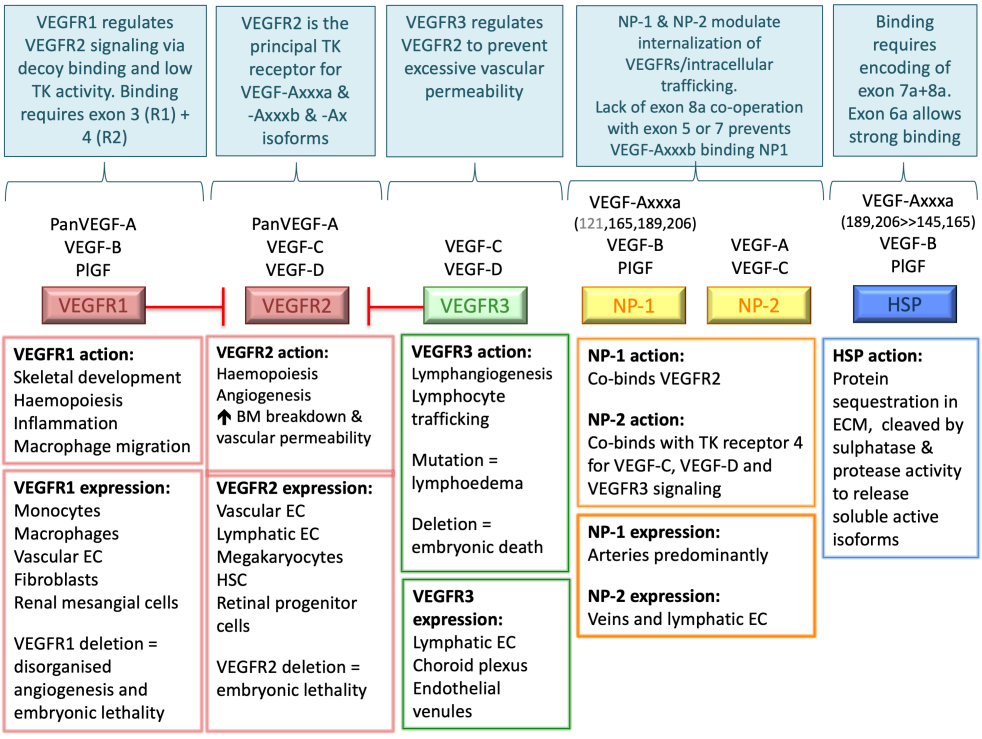

Other members of the VEGF family (VEGF-B-D and PIGF) also promote angiogenesis through co-binding of VEGFR1 and NP-1 (268). VEGF-B also plays a role in fatty acid transport and may therefore provide a therapeutic target for insulin resistance and type 2 diabetes (268). VEGF-C and VEGF-D signal through an alternative VEGFR3 to promote lymphangiogenesis in embryonic and postnatal period respectively (268).

1.9.3 The potential role of VEGF in SSc related vasculopathy

In view of the characteristic microvascular manifestations of SSc, VEGF-A pathways have attracted interest as potentially important drivers of disease pathogenesis. In view of the pronounced capillary drop out found in SSc, the authors of early studies were surprised to identify high levels of circulating serum VEGF-A in both early (270) and established SSc (123, 271), although serum VEGF-A was noted to be comparatively lower in SSc patients with DU (270, 272). VEGF associations with systemic organ manifestations of SSc have been less extensively studied and are notably varied. Circulating VEGF-A levels in SSc pulmonary vasculopathy are contradictory (246, 273, 274). Limited data show no correlation between elevated serum VEGF-A with ultrasound parameters of renal vasculopathy (275). One study has reviewed VEGF-A through non-invasive sampling of tears of SSc patients and found levels to be surprisingly low possibly explained by reduced tear secretion associated with dry eye syndrome (276).

The elevated VEGF-A levels initially appeared at odds with the obliterative microangiopathy associated with progressive capillary loss (270, 277, 278). A proposed explanation for these apparently conflicting findings is cellular compartmentalization of VEGF-A and its receptors, a biological concept that might be important in healthy lung homeostasis (279). However, the

identification of VEGF-A splice variants with opposing angiogenic function provides a deeper and more compelling explanation. VEGF-A_{165}a and VEGF-A_{165}b isoforms differ by only six amino acids at exon 8. Commercially available VEGF-A ELISAs are unable to differentiate between these isoforms. Thus, aforementioned studies (123, 270, 271, 277, 278) likely detected panVEGF-A (representing co-detection of VEGF-A_{xxx}a and VEGF-A_{xxx}b soluble isoforms). Subsequent studies used isoform VEGF-A_{165}b specific detection methods to confirm an association between VEGF-A_{165}b and the 'late' avascular patterns on NC (280). Furthermore, those with 'early' nailfold changes (i.e. few microvascular changes) have similar VEGF-A_{165}b levels to healthy controls (280), suggesting that anti-angiogenic isoform expression evolves with disease progression, although longitudinal studies have yet to confirm this.

VEGF receptor status in SSc skin, serum and cell culture is mixed and inconclusive (39, 271, 281-283). However, higher levels of circulating soluble VEGFR2 appear to be associated with telangiectasia (281). Urokinase-type plasminogen activator receptor (uPAR), which is required for VEGFR2 internalization, is reduced in SSc skin (263). Additionally, NP-1 is reduced in skin and serum (263, 282) and associates with DU and more advanced (active/late) NC patterns in SSc (282). Interestingly, despite evidence of microvasculopathy at the nailfold, reduced serum NP-1 does not appear to associate with specific NC patterns in those with pre-SSc (100). However, exposure of MVEC to patient sera attenuates NP-1 expression, a phenomenon demonstrated even by sera from pre-SSc donors (100). In combination, the functional status of VEGFR2 appears to be impaired from multiple co-factors, potentially reducing the pro-angiogenic potential of VEGF-A_{xxx}a and potentiating VEGF-A_{xxx}b inhibitory action.

Given the relationship between NC pattern and VEGF-A_{165}b, and known correlations between capillary density and both gas transfer (123) and the presence of SSc-related pulmonary disease (both interstitial lung disease (ILD) and PAH) (111), the relationship between inhibitory VEGF-A_{xxx}b isoforms and pulmonary vasculopathy is of interest but has not been investigated to date. Interestingly, transgenic mice over-expressing anti-angiogenic pulmonary VEGF-A_{165}b do not develop vascular abnormalities (256) whereas overproduction of VEGF-A_{164}a (the murine equivalent of VEGF-A_{165}a) results in increased vessel number and wall thickness (284) and dilated and disorganized vasculature (285) suggesting it is the relative rather than absolute level of the anti-angiogenic isoforms that dictates vascular morphology.

The roles of VEGF-B-D have been less extensively investigated in SSc. VEGF-C/D regulate lymphangiogenesis and lymphatic endothelium (Figure 1.3). SSc lesional skin displays a progressive reduction in lymphatic number (286, 287) despite the fact that circulating VEGF-C and cutaneous VEGF-D (288) and its receptor (VEGFR3) (287) are increased. This might indicate impaired downstream signalling of VEGFR3 or the presence of splice variants of VEGF-C/D with opposing functions, akin to the aforementioned VEGF-A_{xxx}b isoforms. In one study, plasma VEGF-D levels were shown to increase at the time of PAH diagnosis (289).

1.9.4 The potential role of VEGF-A in fibrosing disease

HIF and VEGF-A have been implicated in a number of fibrosing diseases including graft versus host disease, hepatic fibrosis and idiopathic pulmonary fibrosis (IPF) (290-297).

A pro-fibrotic role for VEGF-A_{165}a in SSc is supported by the demonstration of increased collagen induction in both healthy and SSc dermal fibroblasts in response to VEGF-A_{165}a with more pronounced effects observed in SSc fibroblasts (298). Serum panVEGF-A levels in SSc correlate with skin scores (277) and increased levels are associated with dcSSc (270, 277) and Scl-70 (270, 299). PanVEGF-A and HIF1α are increased in SSc hypoxic lesional skin (39, 300) and over-expressed by dermal fibroblasts cultured under hypoxic conditions (301). Furthermore, panVEGF-A is overexpressed in non-lesional skin predating the onset of fibrosis (39) implicating VEGF-A as an early signalling protein in fibrosis. However, whilst lesional skin is notably hypoxic, the pO_2 of non-lesional skin is normal (39) suggesting that VEGF-A expression may be stimulated by factors beyond hypoxia.

To date, the focus of VEGF-A_{165}b investigation in SSc has been with regard to its anti-angiogenic function and there are few observations reported with regard to fibrosis in SSc. Studies have identified increased VEGF-A_{165}b in the skin (mRNA) and plasma of SSc patients (280, 302), which may account for the majority of panVEGF-A overexpression (302). VEGF-A_{165}b appears to be particularly elevated in certain autoantibody profiles (anti-centromere and anti-Scl-70) (299, 303) although, in contrast to panVEGF-A, VEGF-A_{165}b levels (in skin and plasma) do not apparently correlate with extent of skin involvement (280, 302). Recent data from murine models of an alternative fibrotic disease (IPF), suggest that VEGF-A_{xxx}a isoforms act as pro-fibrotic drivers of IPF whilst the VEGF-A_{165}b isoform has opposing anti-fibrotic properties(256). In this model, the balance between VEGF-A_{165}a and VEGF-A_{165}b expression may also be important in IPF pathogenesis (256). Considering this parallel fibrotic disease, it may be hypothesized that VEGF-

$A_{165}b$ could detrimentally contribute to the progressive vasculopathy in SSc whilst encouraging regression of skin fibrosis later in disease. Interestingly, VEGF-$A_{165}b$ appears to be higher in the skin of early SSc (despite comparable circulating plasma levels) (302). This may suggest the occurrence of early isoform switching.

There are conflicting data regarding the association of circulating panVEGF-A levels with the degree of pulmonary fibrosis on computerized tomography (123, 274, 277, 304). As discussed for SSc-PAH, VEGF-$A_{xxx}b$ isoform expression has not been specifically studied and conflicting reports in SSc-ILD may be a consequence of panVEGF-A detection.

1.9.5 Potential cellular sources of VEGF-A isoforms in SSc

If VEGF-A is at the forefront of disease initiation, then identifying its cell origin is paramount to understanding and modifying its signalling network. In SSc, panVEGF-A and VEGF-$A_{165}b$ is expressed in fibroblasts, endothelial and perivascular inflammatory cells (39, 302) with additional expression of VEGF-$A_{165}b$ in vascular smooth muscle cells in *ex vivo* lesional skin (302). Circulating mononuclear cells (305) and skin keratinocytes (39, 300) also produce increased panVEGF-A levels.

In vitro, cultured microvascular endothelial cells (MVEC) express higher VEGF-$A_{165}b$ (co-localized with increased VEGFR2 but with impaired signalling function) than controls (302) (Figure 1.4). Additionally, when MVEC, from non-lesional SSc skin, are co-cultured in vitro with activated fibroblasts from lesional skin, panVEGF-A and CD31 expression in the former are reduced whilst VEGF-$A_{165}b$ is increased (306). This is associated with reduced microtubule formation and increased endothelial-to-

mesenchymal transition (EndoMT) (306), demonstrating the potential paracrine activity of SSc fibroblasts on the vasculature and potential to perpetuate the cycle posed by the vascular hypothesis (306).

Platelets are an important source of circulating panVEGF-A in SSc (307) and recent investigation has also proven them to be an important source of VEGF-A_{165}b (308). Furthermore, tubule formation by dermal MVEC in vitro is impaired when incubated with SSc platelet releasate (308) potentially due to the anti-angiogenic action of VEGF-A_{165}b. It is not known whether the platelet load of VEGF-$A_{xxx}a_{/xxx}$b isoforms remains consistently elevated in SSc or whether isoform switching occurs at some stage in the disease course.

Figure 1. 4 Cellular sources and inducers of VEGF-A.

Inducers of VEGF-A under the influence of hypoxia and inflammation (240, 249, 268, 309-311) (black/white pathways) in otherwise healthy human cells and the potential interaction with the known cellular sources of VEGF-A isoforms in SSc (39, 300, 302, 305, 307, 308, 312-314) are shown. *Some interleukins provide cell specific inhibitory signalling (311). **TGFβ and HIF1α synergistically increase VEGF-A in endothelial cells (309) with additional hypoxic up-regulation of VEGFR (310). Whilst TGFβ has been shown to favour VEGF-A_{165}b production in SSc-MVEC, similar evidence is not available in other cell lines, where only results for panVEGF-A have been reported. Abbreviations: HRE, hypoxia response elements found in the VEGF-A gene promoter region; AP-1, activating protein-1; MCP-1, monocyte chemoattractant-1; MVEC, microvascular endothelial cells; PBMC, peripheral blood mononuclear cells; TGFβ, transforming growth factor-β. Figure created by VF.

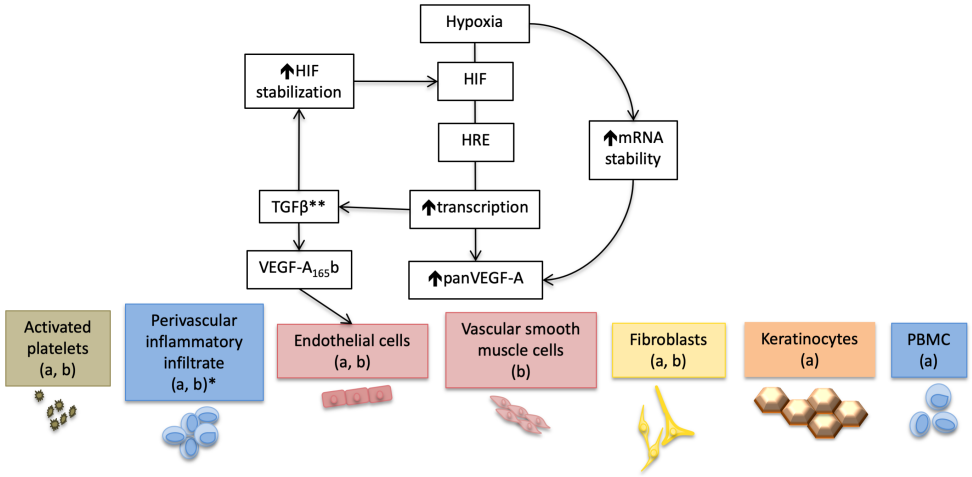

1.9.6 Additional mediators implicated in VEGF-A signalling in systemic sclerosis

Whilst hypoxia is the major driver of VEGF-A expression, other cytokines and growth factors can potentiate VEGF signalling, or are themselves potentiated by VEGF-A expression, which could have important implications for SSc pathogenesis.

1.9.6.1 Angiopoietins

Angiopoietins (Ang-1 and -2) are additional regulators of angiogenesis. Under normoxic conditions, Ang-1 aims to maintain vessel stability through

Tie-2 receptor signalling. Ang-1 drives endothelial microtubule formation through PI3 kinase/Akt pathways but is reliant on the presence of panVEGF-A which may be secreted by neighbouring fibroblasts (315). Ang-2 is released under hypoxic stress and acts differentially to either facilitate angiogenesis or angio-regression depending on the presence or absence of VEGF-A respectively (316). Reported circulating levels of angiopoietins and soluble Tie-2 in SSc are variable in the literature (299, 304, 316-319). However, noting the results of a recent study, there is a reduction in Ang-1/-2 ratio in serum of both pre-SSc and SSc (316). Furthermore, increased vascular expression of Ang-2, reduced Tie-2 and comparable Ang-1 in SSc skin versus controls (316) potentially represents a shift towards an anti-angiogenic environment. Ang-2 correlates with pulmonary arterial pressure and negatively with DLCO in SSc (319) implicating it in pulmonary vasculopathy. Progressive study regarding the association of Ang-2 with VEGF-A_{xxx}b isoforms may help map the divergent nature of Ang-2 with VEGF-A expression and the implications of VEGF-A isoforms on angiopoietin function.

1.9.6.2 Inhibitor of DNA binding protein 1

Inhibitor of DNA binding protein 1 (Id-1) is a transcription factor required for endothelial cell migration and is reduced in SSc endothelial cells, resulting in impaired endothelial cell response to VEGF-A stimulation (320). The influence of Id-1 expression on responses to specific VEGF-A isoforms has not been investigated.

1.9.6.3 Plasma 8-isoprostane

Increased plasma 8-isoprostane reflects increased oxidative stress in SSc (321) and contributes to impaired angiogenesis (321) via increased

TXAR/RhoA/ROCK expression and signalling (321) and subsequent inhibition of VEGF-A induced endothelial cell migration (321). Interestingly, increased plasma 8-isoprostane appears specific to dcSSc and SSc-ILD and not present in lcSSc and SSc-PAH (321). Once again, further investigation of these pathways with respect to specific VEGF-A isoforms and correlation with SSc subtype is of interest.

1.9.6.4 Transforming growth factor-β

Elevated levels of TGFβ are evident in skin and lung tissue (322) and peripheral B cells (323) in SSc alongside increased TGFβ receptor excretion by cultured SSc fibroblasts (324). HIF1 increases TGFβ transcription, which in turn stabilizes HIF1α (301, 325). This provides potential for TGFβ mediated indirect VEGF-A stimulation, but it also directly stimulates VEGF-A production in SSc dermal fibroblasts (314). Furthermore, the effects of HIF and TGFβ on VEGF-A are synergistic in human MVEC in vitro via complementary action at the HRE on the VEGF promoter region (309). However, TGFβ encourages a switch from proximal to distal splicing of VEGF-A exon 8 via p38 MAPK signalling (326) favouring VEGF-A_{165}b production in cultured SSc-MVEC (302). This could ameliorate VEGF-A mediated fibrosis and may explain the late improvement in skin thickening in SSc that characterizes the natural history of the disease. Increased VEGF-A_{165}b in SSc may therefore in part be directed by TGFβ, potentially as part of a negative feedback loop and resulting in mRSS plateau and late improvement.

1.9.6.5 Tumour necrosis factor- α

Treatment of cultured retinal epithelial cells with tumour necrosis factor-α (TNF α) induces a switch from dominant VEGF-A_{165}b at rest to VEGF-A_{165}a

(326). To our knowledge this relationship has not been investigated in SSc specifically. Whilst a previous trial of anti-TNFα agents failed to demonstrate definite improvement in scleroderma (223), the theoretical effects of TNFα inhibition on VEGF-A isoform switching in arresting scleroderma progression is of interest.

1.9.6.6 Platelet derived growth factor

PDGF is known to stimulate VEGF-A via phosphatidylinositol 3 kinase (PI3K) (327). PDGF and its receptors (PDGFR) are increased in SSc and *in vitro*, PDGF can attenuate panVEGF-A production by SSc fibroblasts (39). Furthermore, there is PDGFR up-regulation (in skin and lung fibroblasts) in response to TGFβ stimulation (328). Thus, it is possible that PDGF may compliment TGFβ directed VEGF-A activation in SSc fibroblasts.

1.9.6.7 Connective tissue growth factor

Hypoxia induces increased synthesis of CTGF mRNA in both healthy and SSc dermal fibroblasts via HIF1α dependent pathways (329). Circulating CTGF is increased in SSc and associations have been found with diffuse skin disease, pulmonary fibrosis and disease duration (330). Ex vivo, CTGF levels are over-expressed in SSc mesenchymal stem cells (MSC) and increased further by VEGF-A stimulation (312).

1.9.6.8 Caveolins

Caveolins (Cav) are the principle protein constituent of caveolae (cell membrane invaginations that act as ‘gate keeper’ organelles for a range of cell signalling tasks) (331). Cav-1 and -2 are the principle caveolins in EC, fibroblasts and adipocytes. Cav-1 acts to down-regulate TGFβ (313, 332) and VEGF-A signalling (312) through receptor internalization providing

protection against fibrosis such that Cav-1 knockout mice develop SSc-like features (333). Accordingly Cav-1 levels and therefore VEGFR2 degradation are reduced in SSc (312, 313) with resultant increase in CTGF expression (312). Impaired expression of Cav-1 in SSc may therefore contribute to increased VEGF-$A_{xxx}a_{/xxx}b$ signalling via VEGFR2.

1.9.6.9 Interleukins

Cytokines such as interleukin-1β (IL-1β) and interleukin-6 (IL-6) are pro-inflammatory and pro-fibrotic mediators that induce HIF and VEGF-A through NFκB (268) and signal transducer and activator (Stat3) (334) respectively. Circulating IL-1β is increased in SSc (335) and up-regulates panVEGF-A production in vitro SSc fibroblasts (39). IL-6 is raised in sera (323) and cultured fibroblasts (with further TNFα driven attenuation) (336) and peripheral B cells (323) of patients with SSc, with a correlation between B cell derived IL-6 and mRSS (323). The trend towards improvement in mRSS with Tocilizumab therapy (an IL-6 inhibitor) is therefore expected, although the strength of effect may have been masked by limitations in the mRSS as previously discussed (230, 231).

1.9.7 Effects of hypoxic design on HIF paralog expression and vascular pathology

In rodent models, differential HIF1α and HIF2α paralog expression occur in chronic intermittent hypoxia ((CIH), as is found in obstructive sleep apnoea) as opposed to chronic continuous hypoxia ((CCH), as occurs in chronic lung disease) and important differences in vascular sequelae occur under these varying hypoxic conditions(241). Specifically, CIH exposure *induces* HIF1α and *inhibits* HIF2α in mice resulting in systemic hypertension (337, 338) compared to protective effects of heterozygous HIF1α+/- and HIF2α+/- on

pulmonary vascular remodelling and PAH in transgenic rodents under CCH (339, 340). SSc uniquely demonstrates both patterns of intermittent tissue hypoxia with distinct attacks of RP early in disease course, as well as more continuous tissue ischaemia as structural vascular changes progress. We hypothesize, the transition from early disease where vasculopathy and fibrosis are developing to established RP and scleroderma may both be precipitated by and feed forward to influence differential HIF paralog function and downstream VEGF-$A_{xxx}a/_{xxx}b$ signalling. Notionally, this may explain the heterogeneity of vascular manifestations in lcSSc versus dcSSc. Indeed, an association between a HIF1A (gene encoding HIF1α) polymorphism and ACA lcSSc suggests further evaluation of HIF signalling in SSc is warranted (341).

1.9.8 Implications of VEGF-A signalling in the management of systemic sclerosis

PDE-5 inhibitors and ERA form an integral part of current pharmaceutical therapy for SSc related digital and pulmonary vasculopathy. PDE-5 inhibitors effectively improve SSc-RP and digital blood flow through inhibition of cyclic guanosine monophosphate degradation and potentiation of nitric oxide (NO) driven vasodilation (342). VEGF-A and NO are known reciprocal activators (249), however, PDE-5 inhibition in SSc related RP does not appear to alter circulating panVEGF-A levels in sera (342), which may suggest that either NO/VEGF-A potentiation occurs locally in tissues or that by the time PDE-5 inhibitors are initiated other factors influencing VEGF-A dominate.

In the previously described in vitro model, Corallo et al., (306) demonstrated the ability of ERA to reduce EndoMT and reverse the ratio of panVEGF-A:VEGF-$A_{165}b$ in favour of angiogenesis. Indeed, in some studies NC

patterns demonstrate devolution after ERA therapy (343). Furthermore, Corrado et al., (344) suggested that ERA may have anti-fibrotic potential in SSc-ILD. Further study to examine the potential of ERA to ameliorate progression of both vasculopathy and fibrosis is warranted.

Drugs directly targeting VEGF signalling are now used in a variety of clinical settings including malignancy (268), retinopathy (268) and IPF (345). We have already discussed the beneficial use of nintedanib in SSc-ILD (chapter 1.8.2). The effect of nintedanib on VEGF-A_{165}b signalling specifically is however unknown.

1.9.9 VEGF-A as a potential new paradigm in SSc

The evidence discussed herein implicates VEGF-A as an important signalling factor in SSc pathogenesis. More precisely that the relative ratio of isoform expression may be pivotal. Based on VEGF-A_{xxx}a exhibiting pro-angiogenic pro-fibrotic effects and VEGF-A_{xxx}b being its antithesis, a variable switch in isoform ratio may therefore explain variance in clinical phenotype and progression of disease with VEGF-A_{xxx}a directing early aberrant neovascularisation, obliterative vasculopathy and cutaneous fibrosis whilst VEGF-A_{xxx}b may be responsible for late capillary loss and vascular complications but limit fibrosis and promote a clinical plateau in skin fibrosis. However, arguably against this hypothesis, whilst Manetti et al., (280) demonstrated an isoform specific association with NC stage and early skin disease (302) suggesting a chronological relationship, they also reported an absence of correlation with disease subtype (302). Additionally, increased VEGF-A_{165}b in skin in early disease may be interpreted as either contrary to an anti-fibrotic nature or represent the protein switch occurring pre-diagnosis.

HIFα paralog expression, determined by the nature of tissue hypoxia and local cytokine expression in SSc may also contribute to differential VEGF-A isoform expression. The common cellular expression of HIF1α versus cell specific 2α (including endothelial cells) in addition to endothelial, smooth muscle cell and platelet production of VEGF-A, focuses the attention in the vascular network with additional consideration of overactive SSc fibroblasts and inflammatory effector cells.

Ultimately, identifying a single molecular target in this multifaceted disease continues to be a challenge. However, VEGF-A and its specific isoforms remain in the spotlight as both potential future biomarkers and therapeutic targets.

1.10 Final considerations

SSc is a complex heterogeneous disease that results in significant morbidity and mortality. Further understanding of the inter-relationship between vasculopathy, inflammation and fibrosis is required to comprehend its pathogenesis and advance therapeutic options. VEGF-A isoforms, angiopoietins and HIFα paralogs also warrant further specific investigation as implicated drivers of disease and potential therapeutic targets. The evolution of effective therapeutic options is, however significantly restricted by the limitations of available clinical outcome measures for both vasculopathy and skin disease.

1.11 Hypothesis

As discussed thus far, SSc is a complex and heterogeneous disease whose therapeutic options are limited on two fronts, namely by a lack of detailed

understanding of its pathogenesis and the limitations of some outcome measures available for clinical trials.

Our hypotheses for this thesis are therefore as follows:

- With consideration of outcomes measures for peripheral vasculopathy and skin pathology:
    - LSCI and novel HFUS cSMI are useful non-invasive microvascular assessment tools for SSc vasculopathy.
    - HFUS is able to demonstrate skin pathology (including inflammation and fibrosis) with superiority over the mRSS.
- With consideration of advancing understanding of SSc pathogenesis:
    - There is a relationship between structural and functional microvascular changes in SSc.
    - There is a pivotal relationship between microvasculopathy and skin pathology in SSc.
    - Differential expression of VEGF-A isoforms and angiopoietins are drivers of SSc vascular and skin pathology
    - VEGF-A isoform and angiopoietins are driven by HIF paralogs in response to evolving hypoxia.

1.12 Aims

The overarching aims of this project are:

- To support the development of non-invasive imaging including LSCI and novel HFUS applications for clinical assessment of vasculopathy.
- To support the development of HFUS as an objective assessment tool of skin pathology.
- To better understand the relationship between vasculopathy and skin pathology in SSc as documented by LSCI, NC and HFUS.

- To explore the potential influence of HIF and downstream targets including VEGF-A isoforms and angiopoietins on vasculopathy and skin pathology in SSc.

Specific aims and objectives of each chapter are presented in respective sections. Broadly, the aims of each chapter are:

- Chapter 2 will detail the methodology used for this thesis.
- Chapter 3 will define the demographics of the study cohort to better understand the heterogeneity of the disease group for the benefit of data interpretation of subsequent chapters
- Chapter 4 will investigate LSCI as an objective measure of vascular dysfunction and its relationship to established NC and PROMs.
- Chapter 5 will investigate SSc vasculopathy using a novel HFUS cSMI imaging modality with convergent validation against LSCI, NC and PROMs.
- Chapter 6 will investigate the combined use of 3 HFUS parameters to identify SSc skin pathology and assess convergent validity with skin histological collagen content.
- Chapter 7 will explore the relationship between vasculopathy and skin pathology as demonstrated on non-invasive clinical imaging techniques.
- Chapter 8 will investigate the expression of circulating vascular biomarkers and their relationship to vasculopathy and skin pathology in SSc.
- Chapter 9 will investigate the expression of vascular biomarkers in ex vivo SSc skin.
- Chapter 10 will explore the influence of varying patterns of hypoxia on the expression of HIF paralogs and VEGF-A isoforms in explanted SSc fibroblasts.

Chapter 2. Materials and methods

2.1 Materials

2.1.1 Chemical reagents, buffers and solutions

Acetic acid (glacial)	Fisher, UK 10384970
Adenosine diphosphate (ADP)	Alpha laboratories, UK 101312
Bouin's solution	Sigma, UK HT10132
Ethanol	Sigma, UK E7023
Hydrogen chloride	Sigma, UK H1758
Indomethacin	Sigma Aldrich, UK I7378
Phosphate buffered saline	Sigma, UK P5244 or P4417
Prostaglandin E1	Sigma Aldrich, UK P5515

2.1.2 Commercial kits

Biorad protein assay	Biorad, UK 500006
Ancillary reagent kit 1	R&D systems, UK DY007
Ancillary reagent kit 2	R&D systems, UK DY008
Angiopoietin-1 quantikine	R&D systems, UK DANG10
Angiopoietin-2 quantikine	R&D systems, UK DANG20
HIF1α	R&D systems, UK DYC1935
HIF2α	R&D systems, UK DYC2997
VEGF-A, Tie2, VEGFR1 Angiogenesis panel	Mesoscale discovery, USA K15190D
VEGF-A cytokine panel	Mesoscale discovery, USA K15050D
VEGF-A_{165}b duoset	R&D systems, UK DY3045
Pro collagen I duoset	R&D systems, UK DY6220
RD concentrate 2	R&D systems, UK DY995
Sample activation kit (for TGFβ Duoset)	R&D systems, UK DY010
Sample diluent concentrate 1	R&D systems, UK DY001
TGFβ duoset	R&D systems, UK DY240

2.1.3 Materials for Immunohistochemistry and cytofluorescence

αSMA mouse anti-human	Sigma, UK A5228
Alexa Fluoro plus 488 goat anti-mouse	Invitrogen, UK 15626746
Alexa Fluoro 568 (Fab) goat anti-rabbit	Invitrogen, UK 10032302
Angiopoietin-1 mouse anti-human monoclonal clone 171718	R&D systems, UK 15573572
Angiopoietin-2 rabbit anti-human polyclonal	Fisher, UK 13471487
Cytokeratin-19 mouse anti-human	Sigma, UK SAB4700775
HIF1α mouse anti-human monoclonal clone HIF1a67	R&D systems, UK NB100-105
HIF2α rabbit anti-human polyclonal	R&D systems, UK NB100-102
Normal rabbit IgG control	Fisher, UK 13446524
Normal mouse IgG control	Santa Cruz, USA sc2025
Tie2 rabbit anti-human polyclonal IgG	Fisher, UK 13472697
panVEGF-A rabbit anti-human	Abcam, UK AB52917
VEGF-A_{165}b mouse anti-human	R&D systems, UK MAB3045
Vimentin mouse anti-human	Sigma, UK V2258
Trisodium citrate dihydrate	Sigma, UK W302600
Coverslips thickness 1 (for IHC)	Thermoscientific, UK 25x25-1
Ethanol (IHC grade)	Sigma, UK R8382
IHC mounting media (for Masson's Trichrome)	Fisher, UK 12667746
Masson's trichrome	Sigma, UK HT15
Normal goat serum	Sigma, UK G9023
Prolong diamond antifade mounting media with DAPI (for Immunofluorescence)	Invitrogen, UK 15395816
Tween-20	Sigma, UK P1379
Weigert's haematoxylin A&B	Sigma, UK HT101079
Xylene	Sigma, UK 534056

2.1.4 Materials for cell culture

Amphotericin B	Sigma Aldrich, UK A2942
Cell scrapper	Fisher, UK 11597692
Cobalt chloride, $CoCl_2$	Sigma, UK 15862
Complete miniEDTA free protease inhibitor cocktail	Sigma, UK 04693159001
Culture dish (round ones)	Corning, USA 3261
Culture dish (6 well)	Corning, USA 3516
Culture flasks T75	Fisher, UK 10364131
Culture flask T175	Fisher, UK 10246131
Dimethyl sulphoxide sterile filtered (DMSO)	Sigma Aldrich, UK D2650
Dulbecco's modified Eagle's medium (DMEM)	Sigma Aldrich, UK D6249
PhosphoSTOP	Sigma, UK 4906845001
Foetal bovine serum (FBS)	Gibco, UK 10500-064/Fisher, UK 11550356
Gentamicin	Sigma Aldrich, UK G1272
Lipofectamine RNAimax reagent	Fisher, UK 13778100
Optimem medium	Fisher, UK 31985070
Penicillin-streptomycin	Gibco, UK 15140122 /Fisher, UK 11548876
Phalloidin F actin probe	Invitrogen, UK 10053252
SiRNA HIF1α	Fisher, UK 4390823-s6539
SiRNA HIF2α	Fisher, UK 4390823-s4698
SiRNA scrambler	Fisher, UK 4390824
Sodium Fluoride, NaF	Sigma, UK 67414
TGFβ (recombinant)	Fisher, UK 15112079
Trypsin 0.05%	Gibco, UK 25300-054/Fisher, UK 11580626
Triton-X100	Sigma, UK T8787
Urea	Sigma, UK 15406

2.1.5 Equipment

Aplio A500 ultrasound	Toshiba, UK
Bio Data PAP4 aggregation profiler	Alpha laboratories, UK
Calibration block (for LSCI)	Moor instruments, UK CAL-2PFS
Confocal microscope LSM-880	Zeiss, UK
FLPI laser speckle capture imager	Moor Instruments, UK
PixeLINK 1.3 mega-pixel camera, PL-A742	PixeLINK, USA
Punch biopsy 4mm	Decree Thermo via NHS supply chain, UK FFQ641
SCI-tive UM-025	Baker Ruskinn, UK
Stir bars (for aggregometry	Alpha laboratories, UK 105977

2.2 Participant recruitment

Ethical and regulatory approval was obtained from NRES Southwest-Frenchay (Reference 14/SW/1165), University of Bath and Royal United Hospital (RUH) NHS Foundation Trusts Research and Development department. SSc participants were recruited through the clinical Rheumatology services at the Royal National Hospital for Rheumatic Diseases as well as through the REC-approved SSc database with prior patient consent for contact. Healthy control volunteers were recruited from hospital staff members and relatives of SSc participants. Procedure to study investigations and samples collection occurred after obtaining written informed consent and positive outcome of eligibility screening.

2.2.1 Study eligibility criteria

Participants were recruited based on achieving all inclusion and no exclusion criteria as outlined in Table 2.1.

Table 2. 1 Study inclusion and exclusion criteria.

Willing adult volunteers were recruited as healthy controls providing there was no history of pre-existing vasculopathy. Systemic sclerosis participants were required to meet the ACR/EULAR 2013 classification criteria for SSc (346) and providing they were not currently enrolled in a clinical trial requiring a drug administration. Diabetes was an exclusion criterion for both groups based on the potential to increase VEGF-A.

Healthy Control	Systemic sclerosis
Inclusion criteria	
• Aged 18 years or over	• Aged 18 years or over • Systemic sclerosis as defined by the ACE/EULAR classification criteria
Exclusion criteria	
• Presence of Raynaud's phenomenon or inflammatory rheumatic disease	• Presence of known diabetes
• Presence of diabetes or known peripheral vascular disease	• Current pregnancy
• Current pregnancy	• Current participation in a clinical drug trial
• Volunteer considered unable to comply with the study investigations	• Volunteer considered unable to comply with the study investigations

2.3 Data collection

All consent procedures, interviews, mRSS assessments, clinical study investigations, tissue sampling, laboratory investigations including cell culture and data analysis were performed by Dr Victoria Flower unless otherwise specified.

2.3.1 Demographic data and clinical assessment

Demographic data was collected on all participants to include significant medical history, current drug history and smoking status. Details of disease manifestations (Table 2.2), most recent cardiopulmonary screening test results and historical administration of disease modifying drugs were noted from the medical records. The autoantibody status of SSc participants was

noted from the clinical record based on results from indirect immunofluorescence using Human laryngeal epithelial carcinoma cell line (HEp2) and/or immunoblotting and/or immunoprecipitation. As part of routine clinical care, all patients have indirect immunofluorescence, followed by commercially available line blots to characterise ANA specificity where necessary. Protein immunoprecipitation is used to categorise indeterminate ANA positive samples where required. Active ANA testing for healthy controls was not performed for this study.

An mRSS was also assessed (by VF) for SSc participants at the time of the study visit (139) (as described previously chapter 1.6.2). In brief, skin thickness was assessed at 14 bilateral anatomical locations (fingers, hands, forearms, upper arms, thighs, lower legs, feet) as well as the face, chest, abdomen. Each region was scored according on 0-3 scale (0=normal, 1=mild, 2=moderate, 3=severe thickening). A total score out of a maximum 51 points and local/regional mRSS (to pair with HFUS ROI) was documented.

Table 2. 2 Documentation of the presence of SSc specific manifestations.

SSc manifestation	Requirement for inclusion
Digital ulcers	Documentation of history of DU in the health record *or* clinical evidence at the time of study recruitment of loss of epithelium with depth into the tissue as described by Hughes and Herrick (347) that was not otherwise considered to be a linear fissure.
Telangectasia	Documentation in the health record or clinical evidence at the time of study recruitment of skin capillary malformations in either spider or discoid shape
Gastroesophageal reflux disease or dysphagia	Documentation in the health record or description by patient of acid reflux into the mouth, recurrent indigestion or difficulty swallowing and/or endoscopic or imaging evidence of oesophageal stricture, dilation or dysmotility
Puffy fingers	Documentation in the health record or clinical evidence at the time of study recruitment
Skin thickening	Documentation in the health record or clinical evidence at the time of study recruitment
Sclerodactyly	Documentation in the health record or clinical evidence at the time of study recruitment of finger skin tightness resulting in shiny tapered digits
Calcinosis	Documentation in the health record or clinical evidence at the time of study recruitment
Arthralgia	Patient description of joint pain not felt to be otherwise explained by alternative pathology such as osteoarthritis
Inflammatory arthritis	Clinical evidence of joint swelling with synovitis (either on examination or imaging) and typical inflammatory joint symptoms
Myalgia	Muscle ache without biochemical rise in muscle enzymes
Myositis	Rise is typical biochemistry (CPK) clinically felt to be of skeletal muscle origin with or without muscle symptoms
Interstitial lung disease	Documentation in the health record based on typical features on high resolution CT scan with or without evidence on pulmonary function tests
Pulmonary hypertension/pulmonary arterial hypertension	Documentation in the health record based on typical results for mean pulmonary artery pressure >25mmHg on right heart catheterisation.
Renal crisis	Documentation in the health record of a clinical diagnosis based on acute onset of systemic hypertension with acute kidney injury

2.3.2 Disease classification

SSc disease subset (lcSSc or dcSSc) was noted from the clinical record and examination based on LeRoy and Medsger criteria (348) as illustrated in Figure 1.1 (chapter 1).

The duration of disease was noted from the clinical record for SSc participants in months/years.

SSc participants were classified as early or late disease based on the duration since the first non-RP symptom onset being < or > 3 years at the point of study entry.

2.4 Patient-reported outcome measures (PROMs)

A number of patient-self-reported outcome measures are validated for use in SSc. The health assessment questionnaire disability index (HAQ-DI) (349), documents the level of functional difficulty experienced with activities of daily living. With addition of five SSc specific questions to assess the impact of gastrointestinal, respiratory, RP, DU and pain symptoms the modified HAQ-DI is known as the Scleroderma HAQ (SHAQ) (72).

The Raynaud's diary is a RP specific PROM (a 14 day diary documenting the frequency of RP attacks) together with a patient-visual analogue scale (VAS) for their perceived RP severity (Raynaud's condition score, RCS) (73). Collectively, the SHAQ, RP diary and RCS may all be used to assess SSc peripheral vasculopathy. Whilst some recent studies have raised concerns over the subjectivity of the RP diary (201), these PROMs are an established and validated feature of SSc clinical trials. For our study, each SSc

participant completed the RP diary and SHAQ in close temporal relationship to the study appointment to allow for correlation with HFUS, LSCI, NC and plasma biomarkers. Where participants failed to complete or return their PROMs in a reasonable time, they were not actively chased as it was felt that delayed completion of PROMs would not be temporally relevant to the clinical study assessments.

2.4.1 Analysis of PROMs

The overall SHAQ score as well as individual SSc specific VAS scores from the SHAQ were documented. The mean duration of RP attacks per day and the mean number of attacks per day were calculated from the RP diary. The RCS score was also noted.

2.5 Clinical imaging preparation

All participants were asked to wear light weight clothing for the study assessments, which were performed before midday in the Clinical Measurement department at the RNHRD, Bath. All participants were acclimatised for a minimum of 20 minutes at a mean of 23.1°C +/-1. All clinical investigations were untaken on the non-dominant side of healthy control participants in order that usual daily activities would not be impaired during wound healing in those undergoing skin biopsy. In the SSc group, where RP symptoms were symmetrical, the non-dominant side was used. In the event of a disparity between RP symptoms in the upper limbs, the worst affected side was used.

2.6 Laser speckle contrast imaging and provocation test

2.6.1 Laser speckle contrast imaging

Laser speckle contrast imaging (LSCI) is a method of indirectly assessing cutaneous microvascular perfusion in SSc with reproducible results (62, 350, 351). When a laser light is directed at an object, the reflection of the laser light from its surface creates a speckle pattern. If there is fluid movement within the object such as blood flow within the skin, the reflections cause variation in the speckle pattern representative of the flow and referred to as Flux (352). LSCI has superiority over other laser imaging modalities due to assessment occurring in real time and simultaneously over a wider field (81) and well as low intra-operator variability (62, 353). LSCI has good spatial and temporal resolution which is why it was chosen for his work.

2.6.2 Post occlusive reactive hyperaemia

The application of a post occlusive reactive hyperaemic response to investigate SSc peripheral vascular dysfunction has been discussed in detail (chapter 1.5.4.1). It was chosen for our study methodology in in part due to the relative practical easy of its application and its reproducibility (80).

2.6.3 LSCI image acquisition and study procedure

Settings for the FLPI (Moor Instruments, Axminster, UK) (Appendix A1.1) were chosen in line with the instrument user manual, in order to optimize the balance between spatial resolution and statistical analysis such that too many or too few assigned pixels are respectively limiting (352). The laser was allowed to warm up for a minimum of 30 minutes prior to use and set up according to manufacturer instructions (Appendix A1.1), with the lens focused and the polarizer adjusted to minimise specular reflections. Baseline

perfusion was recorded for 1 minute and then paused for cuff inflation. Two minutes of arterial occlusion were then applied using a sphygmomanometer to the upper arm at 50mmHg above the participants resting systolic pressure. Previous PORH studies have used a wide range of between 1-5 minutes of arterial occlusion in PORH testing (47, 58, 61, 86-88). We chose 2 minutes as an acceptable compromise between sufficient occlusive challenge and acceptable tolerability for participants (ensuring they remained still for the duration of the study to facilitate consistent data gathering across the study cohort). The cuff was rapidly deflated and LSCI recording restarted immediately. Perfusion recorded for 5 minutes after the cuff deflation.

2.6.4 LSCI image analysis

LSCI data was analysed using the corresponding Moor FLPI review version 4.0 software. Regions of interest (ROI) were applied over the distal phalanx of digits 2-5 as well as the dorsum of the hand (Figure 2.1).

Figure 2. 1 Illustration of post occlusive reactive hyperaemic response demonstrated by laser speckle contrast imaging.

Finger blood perfusion on LSCI is measured indirectly by cutaneous Flux. Baseline (B) perfusion in a healthy control demonstrates the typical appearance of increased perfusion (red) at the fingertips compared with the dorsal hand (blue). Following 2 minutes of arterial occlusion and cuff release, there is dramatic vasodilation above baseline levels in response to increase oxygen demand following ischaemia (post occlusive reactive hyperaemic response (PORH) (C)) in the same participant. In contrast, reduced baseline (E) and PORH response (F) are seen in a participant with systemic sclerosis. A transmitted light image (A and D) is shown for anatomical reference. The location of the applied regions of interest are shown overlying the dorsal surface of the distal digits 2-5 and the dorsal hand (D, yellow). The dorsal hand ROI crosses the metacarpophalangeal joints distally and extends proximally over the carpus. Figure created by VF using study images with consent from respective participants.

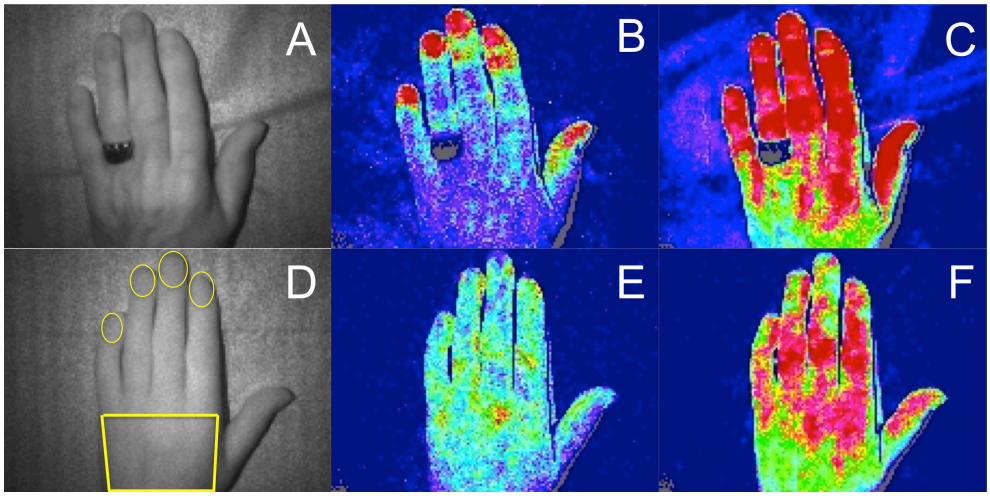

Time points of interest were manually specified by the observer (VF) and were consistent for each participant. The initial 20 seconds of baseline LSCI recording (t = 0-20 seconds) was considered a 'settling' phase for the participant. The median flux over the subsequent 30 seconds (i.e. period of recording T=20-50 seconds) was used as the baseline flux value. The median was chosen as it was felt that this would be less skewed by small peak fluctuations. Following arterial occlusion and cuff deflation, the peak Flux was identified visually and the time point manually entered into the Review v4.0 software. Similarly, the time of cuff deflation until t = 6 minutes

(5 minutes of recording time post cuff release) was identified and manually inputted into the software for data extraction.

Flux within each ROIs at specified time points was calculated and tabulated in a formal report by the software. A macro (written by Darren Hart, Clinical Scientist at RNHRD) was used to export relevant values into an excel file for statistical analysis in SPSS, including baseline median Flux, Flux at peak PORH, time that peak PORH occurred and area under the reperfusion curve following cuff deflation. A reperfusion gradient was calculated as a simplified representation of the velocity of change from baseline Flux to Flux at peak PORH (peak PORH – baseline median/time from cuff deflation to peak PORH). Flux data for each of these parameters was then additionally averaged as a mean across the distal 2^{nd}-5^{th} fingers in line with methodology from previous studies (354, 355). A distal-dorsal difference (DDD) in Flux was also calculated between the distal fingers (mean of distal 2^{nd}-5^{th} fingers) and the dorsal hand to demonstrate the gradient of perfusion towards the extremities (356).

2.7 Nailfold capillaroscopy

2.7.1 Clinical application of nailfold capillaroscopy

Nailfold capillaroscopy (NC) is a non-invasive and established clinical tool used to assess for structural microvascular changes at the nailfold (discussed in detail in chapter 1.5.5-1.5.7). It forms part of SSc classification (346), supports early diagnosis (37) and may be of value as a prognostic factor in SSc (119). As such, we chose to use NC to allow us to undertake a qualitative and quantitative assessment of the structural microangiopathy of SSc.

2.7.2 Nailfold capillaroscopy image acquisition

NC was performed as per the usual protocol for clinical practice at the RNHRD for each of fingers 2-4 on the same hand a used for HFUS and LSCI investigations. In brief, clear oil was wiped across the nailfold to allow light penetration to the capillary layer. A pillar mounted 1.3 mega-pixel camera (PL-A742, PixeLINK) was used to obtain x30 magnification of the whole region of interest followed by several images at x200 magnification to demonstrate capillary density and morphology. Corresponding software (PixeLINK Capture OEM) was used to prepare images (chapter 1, Figure 1.2).

2.7.3 Nailfold capillaroscopy image analysis

There are no fully automated methods for NC analysis at the present time. Semi-automated methods have been developed and tested as research tools elsewhere (357). These methods were not available locally and to our knowledge still require external validation. Images were therefore analysed manually in line with pathological features described in previous published studies (107). Firstly, individual NC parameters (defined in Table 2.3 and illustrated in chapter 1.5.5 Figure 1.2) were quantified manually as a mean across all image fields for each digit with respect to:

- number of capillaries per 1000μm,
- mean inter-capillary distance, μm (106),
- number of enlarged capillaries,
- number of giant capillaries,
- number of haemorrhages,
- number of ramifications.

An overall mean value for each of these NC parameters was also calculated as an average across 3 digits examined.

Table 2. 3 Nailfold capillaroscopy classification criteria

Classification	Enlarged	Capillary number/mm	Neovascularisation[4]	Microhaemorrhages [5]	General description
Normal [1]	≤ 2 dilated capillaries [2] No giant	6-9	Nil	Nil	Preserved capillary number
Non-specific	≥2 dilated No giant	6-9	Nil/some	Nil	-
Early	Some enlarged + at least 1 giant [3]	≥6 (preserved number)	Nil	Nil or few	Preserved capillary number with enlarging capillaries
Active	Frequent enlarged, at least 1 giant but typically several giant	4-6	Absent or few	Frequent	Numerous dilated capillaries with capillary loss
Late	May have enlarged capillaries but typically absent (or few) giant	<4	Typically present	Typically absent but may have few	Severe capillary loss with neovascularisation

[1] any single abnormality in isolation is not considered pathological. [2] afferent, efferent or apical limb is ≥20μm. [3] afferent, efferent and apical limb are all homogenously ≥50 μm. [4] 1 neovascularisation = ramified, bushy or tree-like structure arising from a single afferent-efferent capillary. [5] 1 microhaemorrhage = any single haemosiderin deposit or cluster sharing a spatial relationship to indicate they occurred as part of the same capillary haemorrhage.

Secondly, a qualitative assessment was undertaken in which each finger (digits 2-4) was classified as 'normal', 'non-specific' changes or 'early', 'active' or 'late' SSc-specific pattern according to defined criteria in line with the CAP study (107) (Table 2.3). Additionally, the most advanced classification across the 3 digits was also noted and recorded as an 'overall' NC pattern for that participant.

Image analysis was performed in batches and blinded, by the same investigator (VF).

2.8 Assessment of peripheral vascularity by high frequency ultrasound

2.8.1 High frequency ultrasound for microvascular imaging

As discussed in detail in chapter 1.5.8, high frequency ultrasound (HFUS) is a non-invasive and readily available clinical tool that has been used to assess micro- (65, 131) and macrovascular flow (130-133). Its non-invasive and accessible nature is in part why it was chosen to quantify microvascular flow in our study.

'Superb microvascular imaging with colour overlay' (cSMI) is a novel HFUS application using colour Doppler imaging but with added proficiency of being able to remove low level tissue artefact from vessel walls whilst still reporting low frequency echoes reflected by areas of lower blood flow (typically in capillary beds). It also utilizes high frame rates for more accurate reporting of flow. To our knowledge, there is no published data on the use of novel cSMI in SSc. HFUS with cSMI was therefore chosen for our study for its novel and comprehensive application for microvascular imaging.

2.8.2 HFUS cSMI image acquisition

Images were captured from three views: dorsovolar sagittal, transverse of the nailbed and transverse of the fingertip (Figure 2.2) in line with previous studies using similar ultrasound based techniques to allow for relative comparison of results (65). Images were captured using a thick layer of gel between the transducer and the skin surface with adequate contact but avoiding excess pressure in order to avoid external compression of microvasculature. This was achieved by ensuring that a visible layer of gel was present on the B mode HFUS image whilst ensuring there were no ultrasound free shadows within the ROIs. Images were captured with consistent cSMI HFUS settings and zoom (Appendix 1.2).

Figure 2. 2 Superb microvascular imaging on high frequency ultrasound used to assess vascularity at the distal middle finger.

Three fields of view were captured: dorsovolar sagittal, transverse nailbed and transverse fingertip. Images demonstrate subjective reduction in vascularity in SSc which was quantified using Image J. Figure created by VF using study images with consent from respective participants.

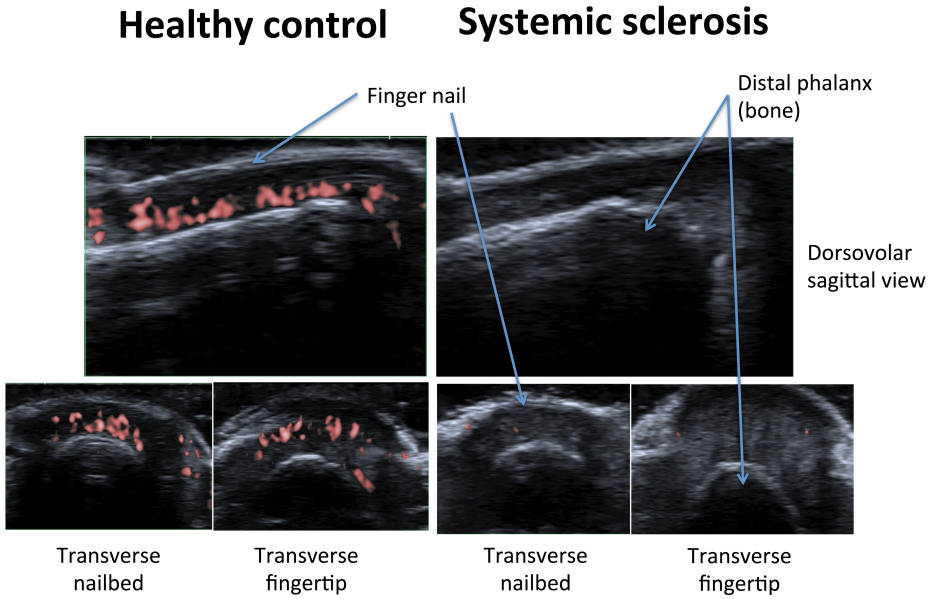

2.8.3 HFUS cSMI image analysis

Images were analysed using Image J (https://imagej.nih.gov/ij/). The regions of interest were outlined manually within Image J as defined by:

- Dorsovolar sagittal - the nailfold proximally to the tip of the finger distally and the nail superiorly down to the bony phalanx inferiorly
- Nailfold - the nail superiorly to the bony phalanx inferiorly and excluding the lateral digital arteries
- Fingertip - all central red colour and excluding the lateral digital arteries.

The mean vascularity (mean intensity of the red colour pixels) as well as the area (cumulative area occupied by the red colour pixels) within the respective regions of interest, were documented.

2.9 Assessment of skin pathology by high frequency ultrasound

2.9.1 High frequency ultrasound for cutaneous imaging

HFUS was chosen as a safe, non-invasive assessment tool due to its established applications in a number of skin diseases (180, 182) and its ability to reproducibly document both quantitative and qualitative data in SSc (as described in chapter 1.6.2) (141, 171-173, 175, 176).

APLIO A500 HFUS (Toshiba) was used for this study combining several novel imaging modalities to assess inflammation (low echogenicity reflecting increased oedema) and fibrosis (skin thickness, increased echogenicity and shear wave elastography.) HFUS beneficially provides better spatial resolution than lower frequency applications. The resultant reduction in

penetrance is inconsequential in this study as the region of interest is limited to maximally a centimetre depth.

2.9.2 Skin thickness

2.9.2.1 Skin thickness image acquisition

The image capture protocol and ROIs were adapted from previous studies (141, 165), considering the anatomical sites of previous optimal correlation with mRSS (171), for practicality of assessment for the participants and areas that were most likely to have pathological skin (finger, hand and forearm). By design, we also wanted to assess an area of clinically uninvolved skin for each participant. The abdominal epigastrium was chosen as a specific ROI, as it was felt that this was the most likely location that clinically uninvolved skin would be found.

Consistent HFUS settings were used for each participant (Appendix 1.2) using the Aplio A500 (Toshiba, 18MHz). All images were obtained before midday to reduce natural variations occurring in cutaneous fluid content. The transducer was applied perpendicular to the skin at specific anatomical areas:

- over the proximal phalanx of the middle finger,
- dorsal hand in the valley between and just proximal to the 2nd and 3rd metacarpophalangeal joints,
- 7-10cm proximal to the wrist over the dorsal forearm
- abdominal epigastrium at mid-point between the xiphisternum and the umbilicus.

A visible layer of gel on the 2D B mode HFUS image, was maintained between the transducer and the skin surface, thus avoiding data confounding through variable applied pressure. Two images were taken per ROI to assess for intra-observer variability. The transducer was removed from the skin surface and reapplied for successive image capture.

2.9.2.2 Skin thickness image analysis

Skin thickness was assessed by placement of electronic calipers on to the images by the observer (milimeters) and using the APLIO A500 in-built software. It was noted that for a number of SSc participants, the dermo-subcutis junction at the proximal finger was not easily distinguishable which we hypothesised may be due to a combination of scleradermatous changes in the dermis creating a similar echo to the hypodermis thus reducing the echo interface, as well as pathological subcutaneous fat atrophy in the disease group at a site which naturally has little fatty tissue. This is a feature also observed in other studies on OCT with reduced clarity of the dermo-epidermal junction and papillary-reticular dermis interface in the scleroderma disease state (146). The skin thickness at the finger was therefore judged as the interface between the external gel and epidermis down to the extensor tendon in the middle of the proximal phalanx (Figure 2.3), which was clearly visible in all participants, in line with a previous study (358). Skin thickness at the hand, forearm and abdomen was reference from the gel-epidermis interface down to the dermo-subcutis interface as this was clearly distinguishable at these ROIs (Figure 2.3) to assess the skin thickness (epidermis + dermis) as per methodology by others (171, 172, 359).

Figure 2. 3 Example images obtained using high frequency ultrasound to assess skin pathology.

HFUS was used to assess skin thickness at 4 anatomical regions of interest: proximal middle finger (A), dorsal hand (B), distal forearm (C) and the abdomen (D). Skin thickness at the proximal finger was assessed as a total depth of the epidermis, dermis and subcutis from the external surface of the skin down to the extensor tendon (red arrow). Skin thickness at the other 3 regions was assessed as the depth of the epidermis and dermis combined (red arrows). Depth is illustrated by the scale on the left-hand side of each image (cm). Figure created by VF using study images with consent from respective participants.

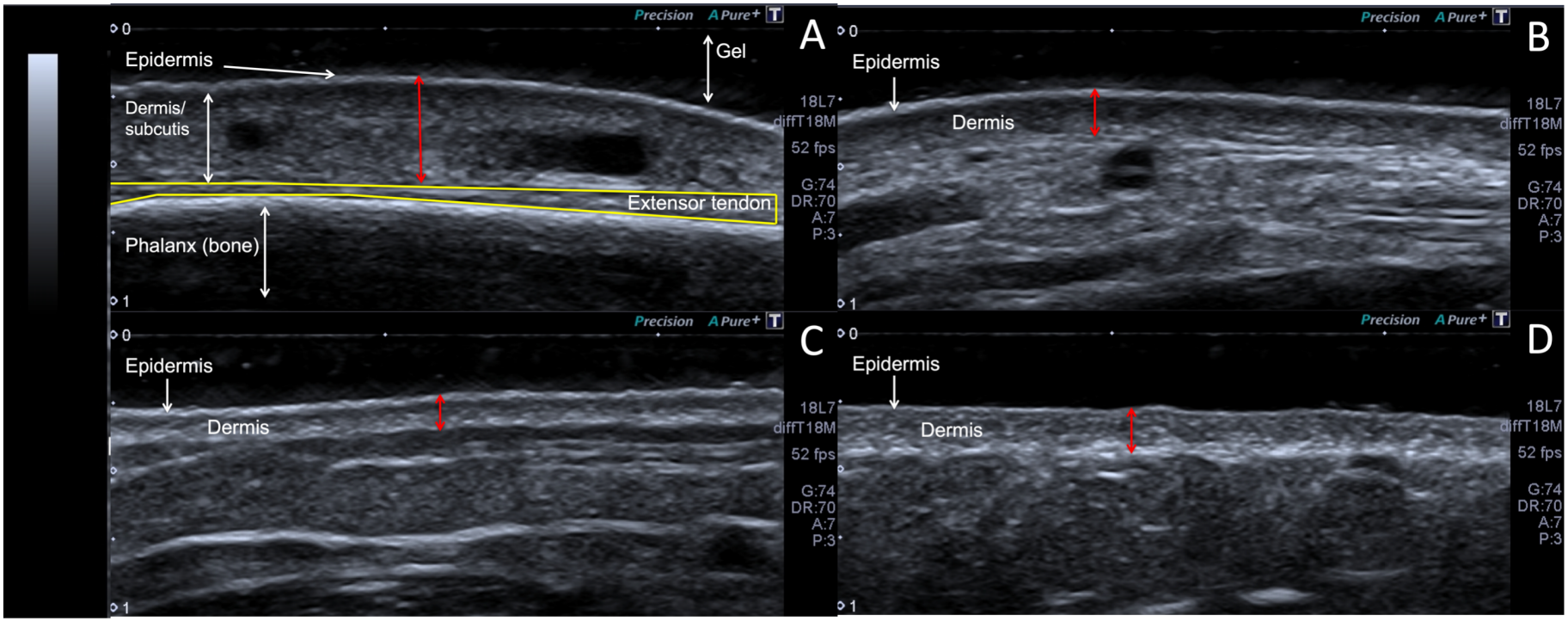

2.9.3 Echogenicity

Echogenicity is the measure of skin brightness on HFUS and can be used as an indirect measure of cutaneous inflammation. During the 'oedematous' phase of SSc skin disease the dermis appears hypoechoic (darker) as there is increased water content from oedema, which resolves and becomes hyperechoic (brighter) towards the fibrotic phase (141, 172).

2.9.3.1 Echogenicity image acquisition and analysis

The same images were used to quantify skin echogenicity as were used for skin thickness. ROIs were drawn using Image J (https://imagej.nih.gov/ij/), encompassing the same depth as per skin thickness measurement and spanning the whole width of the HFUS image. Echogenicity was recorded as the mean 'brightness of gray scale' (scale 0-255) across the ROI, as calculated by Image J software.

2.9.4 Elastography

Elastography is the use of ultrasound to indirectly measure the elastic qualities of the skin by either measuring tissue strain (the pressure required to produce 100% strain in the tissue) or shear velocity (the time taken for an applied force to propagate through the tissue). The elastic properties of the skin may change in response to disease states including inflammation, fibrosis and malignancy and elastography is already an established tool for assessing such in a number of diseases (360). A small number of studies demonstrated good reproducibility in SSc skin disease (175, 176). However, previous methods utilized manual displacement of tissues by the investigator, which is subject to intra- and inter-observer variation in the applied force. Newer shear wave elastography (SWE) technology provided

by the APLIO A500 generates a consistent ‘pushing pulse’ from the transducer, which produces more consistent and reliable results. As the sound wave propagates through the tissues, SWE ‘maps’ are generated. The first ‘propagation’ map demonstrates the movement of the sound wave through the tissue. This is visualized in the form of lines across the 2D B-mode ultrasound image. Where the lines are approximately parallel through the tissue of interest, the measure of elastography can be considered reliable. A ‘colour’ map corresponding to a quantifiable scale (KPa) is then generated depending on how the wave propagates through the tissue. Higher values (KPa) in this application represent stiffer skin.

2.9.4.1 SWE image acquisition

The elastography protocol was generated in line with APLIO A500 user instructions and with consideration of European Federation of Societies for ultrasound in Medicine and Biology guidelines (360, 361) with consistent HFUS settings (Appendix 1.2). In brief, the ultrasound transducer was applied perpendicular to the skin at the same anatomical ROIs as for skin thickness/echogenicity. A solid gel pad of 2cm depth (Aquaflex, 04-02, Parker Laboratories Inc.) was used as a standoff for the transducer in order to focus the shear wave within the correct depth of the tissues. Contact between the transducer and pad as well as the pad and skin were ensured with a thin layer of ultrasound gel on either side of the pad. Adequate but not excessive force was applied to maintain contact but avoid external compression of the skin, which would falsely elevate the elastograph. A region of interest was applied by the observer, covering the depth of the dermis and crossing two parallel propagation lines using the APLIO A500

software. Elastography parameters were then calculated by the inbuilt software as a mean across the ROI (Figure 2.4).

Figure 2. 4 Shear wave elastography (SWE) application in systemic sclerosis skin disease.

Example SWE at the forearm for healthy control (top) and SSc (bottom) are shown. Healthy control skin demonstrates blue/green colour maps representing lower SWE values and more elastic skin properties. The SSc participant represented here has mRSS = grade 2 skin involvement (moderate scleroderma) at the site of elastography assessment. Firmer skin in SSc participant has higher SWE values (red). Figure created by VF using study images with consent from participants.

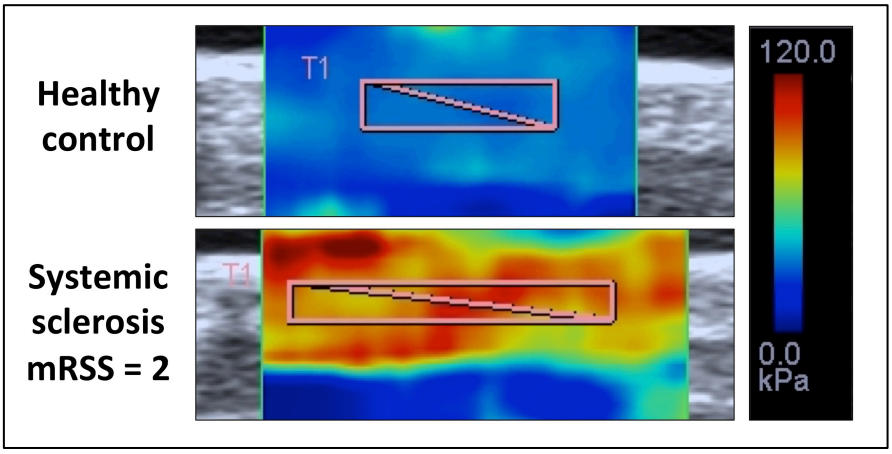

2.10 Plasma and platelet collection

Blood samples were collected by uncuffed phlebotomy using anticoagulated citrate and EDTA vacutainers and processed within 3 hours of collection. First stage centrifugation at low speed (250g, 10 minutes, 22°C) allowed isolation of platelet rich plasma (P-RP). 2x 450µL P-RP was removed for platelet aggregometry. Prostaglandin E1 (0.1µg/mL final concentration) and indomethacin (10µM final concentration) were added to the bottom of the aliquot for remaining P-RP (citrate and EDTA) to prevent platelet activation during the second stage centrifugation (500g, 10 minutes, 22°C) and obtain platelet poor plasma (P-PP). P-PP was stored at -80°C in 250µL aliquots until analysis of circulating biomarkers by ELISA.

2.10.1 Platelet aggregometry

Platelet aggregometry measuring percentage light penetration through P-RP was performed to demonstrate that platelet activation had taken place. As platelets activate, they change morphology resulting in increased transparency and light transmission through P-RP. Values for rate of change of light transmission (slope) and maximal light transmission achieved after addition of ADP agonist were recorded for each participant sample in duplicate, as a reflection of platelet activation (Figure 2.5). In order to record platelet aggregation, 450µL of P-RP (citrate) was placed in each of 2 glass cuvettes from each participant and incubated in a light transmission aggregometer (PAP4, BioDATA Corp) at 37°C for 3 minutes. Platelets in P-RP were activated by addition of 50µL of $1x10^{-4}$M adenosine diphosphate (ADP) (terminal ADP concentration $1x10^{-5}$M equivalent to 10µM/L) to release contents of alpha granules including VEGF-A (362). Aggregometry was performed in duplicate and within 3 hours of phlebotomy. Activated P-RP was then centrifuged (500g, 10 minutes, 22°C) to remove the platelet pellet. Releasate was stored at -80°C until analysis by ELISA.

Figure 2. 5 Platelet activation by ADP recorded by light transmission aggregometry.

Light transmission aggregometer PAP4 (A) and percentage light transmission profile (B) demonstrating platelet aggregation following activation with ADP. Arrows demonstrate the point of addition of ADP agonist to P-RP for sample 1 (red) and sample 2 (blue). Vertical axis shows percentage light transmission. Horizontal axis shows time (4 squares = 1 minute). Both samples demonstrate single-phase aggregation and 100% light penetrance 2 minutes post activation. Figure created by VF using own study images.

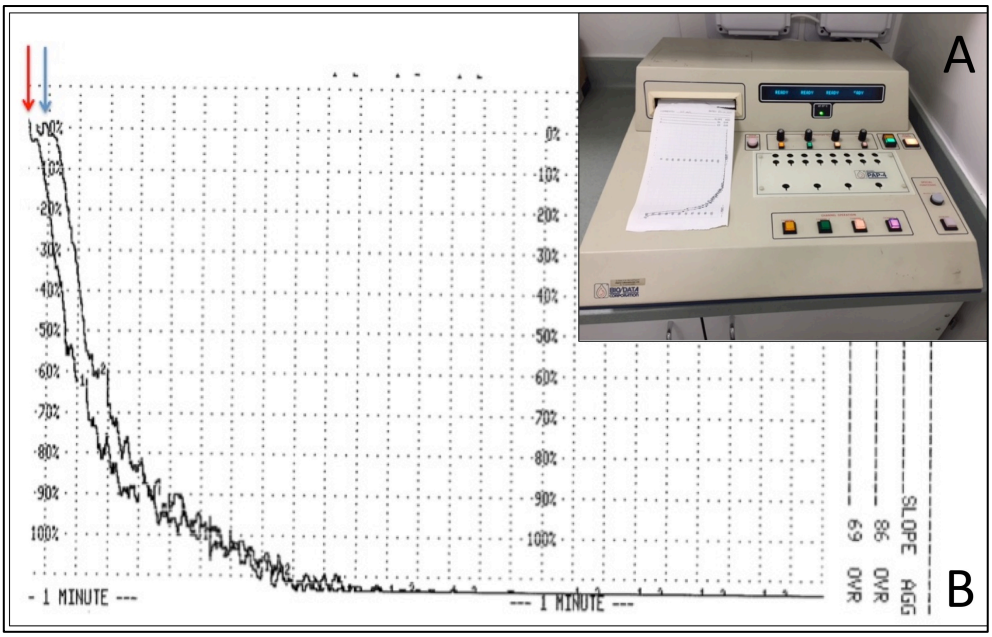

2.10.2 Plasma enzyme linked immunosorbent assay (ELISA)

After thawing at room temperature, all samples were centrifuged at 2000g for 3 minutes before assaying. All assay steps were performed at room temperature with buffers and reagents at room temperature unless otherwise specified. Samples and standards were assayed in 96-well plates in duplicate with 2 intra-plate repeats and 3 inter-plate repeats across multiple plates. Thorough vortexing was used at all mixing stages.

2.10.2.1 Multiplex assay for panVEGF-A, sVEGFR1 and sTie-2

Multiplex ELISA plates (Angiogenesis panel, K15190D MSD) were blocked with 150uL of blocking buffer (5% BSA in PBS), sealed and incubated for 1 hour with plate shaking followed by 3 washes in wash buffer (0.05% Tween-20 in PBS for all wash steps). 7 stage serial dilutions of standards were made in the supplied diluent-7 (VEGF-A 0.427 – 1750 pg/mL, sVEGFR1 2.01 – 8250pg/mL, sTie-2 20.1 – 82400pg/mL). Plasma (EDTA) samples were diluted 1:1 in the same diluent-7 as per manufacturer's recommendations. 50uL of samples, standards and blank (diluent-7) were added to the plate. Plates were sealed and incubated on a plate shaker for 2 hours. Plates were washed 3 times prior to addition of 25uL of detection antibodies (1:50 in diluent-11) to each well and incubated for a further 2 hours with shaking and shielded from direct sunlight. Plates were washed 3 times followed by addition of 150uL of a read buffer (2x concentrate) to each well. Plates were read without delay (Sector 6000, Mesoscale discovery).

2.10.2.2 VEGF-A_{165}b duoset ELISA

ELISA plates (R&D duoset DY3045) were coated with 100uL per well of capture antibody (2μg/mL), sealed and incubated overnight. The following

day, plates were washed 3 times in wash buffer (0.05% Tween-20 in PBS, pH 7.2-7.4 for all wash steps) and then blocked with 300uL per well of blocking buffer (1% BSA in PBS, pH 7.2-7.4) for 1 hour. Plates were washed 3 times before adding 100uL of samples (neat) and standards after vortexing. Standards were prepared with 7 serial dilutions (31.25 – 4000pg/mL) in reagent diluent (1% BSA in PBS). The same diluent was used as the blank for the standard curve. Plates were sealed and incubated for 2 hours followed by a further triple wash step. 100uL of detection antibody (250ng/mL) per well was incubated for a further 2 hours and again washed 3 times. 100uL of Strep-HRP (1:200) was added to each well and incubated in the dark for 20 minutes followed by 3 washes. 100uL of 1:1 mix of substrate solutions A and B (H_2O_2 + tetramethylbenzidine respectively) were added to each well and incubated in the dark for 20minutes. 50uL of stop solution (2N H_2SO_4) was added to each well (without washing). Plates were read immediately at 450nm (Fluostar optima, BMG lab tech).

2.10.2.3 Angiopoietin-1 and -2 quantikine ELISA

For angiopoietin-1 assay (DANG10 R&D), samples were diluted 15-fold in RD5P diluent. Standards were prepared using 7 serial dilutions of angiopoietin-1 calibrator in RD5P diluent (31.25-4000pg/mL). The same RD5P diluent was used as a blank for the standard curve. A further dilution of 1-part sample/standard in 2-parts diluent RD1-20 (total 150uL) was performed in-plate and incubated on a plate shaker for 2 hours. Plates were washed 4 times in wash buffer (0.05% tween-20 in PBS, pH 7.2-7.4 for all wash steps). 200uL of angiopoietin-1 conjugate was added to each well and incubated for a further 2 hours on a plate shaker followed by a further 4 washes in wash buffer. 200uL of substrate solution made from a 1:1 mix of

colour reagents A and B (H_2O_2 + tetramethylbenzidine respectively) was added to each well for 30 minutes of static incubation and with protection from light. 50uL of stop solution (2N H_2SO_4) was added to each well and spectroscopy performed immediately at 450nm (Fluostar optima, BMG lab tech).

Angiopoietin-2 assay (DANG20 R&D) protocol was as for angiopoietin-1 above. Variations in the diluent, calibrator and conjugate used were as follows:

Samples were diluted 5-fold in RD5-5 diluent. Standards were made using serial dilutions of angiopoietin-2 calibrator in the same diluent (23.4-3000pg/mL), which was also used as a blank. Samples and standards were further subject to a 3-fold in-plate dilution in RD1-76 diluent. 200uL of angiopoietin-2 conjugate was added to each well after the first wash step.

2.11 Skin tissue sampling

2.11.1 Participants

A proportion of volunteers from both participant groups underwent skin punch biopsies (2x 4mm diameter) from the forearm. A proportion of SSc participants who underwent forearm biopsy also had paired abdominal samples from an area of clinically uninvolved skin. A purposive sampling framework was applied to obtain samples from a range of early and late SSc and lcSSc and dcSSc.

2.11.2 Skin biopsy procedure

Punch biopsies were undertaken by usual clinical practice and protocols, but with care to avoid use of excessive lignocaine and without co-administration

of adrenaline to avoid inadvertent activation of HIF. Anatomical site and biopsy size were chosen to minimize risk to participants in line with EUSTAR guidelines (363) as well as correspond with site of HFUS assessment. Participants on warfarin or direct oral anticoagulants (e.g. apixaban) were excluded from skin biopsy due to the risk of significant bleed in the absence of adrenaline use.

2.11.3 Skin biopsy processing

Biopsies were processed as follows:

Biopsy 1 - The sample was formalin fixed, paraffin embedded (FFPE) and sectioned at 4μm thickness, (undertaken by the pathology department at the Royal United Hospital NHS Foundation Trusts.)

Biopsy 2 – was briefly stored in DMEM culture medium (Sigma D6249) with 10% foetal bovine serum (Gibco, 10500-064 or Fisher 11550356) and antibiotics (penicillin-streptomycin 100U/mL (Gibco 15140122 or Fisher 11548876), gentamicin 50ug/mL (Sigma G1272), amphotericin B 2.5ug/mL (Sigma A2942), Appendix 3.1) during transport to the laboratory and subsequently used for fibroblast explant culture at the University of Bath.

2.12 Immunohistochemistry on skin sections

2.12.1 Masson's trichrome

Skin collagen content was quantified using Masson's trichrome stain which stains collagen blue through successive levels of progressive staining displacement (Sigma HT15). All stages were performed at room temperature unless otherwise specified. FFPE skin tissue sections (chapter 2.10.3) were deparaffinised in xylene (Sigma 534056) twice for 3 minutes each followed

by rehydration in decreasing concentrations of histological grade ethanol (Sigma 534056) for 2 minutes each (100%, 100%, 95%, 80%, 50%). Sections were incubated overnight in Bouin's solution (Sigma HT10132) and then rinsed in running tap water for approximately 5 minutes until the water ran clear. Sections were then incubated in 50:50 mix of Weigert's haematoxylin A and B (Sigma HT101079) for 8 minutes to stain the nuclei black and then rinsed in warm running tap water for 5 minutes followed by brief rinsing in mqH_2O. Sections were placed in Biebrich's scarlet-acid fuchsin (0.9% Biebrich's scarlet, acid fuchsin 0.1% in 1% acetic acid) for 5 minutes and then rinsed in running tap water until the water was almost clear. Sections were then incubated in 10% phosphotungstic : 10% phosphomolybdic acid (in a ratio of 1:1:2 mqH_2O) for 5 minutes to remove the red dye by displacement and create the acidic environment required for staining with alanine blue. Sections were transferred straight to alanine blue (2.4% alanine, 2% acetic acid) for 5 minutes to stain the collagen blue. Sections were incubated in 1N glacial acetic acid (Fisher 10384970) for 2 minutes to enhance the alanine blue stain and then briefly rinsed in mqH2O. Sections were dehydrated in increasing ETOH concentrations (80%, 95%, 100%, 100%) for 2 minutes each. Sections were cleansed in xylene (2 minutes) and mounted (Fisher 12667746) and cover slipped.

2.12.1.1 Imaging of Masson's trichrome stain

Sections were imaged immediately using Leica microscope (CTR40000) and corresponding imaging software (LAS v4.3).

2.12.1.2 Image analysis

Image analysis for Masson's trichrome is described in the respective results chapter (chapter 6).

2.12.2 Indirect immunofluorescence staining of skin sections

Immunofluorescent (IF) staining of skin tissue sections was undertaken on FFPE skin sections (chapter 2.10.3). Methodology was derived and adapted from previous studies (256, 300, 302). All stages were performed at room temperature unless otherwise specified. A wash step involved 3 washed in PBS for 2 minutes each unless otherwise specified.

Skin tissue sections were deparaffinised in xylene (Sigma 534056) twice for 3 minutes each followed by rehydration in decreasing concentrations of histological grade ethanol (Sigma R8382) for 2 minutes each (100%, 100%, 95%, 80%, 50%). Sections were rinsed briefly in mqH_2O before heat induced antigen retrieval in a pre-warmed citric acid buffer (10mM in 0.05% Tween-20, pH6, Appendix 2.1) (Sigma W302600) for 15 minutes. Sections were left to cool to room temperature in the same buffer. Sections were wash twice in mqH_2O followed by PBS wash. After optimisation of the block buffer (Appendix 2.2), sections were blocked in 5% normal goat serum (NGS in PBS, G9023 Sigma) for 1 hour at room temperature. The sections were incubated with primary antibody (Table 2.4) diluted in 5% NGS overnight at 4°C in a humidified chamber. Dual staining was performed by mixing 2 primary antibodies.

Table 2. 4 Antibody dilutions used for immunofluorescent tissue staining.

Antibody dilutions in 5% normal goat serum used for IF of human skin tissue sections. Co-staining was performed by mixing primary antibodies from mouse and rabbit hosts or by mixing appropriate target secondary antibodies raised in a goat and conjugated to fluorescent antibodies. Dilutions were determined by manufacturer recommendation, previous studies and optimisation.

Antibody	Supplier	Dilution	Final concentration (μg/mL)
Primary antibody			
HIF1α	Novus NB100-105 Clone HIF1a67	1:25	40
HIF2α	Novus NB100-122	1:100	10
panVEGF-A	Abcam AB52917	1:100	2.96
VEGF-A_{165b}	R&D DY3045	1:50	10
Angiopoietin-2	Fisher PA5-27299	1:100	14.4
Tie-2	Fisher PA5-28582	1:100	10
CD31	Sigma SAB5500059	1:50	
Secondary antibody			
Goat anti-mouse (Alexa-488)	Invitrogen 15626746	1:200	10
Goat anti-rabbit (Alexa-568)	Invitrogen 10032302	1:200	10

Sections were washed in PBS before incubation with the secondary antibody for 1 hour in the dark. Dual staining was performed by mixing 2 secondary antibodies. A further wash step in PBS was performed before mounting in mounting media with DAPI (Invitrogen prolong diamond antifade, 15395816) and cover-slipped (Thermoscientific, UK thickness 1). Mounting media was allowed to cure overnight in the dark.

Primary controls were performed using non-immune primary antibodies (Appendix 2.3). Secondary controls were performed by omission of the primary antibodies (incubation with NGS only) (Appendix 2.3). Staining of serial sections using CD31 allowed confirmation of staining within the vasculature.

2.12.2.1 Image acquisition of Immunofluorescent staining of skin sections

Sections were imaged the next day using a confocal microscope (LSM-880, Zeiss, U.K) and accompanying software Zen black version 2.3 (Zeiss, U.K.). Images were acquired using individual laser tracks to minimize spectral overlap between the fluorophore emission wavelengths.

2.12.2.2 Immuofluorescent image analysis

Post-acquisition image processing and epidermal quantification was performed using Zen blue Lite software version 2.3 (Zeiss, U.K.). Further detail is described in the respective results chapter 9.2.1.1.

2.13 Fibroblast culture

2.13.1 Explant culture

Fibroblast explant culture was performed in line with EUSTAR guidelines (363). Briefly, under sterile technique, the tissue was cut into small (approximately 1mm) sections and placed with the dermis in contact with the culture dish surface (Corning, USA 3261). Tissue was left to dry for 15 minutes before adding 3mL culture medium (supplemented with FBS and antibiotics as above). Media was changed twice a week and tissue sections removed when adherent fibroblasts could be seen growing outside of the sample (Figure 2.6). Media was supplemented with all four antibiotics for passage 0 and 1. Thereafter, penicillin-streptomycin were used only. To passage cells, adherent cultures were incubated for 5 minutes with warmed 0.05% trypsin (Gibco 25300-054 or Fisher 11580626), followed by neutralisation using cold DMEM supplemented with 10% FBS. Cells were then either reseeded at a minimum of 5000 cells/cm^2 in T75 or T175 flask (Fisher 10363141 or 10246131 respectively) or suspended in freezer media (Appendix 3.2) and frozen at $1x10^6$ cells per cryotube in -80°C overnight before transfer to liquid nitrogen for longer term storage.

Figure 2. 6 Fibroblast explant culture.

Image demonstrates typical spindle shaped fibroblast morphology. Scale bar represents 100μm. Figure created by VF using own image.

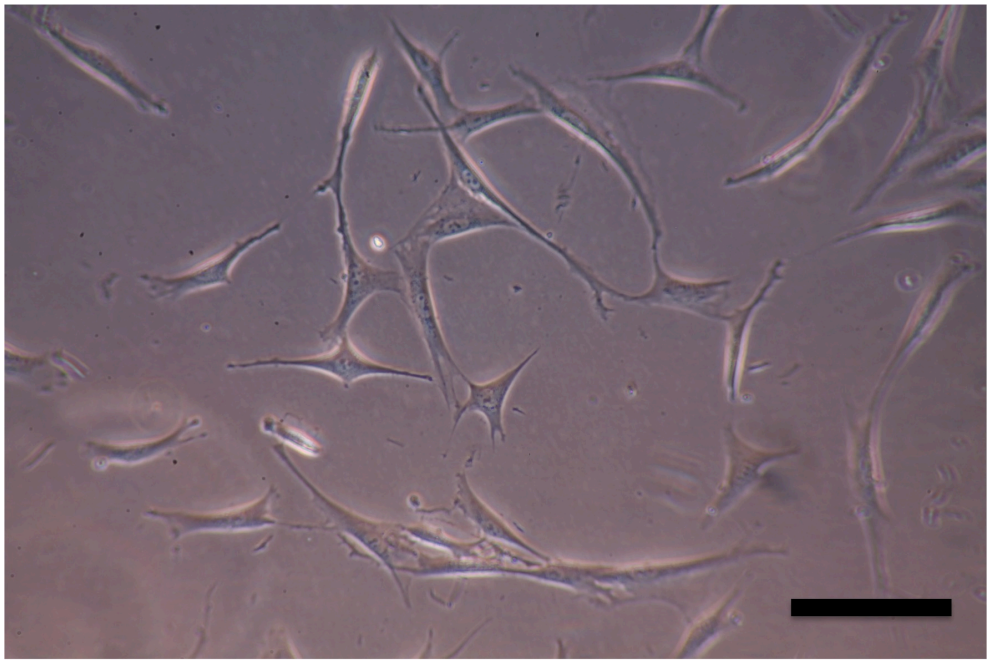

2.13.2 Hypoxic chamber experiments

2.13.2.1 Fibroblast donors

Fibroblast cultures were chosen for hypoxic experimentation from 3 early diffuse donors for homogeneity and with the aim of capturing the most active fibroblast phenotype. Age and sex matched control samples were chosen from non-smokers.

2.13.2.2 Fibroblast culture conditions

Cells were revived from liquid nitrogen for use in experiments by rapid rewarming in a water bath (37°C), washing in DMEM culture media to remove freezer media containing DMSO and reseeded as for cell passage (described chapter 2.11.1). Cells were grown to 70-90% confluence for experimentation in 6 well plates (Costar). All experiments were undertaken on fibroblasts between passage 4-6. During the experiments cells remained in

supplemented media (DMEM + 10% FBS), as HIF1α expression investigated in previous studies was reduced in low serum conditions compared to supplemented media (39).

Cells from each donor were cultured under the following conditions (Figure 2.7):

- Normoxia (21% O_2, 5% CO_2, 37°C for 48 hours) in a humidified incubator (Thermoscientific, BB15).
- In situ normoxia (5% O_2, 5% CO_2 for 48 hours) in a gloved hypoxic chamber (SCI-tive UM-025, Baker Ruskinn).
- Chronic continuous hypoxia (CCH) (1% O_2, 5% CO_2 for 48 hours) in a gloved hypoxic chamber (SCI-tive UM-025, Baker Ruskinn).
- Chronic intermittent hypoxia (CIH) (4 hour cycles of 5% and 1% O_2 for 48 hours) in a gloved hypoxic chamber (SCI-tive UM-025, Baker Ruskinn).

Samples were additionally stimulated or inhibited as outline in Figure 2.7 in order to investigate the influence of hypoxia and HIF1α, HIF2α and TGFβ on VEGF-A isoform expression in fibroblasts. Recombinant TGFβ, TGFβ neutralising antibodies and $CoCl_2$ were added at the start of experimentation.

Figure 2. 7 Plate layout for fibroblast cell culture experiments.

Cultured cells in 6-well plates were stimulated by under varying oxygen concentration and chemical stimulation as shown. (A) normoxia (21% oxygen), (B) chronic continuous hypoxia (CCH, 1% oxygen), (C) in situ normoxia (5% oxygen), (D) chronic intermittent hypoxia (CIH, alternating 5% & 1% oxygen). Abbreviations: rhTGFβ, recombinant TGFβ; $CoCl_2$, cobalt chloride; SiRNA, small interfering RNA.

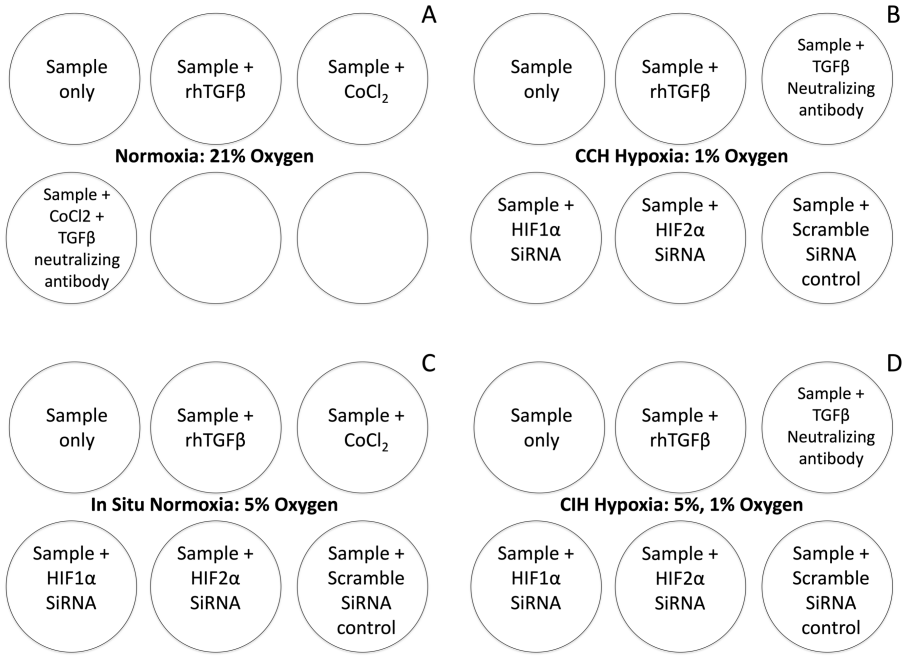

2.13.2.3 SiRNA

HIF1α, 2α and scrambler control SiRNA (Fisher 4390823 and 4390824) were reconstituted and diluted (30pmol in low serum opti-mem medium (Fisher 31985070)) as per manufacturer instructions (Appendix 3.4). 9uL of lipofectamine RNAiMAX reagent (Fisher 13778100) was diluted in 150uL of opti-mem medium (Fisher 31985070). The dilute SiRNA and lipofectamine solutions were then mixed 1:1 and incubated at room temperature for 5 minutes. 24 hours prior to the start of the experiment, SiRNA solutions were added to respective wells (1:8 dilution in DMEM/10% FBS/abx) for a terminal concentration of 25pmol SiRNA and 7.5uL of lipofectamine per well (Appendix 3.4). DMEM was changed 4 hours after transfection to reduce the

toxicity of the lipofectamine to fibroblasts. RNAse and DNAse free plastics were used throughout.

2.13.2.4 Experiment termination and sample storage

Experiments were terminated on ice, supernatant removed and stored on ice until centrifugation. Cells were lysed using 150uL of ice-cold lysis buffer (Appendix 3.3) facilitated by cell scrapping (Fisherbrand). Cell lysis and supernatant were transported on ice and centrifuged to remove debris (10,000 rpm, 3 minutes, 4°C) before storage at -80°C.

2.13.3 Protein quantification

2.13.3.1 Biorad protein assay on cell lysate

Total protein quantification was performed using Biorad protein assay (BioRad 500006) by MSc student, MS (Pharmacy & Pharmacology department). 10uL of cell lysate and 200uL of dye reagent were incubated at room temperature with gentle agitation on a plate shaker for 5 minutes and then read on microplate reader (Fluostar Optima, BMG Lab Tech) at 595nm against a BSA standard curve (diluted in the lysis buffer used for fibroblast cell lysis and also used as a blank.)

2.13.3.2 HIF ELISA on cell lysate

HIF1α and HIF2α expression was quantified from cell lysates by ELISA (R&D duoset DYC1935, DYC2997) within 7 days of cell culture experiments to avoid HIF degradation. HIF1α and HIF2α ELISAs were performed by VF.

HIF1α/2α duoset ELISAs were performed as per protocol previously described for VEGF-A_{165}b Duoset ELISA (chapter 2.9.2.2) with respective variations described below.

HIF1α capture antibody was prepared and used at 4μg/mL. Reagent diluent (5% BSA in wash buffer, pH 7.2-7.4) was used as a blocking buffer, for dilution of standards and as a blank for standards. A 7-point standard curve between 125-8000pg/mL of HIF1α was used. 100μL of cell lysates were added to wells neat and in duplicate. HIF1α detection antibody was used at a concentration of 100ng/mL.

For HIF2α duoset ELISA, HIF2α capture antibody was prepared and used at 4μg/mL. Plates were blocked with blocking buffer (1% BSA in PBS with 0.05% NaN_3, sterile filtered, pH 7.2-7.4). Cell lysate samples were diluted 6-fold (in 1mM EDTA, 0.5% Triton X-100, 5mM NaF in PBS, pH 7.2-7.4) in order to reduce the urea from the lysis buffer to 1M for assay compatibility and added to the plate as 100μL in duplicate. HIF2α standard was reconstituted to 70ng/mL stock solution (in 1mM EDTA, 0.5% Triton X-100, 5mM NaF, 6M urea in PBS, sterile filtered, pH 7.2-7.4), followed by a further 6-fold dilution (in 1mM EDTA, 0.5% Triton X-100, 5mM NaF in PBS, pH 7.2-7.4). Serial dilutions were then made (in 1mM EDTA, 0.5% Triton X-100, 5mM NaF, 1m urea in PBS, sterile filtered, pH7.2-7.4) to create a 7-point standard curve (125-8000pg/mL). The latter diluent was used as a standard curve blank. The detection antibody was used at a working concentration of 200ng/mL.

2.13.3.3 panVEGF-A ELISA on cell culture supernatant

PanVEGF-A ELISA (Cytokine panel K-15050D, MSD) was performed by MSc students (MS & TW) as per protocol previously described for Angiogenesis multiplex assay (chapter 2.9.2.1). Standards were prepared in the supplied diluent-43 (0.342-1400pg/mL) which was also used as a blank. The detection antibody was prepared as a 1x working concentration (1:50 in supplied diluent-3).

2.13.3.4 VEGF-A_{165}b ELISA on cell culture supernatant

VEGF-A_{165}b ELISA (R&D duoset DY3045), was performed by MSc students (MS, TW) as per protocol (described previously chapter 2.9.2.2.).

2.13.3.5 TGFβ ELISA on cell culture supernatant

TGFβ (R&D DY240) ELISAs were performed by MSc students (MS and TW) as per the protocol for VEGF-A_{165}b duoset (chapter 2.9.2.2). Alternatively, for the TGFβ assay, the capture antibody was used at a working concentration of 2μg/mL. The block buffer was prepared as 5% Tween-20 (in PBS, pH 7.2-7.4, sterile filtered). Standard curve was created with serial dilutions (15.625-2000pg/mL) in reagent diluent which was also used as a blank for the curve. A sample of supplemented DMEM culture media was also used as a separate control. Cell culture supernatant samples were activated prior to assay with 5:1 addition of 1N HCL, incubated for 10 minutes. Samples were then neutralised with 12N NaOH/0.5M Herpes. Samples had a final dilution in reagent diluent before assaying (final dilution factor 16.4). The detection antibody was used at a working concentration of 50ng/mL in reagent diluent.

2.13.3.6 Pro-Collage I ELISA on cell culture supernatant

Pro collagen I (Pro Col I, R&D DY6220) ELISA of the cell supernatant was performed by MSc students (MS & TW) as per the protocol for VEGF-A_{165}b (chapter 2.9.2.2). The capture antibody was diluted to a working concentration of 2μg/mL in PBS. Standards were prepared using serial dilutions in reagent diluent (31.25-2000pgmL) which was also used as a blank. A sample of supplemented DMEM culture media was also used as a separate control. Cell culture supernatant samples were diluted 125-fold in reagent diluent prior to assay. The detection antibody was prepared at a working concentration of 100ng/mL in reagent diluent.

2.13.4 Fibroblast phenotyping

Fibroblasts were grown as previously described (chapter 2.12.2.2) on slides. Cells were washed in ice cold PBS and then fixed in 4% paraformaldehyde (pH 7.4 in PBS at room temperature). Cells were then permeabilised (0.3% Triton -100 in PBS) for 10 minutes and then washed in PBS. Cells were incubated with blocking solution (5% normal calf serum, 2% BSA, 0.1% Tween-20 in PBS) for 30 minutes. Cells were incubated with primary antibodies (1 in 100 dilution in blocking solution) for 1 hour at room temperature. Primary antibodies included vimentin, cytokeratin-19, αSMA and normal mouse IgG control. Cells were washed twice in PBS and then incubated with the secondary antibody (1 in 200 in blocking solution, Table 2.4) as well as conjugated phalloidin (a bicyclic peptide from fungi that binds to F-actin to highlight the cytoskeleton, 1 in 200 in blocking solution) for 1 hour in the dark. Cells were then washed twice in PBS (in the dark) and mounted in mounting media with DAPI and cover slipped.

2.13.4.1 Fibroblast imaging

Cells were imaged the same day using a Confocal microscope (LSM-880, Zeiss, U.K) and accompanying software Zen Black version 2.3 (Zeiss, U.K.) with appropriate laser wavelengths for respective secondary antibodies as well as wavelength 633 for phalloidin. Phenotypes are demonstrated in Appendix 3.

Chapter 3. Description of demographic data and systemic sclerosis specific clinical manifestations in the study cohort

3.1 Introduction

The notorious heterogeneity in the clinical phenotype expressed across systemic sclerosis cohorts (chapter 1.2), necessitates additional scrutiny when both interpreting and critically appraising collective data. This chapter therefore aims to describe the demographic and clinical parameters of the study groups in order to allow appropriate interpretation of the data presented in subsequent chapters.

3.2 Methods

3.2.1 Study population

Healthy controls and SSc participants were recruited as described previously (chapter 2.1).

Participant demographics were collected using the study proforma, participant interview and (for SSc participants) also the clinical case notes (as described in chapter 2.2.1).

3.2.2 Statistical analysis

Statistical analysis was performed using SPSS with parametric (normally distributed data) and non-parametric tests as appropriate. Non-parametric continuous data are described as median, [IQR]. Data displayed as box plots show median (horizontal line), interquartile ranges (box plot) and range (whiskers) with group outliers shown as asterisks and circles.

3.3 Results

3.3.1 Cohort demographic data

Fifteen healthy controls were enrolled and completed the study with a mean age of 49.6 years (S.D. 8.9, range 36 – 66). Fifty-three patients meeting the 2013 ACR/EULAR classification criteria for SSc (detailed in chapter 2.1) were enrolled. The mean age of SSc participants was 62.2 years (S.D. 11.2, range 36 – 81). Group ages were normally distributed with equal variance. SSc participants were statistically significantly older than controls (t test $p < 0.01$). There was no difference in mean age between SSc disease subtypes.

The SSc group consisted of 45 lcSSc (84.9%) and 8 dcSSc (15.1%) participants (Table 3.1). The majority (79.2%) of the SSc cohort had a disease duration greater than 3 years (i.e. late SSc, chapter 2.2.2). The mean age of SSc patients did not differ between early and late SSc (Table 3.1).

There was no significant difference between healthy controls and SSc, early versus late SSc or lcSSc versus dcSSc for gender distributions (Pearson's Chi squared, χ^2 p = 0.767, 0.061, 0.185 respectively), smoking status (χ^2 p=0.861, 0.464, 0.385 respectively) or ethnicity (χ^2 p=0.445, 0.461, 0.543 respectively). The majority of the study cohort were white caucasian (Table 3.1), which is typical of the demographic for the geographical area of recruitment.

There was no difference in alcohol consumption between SSc and healthy controls or early versus late SSc (Pearson's Chi squared, χ^2 p=0.319, 0.905 respectively). However, proportionally more dcSSc had a higher average alcohol consumption (Pearson's Chi squared, χ^2 p=0.007).

Two healthy controls had treated thyroid disease and 1 had treated hypertension. There was no history of previous cardiovascular events in the control group. Seven SSc participants had treated thyroid disease and 13 had treated hypertension. No SSc participants had a history if ischaemic heart disease.

Table 3. 1 Study cohort demographics.

p<0.01ø using Independent t test, p<0.01** using Pearson's Chi squared. Comparator group is shown in **bold**. [1]SSc was classified as early or late disease based on < or > 3 years duration since the onset of the first non-RP symptom at the point of study entry.

	SSc Overall	**Disease subset**		**Disease duration**		**Healthy control**
		LcSSc	DcSSc	Early SSc	Late SSc	
Subgroup total, n. (% of SSc)	53	45 (84.9)	8 (15.1)	11 (20.8)	42 (79.2)	15
Age, mean, (S.D.)	**62.2, (11.2)ø**	62.1 (11.1)	62.9 (12.6)	62.0 (13.6)	62.3 (10.7)	**49.6 (8.9)**
Female, n. (% of subgroup)	47 (88.7)	41 (91.1)	6 (87.5)	8 (72.7)	39 (92.9)	12 (80.0)
Disease duration mean years, (S.D.)	11.7 (11.6)	12.3 (12.2)	8.7 (6.9)	1.7 (1.1)	14.5 (11.6)	-
Ethnicity, n. (% of subgroup)						
White Caucasian	51 (96.2)	43 (95.6)	8 (100)	11 (100)	40 (95.2)	15 (100)
Asian (Chinese)	2 (3.8)	2 (4.4)	0 (0)	0 (0)	2 (4.8)	0 (0)
Smoking status, n. (% of subgroup)						
Current	6 (11.3)	4 (8.9)	2 (25)	2 (18.2)	4 (9.5)	1 (6.7)
Ex-smoker	11 (20.8)	10 (22.2)	1 (12.5)	1 (9.1)	10 (23.8)	3 (20)
Non-smoker	36 (67.9)	31 (68.9)	5 (62.5)	8 (72.7)	28 (66.7)	11 (73.3)
Alcohol, n. (% of subgroup)						
>14 units/week	9 (17)	**5 (11.1)**	**4 (50)****	2 (18.2)	7 (16.7)	1 (6.7)

3.3.2 Serological autoantibody status of the disease group

The autoantibody status across the SSc cohort is detailed in Table 3.2. With the exception of one participant for whom their autoantibody status was not known, all SSc participants were positive for autoantibodies and >92% had SSc-specific or SSc-associated autoantibodies. One late dcSSc participant had dual positivity for Scl-70 and U1RNP.

The majority of lcSSc participants were anti-centromere antibody positive, followed by anti-Scl-70 positivity reflecting that seen in the general European SSc population (5). There were more anti-RNAPIII and anti-U3RNP in dcSSc as expected.

Table 3. 2 Autoantibody profile of SSc cohort.

Statistical comparison using Pearson's χ^2 is illustrated for lcSSc versus dcSSc.

Autoantibody	% SSc (all patients)	SSc overall	LcSSc	DcSSc	p value (χ^2)
Systemic sclerosis-specific Autoantibody, n. (early, late)					
Anti-centromere	56.6%	30 (5, 25)	30** (5, 25)	0 (0, 0)	**<0.001**
Anti-Scl-70	17.0%	9 (1, 8)	6 (1, 5)	3 (0, 3)	0.093
Anti-RNAPIII	3.8%	2 (2, 0)	0 (0, 0)	2 (2, 0)	**0.001**
Anti-U3RNP	1.9%	1 (0, 1)	0 (0, 0)	1 (0, 1)	**0.017**
Anti-Th/To	1.9%	1 (0, 1)	1 (0, 1)	0 (0, 0)	0.670
Unknown	1.9%	1 (0, 1)	1 (0, 1)	0 (0, 0)	-
Systemic sclerosis-associated Autoantibody, n. (early, late)					
Anti-U1RNP	5.7%	3 (0, 3)	2 (0, 2)	1 (0,1)	0.364
Anti-PmScl	3.8%	2 (1, 1)	2 (1, 1)	0 (0, 0)	0.543
Anti-Nor-90	1.9%	1 (1, 0)	0 (0, 0)	1 (1, 0)	**0.017**
Other autoantibodies, n. (early, late)					
Non-specific ANA	7.5%	4 (1, 3)	3 (1, 2)	1 (0, 1)	0.565
Anti-Ro	13.2%	7 (2,5)	7 (2,5)	0 (0, 0)	0.231
Rheumatoid factor	5.7%	3 (0,3)	3 (0,3)	0 (0, 0)	0.452
Anti-β2GPI	1.9%	1 (0,1)	1 (0,1)	0 (0, 0)	0.670
Anti-mitochondrial	1.9%	1 (0, 1)	1 (0, 1)	0 (0, 0)	0.670

3.3.3 Clinical manifestations in systemic sclerosis

All SSc participants had a clinical diagnosis of RP, in line with expectations. Significantly more late SSc participants had calcinosis, reflux and telangiectasia than those with early disease (Table 3.3). One patient had pulmonary hypertension relating to severe aortic stenosis, which was incidental to SSc, but is noted in view of the potential to influence plasma biomarkers.

Table 3. 3 Clinical manifestations of SSc cohort.

Abbreviations: DU, digital ulcers; GORD, gastro oesophageal reflux disease; ILD, interstitial lung disease; n, number; PH, pulmonary hypertension; SSc-PAH, SSc related pulmonary arterial hypertension. *p<0.05 and **p≤0.01 using Pearson's Chi-squared (χ^2) between lcSSc versus dcSSc or early versus late disease with comparator group in **bold**.

	SSc overall	**Disease subset**		**Disease duration**	
		LcSSc	DcSSc	Early SSc	Late SSc
Cutaneous subtype, n. (%)					
LcSSc	45 (84.9)	45	-	8 (72.7)	37 (88.1)
DcSSc	8 (15.1)	-	8	3 (27.3)	5 (11.9)
Vascular features, n. (% of subgroup)					
Raynaud's	53 (100)	45 (100)	8 (100)	11 (100)	42 (100)
DU ever	16 (30.2)	15 (33.3)	1 (12.5)	1 (9.1)	15 (35.7)
Telangectasia	46 (86.8)	40 (88.9)	6 (75)	**7 (63.6)**	**39 (92.9)****
SSc-PAH	4 (7.6)	4 (8.9)	0 (0)	0 (0)	4 (9.5)
PH	1 (1.9)	1 (2.2)	0 (0)	0 (0)	1 (2.4)
Renal crisis	0 (0)	0 (0)	0 (0)	0 (0)	0 (0)
Fibrotic features, n. (% of subgroup)					
Scleroderma	49 (92.5)	41 (91.1)	8 (100)	10 (90.9)	39 (92.9)
GORD	45 (84.9)	38 (84.4)	7 (87.5)	**7 (63.6)**	**38 (90.5)***
ILD	17 (32.1)	12 (26.7)	5 (62.5)	2 (18.2)	15 (35.7)
Other, n. (% of subgroup)					
Calcinosis	24 (45.3)	21 (46.7)	3 (37.5)	**1 (9.1)**	**23 (54.8)***
Inflammatory arthritis	11 (20.8)	**10* (22.2)**	**1 (12.5)**	4 (36.4)	7 (16.7)
Time from Raynaud's onset to first non-Raynaud's symptom					
Data available, n.	47	40	7	10	37
Time (median, years)	1.8 (0.0-11.0)	2.5 (0.0-11.8)	0.7 (0.0-3.5)	0.5 (0.1-3.4)	3.5 (0.0-12.0)

3.3.4 Medication use within the Study cohort

The SSc group (all patients) had significantly more participants currently using vasodilator therapy (single or multiple prescription) than healthy controls (χ^2 $p<0.01$) (Table 3.4). fluoxetine (an antidepressant) also has vasoactive properties. It is therefore counted in the 'number of vasodilators' for each group. One healthy control was taking multiple vasodilators for hypertension and one was taking fluoxetine. There was no significant difference in current vasodilator use between lcSSc and dcSSc (Pearson's Chi squared, χ^2 $p=0.561$) or early and late disease (χ^2 $p=0.599$). There was no significant difference between SSc versus controls or lcSSc versus dcSSc in antiplatelet (χ^2 $p=0.739$, 0.102 respectively) or anticoagulation (χ^2 $p=0.273$, 0.380 respectively) administration. There was a significantly increased current use of anti-platelet therapy in early compared to late SSc (χ^2 $p=0.023$), but no difference in anticoagulant use (χ^2 $p=0.287$).

Table 3. 4 Medication use in the study cohort.

p<0.05* and p≤0.01** using Pearson's Chi-squared (χ^2) with comparator groups illustrated in **bold**. Abbreviations: ACEI, angiotensin converting enzyme inhibitor; ARB, angiotensin receptor blocker; AIIRB, angiotensin II receptor blocker; CCB, calcium channel blocker; ERA, endothelin receptor antagonist; PDE-5 inhibitor, phosphodiesterase-5 inhibitor.

	SSc overall	**Disease subset**		**Disease duration**		**Healthy control**
		LcSSc	DcSSc	Early	Late	
n.	53	45	8	11	42	15
Number of Vasodilators used per participant, n. (subgroup %)						
Any Vasodilator	**35 (66.0)****	29 (64.4)	6 (75.0)	8 (72.7)	27 (64.3)	**2 (13.3)**
0 Vasodilator	**18 (34.0)****	16 (35.6)	2 (25.0)	3 (27.3)	15 (35.7)	**13 (86.7)**
1 Vasodilator	**21 (39.6)****	17 (37.8)	4 (50.0)	7 (63.6)	14 (33.3)	**1 (6.7)**
2 Vasodilator	**11 (20.8)****	10 (22.2)	1	1 (9.1)	10 (23.8)	**1 (6.7)**
3 Vasodilator	0 (0)	0 (0)	0 (0)	0 (0)	0 (0)	0 (0)
4 Vasodilator	3 (5.7)	2 (4.4)	1(12.5)	0 (0)	3 (7.1)	0 (0)
Medication use by Drug Class, n. (subgroup %)						
CCB	**23 (43.4) ****	21 (46.7)	2 (12.5)	5 (45.5)	18 (42.9)	1 (6.7)
ACEI	4 (7.5)	3 (6.7)	1 (12.5)	1 (9.1)	3 (7.1)	1 (6.7)
ARB	3 (5.7)	1 (2.2)	2 (25)	2 (18.2)	1 (2.4)	0 (0)
AIIRB	7 (13.2)	5 (11.1)	2 (25)	0 (0)	7 (16.7)	0 (0)
Fluoxetine	5 (9.4)	3 (6.7)	2 (25)	1 (9.1)	4 (9.5)	1 (6.7)
PDE-5 Inhibitor	8 (15.1)	7(15.6)	1 (12.5)	0 (0)	8 (19.0)	0 (0)
ERA	3 (5.7)	3 (6.7)	0 (0)	0 (0)	3 (7.1)	0 (0)
Beta blocker	1 (1.9)	0 (0)	1(12.5)	1 (9.1)	0 (0)	1 (6.7)
Antiplatelet therapy	5 (9.4)	3 (6.7)	2 (25)	**3 (27.3)***	**2 (4.8)**	1 (6.7)
Anticoagulant therapy	4 (7.5)	4 (8.9)	0 (0)	0 (0)	4 (9.5)	0 (0)
Medication Administered on the day of Study Assessment, n. (subgroup %)						
Vasodilator	30 (56.6)	25 (55.6)	5 (62.5)	6 (54.5)	24 (57.1)	1 (6.7)
Beta blocker	1 (1.9)	0 (0)	1 (12.5)	1 (9.1)	0 (0)	1 (6.7)

As expected, there was a trend for more SSc participants with a history of DU to be taking 2 or more vasodilator therapies than SSc without a history of DU (Pearson's χ^2 p=0.053). Furthermore, a greater number of SSc-DU participants were taking a potent vasodilator, PDE-5 inhibitor (sildenafil), than those with no DU (Pearson's Chi-squared, χ^2 <0.001) (Table 3.5). One SSc participant without any history of DU (2.7%) was prescribed an ERA for SSc-PAH compared to 2/16 (12.5%) of those with a history of DU. The low numbers of ERA therapy in either group of our cohort did not reach statistical significance.

Table 3. 5 Vasodilator use between SSc with and without Digital Ulcer history.

Significance is illustrated using Pearson's Chi-squared (χ^2). Abbreviations: DU, digital ulcers; ERA, endothelin receptor antagonist (bosentan); PDE-5 inhibitor, phosphodiesterase-5 inhibitor (sildenafil).

	No History of Digital Ulcers	**History of Digital Ulcers**	**p value (χ^2)**
DU history, n.	34	19	-
Any vasodilator	20 (58.8)	15 (78.9)	0.138
Number of co-prescribed Vasodilators			
0	14 (41.2)	4 (21.1)	
1	14 (41.2)	7 (36.8)	
2	5 (14.7)	6 (31.6)	
4	1 (2.9)	2 (10.5)	0.219
≥2	6 (17.6)	8 (42.1)	0.053
PDE-5 Inhibitor	**1 (2.9)**	**7 (36.8)**	**0.001**
ERA	1 (2.9)	2 (10.5)	0.252

Historic and current use of disease modifying anti-Rheumatic drugs (DMARDs, typically immunosuppressant in action) is illustrated in Table 3.6. As expected, proportionally more dcSSc than lcSSc had required DMARDs at some point in their disease course (Pearson's $\chi^2 = 0.006$) (Table 3.6). There was no difference in DMARD use between early and late SSc.

Table 3. 6 DMARD exposure in the SSc cohort.

The frequency of disease modifying anti-Rheumatic drugs (past or current) are shown. $p<0.05$* and $p<0.01$** using Pearson's χ^2 is demonstrated by between lcSSc and dcSSc or early versus late SSc, with the comparator group in **bold**.

	SSc overall	**Disease subset**		**Disease duration**	
		LcSSc	DcSSc	Early SSc	Late SSc
Subgroup total, n.	53	45	8	11	42
DMARDs exposure ever, n. (%)	23 (43.4)	**16 (35.6)**	**7 (87.5)****	5 (45.5)	18 (42.9)
Previous DMARD use alone or in combination, n. (%)					
Prednisolone	3 (5.7)	3 (6.7)	0 (0)	1 (9.1)	2 (4.8)
Hydroxychloroquine	3 (5.7)	3 (6.7)	0 (0)	0 (0)	3 (7.1)
Penicillamine	1 (1.9)	1 (2.2)	0 (0)	0 (0)	1 (2.4)
Sulfasalazine	1 (1.9)	1 (2.2)	0 (0)	0 (0)	1 (2.4)
Methotrexate	2 (3.8)	2 (4.4)	0 (0)	0 (0)	2 (4.8)
Azathioprine	1 (1.9)	1 (2.2)	0 (0)	0 (0)	1 (2.4)
Mycophenolate mofetil	2 (3.8)	**0 (0)**	**2 (25)****	0 (0)	2 (4.8)
Cyclophosphamide	10 (18.9)	**3 (6.7)**	**7 (87.5)****	4 (36.4)	6 (14.3)
Rituximab	1 (1.9)	**0 (0)**	**1 (12.5)***	0 (0)	1 (2.4)
Current DMARD use alone or in combination, n. (%)					
Any current DMARD	17 (32.1)	**11 (24.4)**	**6 (75)****	5 (45.5)	12 (28.6)
Prednisolone	12 (22.6)	**8 (17.8)**	**4 (36.4)***	3 (27.3)	9 (21.4)
Hydroxychloroquine	4 (7.5)	3 (6.7)	1 (12.5)	1 (9.1)	3 (7.1)
Methotrexate	3 (5.7)	3 (6.7)	0 (0)	1 (9.1)	2 (4.8)
Azathioprine	1 (1.9)	1 (2.2)	0 (0)	0 (0)	1 (2.4)
Mycophenolate mofetil	9 (17)	**4 (8.9)**	**5 (62.5)****	3 (27.3)	6 (14.3)

3.3.5 Description of the SSc cohort by fibrotic burden

When considering the burden of fibrosis within the SSc group, more than 90% had a previous history of documented clinically detectable skin thickening proximal to the proximal inter-phalangeal joint. The median total mRSS at the time of the study assessment for SSc group overall was 3 [2-7], which reflects a low median burden of skin disease due to the large number of lcSSc participants (Table 3.7). There was a significantly higher total mRSS in dcSSc than lcSSc (median 15, [2-18] versus median 2, [2-5], p=0.034) as expected (Table 3.7, Figure 3.1). The site-specific local mRSS score at the time of assessment, corresponding to each of four HFUS assessment locations is reported in Table 3.7.

Those with dcSSc were significantly more likely to have clinically detectable skin thickening (mRSS ≥ 1) at all HFUS sites other than the finger, when compared to lcSSc (χ^2 hand p=0.003, forearm p=0.002, abdomen p=0.001), as were those with early compared to late SSc (χ^2 hand p=0.048, forearm p=0.023, abdomen p=0.005) reflecting the tendency for skin regression with time and therapy. DcSSc were also more likely to have higher skin scores (mRSS≥ 2) at finger, hand and forearm than lcSSc. This was not true at the abdominal HFUS site, by design as the abdominal epigastrium was chosen as a ROI as it was most likely to be an area of palpably normal skin. With the exception of 2 participants with early dcSSc, all SSc had clinically uninvolved skin at the abdominal epigastrium at the site of HFUS assessment.

Table 3. 7 Local mRSS at HFUS assessment site in SSc sub-groups.

Statistical comparison between lcSSc versus dcSSc and early versus late using Mann Whitney-U for total mRSS and Chi-squared (χ^2) for comparison of local mRSS at the finger, hand, forearm and abdomen corresponding to HFUS regions of interest.

	SSc overall	**Disease subset**		**Disease duration**	
		LcSSc	DcSSc	Early	Late
n.	53	45	8	11	42
Total mRSS (0-51)					
median [IQR]	3 [2-7]	2 [2-5]	15 [2-28]	4 [2-18]	3 [1-6]
p value (MWU)		**0.034**		0.369	
Local mRSS Proximal phalanx of middle finger, n. (% of subgroup)					
0	11 (20.8)	9 (20)	2 (25)	1 (9.1)	10 (23.8)
1	33 (62.3)	32 (2.2)	1 (12.5)	7 (63.6)	26 (61.9)
2	7 (13.2)	4 (8.9)	3 (37.5)	2 (18.2)	5 (11.9)
3	2 (3.8)	0 (0)	2 (25)	1 (9.1)	1 (2.4)
p value (χ^2)	-	**<0.001**		0.529	
mRSS ≥ 1	42 (79.2)	36 (80)	6 (75)	10 (90.9)	32 (79.2)
p value (χ^2)	-	0.748		0.284	
Local mRSS Dorsal hand (n.)					
0	37 (69.8)	35 (77.8)	2 (25)	5 (45.5)	37 (88.1)
1	12 (22.6)	8 (17.8)	4 (50)	5 (45.5)	7 (16.7)
2	3 (5.7)	2 (4.4)	1 (12.5)	1 (9.1)	2 (4.8)
3	1 (1.9)	0 (0)	1 (12.5)	0 (0)	1 (2.4)
p value (χ^2)	-	**0.007**		0.178	
mRSS ≥ 1	16 (30.2)	10 (22.2)	6 (75)	6 (54.5)	10 (23.8)
p value (χ^2)	-	**0.003**		**0.048**	
Local mRSS Distal forearm (n.)					
0	42 (79.2)	39 (86.7)	3 (37.5)	6 (54.5)	36 (85.7)
1	9 (17)	6 (13.3)	3 (37.5)	4 (36.4)	5 (11.9)
2	2 (3.8)	0 (0)	2 (25)	1 (9.1)	1 (2.4)
p value (χ^2)	-	**<0.001**		0.075	
mRSS ≥ 1	11 (20.8)	6 (13.3)	5 (62.5)	5	6 (14.3)
p value (χ^2)	-	**0.002**		**0.023**	
Local mRSS Abdomen (n.)					
0	51 (96.2)	45 (100)	6 (75)	9 (81.8)	42 (100)
1	2 (3.8)	0 (0)	2 (25)	2 (18.2)	0 (0)
p value (χ^2)	-	**0.001**		**0.005**	

Figure 3. 1 Total mRSS in SSc subsets.

Significantly greater median total mRSS is seen in the dcSSc subgroup compared to lcSSc (Mann Whitney-U) as expected. Box plots show median (line) and interquartile ranges (whiskers). Outliers are shown by * and °.

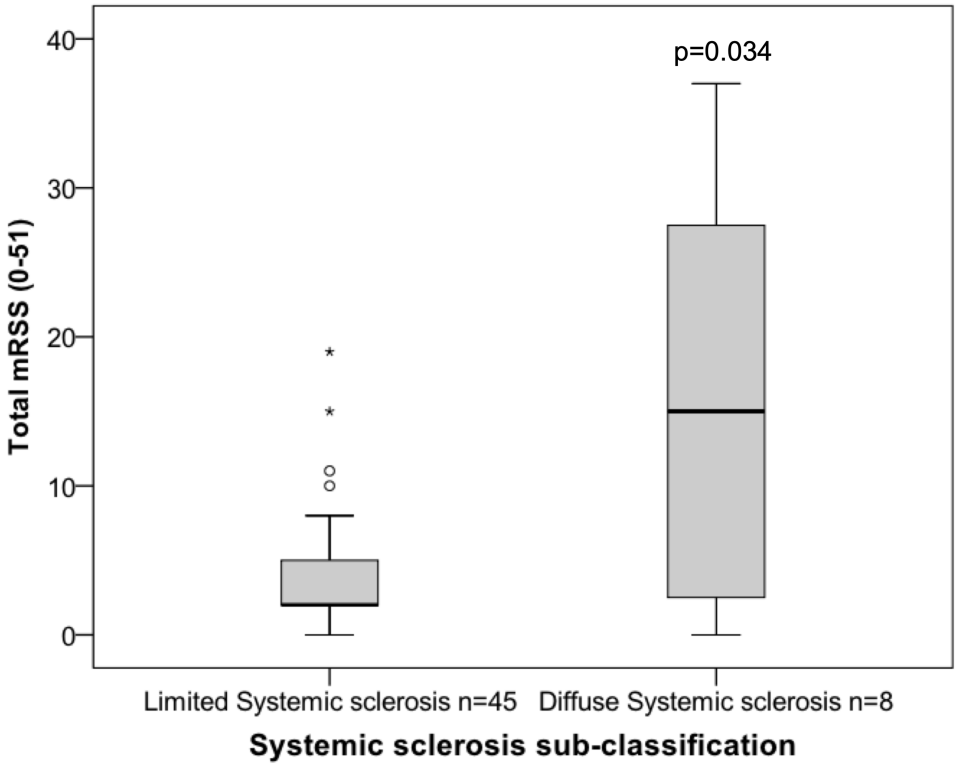

3.3.6 Demographic description and clinical features of skin tissue donors

Within the participant groups described thus far, forearm skin biopsies were obtained from 10 SSc patients and 10 HC. Amongst those who provided skin biopsies used for trichrome staining, healthy controls were significantly younger than SSc (mean 50.4 (S.D. 9.9) versus 65.3 (S.D. 10.5), p=0.004) (Table 3.8), as reflected for the overall cohort described above (chapter 3.3.1). Among those whose forearm skin biopsies were used for IHC-IF, there was no significant difference in age between HC and SSc donors (mean 55.8 (S.D. 9.6) versus 65.3 (S.D. 10.5), p=0.113).

Similarly, the greater use of vasodilators seen in SSc from the whole cohort compared to controls translated to the skin biopsy donors also (7/10 SSc versus 2/10 HC trichrome samples, χ^2 p=0.025 and 0/5 HC IHC-IF samples, χ^2 p=0.01). A greater proportion of dcSSc currently administered vasodilators and had a history of current or previous DMARD exposure compared to lcSSc (χ^2 p=0.038 for both) amongst the forearm skin donors.

Table 3. 8 Demographic data for forearm skin biopsy donors.

p<0.05π and p<0.01ø using Independent t test compared to controls. p<0.05* and χ^2 p=0.01** using Pearson's Chi-squared, χ^2 for control groups versus SSc overall and for lcSSc versus dcSSc.

	Healthy control (Trichrome stain)	**Healthy control (IHC-IF)**	**SSc overall**	**LcSSc (early, late)**	**DcSSc (early, late)**	**Early SSc**	**Late SSc**
Subgroup total, n.	10	5	10	5 (2, 3)	5 (3, 2)	5	5
Age mean, years (S.D.)	**50.4 (9.9)**	55.8 (9.6)	**65.3 (10.5)ø**	**65.5 (10.1)π**	**65 (12)π**	**69 (10.7)ø**	61.6 (9.9)
Female, n. (%)	7 (70)		8 (80)	4 (80)	4 (80)	3 (60)	5 (100)
Disease duration, mean years (S.D.)	-	-	13.9 (20.1)	23.3. (25.9)	4.5 (3.7)	1.8 (1.1)	25.9 (23.3)
Total mRSS, median (mean, IQR)	-	-	6.5 (13, 2-27)	3 (4, 2-7)	26 (22,9-33)	18 (16, 4-28)	3 (10, 1-22)
Autoantibody status, n. (%)							
Anti-centromere	-	-	1 (10)	1 (20)	0 (0)	0 (0)	1 (20)
Scl-70	-	-	4 (40)	2 (40)	2 (40)	0 (0)	4 (80)
RNAPIII	-	-	2 (20)	0 (0)	2 (40)	2 (40)	0 (0)
U1RNP	-	-	1 (10)	0 (0)	1 (20)	0 (0)	1 (20)
PmScl	-	-	1 (10)	1 (20)	0 (0)	1 (20)	0 (0)
Nor-90	-	-	1 (10)	0 (0)	1 (20)	1 (20)	0 (0)
Non-specific ANA	-	-	1 (10)	1 (20)	0 (0)	1 (20)	0 (0)
Drug exposure, n. (%)							
Current vasodilator, n. (%)	**2 (20)***	**0 (0)****	**7 (70)**	**2 (40)***	**5 (100)**	3 (60)	4 (80)
DMARD ever, n. (%)	-	-	7 (70)	**2 (40)***	**5 (100)**	4 (80)	3 (60)

3.4 Discussion

The data described demonstrate that our study cohort is representative of the general European SSc population when compared to the large EUSTAR database (5), in particular with a female ACA+ lcSSc predominance. Overall, with respect to the 3 principle SSc-specific autoantibodies, our cohort exhibited similar expression to the EUSTAR database, but with a greater proportion of ACA+, (ACA 56.6% versus 32%, Scl-70 17% versus 36%, RNAPIII 3.8% versus 2.4% in our study cohort versus EUSTAR database respectively). One of our participants expressed dual autoantibody positivity, which has been described in the literature (364). Additionally, our cohort is comparable with the EUSTAR database for DU frequency and inflammatory arthritis, although exhibits less PAH (7.5% versus 21%), which may reflect patients with more advanced disease and mobility restrictions being less able to attend additional research visits (5).

The high proportion of ACA+ lcSSc in our late disease group was expected, as this subtype tends to exhibit a more indolent progression and better overall survival than the more rapidly progressive dcSSc counterpart (188). The greater occurrence of calcinosis, reflux and telangiectasia in the late SSc group was also therefore expected as these features are commonly expressed in the ACA+ lcSSc phenotype, (formally described by the acronym CREST syndrome: calcinosis, Raynaud's, oesophageal dysmotility, sclerodactyly, telangectasia) (365).

The ratio of lcSSc:dcSSc (84.90% : 15.09% respectively) in our cohort was a greater proportion of lcSSc compared to the reported background population (typically 60% lcSSc versus 40% dcSSc) (5). This may due to the

comparatively more aggressive disease course in dcSSc resulting in fewer patients who were able and willing to take part in the study.

There was a significantly higher mean age in the SSc group (all patients) compared to controls, which is note-worthy with respect to data interpretation in forward chapters and will be discussed for relevant results. Study recruitment for healthy control group was predominantly from willing staff under employment at the RNHRD, which resulted in a number of control participants being of pre-retirement age compared to the SSc group.

Similarly, there was significantly more vasodilator use in the SSc group, both as single and multiple co-prescription. Vasodilator therapies are frequently prescribed for RP and pulmonary vascular disease in SSc, as well as other cardiovascular comorbidities (190) and therefore this was expected. Indeed, there was a non-significant trend for SSc with a DU history to be administering 2 or more vasodilators at the time of study assessment as well as significantly more SSc-DU to be using PGE-5 inhibitors. The study design did not incorporate inclusion criteria for treatment naïve participants or a washout phase of medications as it was considered that this would both reduce voluntary participation and also result in selection bias of those with milder disease phenotype who would be clinically more able to withdraw medication. The potential effect of vasodilator and DMARD use on study results will be discussed in respective subsequent chapters.

Chapter 4. Evidence of vasculopathy in systemic sclerosis

4.1 Introduction

The multifaceted nature of SSc related vasculopathy involves both functional and structural changes that are further complicated by evolution over the disease course and discussed in detail in chapter 1.4 and 1.5. As such, in addition to acute ischaemic attacks in response to cold, SSc patients have impaired blood flow even at ambient temperatures (chapter 1.5). Several different imaging modalities and functional vascular challenge techniques have been used to demonstrate the more severe RP and peripheral vasculopathy experienced by SSc patients compared to either healthy individuals or primary RP (chapter 1.5.4). As discussed, the PORH test is logistically easier to perform for both the patient and clinician.

4.1.1 Use of laser based imaging techniques to assess baseline perfusion and PORH kinetics in SSc

Most studies that have used laser technologies (either LDF or LSCI) to examine PORH have demonstrated abnormal PORH kinetics in SSc (chapter 1.5.4.1). Very few PORH studies (61, 88-90) have utilised LSCI despite its potential as a superior laser imaging modality (81) (discussed in chapter 1.5.4.1). The consensus of these studies is that PORH kinetics are impaired in SSc (chapter 1.5.4.1). However, most of these studies had relatively small SSc cohorts (median 26, IQR 15-48). More data are needed for the application of LSCI and PORH in SSc vasculopathy.

4.1.2 Peripheral tissue perfusion in SSc-DU

On review of the PORH literature (chapter 1.5.4.1), it is noted that none of the studies report on post-hoc analysis of SSc with a history of DU, a sub-group of patients where perfusion is expected to be most impaired. The explanation for this gap in the literature is due to a combination of active exclusion of SSc-DU patients from some studies as well as vasodilator withdrawal in many other study methodologies, which may have contributed to negative selection bias of DU patients.

4.1.3 The relationship between structural nailfold capillaroscopy changes and functional LSCI PORH in SSc

The relationship between structural microvascular changes and tissue perfusion reported by LSCI has only been reported in 2 studies from the same group (88, 90) (chapter 1.5.4.1), between which there were conflicting results. In their earlier study, Della Rossa et al., (88) reported no difference in either baseline perfusion or PORH kinetics between progressive NC patterns. In contrast, a subsequent study with an additional VEDOSS subset reported that peak PORH correlates with capillary density and worsens with progressive NC patterns (90). Given the potential predictive value of NC (discussed in chapter 1.5.6), the relationship between finger perfusion on LSCI and NC changes warrants further study.

4.1.4 Chapter hypothesis, aims and objectives

Our hypotheses for this chapter are two-fold. Firstly, that LSCI with PORH testing is a useful, objective and non-invasive assessment tool for SSc vascular dysfunction. Secondly, that there is a relationship between structural and functional microvascular changes in SSc. The overriding aim

of this chapter was to use nailfold capillaroscopy and LSCI with PORH testing to investigate this relationship. The specific objectives were:

1. To examine functional vascular impairment in SSc following a PORH test measured using LSCI.
2. To compare functional assessment of digital perfusion with the structural microvascular changes at the nailfold using nailfold capillaroscopy in SSc.
3. To investigate if functional and structural vascular changes are worse in SSc with a history of DU.
4. To investigate the inter-relationship between PORH assessment using LSCI, structural microvascular changes on nailfold capillaroscopy and patient-reported outcome measures of peripheral vasculopathy.

4.2 Methods

4.2.1 Study population

Healthy controls and SSc participants were recruited as described previously (chapter 2.1).

4.2.2 Microvascular assessment

Healthy control and SSc participants attended for microvascular imaging as described previously (chapter 2.4). Participants underwent LSCI with PORH testing and NC as described in chapter 2.5 and 2.6 respectively. PROMs for the RP diary and SHAQ were collected as described in chapter 2.3.

4.2.3 Imaging analysis

4.2.3.1 LSCI image analysis

Detailed description of LSCI parameters are discussed in chapter 2.5.4. In brief, LSCI data described in this chapter includes:

- Overall distal finger average (mean across the distal phalanx of each of 2^{nd}-5^{th} fingers) for
    - median baseline (Perfusion Units, PU)
    - peak PORH (PU)
    - time to peak PORH (seconds)
    - reperfusion gradient (ΔPU/s) following an ischaemic challenge
    - Area under the reperfusion curve (AUC)
- Distal dorsal difference demonstrating the perfusion gradient between the distal fingers (average of 2^{nd}-5^{th} fingers) and the dorsal hand.

4.2.3.2 NC image analysis

Nailfold capillaroscopy images were analysed as described in chapter 2.6.3. Data for NC in this chapter describes the overall NC classification as judged by the most advanced NC pattern represented across the 3 investigated fingers. Individual NC parameters e.g. the mean number of capillaries/mm are calculated as an overall mean across the 3 investigated fingers.

4.2.4 Statistical analysis

Statistical analysis utilised non-parametric test in SPSS and therefore describe the median of the mean for LSCI and NC parameters where applicable (median, [IQR]). Data displayed as box plots show median

(horizontal line), interquartile ranges (box plot) and range (whiskers) with group outliers shown as asterisks and circles.

4.3 Results

4.3.1 Participants

The cohort demographics have been described in chapter 3.3.1.

Fifteen HC underwent LSCI and NC. LSCI data was available for 52 SSc participants due to technical failure at the time of study visit for one SSc participant (62-year-old female with late lcSSc and no history of prior DU). Baseline LSCI data was available for all 52 SSc participants. Movement artefact on LSCI degraded the PORH data quality and reliability in three SSc participants who were excluded from PORH analysis (50-year-old female with early lcSSc, a 74-year-old female with late lcSSc and a 70-year-old female with late lcSSc, final PORH n=49). All 53 SSc subjects underwent NC with good quality images to assess the overall NC classification. PROMs were successfully completed and returned by SSc participants as follows: Raynaud's diary n=44, SHAQ-RP n=47, SHAQ-DU n=39 (chapter 2.3).

4.3.2 Laser speckle contrast imaging to assess functional peripheral vascular response to ischaemic challenge

We first investigated the ability of LSCI to differentiate diagnostic groups in our cohort based on both baseline and functional microvascular perfusion. There was no significant difference in the median baseline flux between SSc (median 532.1, [241.1-725.9]) and healthy controls (478.4, [159.1-720.8], p=0.599) (Figure 4.1). However, there was evidence of impaired peripheral vascular response to ischaemic challenge including a non-significant trend towards reduced peak PORH in SSc versus controls (median 715.7, [582.3-

956.8] versus 840.3, [670.2-1078.0], p=0.134, respectively) and a significantly reduced reperfusion gradient (median 3.0, [2.2-4.8] versus 7.1, [3.5-10.1], p<0.001). The two factors contributing to the latter were a prolonged time to reach peak PORH in the disease group (median 127.0, [88.8-184.6] versus 78.5, [64.0-94.3] respectively, p=0.001) and secondly a trend towards a reduced percentage increase in flux after ischaemic challenge reflected in the disease group (74.8%, [38.9-171.3] versus 128.6%, [41.6-314.0] respectively; p=0.161.). The collective result of such was a significantly increased area under the curve in the disease group compared to controls after occlusive challenge (4998.3, [3220.1-10412.8] versus 1842.3, [1487.5-4449.5] respectively, p=0.015) (Figure 4.1).

Figure 4. 1 Peripheral perfusion in SSc and healthy controls.

LSCI parameters demonstrated (A) no difference between groups in baseline distal finger perfusion (mean across digits 2-5). A significant delay in vascular response to an ischaemic challenge is, however, observed through (B) increased time to reach peak PORH, (C) reduced reperfusion gradient in flux from baseline to peak PORH, and (D) increased area under the curve. Significance illustrated using Mann-Whitney U.

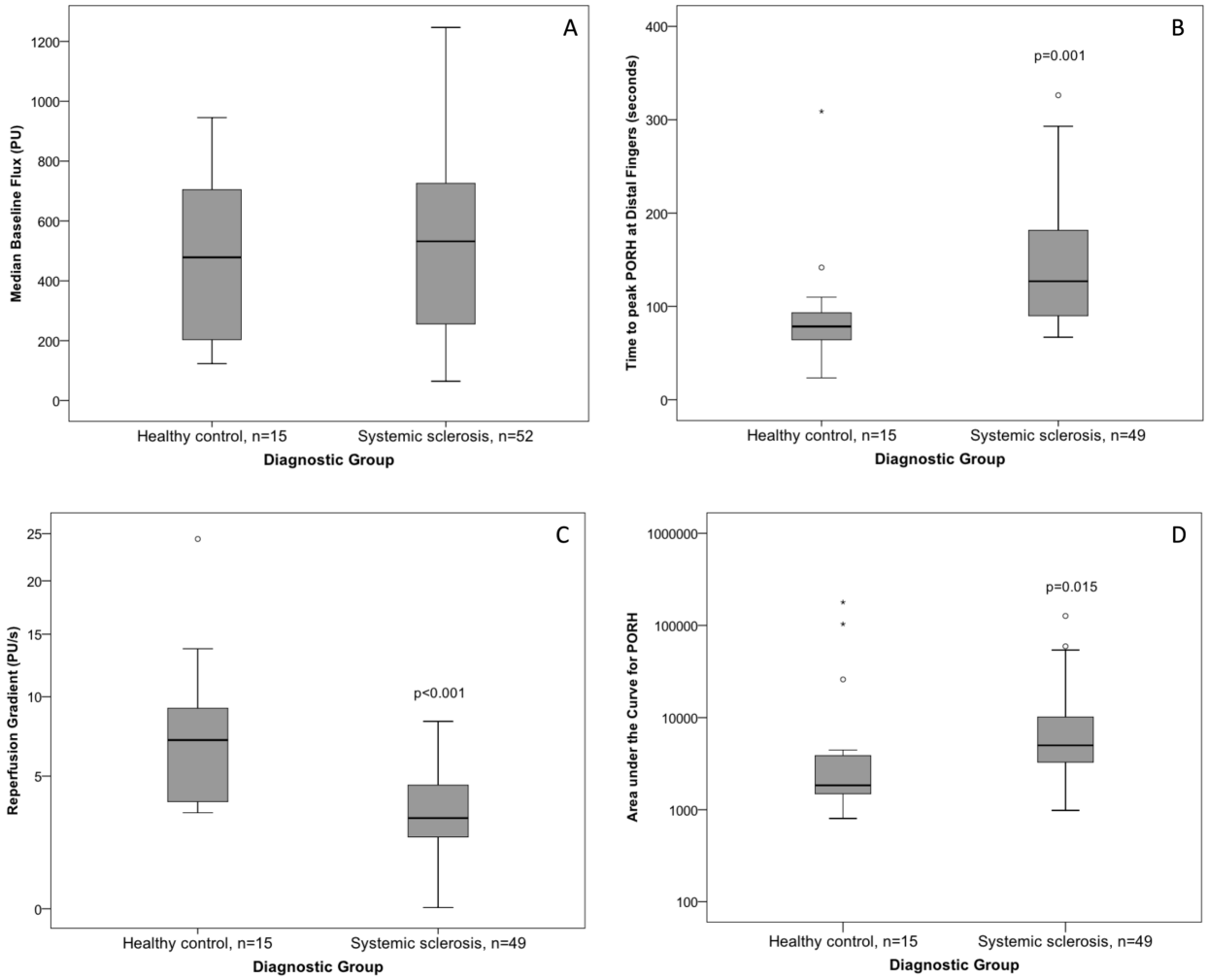

4.3.2.1 Impaired perfusion and PORH kinetics in SSc-DU

Despite similar baseline flux between SSc and controls, within the SSc group, those with a history of DU (n=16) had significantly reduced perfusion at baseline compared to those without SSc-DU (n=34) (median 406.5 [133.8-633.8] versus 654.0 [382.0-873.6], p=0.011) (Figure 4.2). In addition, LSCI demonstrated a significant reduced peak PORH response in SSc-DU compared to SSc without DU history (median 649.2 [237.4-711.1] versus 895.2 [709.8-1085.2], p=0.001). Coupled with a non-significant trend towards

an increased time to reach peak PORH (median 171.3 [105.5-203.3] versus 108.1 [71.8-171.2], p=0.075), there was a significantly reduced reperfusion gradient after ischaemic challenge (median 2.5 [1.5-3.3] versus 3.3 [2.5-5.1], p=0.027) in patients with a history of SSc-DU compared to SSc without DU history (Figure 4.2).

Figure 4. 2 Peripheral perfusion and PORH kinetics in SSc-DU.

Significantly impaired distal finger perfusion in SSc with a history of digital ulcers is demonstrated at baseline compared to SSc without DU (A). Impaired functional vascular response to ischaemic challenge is observed in: (B) the reduced median peak PORH, (C) reduced reperfusion gradient following ischaemic challenge. (D) The difference in flux between the distal fingers and the dorsum of the hand (distal-dorsal difference, DDD) is seen both at baseline (white) and at peak PORH (grey). Statistical significance demonstrated using Mann-Whitney U. Data are sub-analysis of SSc patients from overall cohort.

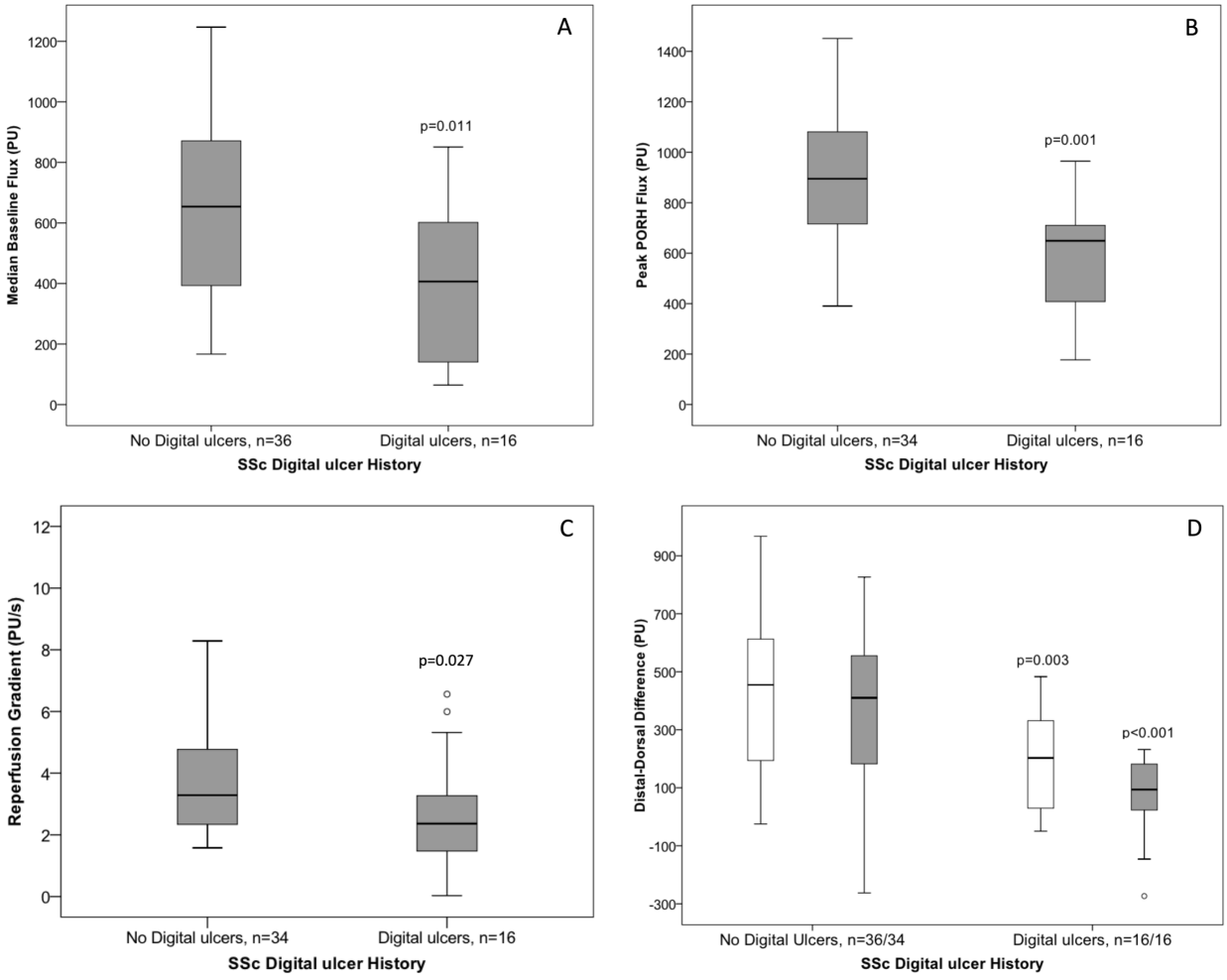

We calculated a distal dorsal difference (DDD) from the flux at the distal fingertips compared to that at the dorsum of the hand. No difference was

noted either at baseline or at the point of peak PORH response between SSc and controls (median 314.2 [110.1-483.4] versus 320.8 [70.2-558.7], p=0.904 and 182.4 [62.2-411.6] versus 374.2 [113.3-562.8], p=0.101 respectively). However, there was a significant reduction in the DDD both at baseline (median 202.8 [19.8-335.0] versus 454.9 [189.1-639.9], p=0.003) and peak PORH (median 93.9 [20.6-181.7] versus 410.1 [180.4-555.3], p<0.001) in those with a history of SSc-DU compared to SSc without DU (Figure 4.2). A contributing factor towards a reduced baseline DDD was a trend towards a reduced baseline flux over the back of the hand in SSc-DU compared to no DU (median 140.3 [116.2-300.8] versus 195.9 [160.9-231.4], p=0.057), possibly indicating evidence of vasculopathy extending more proximally (i.e. more severe) in those patients susceptible to DU disease.

There were no significant differences between lcSSc and dcSSc or early and late SSc and no correlation with disease duration for any LSCI parameter at the distal fingers (data not shown).

4.3.3 Systemic sclerosis specific structural microvascular changes at the nailfold

4.3.3.1 Qualitative assessment of NC abnormalities

All healthy controls were given an overall NC classification of either structurally normal (n=12) or non-specific changes (n=3). In contrast, only 2 participants with SSc were considered to have normal NC (Pearson's Chi-squared for normal versus abnormal NC, χ^2 p<0.001) (Figure 4.3). There was no significant association between overall NC pattern and SSc-DU history (χ^2 for early NC p=0.135, active NC p=0.372, late NC p=0.311, any pattern p=0.323) although the active and late NC pattern appeared to be more frequent (Figure 4.4).

Figure 4. 3 Nailfold capillaroscopy classification.

The number of participants for each diagnostic group, classified according to overall worst nailfold capillaroscopy (NC) pattern across 3 fingers are shown. The majority of healthy controls (n=12/15) exhibited normal pattern NC compared with few SSc (n=2/53), (Pearson's Chi-squared for normal versus abnormal NC, χ^2 <0.001). Percentages represent proportion of the diagnostic group with respective NC patterns.

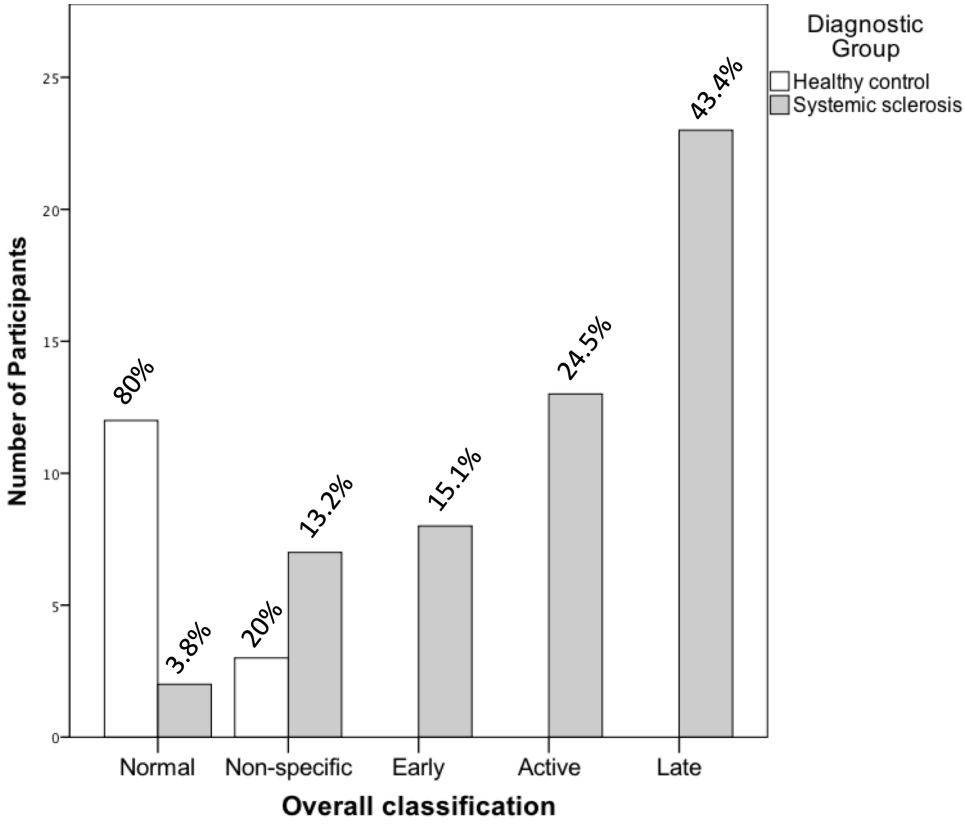

Figure 4. 4 Nailfold capillaroscopy classification in SSc-DU.

No significant association was noted for the NC classification in SSc participants with and without a history of digital ulcers, (Pearson's Chi-squared, χ^2 p=0.323). Normal, non-specific and early NC patterns did appear to be less frequent in the SSc-DU with proportionally more SSc-DU participants having active or late NC patterns. Percentages represent proportion of the NC group assigned to SSc-DU or no DU. Data are sub-analysis of SSc patients from the overall cohort.

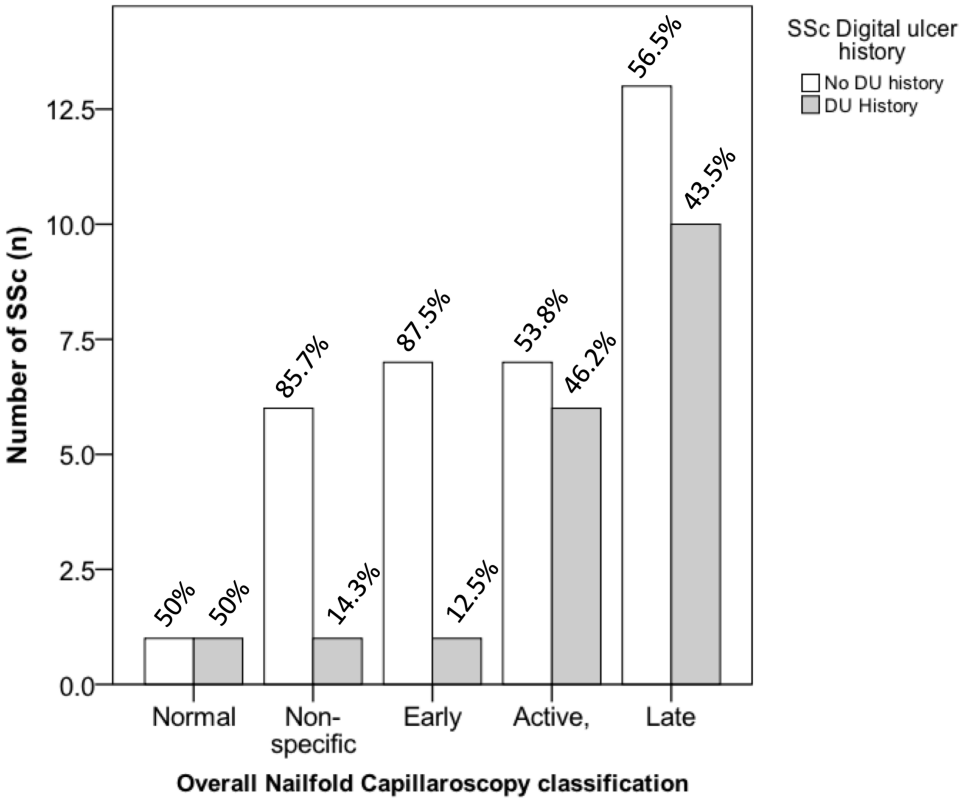

In the SSc group, disease duration was significantly longer in those with NC pattern classified as being late versus active or non-specific only (overall classification, Figure 4.5). Interestingly, there was not a progressive increase in median disease duration with progressive NC patterns, which may be due to small numbers in each group as well as treatment effect. Indeed, there was also a trend for those with more advanced NC patterns to be using more vasodilators (Table 4.1).

Figure 4. 5 Median disease duration for SSc group according to overall qualitative NC classification.

Statistically significantly longer disease duration is seen in those classified as late compared to non-specific and active patterns. Statistical significance by Kruskal-Wallis testing demonstrated an overall p=0.006. Individual p values (post hoc Dunn test) are illustrated in Figure.

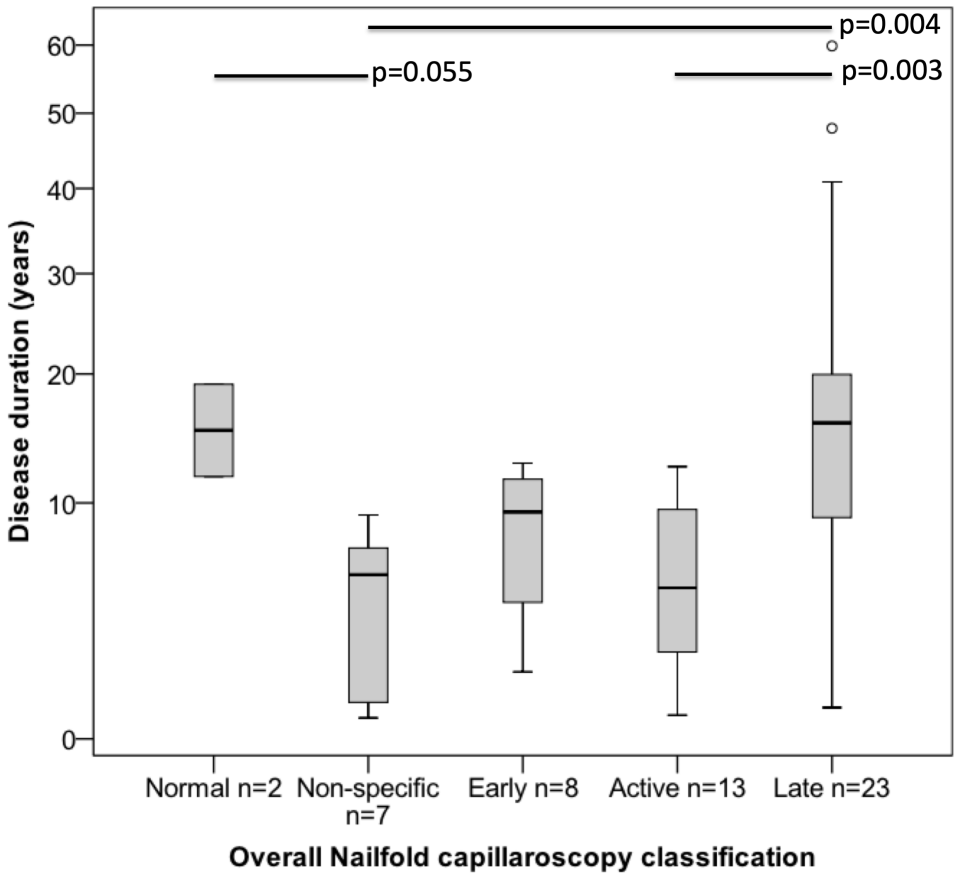

Table 4. 1 Vasodilator use according to overall nailfold capillaroscopy pattern in SSc.

The use of vasodilators in SSc is shown according to nailfold capillaroscopy pattern. There was a trend for those with more advanced NC patterns to be taking more vasodilators. Similarly, only patients with more advanced NC patterns were taking 4 vasodilators. Statistical analysis by Pearson's Chi squared, χ^2.

	No. of SSc taking vasodilators (n.)	**Nailfold Capillaroscopy pattern n. (%)**					
		Normal	Non-specific	Early	Active	Late	**p value (χ^2)**
Total, n.	53	2	7	8	12	23	-
No. of prescribed vasodilators, n.							
0	18	1 (50)	2 (28.6)	7 (87.5)	1 (8.3)	7 (30.4)	
1	21	0 (0)	5 (71.4)	0 (0)	7 (58.3)	9 (39.1)	
2	11	1 (50)	0 (0)	1 (12.5)	4 (33.3)	5 (21.7)	
4	3	0 (0)	0 (0)	0 (0)	1 (8.3)	2 (8.7)	0.055
PDE-5	8	1 (50)	0 (0)	0 (0)	3 (25)	4 (17.4)	0.257
ERA	3	1 (50)	0 (0)	0 (0)	0 (0)	2 (8.7)	0.051

4.3.3.2 Quantitative assessment of NC abnormalities

Individual NC parameters were subsequently compared between study groups. Participants with SSc had significantly reduced overall mean capillary number per 1000μm (median 5.1 [4.1-6.3] versus 8.3 [7.9-8.6], $p<0.001$) and accordingly increased overall mean inter-capillary distance (202um, [160.5-258] versus 121um, [116-127], $p<0.001$) compared to healthy controls, reflecting capillary loss associated with SSc related vasculopathy (Figure 4.6). Consistent with our qualitative analyses, SSc participants with a history of DU demonstrated significantly fewer capillaries per 1000μm (median 4.5 [3.2-5.9] versus 5.9 [4.9-7.5], $p=0.012$) and increased overall mean inter-capillary distance compared to SSc without a history of DU (median 234um [174.5-337] versus 169um [136-210.5] respectively, $p=0.01$) (Figure 4.6).

Figure 4. 6 Reduced inter-capillary distance associated with SSc.

Systemic sclerosis related peripheral vasculopathy is demonstrated with respect to the highly significant reduction in mean number of capillaries at the nailfold (across 3 digits) in (A) SSc versus controls and (c) SSc-DU versus no DU history. The ensuing increased inter-capillary distance is demonstrated (B, D respectively). Statistical analysis of medians of the mean by Mann Whitney-U.

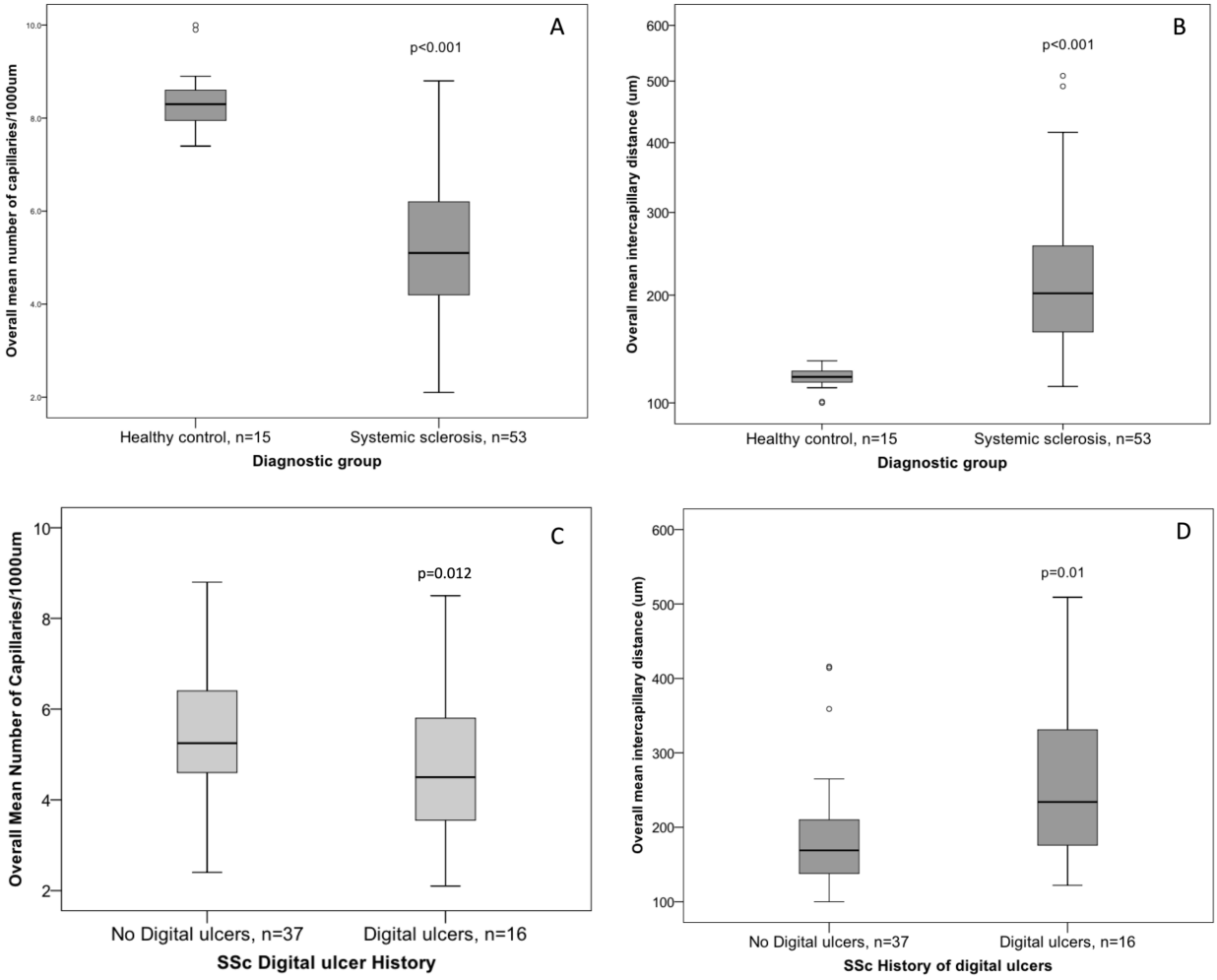

There was no significant difference between either lcSSc versus dcSSc or early versus late disease with respect to individual nailfold capillaroscopy parameters (Mann-Whitney U, data not shown). However, overall mean inter-capillary distance did correlate weakly with disease duration (Spearman's Rho +0.304, p=0.032).

4.3.4 The relationship between functional and structural vascular impairment in systemic sclerosis

There was no significant difference in baseline finger perfusion between NC patterns in SSc (median, early NC 624.4 [226.2-835.6] versus active NC 488.0 [231.6-806.8] versus late NC 504.1 [226.2-670.0], p=0.882 Kruskal-Wallis) (Figure 4.7).

However, there were notable differences in reperfusion kinetics after an ischaemic challenge in SSc. There was a trend for an increase in the time to reach peak PORH (median time for early NC 84.8, [5.7-104.6] versus active 118.3 [94.0-217.0] versus late 146.3 [103.4-189.5], p=0.096, respectively) and reduced peak PORH (median for early 880.3 [616.2-1017.0] versus active 651.4 [431.2-1246.2] versus late 700.8 [519.4-849.8], p=0.202, respectively), with a resultant reduction in reperfusion gradient (median gradient for early NC 4.5 [3.4-5.3] versus active 2.5 [2.0-6.0] versus late 2.6 [1.8-3.4], p=0.104) across progressive NC patterns (Figure 4.7). Baseline DDD (median for early NC 426.4 [70.0-630.1] versus active 280.4 [29.7-639.1] versus late 204.0 [106.9-451.0], p=0.648, respectively) and DDD at peak PORH (median for early NC 204.6 [104.4-488.1] versus active 181.7 [68.9-666.8] versus late 180.4 [37.7-333.8], p=0.202) both progressively reduced across NC patterns also, which was due to a reduction in perfusion at both the fingers and the back of the hand reflecting worse perfusion at more proximal sites with more advanced NC pattern (Figure 4.7).

Figure 4. 7 Changes in Finger Perfusion across Nailfold capillaroscopy classification.

Progressive changes are shown in distal finger perfusion (mean across 2nd-5th digits) across SSc-specific nailfold capillaroscopy patterns (overall classification). Significance using Kruskal-Wallis p value indicated (brackets, legend text). Individual comparison p values (comparator lines in Figure) demonstrate post-hoc Dunn test. There is a trend towards reduction in (A) baseline perfusion (p=0.882) and (B) peak PORH (p=0.162) and significant reduction in (D) reperfusion gradient (p<0.001) across SSc specific NC patterns. Similarly, there is an increase in (C) time to peak PORH (p=0.001) and (E) PORH area under the curve (AUC) (p=0.059). (F) Baseline distal-dorsal difference (DDD) (white, p=0.0863) and DDD at peak PORH (grey, p=0.282) progressively reduce across the NC patterns due to a reduction in the perfusion both at the distal fingers and the at the back of the hand.

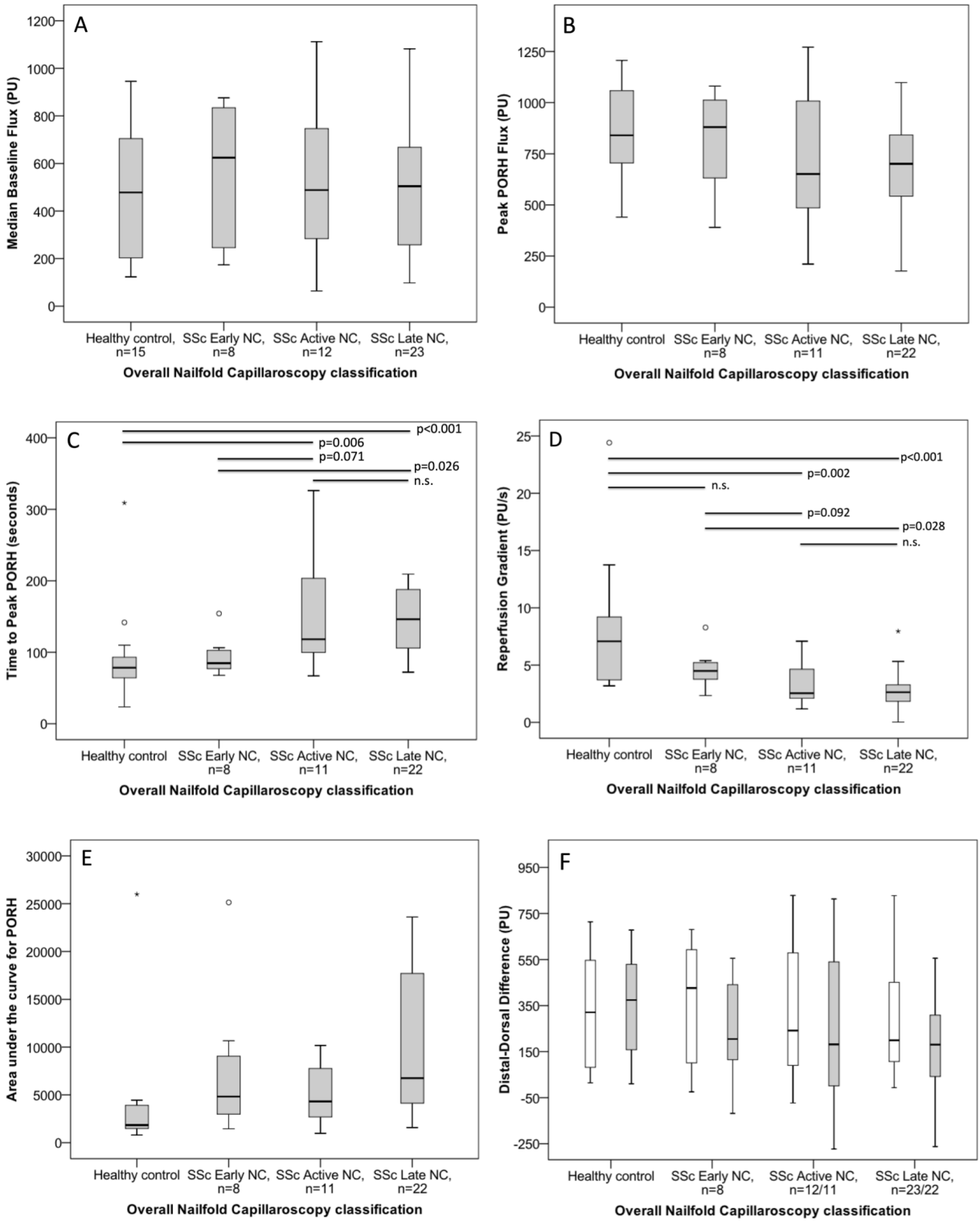

A number of LSCI and NC parameters demonstrated significant correlations for the overall study cohort (all participants) and SSc group (Table 4.2). For the overall study cohort, all correlations with the mean number of capillaries and in turn the mean ICD demonstrated that in the presence of capillary loss there is impaired vascular response to an ischaemic event such that there is reduced peak PORH, increased time to reach peak PORH, slower rate of reperfusion (reperfusion gradient) and reduced DDD at peak PORH. There were no significant correlations with ICD for the overall cohort at baseline, which may be due to vasodilator use in the disease group. The reperfusion gradient demonstrated the strongest correlations with ICD (followed by the time to peak PORH) which suggests the rate of reperfusion capacity is more dependent on the number of capillaries than the absolute maximum perfusion.

In the SSc only group, ICD had a weak negative correlation with the DDD at baseline. Significant positive relationships with ICD were noted with peak PORH and the reperfusion gradient in SSc (Table 4.2). In comparison to the overall study cohort, there were no significant relationships between ICD and time to peak PORH or DDD at peak PORH in SSc.

The presence of giant capillaries in SSc also related to reduced baseline perfusion, peak PORH response and DDD at peak PORH, which reflects that seen in Figure 4.7. This may be due to the association of giant capillaries with reducing capillary number or may suggest that giant capillaries themselves contribute to vascular dysfunction. There were no correlations between the number of haemorrhages, enlarged (but not giant)

capillaries or neovascularisations and LSCI parameters in SSc (data not shown).

Table 4. 2 Correlation between functional vascular kinetics and structural nailfold capillary changes.

*p<0.05, **p≤0.01 using Spearman's Rho. Abbreviations: AUC, area under the curve; DDD, distal-dorsal difference; PORH, post occlusive reactive hyperaemia.

LSCI parameters	**Nailfold Capillaroscopy parameters (mean)**					
	Overall cohort (SSc+HC)		**Systemic sclerosis**			
	No. of Capillaries/mm	ICD (μm)	No. of Capillaries/mm	ICD (μm)	No. of Giant capillaries	No. of Neovascularisations
Baseline						
Subgroup total, n.	67		52			
Median baseline	+0.120	-0.135	+0.206	-0.240	**-0.305***	-0.054
DDD at baseline	+0.208 (p=0.091)	-0.216 (p=0.079)	+0.261 (p=0.062)	**-0.282***	**-0.290***	-0.028
PORH kinetics						
Subgroup total, n.	64		49			
Peak PORH	**+0.336****	**-0.347****	**+0.308***	**-0.320***	**-0.327***	+0.022
Time to peak PORH	**-0.414****	**+0.419****	-0.227	+0.235	-0.026	+0.167
Reperfusion gradient	**+0.551****	**-0.550****	**+0.420****	**-0.399****	+0.065	-0.032
AUC	-0.245 (p=0.051)	**+0.254***	-0.069	+0.073	+0.058	+0.069
DDD at peak PORH	**+0.318****	**-0.328****	+0.226	-0.233	**-0.338***	+0.022

4.3.5 The Relationship between peripheral vasculopathy and PROMs

There were no correlations between PROM instrument endpoints and LSCI (Spearman's Rho, data not shown).

Significant moderate associations were found between each of the mean number of RP attacks per day (Spearman's Rho +0.403, p=0.007), the mean daily RP duration (Spearman's Rho +0.427, p=0.004) and Raynaud's physician's score (Spearman's Rho +0.342, p=0.009) with the mean overall number of haemorrhages per digit only. No significant correlation was identified with other NC parameters or the patient RCS.

4.4 Discussion

4.4.1 Systemic sclerosis exhibits reduced peripheral vascular kinetics in response to functional ischaemic challenge

In our SSc cohort there was no difference in baseline LSCI perfusion of the distal fingers compared to controls, which is in conflict with previous LSCI studies reporting reduced (61, 62, 105, 366) or even increased baseline perfusion (88). This may be in part due to variations in methodology with different focal anatomical regions of the hand and fingers examined or volar versus dorsal presentation. Most notably however, the studies reporting a reduced baseline perfusion in the disease group protocolled a drug washout phase of some (366) or all (61, 62, 105) vasodilator drugs prior to study investigations. Indeed, the only study permitting concomitant use of vasodilators during study assessment reported a surprising increase in baseline perfusion in SSc (88), which is similar to our non-significant trend. We therefore conclude from the literature pool that SSc do have reduced baseline finger perfusion but that vasodilator use can abrogate this at

ambient temperatures (with encouraging implications for the potential efficacy of vasodilator medications in SSc).

Despite the concurrent use of vasodilators, we have demonstrated for the first time with LSCI that there is a reduced rate of reperfusion in SSc reflecting the impaired recovery response following a period of ischaemia. This compliments the findings of reduced peak PORH (61, 89) and increased time to reach peak PORH in SSc compared to controls that others have demonstrated (61, 89).

A DDD of greater than -1°C difference on infrared thermography between the fingers and dorsum of the hand has previously been reported as a differentiating tool between primary and secondary RP (367). We did not observe a significant difference in DDD between SSc and healthy controls with LSCI as demonstrated by previous studies either at baseline (61, 105) or after ischaemic challenge (using arterial occlusion) (61). Vasodilator use may have contributed to this. LSCI and IRT also measure different aspects of tissue perfusion. Whereas LSCI primarily measures microangiopathy, skin temperature recorded by IRT is considered an indirect measure of macro- and microvascular perfusion of the skin. This may suggest that the specific thermal gradient described by the DDD in SSc-RP is partly due to macrovascular disease which we did not examine in out cohort. Indeed, we did demonstrate a reduced DDD at baseline and peak PORH in SSc-DU, a group with which macrovasculopathy has been associated in other studies (130, 131, 133).

This study has further clarified the nature of functional vascular impairment in SSc overall using a PORH assessment. However, there are mixed reports

with regard to SSc sub-groups. As for our data, no difference in LSCI perfusion was noted by Della Rossa et al., (88), between lcSSc and dcSSc subtypes. In contrast to this, some groups have shown less severe reduction in volar hand perfusion in lcSSc than dcSSc (62) where others reported reduced finger perfusion dcSSc versus lcSSc (105, 366). Similarly, it has been reported that reperfusion dynamics are comparable between early and late SSc in one study (88) and progressively impaired with increasing disease duration, from VEDOSS to established SSc in another by the same author (90). Little conclusion can therefore be drawn from these contrasting reports.

Della Ross et al., reported that several of the altered vascular kinetics discussed herein are more severe in SSc-RP than PRP (88). Given the limited number of studies available for these specific comparisons, an extension of our study to include both VEDOSS and PRP as additional comparator groups would be of interest.

4.4.2 Microvascular loss at the nailfold is associated with systemic sclerosis related digital ulceration

The appearances of SSc-specific changes at the nailfold are visually striking to even the untrained eye. However, a significant limitation of Nailfold capillaroscopy is that the most robust method of analysis that incorporates all of the microvascular features is qualitative/semi-quantitative and open to inter-observer variation. Quantification of individual parameters such as haemorrhages or giant capillaries for clinical correlation is limited due to these predominantly occurring in the active phase and thus the absolute numbers of these features do not distinguish early from late patterns, and is a feature that has limited the application of the CSURI composite index for

DU risk (368). We suggest that capillary number and in turn ICD are therefore potentially the most useful parameter for comparison.

In line with previous reports, our cohort ICD was increased in our SSc cohort (109) and more so in SSc-DU (107, 108, 131, 369). We identified a weak correlation between disease duration and ICD which has been positively reported by some (370) and a specific lack of relationship reported by others (108). Additionally, our cohort had longer disease duration in those classified as late NC pattern compared to some other NC classifications. Other studies have implied such an association through reference to progression of NC patterns in longitudinal studies (95, 116). The variation in reports may be a consequence of treatment effect such that capillary number at the nailfold improves with ERA therapy (371-373) as well as Botulinum induced vasodilation (374).

We did not however, identify any difference between individual NC parameters between SSc subtypes or autoantibody status. In contrast, others have reported more severe grading of capillary loss in diffuse disease (118) as well as more severe NC changes in RNAPIII+ SSc and Scl70 that tend to associate with dcSSc than ACA (118).

4.4.3 Microvascular dysfunction worsens with progressive structural vasculopathy

We have described a progressive impairment of the functional PORH reperfusion response to ischaemia with progressive NC patterns. We describe for the first time a correlation between reperfusion gradient following an ischaemic challenge and capillary density on NC, which compliments previous reports of the respective relationship with peak PORH (88, 90).

Similarly, the increased time to peak PORH and reduced reperfusion gradient across NC classifications presented in this chapter has not be described previously. The strong trend for reduced peak PORH in our cohort is in line with data from Della Rossa et al., (90).

We found fewer notable LSCI results at baseline however, which was surprising. Previous published data has described the relationship between baseline LSCI perfusion and NC (62, 105, 366, 375), with a progressive reduction in finger perfusion with progressive NC changes (significance achieved for early vs late only (62, 366) and reported as overall Kruskal-Wallis comparison (105, 375)), which is in line with our data trend. Ruaro et al., (105) further support this relationship through a negative correlation between baseline perfusion and capillary number, a significant association that we did not observe in our cohort. Alternative laser methods such as LDF examined by the same group, further confirm this principle with significant reduction in hand perfusion in early and active NC versus late (62) and early versus active and late (122). Ruaro et al., (105) also specifically found reduced periungual perfusion between NC patterns (reported as overall Kruskal-Wallis significance only). A notable difference in the methodology of these studies was a washout of some or all vasodilators for 1 month before the study assessments, which may account for our lack of significant findings. Indeed, Della Rossa et al., (88) had a high proportion of vasodilator use in their SSc cohort and like us did not find a significant difference in baseline perfusion between NC patterns.

4.4.4 Structural and functional vasculopathy is attenuated in digital ulcer disease

Collectively, the data discussed above demonstrates impaired and progressive tissue perfusion in SSc that from a clinical point of view may lead to tissue compromise and digital ulceration. Peripheral digital perfusion at ambient temperatures is more severely impaired in SSc-DU as described using LDF and LSCI previously (62). We report for the first time using LSCI a reduction in DDD at baseline in SSc-DU. We also report novel findings of impaired vascular kinetics with a reduced peak PORH, reperfusion gradient and DDD at peak PORH compared to SSc without DU.

The significant relationship between ICD and peak PORH suggest that in the presence of structural microvascular changes, there is a reduced capacity for vascular reperfusion after an ischaemic event. In clinical terms, this means that in patients who have worse NC changes may have worse recovery after a RP attack which may contribute to a greater risk of tissue damage in the form of DU. Alternatively, it may be that increased capillary drop out results in more profound irreversible tissue ischaemia and acts as a barrier to successful PORH (due to lower possible cutaneous perfusion). This can be linked with both our data showing an association with a greater increase in ICD in SSc-DU as well as an association between a history of DU in patients with late NC changes in the literature (107, 108, 110, 111, 272).

We have found a novel and interesting negative association between giant capillaries and baseline perfusion, peak PORH and respective DDDs. Whilst our correlations are weak, there are previous reports demonstrating that in the presence of enlarged nailfold capillaries there is reduced hand

temperature on IRT (106) and increased risk of digital ulcers (112). As such, we conclude that these associations are likely linked by reduced tissue perfusion and reperfusion responses after RP ischaemic attacks (Figure 4.8).

Figure 4. 8 Proposed relationship between structural capillary changes and digital ulcer risk through microvascular dysfunction.

Figure created by VF using study images.

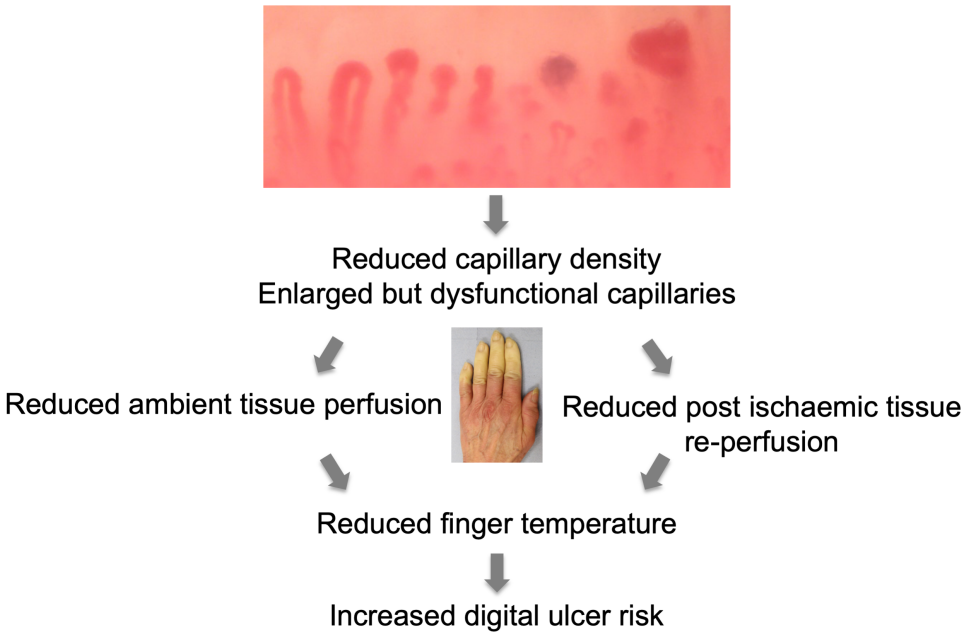

4.4.5 Patient-reported outcome measures poorly reflect peripheral vasculopathy

As for previous published data from local colleagues (351), PROM for SSc-RP did not correlate well with LSCI data in our study. With respect to NC, PROM from the RP diary only correlated modestly with the number of haemorrhages and therefore we again conclude that existing PROMs are likely influenced by other aspects of digital vasculopathy and health beliefs beyond digital perfusion. Whilst PROMs such as the RCS diary are the preferred method for assessing the impact of peripheral vasculopathy in SSc (73), the poor convergent validity of with objective quantitative and qualitative assessment of digital structure and function is concerning. The RCS diary has limitations. For example, it fails to capture all of the patient interventions

undertaken in order to minimize their RP attacks coupled with the difficulty that patients often have in defining ‘a single RP episode’ (69, 70, 376). Such limitations of the RP diary may have contributed to recent negative clinical trials of promising vasodilator therapies where placebo appeared to have better outcomes than the active treatment arm (201). Work is currently underway by the scleroderma clinical trials consortium to establish a new PRO instrument that aims to better capture the severity and patterns of SSc-RP that may be utilised in clinical trials.

4.4.6 Concluding remarks

Our results shed light on the complex relationship that exists between the structural and functional vasculopathy of SSc. We have shown for the first time that the PORH recovery responses to ischaemia are poorer in those with SSc-DU. The RCS diary and other PROM instruments are not concordant with the severity of SSc peripheral vasculopathy assessed using objective assessment of the microvasculature using LSCI and NC.

Chapter 5. The role of high frequency ultrasound in assessment of systemic Sclerosis-related vasculopathy

5.1 Introduction

We have demonstrated the differentiation of vascular kinetics and microvascular structure between SSc and healthy subjects (chapter 4). As discussed in chapter 1.5.8, a disadvantage of both NC and LSCI is that their use is limited to specialised rheumatology centres. Data from NC in particular may be degraded by image quality (377). Formal data analysis of each can also be time consuming. In contrast, ultrasound is a readily available apparatus in every hospital. There are a small number of studies in the literature applying ultrasound to the study of SSc vasculopathy and examine both microvascular and macrovascular disease through an assortment of specific methodology. Ultrasound differentiates primary from secondary RP through assessment of macrovascular occlusion of palmar digital arteries (378, 379). It also identifies macrovascular changes in SSc associated with finger (130, 133) and lower limb ulceration (380). It has also been used to assess erectile dysfunction in SSc males (381). Only two studies have evaluated the potential role of ultrasound in quantifying microvascular pathology in SSc (65, 131) (Table 5.1). One of these studies used small SSc numbers and a mixed cohort including other connective tissue disease diagnoses, and both studies utilised ultrasound frequencies below 15 MHz (Table 5.1). Only one study examined the relationship of ultrasound with NC and SSc-DU. To date there has been no published data to validate

vascularity on ultrasound against other imaging applications of microvascular perfusion or PROMs. Further SSc specific study using higher frequency ultrasound is therefore warranted.

HFUS applications are continually evolving and upgrading to provide superior assessment. ‘Superb Microvascular Imaging’ with colour overlay (cSMI) is a novel HFUS application using colour doppler imaging but with added proficiency of being able to remove low level tissue artefact from vessel walls whilst still reporting low frequency echoes reflected by areas of lower blood flow (typically in microvascular capillary beds) (382). It also utilizes high frame rates for more accurate reporting of flow (382). cSMI technology therefore has potential to provide useful information about the microvasculopathy in SSc.

Table 5. 1 Summary of studies utilising ultrasound to investigate microvascular pathology in SSc.

Abbreviations: CDU, colour Doppler ultrasound; CTD, Connective tissue diseases; PRP, Primary Raynaud's phenomenon; SLE, Systemic Lupus Erythematosus; SRP, secondary Raynaud's phenomenon.

Studies examining the use of Ultrasound to investigate microvasculature in systemic sclerosis				
Study & purpose	**Sample size**	**Exclusions**	**Methodology**	**Main findings**
Keberle et al., 2000 (65) Cross sectional study using peripheral microvascularity and functional response to thermal challenges to differentiate between HC, PRP and SRP	n = 60 15 HC 10 PRP 35 CTD 18 SSc 17 SLE	Exclusions included smokers and concurrent vasoactive medications	Sonoline Elegra advance colour doppler ultrasound 9-12 MHz performed before and after cold and warm functional challenge on 2nd & 3rd finger.	• Baseline vascularity showed SRP < PRP = HC. • Baseline vascularity showed SSc < CTD without skin lesions. • Vascularity after cold stress PRP = SRP < HC. • After warming vascularity HC > CTD without skin lesions > SSc.
Schioppo et al., 2019 (131) Cross sectional study examining the association between a history of digital ulcers and microvascular (and macrovascular) changes in the finger.	n = 106 SSc 93 LcSSc	None specified	Esaote MyLab power doppler ultrasound, 14.3 MHz 3rd & 4th finger pulp and nailbed of the dominant hand examined.	• Finger pulp and nailbed vascularity were reduced with reducing nailfold capillary number. • Odds ratio (n.s.) suggested reduced vascularity in SSc-DU.

5.1.1 Chapter hypothesis, aims and objectives

We hypothesised that HFUS with cSMI application is a useful tool for assessment of SSc peripheral vasculopathy. The principal aim of this chapter was therefore to assess the relationship between novel HFUS cSMI application in the assessment of digital microvascular pathology in SSc against more establish assessment tools. The specific objectives were to assess the convergent validity between digital perfusion on HFUS cSMI with:

1. Baseline and functional microvascular assessment by LSCI
2. Structural microvasculature changes at the nailfold using Nailfold capillaroscopy
3. Patient-reported outcome measures (RP diary and vascular features of the SHAQ).

5.2 Methods

5.2.1 Study population

Healthy controls and SSc participants were recruited as described previously (chapter 2.1).

5.2.2 Microvascular imaging

Participants underwent LSCI, NC and HFUS cSMI as described in detail in chapter 2.5, 2.6 and 2.7 respectively.

5.2.3 Imaging analysis

5.2.3.1 HFUS cSMI image analysis

Vascularity on HFUS was assessed at 3 ROI as previously described (chapter 2.7.3).

5.2.3.2 Nailfold capillaroscopy analysis

Nailfold capillaroscopy was analysed as described chapter 2.6.3. Participants were classified according to the specific NC pattern represented at the middle finger in order to relate to the digit investigated with HFUS cSMI. Similarly, individual NC parameters (e.g. mean number of capillaries per mm) were calculated for the middle finger specifically.

5.2.3.3 LSCI image analysis

LSCI was analysed as described previously in chapter 2.5.4. LSCI parameters discussed in this chapter were calculated for:

- ROI at the distal 3rd finger only (for comparison with the same anatomical location as HFUS) (chapter 2.5.4 Figure 2.1)
    - median baseline (Perfusion Units, PU)
    - peak PORH (PU)
    - time to peak PORH (seconds)
    - reperfusion gradient (ΔPU/s) following an ischaemic challenge
    - area under the reperfusion curve (AUC)
- Overall distal finger average (mean across the distal phalanx of each of 2nd-5th fingers)
    - median baseline (perfusion Units, PU)
    - peak PORH (PU)
    - time to peak PORH (seconds)
    - reperfusion gradient (ΔPU/s) following an ischaemic challenge
    - area under the reperfusion curve (AUC)
- distal dorsal difference demonstrating the perfusion gradient between the distal fingers (average of 2nd-5th fingers) and the dorsal hand.

5.2.4 Statistical analysis

Non-parametric statistical tests were used across all data points. HFUS vascularity indices are reported to the nearest $1x10^3$. Non-parametric statistical analysis of LSCI data compares the group median of the means (median [IQR]). Data displayed as box plots show median (horizontal line), interquartile ranges (box plot) and range (whiskers) with group outliers shown as asterisks and circles.

5.3 Results

Participant demographics are as described in chapter 3.3. Fifteen HC underwent HFUS, LSCI and NC with uninterrupted data available for analysis.

53 SSc were assessed by HFUS and NC. 1 SSc had poor quality images at the middle finger and therefore n=52 when comparisons are made with middle finger NC specifically.

52 SSc had data available for LSCI due to technical failure at the time of study visit for one SSc participant (as discussed in chapter 4.3.1). Baseline LSCI data was available for all of the 52 SSc participants. Movement artefact on LSCI degraded the PORH data quality and reliability for 3 additional SSc participants who were then excluded from PORH analysis (n=49) (as discussed in chapter 4.3.1).

PROMs were returned by SSc participants and available for analysis as follows: Raynaud's diary n=44, SHAQ-RP n=47, SHAQ-DU n=39.

5.3.1 Quantification of systemic sclerosis related vasculopathy on high frequency ultrasound

A significant reduction in the median vascularity of the middle finger on HFUS was only observed at the transverse fingertip view in SSc compared to healthy controls (median 89.3 [80.8-101.0] versus 100.3 [92.5-110.4], p=0.002). It was noted that vascularity (= mean intensity or gray scale of colour pixels within the ROI) does not differentiate small areas of intense vascular flow from larger diffuse areas (Figure 5.1). Therefore the integrated density (hereafter referred to as 'vascularity index', Vi) was calculated as a composite value = mean intensity of red pixels x the total area of the red colour pixels). The Vi at each ROI (dorsovolar DVVi, nailfold NVi, fingertip FVi) are used to report all statistical analysis hereafter and reported to the nearest 1 $x10^3$.

Figure 5. 1 Illustration of vascularity assessment by HFUS with quantification by Image J.

The mean vascularity (mean intensity of the red pixels) and vascularity index at the dorsovolar view (DVVi) at the distal middle finger on HFUS are shown for (A) SSc and (B) healthy control participant. Visually, there is a notable reduction in microvascular flow on HFUS in the SSc compared to the control. Quantification of mean vascularity assigns similar figures to both participants. However, the DVVi provides better differentiation by taking the area of blood flow into consideration. Figure created by VF using study images with participant consent.

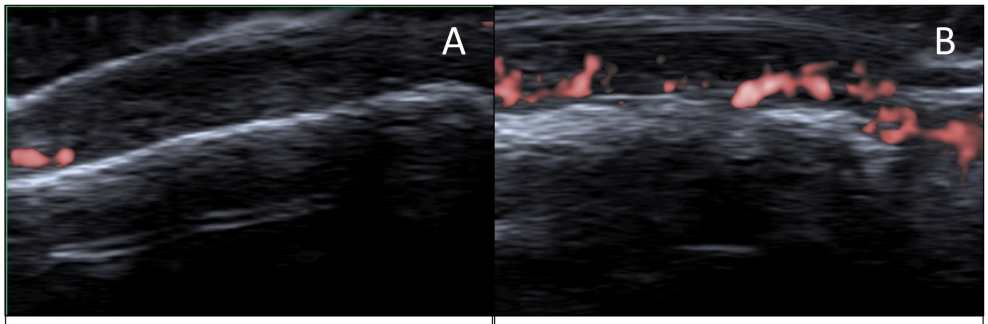

Systemic sclerosis	**Healthy control**
mean vascularity = 118	mean vascularity = 96
DVVi = 99,018	DVVi = 882,904

The Vis demonstrated a significant reduction at all three regions of interest in SSc compared to controls (Table 5.2). Furthermore, despite an increased use of vasodilators in SSc-DU (chapter 3.3.4 Table 3.5), the DVVi and FVi both demonstrated a significant reduction in SSc with a history of DUs compared to those without (Table 5.2 and Figure 5.2).

There was a strong trend towards reduced Vis in lcSSc compared to dcSSc (DVVi median 40 [12-12] versus 124 [60-250], p=0.06; NVi median 76 [21-205] versus 185 [51-530], p=0.067; FVi median 74 [49-267] versus 184 [120-413], p=0.179). Late disease was associated with a lower FVi than early SSc (median 76 [48-212] versus 207 [72-410] respectively, p=0.087) but there was no relationship between disease duration and DVVi (median 51 [19-140] versus 55 [15-160], p=0.776), or NVi (median 86 [22-215] versus 122 [20-256], p=0.878) (Table 5.2 and Figure 5.2).

Table 5. 2 Vascularity indices between healthy controls and SSc subgroups.

Statistical significance is illustrated using Mann Whitney-U for SSc versus control, lcSSc versus dcSSc, early SSc versus late SSc and SSc with and without a history of DU. Abbreviations: DVVi dorsovolar vascularity index, FVi fingertip vascularity index, NVi nailfold vascularity index.

Diagnostic group	**Subgroup total, n.**	**DVVi median x10^3, [IQR x10^3]**	**NVi median x10^3, [IQR x10^3]**	**FVi median x10^3, [IQR x10^3]**
Healthy control	15	215 [62-818]	247 [102-551]	618 [176-1103]
Systemic sclerosis	53	**55 [15-141]**	**96 [22-233]**	**85 [50-277]**
p value		**0.002**	**0.01**	**<0.001**
LcSSc	45	40 [12-121]	76 [21-205]	74 [49-267]
DcSSc	8	124 [60-250]	185 [51-530]	184 [120-413]
p value		0.06	0.067	0.179
Early SSc	11	55 [15-160]	122 [20-256]	207 [72-410]
Late SSc	42	51 [19-140]	86 [22-215]	76 [48-212]
p value		0.776	0.878	0.087
SSc History of DU				
Not present	37	110 [27-282]	138 [40-266]	195 [59-490]
Present	16	**40 [8-68]**	38 [21-178]	**52 [32-95]**
p value		**0.015**	0.146	**0.006**

Figure 5. 2 Vascularity indices at the proximal middle finger.

Box plots from left to right: dorsovolar vascularity index DVVi (grey stripe), nailfold NVi (white dots), fingertip FVi (grey). (A) All three Vis are significantly reduced in SSc. (B and C) An additional non-significant trend towards Vi reduction in lcSSc (p=0.06 DVVi and p=0.067 NVi) and late disease (p=0.087 FVi) is also noted. (D) A significant reduction in Vis is noted at all 3 regions in SSc-DU compared to SSc without a DU history. Significance is demonstrated using Mann Whitney-U. Data are re-presentation of Table 5.2.

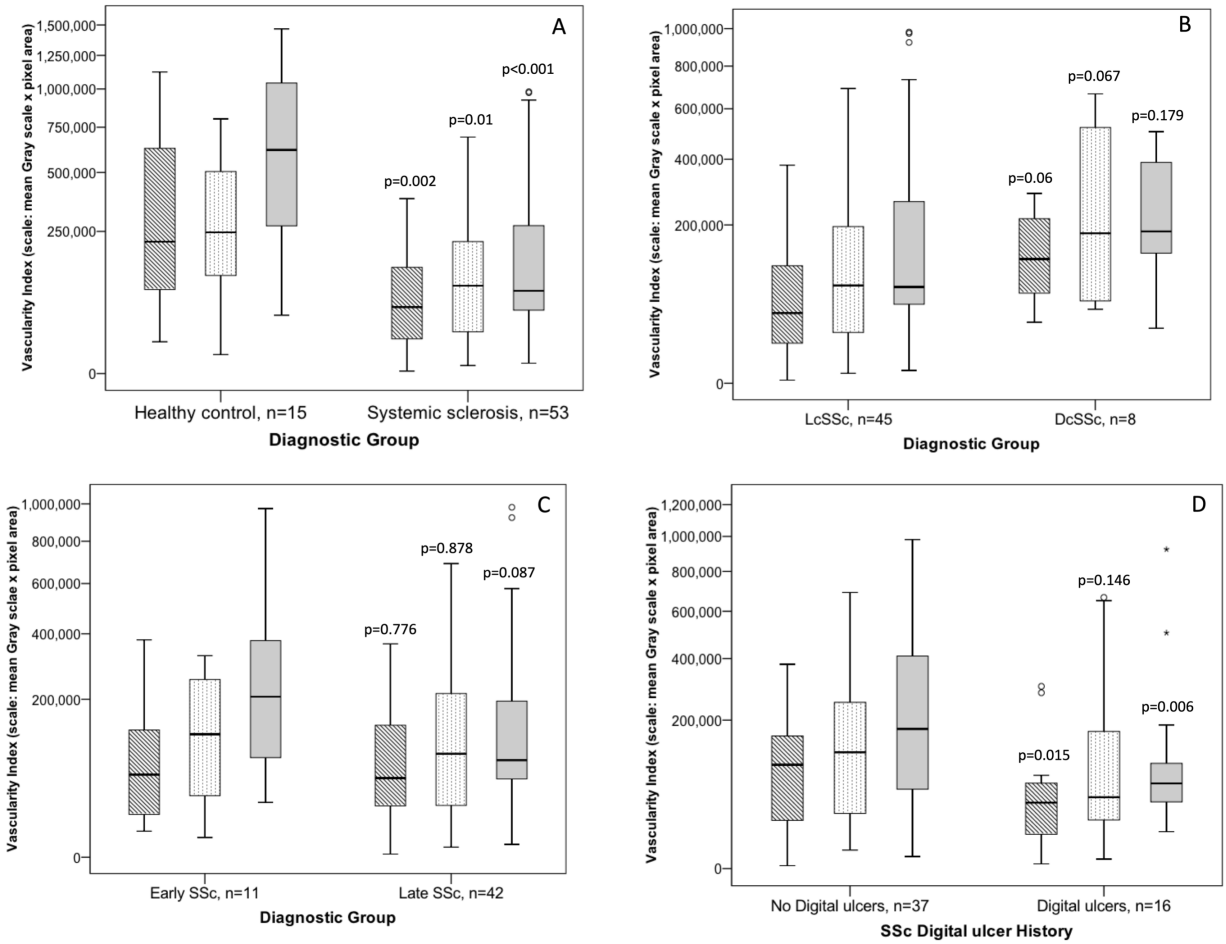

5.3.2 Convergent validity of HFUS vascularity indices with LSCI

Correlation was made between localized flux at the distal middle finger (at the same anatomical location as HFUS) as well as with the overall average of distal finger perfusion. Vascularity indices correlated with finger perfusion on LSCI at baseline and peak PORH across the whole cohort, SSc group alone and lcSSc subtype, with the strongest correlations occurring with the FVi (Table 5.3). Significant correlations were not seen in dcSSc possibly due to

small group size or outliers. No significant correlations were seen with reperfusion gradient or AUC.

Table 5. 3 Correlation of vascularity indices with laser speckle contrast imaging parameters.

*p<0.05, **p≤0.01 using Spearman's rank correlation coefficient. Overall cohort reflects data for SSc + healthy control groups combined.

LSCI parameter	**Dorsovolar vascularity index**				**Nailbed vascularity index**				**Fingertip vascularity index**			
	Overall cohort	SSc overall	LcSSc	DcSSc	Overall cohort	SSc overall	LcSSc	DcSSc	Overall cohort	SSc overall	LcSSc	DcSSc
Mean of distal 2nd-5th fingers												
n.	67	52	44	8	67	52	44	8	67	52	44	8
Median baseline perfusion (PU)	**+0.371 ****	**+0.378 ****	**+0.389 ****	-0.071	**+0.342 ****	**+0.393 ****	**+0.383 ****	+0.381	**+0.533 ****	**+0.638 ****	**+0.703 ****	-0.024
n.	64	49	41	8	64	49	41	8	64	49	41	8
Peak PORH	**+0.487 ****	**+0.413 ****	**+0.472 ****	-0.048	**+0.449 ****	**+0.459 ****	**+0.498 ****	+0.333	**+0.677 ****	**+0.674 ****	**+0.746 ****	+0.143
Reperfusion Gradient	+0.122	+0.026	+0.11	-0.548	+0.093	+0.005	+0.092	-0.5	+0.149	-0.03	-0.007	-0.310
Area under the curve for peak perfusion	-0.129	-0.028	-0.054	0.0	-0.031	+0.016	-0.077	+0.238	-0.001	+0.184	+0.163	+0.310
Distal middle finger only												
n.	67	52	44	8	67	52	44	8	67	52	44	8
Median baseline perfusion (PU)	**+0.400****	**+0.444****	**+0.438****	+0.310	**+0.321****	**+0.411****	**+0.392****	+0.429	**+0.491****	**+0.611****	**+0.641****	+0.357
n.	64	49	41	8	64	49	41	8	64	49	41	8
Peak PORH	**+0.494****	**+0.434****	**+0.499****	+0.024	**+0.436****	**+0.448****	**+0.497****	+0.167	**+0.627****	**+0.635****	**+0.669****	+0.238
Reperfusion Gradient	+0.245 (p=0.05)	+0.185	+0.258	-0.476	+0.119	+0.006	+0.103	-0.548	+0.208	+0.047	+0.083	-0.333
Area under the curve for peak perfusion	-0.099	+0.000	-0.021	+0.214	-0.022	+0.030	-0.053	+0.262	+0.008	+0.194	+0.172	+0.452

5.3.3 The relationship between nailfold capillaroscopy classification and HFUS vascularity indices

NC classification and individual parameters in this section refer to the middle finger specifically. There were significant differences between DVVi, transverse NVi and FVi at the middle finger across one or more NC classifications (Table 5.4). Detailed review of all 3 Vis according to the middle finger NC classification, demonstrated that for each of the SSc-specific NC classifications (early, active and late), Vis were reduced compared to normal NC across most of the study groups and subgroups (Table 5.4 and Figure 5.3 and 5.4). Universal significance was not, however, achieved for each group/subgroup, but most consistently observed for the DVVi.

Vascularity indices were reduced in each of early, active and late NC classifications at the middle finger compared to normal NC for the study cohort overall, SSc group and lcSSc, with significance being achieved most consistently for DVVi.

Table 5. 4 Vascularity indices according to nailfold capillaroscopy classification at the middle finger.

p value using statistical analysis by Kruskal-Wallis is illustrated in the terminal row of the table. p=0.05† and p≤0.01¥ using post-hoc Dunn test versus normal nailfold capillaroscopy classification. p<0.05 *ƒ* using post-hoc Dunn test versus non-specific NC classification. Significant reductions in Vis were noted in some SSc-Specific NC classifications compared to non-specific NC in the overall cohort: DVVi in early (p=0.019) and active (0.017) NC changes, NVi in active (p=0.047), FVi for early (p=0.037) and late (p=0.036) and borderline significance for active (p=0.05).

NC classification of middle finger	**Dorsovolar vascularity index (median x10^3, [IQR])**				**Nailbed vascularity index (median x10^3, [IQR])**				**Fingertip vascularity index (median x10^3, [IQR])**			
	Cohort overall (HC+SSc)	SSc overall	LcSSc	DcSSc	Cohort overall (HC+SSc)	SSc overall	LcSSc	DcSSc	Cohort overall (HC+SSc)	SSc overall	LcSSc	DcSSc
n.	17	4	4	0	17	4	4	0	17	4	4	0
Normal	204 [90-302]	240 [149-302]	240 [149-302]	-	262 [100-564]	278 [31-629]	278 [31-629]	-	397 [98-1014]	123 [14-742]	123 [14-742]	-
n.	13	11	8	3	13	11	8	3	13	11	8	3
Non-specific	145 [35-333]	102 [15-287]	97 [8-303]	145 (55-)	139 [34-249]	122 [21-251]	109 [20-190]	251 [47-]	410 [120-687]	344 [60-448]	340 [53-662]	344 [181-]
n.	9	9	7	2	9	9	7	2	9	9	7	2
Early	**27 [12-49] ¥*ƒ***	**27 [12-49] ¥**	**15 [12-35] ¥**	95 (30-)	124 [32-321]	124 [32-321]	157 [21-324]	82 [44-]	**88 [44-142]†*ƒ***	88 [44-142]	88 [54-174]	64 [24-]
n.	10	10	10	0	10	10	10	0	10	10	10	0
Active	**33 [2-76]¥*ƒ***	**33 [2-76] ¥**	**33 [2-76] ¥**	-	**26 [21-49]¥*ƒ***	26 [21-49]	26 [21-49]	-	**72 [41-312]†**	72 [41-312]	72 [41-312]	-
n.	18	18	15	3	18	18	15	3	18	18	15	3
Late	**58 [24-116]†**	**58 [24-116]†**	**38 [21-110]†**	103 (76-)	98 [26-261]	98 [26-261]	48 [16-216]	539 [62-]	**73 [46-211]†*ƒ***	73 [46-211]	69 [37-182]	187 [171-]
p value (Kruskal-Wallis)	**0.002**	**0.021**	**0.041**	0.790	**0.020**	0.243	0.346	0.291	**0.019**	0.401	0.694	0.133

Figure 5. 3 Vascularity indices across nailfold capillaroscopy classifications in SSc and controls.

Box plots from left to right: dorsovolar vascularity index DVVi (grey stripe), nailfold NVi (white dots), fingertip FVi (grey). (A) the overall cohort (systemic sclerosis and healthy controls combined) and (B) systemic sclerosis alone. Across the whole cohort, DVVi and FVi are significantly reduced in each of early, active and late NC classifications compared to normal NC. Only those classified as active demonstrated significantly reduced Vi for NVi, with an additional trend towards reduction in NVi in early and late compared to normal. Significant reductions in some Vis were also noted in the 3 SSc-specific classifications compared to non-specific NC classification. In the SSc only group, all Vis were reduced in early, active and late compared to Normal NC patterns but significance only achieved with respect to the DVVi. $p<0.05$† and $p\leq0.01$¥ using post-hoc Dunn test. Data are re-presentation of Table 5.4.

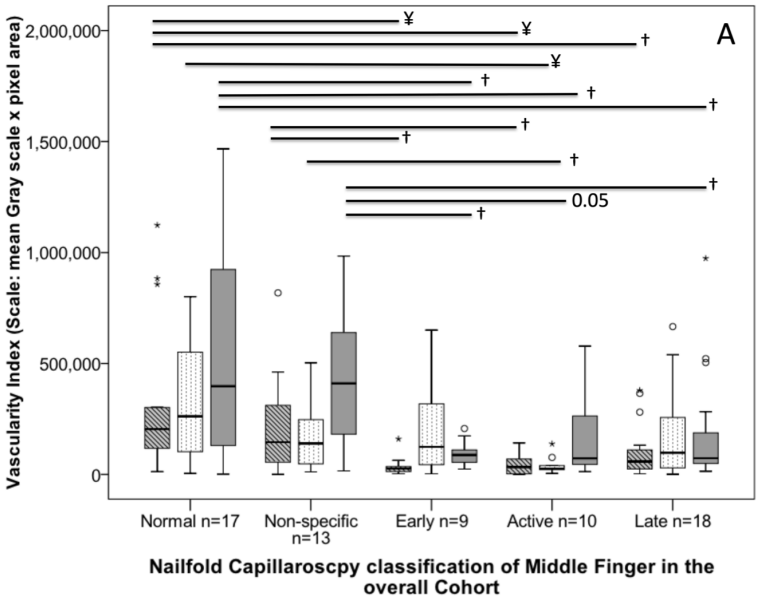

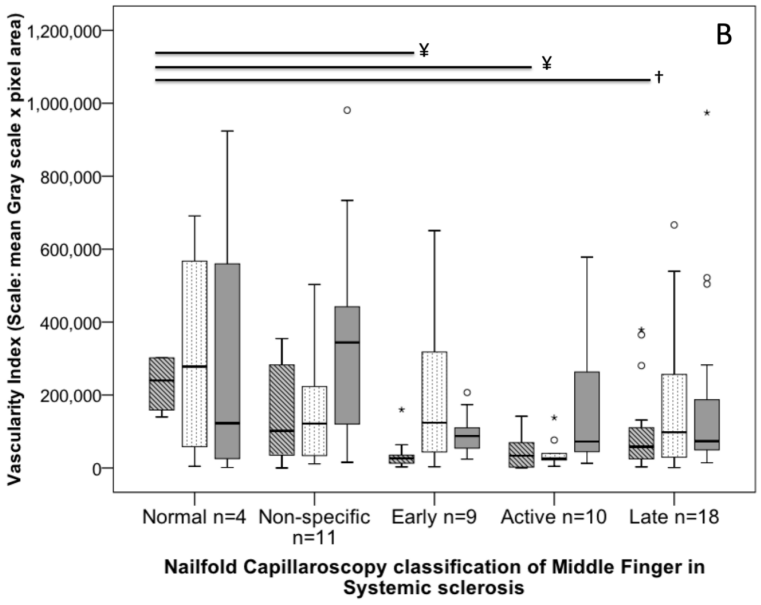

Figure 5. 4 Vascularity indices according to nailfold capillaroscopy classification and disease sub-group.

Box plots from left to right: dorsovolar vascularity index DVVi (grey stripe), nailfold NVi (white dots), fingertip FVi (grey). (A) Vascularity indices across nailfold capillaroscopy classification in lcSSc demonstrate a significant reduction in Vis in each of early, active and late patterns compared to normal NC. (B) No dcSSc patients had normal or active NC classification. No significant differences in Vis were seen in patients with diffuse cutaneous systemic sclerosis across nailfold capillaroscopy classifications. The lack of significance between classifications may be due to small numbers in each group. $p<0.05$† and $p\leq0.01$¥ using post-hoc Dunn test. Data are sub-analysis of SSc from the overall cohort.

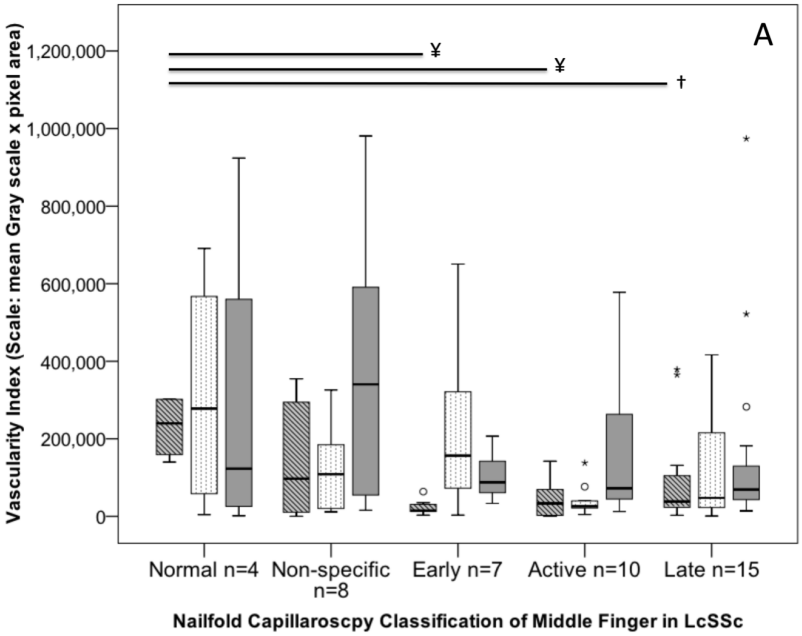

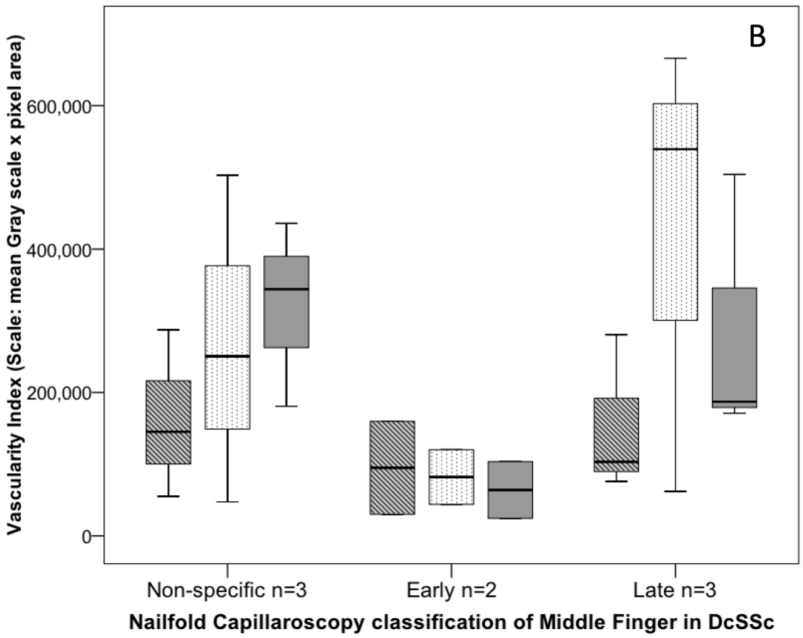

When considering the individual NC parameters, all 3 Vis correlated weakly with overall mean inter-capillary distance, mean number of capillaries per 1000μm and the number of giant capillaries for the combined cohort (HC+SSc). Strong correlations were seen for dcSSc across these parameters also. Due to small numbers, the strength of this relationship should be interpreted with caution. Additional weak correlations were noted for DVVi and NVi for the combined cohort (HC+SSc) for the number of enlarged capillaries which may reflect the association with the active phase during which there is initial capillary loss, (Table 5.5).

Table 5. 5 Correlation of vascularity indices with nailfold capillaroscopy parameters at the middle finger.

*p<0.05, **p≤0.01 using Spearman's Rho.

NC parameters at the middle finger	**Dorsovolar vascularity index**				**Nailbed vascularity index**				**Fingertip vascularity index**			
	Cohort overall (HC+SSc)	SSc overall	LcSSc	DcSSc	Cohort overall (HC+SSc)	SSc overall	LcSSc	DcSSc	Cohort overall (HC+SSc)	SSc overall	LcSSc	DcSSc
n.	67	52	44	8	67	52	44	8	67	52	44	8
Mean inter-capillary distance	**-0.372****	+0.061	-0.177	+0.143	**-0.288 ***	-0.159	-0.181	+0.548	**-0.359****	-0.117	-0.181	**+0.714***
Mean number of capillaries/1000µm	**+0.370****	+0.204	+0.178	-0.143	**+0.299 ****	+0.178	+0.206	-0.548	**+0.363****	+0.125	+0.193	**-0.714 ***
Number of enlarged capillaries/digit	**-0.292***	-0.203	-0.130	-0.374	**-0.316 ****	-0.184	-0.170	-0.096	-0.156	+0.087	+0.108	-0.157
Number of giant capillaries/digit	**-0.360****	**-0.361 ****	**-0.30 ***	-0.327	**-0.302 ****	**-0.301 ***	-0.235	-0.452	**-0.308****	-0.246 (p=0.079)	-0.178	**-0.733 ***
Number of Haemorrhages	-0.093	-0.09	-0.102	+0.265	-0.069	-0.003	+0.053	-0.327	-0.145	-0.151	-0.045	-0.546
Number of neovascularisation/digit	-0.100	+0.09	+0.102	+0.386	-0.077	+0.111	+0.185	-0.283	-0.146	+0.065	+0.007	+0.514

5.3.4 The relationship between patient-reported outcome measures and HFUS Vascularity Indices in systemic sclerosis

There were no significant monotonic correlations between vascularity indices and parameters of the RCS diary, SHAQ-RP or SHAQ-DU (Spearman's Rho, data not shown).

5.4 Discussion

5.4.1 High frequency ultrasound identifies reduced peripheral vascularity in systemic sclerosis

Using a novel cSMI HFUS application, we have demonstrated that vascularity indices as assessed by HFUS cSMI at three ROI, reflect the significant peripheral vasculopathy in SSc compared to controls. Our larger SSc specific study reflects the results reported by Keberle et al., (65) who examined a mixed group of SRP using a different CDU application on which our study ROIs are based. We have demonstrated a potential useful application of HFUS in microvascular assessment in SSc.

Our use of novel HFUS cSMI technology also demonstrated further reduction in vascularity indices in those with a history of SSc-DU despite an increased use of therapeutic vasodilators (vasodilator use described in chapter 3.3.4, Table 3.5). A very recent publication by Schioppo et al., (2019) identified a similar non-significant trend in nailbed or fingertip pulp power Doppler signals in SSc with a DU history than without (131). Tentatively, we consider this *may* suggest superiority of HFUS cSMI as an imaging modality. There is a lack of clear understanding of how variations in specific HFUS technology with ever evolving 'next generation' technologies might impact on the quantification of microvascularity described in this chapter. Certainly, if HFUS

is to progress from a novel to establish method of SSc microvascular assessment, further studies need to be done to examine specific HFUS modalities in head to head trials.

5.4.2 High frequency ultrasound provides superior assessment of digital perfusion in SSc

We have demonstrated the convergent validity of vascularity indices with baseline LSCI perfusion for the first time. Whilst associations with DVVi and NVi were weak, we have reported strong associations between LSCI and FVi. In view of previous validation of LSCI as a SSc-RP assessment tool, this suggests that at controlled temperatures HFUS cSMI reflects distal digital blood flow in SSc. Additionally, the correlation between HFUS and peak PORH suggests that those with low ambient digital perfusion may have a limited capacity to maximally vasodilate in response to increase oxygen demand.

Given that ambient HFUS vascularity successfully differentiated SSc and HC where baseline LSCI perfusion did not (chapter 4.3.2), we suggest that HFUS cSMI is a useful application to investigate SSc microvasculopathy.

The mirrored correlations between HFUS Vis and each of LSCI baseline and peak PORH suggests that additional time-consuming functional challenge may not provide additional useful data. Ultrasound colour doppler and warm water challenges have been combined by others, to demonstrate reduced hyperaemic flow in Secondary RP (65). Further exploration of the relationship between HFUS and LSCI could be considered with an addition of a PORH

challenge on HFUS cSMI, however anecdotally we feel this may be of limited benefit.

There were notably few significant differences between NC classifications with respect to local HFUS at the nailfold (FVi), which suggests that the structural microvascular changes do not dictate focal areas of vascularity on HFUS. Likewise, we have not demonstrated a progressive relationship between evolving NC changes and finger vascularity measured by any of the Vis. This is in contrast to similar comparisons between NC and focal LSCI at the nailfold (105). However, the significant reduction in DVVi and FVi across all 3 SSc-specific NC classifications compared to normal NC does demonstrate that SSc experience reduce finger perfusion even when capillary number is preserved in the early NC phase. Furthermore, significant and expected relationships were identified using individual NC parameters including positive correlations between Vis and capillary number. Schioppo et al., recently reported a similar reflection using power Doppler (131). Similarly, others have demonstrated reduced localised nailfold microvascular flow on OCT in those with prominent capillary loss (104). Of interest, enlarged and giant capillaries in our cohort associated with worse digital perfusion on HFUS Vis which may reflect the association with DU reported by some (112).

HFUS does therefore demonstrate reduced perfusion associated with structural microvascular changes in SSc but does not differentiate between qualitative NC classifications.

5.4.3 PROMs do not adequately reflect the severity of SSc vasculopathy on HFUS

Similar to correlations with LSCI and NC data (chapter 4.3.5), our results suggest that the RP diary and SHAQ do not reflect the severity of peripheral vasculopathy on HFUS, a feature that to our knowledge has not been previously investigated but again demonstrates the limitations of subjective patient-report data.

5.4.4 Concluding remarks

We have demonstrated that HFUS with novel cSMI application and quantification using vascularity indices can delineate SSc from controls as well those with a history of SSc-DU. Our data demonstrates for the first time that ambient HFUS cSMI can beneficially differentiate SSc from controls despite the concurrent use of vasodilators where LSCI could not and potentially therefore has superior clinical and research application. HFUS cSMI also reflects reduced perfusion associated with capillary loss at the nailfold. PROMs however, appear to have little or no relationship with HFUS which we report for the first time.

Chapter 6. Validation of the use of high frequency ultrasound in assessment of systemic sclerosis related skin disease

6.1 Introduction

The modified Rodnan skin score (mRSS) remains the Gold standard for clinical assessment of SSc related skin disease. However, as discussed in chapter 1.6.2, this technique was devised to quantify skin thickness alone and lacks the sensitivity for qualitative assessment of the complex and evolving SSc skin pathology. The mRSS is easy to perform and requires no specialised equipment making it an attractive tool for skin assessment in daily clinical practice. However, in order for real progress to be made in the management of SSc, the methods of assessing and monitoring skin disease must be improved, in the least for the benefit of clinical trials.

Ultrasound provides an objective measure of both quantitative and qualitative data and with the added advantage of a greater penetration depth than OCT (170). The academic application of ultrasound in SSc skin disease to date has been previously discussed (chapter 1.6.2.1). Overall, the use of HFUS for skin assessment in SSc has been shown to be reproducible both for quantitative (122, 165, 172-174) and qualitative (172, 174-176) data and is reportedly sensitive and specific (359). It therefore shows promise as a useful tool in SSc skin disease. However, the available data are limited on several fronts. Firstly, there are a relatively small number of studies spanning decades each using models of Ultrasound technology applicable in their time. For example, studies investigating elastography originally used manual

displacement of the skin, which is subject to variation. Newer technology allows a 'pushing' pulse to be generated by the ultrasound transducer itself, which theoretically may give more consistent results by generating a more consistent displacing waveform. Secondly, skin thickness, echogenicity and elastography have yet to all be examined within the same study. We therefore are not able to draw conclusions about their inter-relationships or whether there is added value in measuring all three parameters. Thirdly, the true academic and clinical benefit of HFUS over skin scoring by palpation alone is its potential to act as a virtual skin biopsy, which requires correlation with histological findings. Only one study to date has also taken anatomically paired skin biopsies and reported binary normal or abnormal skin based on thickening of collagen bundles (359). However, no direct correlation was made with HFUS data. A further study has examined expression of ECM markers in patients examined by HFUS, but histological analysis was not performed (383).

6.1.1 Chapter hypothesis, aims and objectives

We hypothesised that HFUS is a useful objective assessment tool for SSc skin pathology with superiority over the mRSS. The aim of this chapter was to explore the potential of HFUS as a useful non-invasive biomarker and virtual skin biopsy in SSc skin disease. The specific objectives were to:

1. Use 3 HFUS modalities, namely skin thickness (ST), echogenicity and novel shear wave elastography (SWE) to demonstrate the presence of SSc related skin pathology.
2. Assess the relationship between 3 HFUS modalities with traditional clinical assessment by mRSS.
3. Assess the convergent validity of HFUS parameters with histological analysis of dermal collagen content.

6.2 Methods

6.2.1 Study population

Healthy controls and SSc participants were recruited as described previously (chapter 2.1).

6.2.2 Study procedures

Skin thickness, echogenicity and SWE were assessed using HFUS as described previously (chapter 2.8). mRSS was assessed at each of 51 anatomical locations to provide a total mRSS. Local mRSS was also documented for each of the HFUS ROI (as described previously, chapter 2.2.1).

6.2.2.1 HFUS image analysis

Images for ST, echogenicity and SWE were analysed as previously described (chapter 2.8.2.2, 2.8.3.1, 2.8.4.1 respectively).

6.2.3 Ex vivo collagen quantification of skin

Skin biopsies were taken from the distal forearm at the site of HFUS assessment as described in chapter 2.10. Skin collagen content was quantified using Masson's trichrome stain (Sigma HT15, detailed methodology described in chapter 2.11.1).

Collagen staining was then quantified using Image J to calculate a mean intensity (gray scale) of blue colour across the tissue section, integrated density (mean intensity x blue pixel area) and total sum of the gray scale (total sum of the intensity of each blue pixel) (as described for vascularity, chapter 5.3.1).

6.2.4 Statistical analysis

For each of the HFUS parameters the first of two readings were used for each participant and compared between groups using non-parametric tests in SPSS v24. HFUS results are reported to 1 decimal place in line with the format reported by the Aplio technology. Median [IQR] group values are reported for skin thickness. Individual participant echogenicity and SWE results represent a mean value across the ROI. Group results are therefore reported as a median [IQR] of the mean values for echogenicity and SWE.

Statistical comparison of ultrasound data between SSc (whole group) and HC utilized Mann-Whitney U (presented as group median [interquartile range]). Comparisons made with grades of local mRSS utilized Kruskal-Wallis tests. Post-hoc analysis (Dunn test) was applied for comparison between 2 individual groups when K-W achieved significance.

Repeat ultrasound assessments were used to calculate inter-class correlation coefficient (ICC) for intra-observer variability of the single assessor.

SSc HFUS data for skin thickness at each site was sub-categorized according to atrophic skin (<mean +2 S.D. of controls), thickened skin (>mean + 2 S.D. of controls) or normal skin thickness. Multiple linear regression analysis for the 3 HFUS parameters to predict skin collagen content was performed using backwards exclusion (for echogenicity).

Data displayed as box plots show median (horizontal line), interquartile ranges (box plot) and range (whiskers) with group outliers shown as asterisks and circles.

6.3 Results

HFUS was performed on 15 HC and 53 SSc participants. Participant demographics are as described in chapter 3.3.1.

The normal range of HFUS parameters was calculated from HC data using mean +/-2 S.D. (Table 6.1).

Table 6. 1 Normal range of HFUS skin parameters.

A normal range determined from the mean +/- 2 S.D. of the health control group (n=15) for each parameter.

	Finger	Hand	Forearm	Abdomen
Skin thickness (mm)	1.7-4.1	1.0-1.7	1.0-2.3	1.4-3.0
Echogenicity (mean, gray scale 0-255)	40.1-100.9	12.5-105.6	33.7-91.3	23.2-109.2
SWE (mean, KPa)	8.9-56.5	0-56.0	5.1-56.7	0.5-34.4

6.3.1 HFUS identifies SSc skin pathology

Across the whole cohort, skin thickness and SWE were generally higher at each ROI in SSc compared to controls (Table 6.2). Dermal echogenicity was lower at the finger but higher at the forearm in patients with SSc compared to controls.

Table 6. 2 HFUS assessment of SSc skin pathology.

Significance illustrated using Mann-Whitney U.

HFUS parameter (median [IQR])	Healthy control	SSc	Sig.
n.	15	53	
Proximal Phalanx			
Skin thickness (mm)	2.9 [2.6-3.4]	**3.4 [2.8-4.05]**	**0.047**
Echogenicity (mean, gray scale 0-255)	67 [55-81]	**48 [40.5-63.5]**	**<0.001**
SWE (mean, KPa)	33.3 [21.8-40.6]	**39.8 [32.4-53.3]**	**0.02**
Dorsal Hand			
Skin thickness (mm)	1.4 [1.2-1.5]	1.6 [1.3-1.8]	0.052
Echogenicity (mean, gray scale 0-255)	55 [37-74]	46 [34.5-58]	0.112
SWE (mean, KPa)	27 [15.9-40.4]	**38.9 [31.8-50.1)]**	**0.003**
Distal Forearm			
Skin thickness (mm)	1.5 [1.3-1.7]	1.4 [1.2-1.6]	0.183
Echogenicity (mean, gray scale 0-255)	64 [57-71]	**73 [63-84]**	**0.025**
SWE (mean, KPa)	27.9 [21.1-41.1]	35.4 [28.6-43.2]	0.117
Abdomen			
Skin thickness (mm)	2.0 [1.9-2.5]	**1.8 [1.5-2.2]**	**0.016**
Echogenicity (mean, gray scale 0-255)	62 [49-81]	69 [61-85]	0.107
SWE (mean, KPa)	15.8 [9.4-25.9]	**25.9 [19.5-29.4]**	**0.01**

6.3.2 Relationship between HFUS assessment of skin thickness and clinical assessment using mRSS

There was a linear relationship between HFUS median skin thickness and the local mRSS at all 4 ROIs (Table 6.3). ST was significantly higher at the hand in patients with mRSS of 1 and 2 compared with HC (1.75mm [1.2-], p=0.043 and 2.1mm [1.6-], p=0.015 versus 1.4mm [1.2-1.5] respectively) (Figure 6.1). Similar trends were evident at the finger and forearm. For example, the skin thickness at the forearm in patients with a mRSS of 1 was significantly higher than in patients with a skin score of 0 (1.6mm [1.5-2.1] versus 1.4mm [1.2-1.5], p=0.009). When the mRSS was 0, the median skin thickness at the forearm (SSc 1.4mm [1.2-1.5] vs. HC 1.5mm [1.3-1.7], p=0.046) and abdomen (SSc 1.8mm [1.5-2.0] vs. HC 2.0mm [1.9-2.5],

p=0.026) was actually lower in SSc compared with HC reflecting atrophic skin. Skin thickness at the hand and fingers was similar in SSc and controls when the skin score was 0.

With consideration of the influence of age on skin thickness, ST only correlated with age in the control group at the forearm ROI (Spearman's Rho = -0.390, p=0.001), a site at which there was no significant difference between diagnostic groups. There was no correlation between ST and age at any site for SSc or finger, hand or abdomen in HC.

Table 6. 3 High frequency ultrasound assessment of scleroderma according to clinical grading by local mRSS.

p values illustrated using Kruskal-Wallis. Post-hoc Dunn test p values between two individual groups are shown in Figure 6.1 and 6.2.

HFUS parameter median [IQR]	Healthy control	Systemic sclerosis local mRSS				
		mRSS 0	mRSS 1	mRSS 2	mRSS 3	p value
Proximal Finger, n.	15	11	33	7	2	
Skin thickness (mm)	2.9 [2.6-3.4]	3.0 [2.5-3.8]	3.4 [3.0 - 4.3]	3.3 [2.1 - 4.0]	3.6 [3.3 – 3.8]	0.137
Echogenicity (gray scale)	67.0 [55-81]	52.0 [33.0-73.0]	47.0 [40.0 - 63.5]	50.0 [46.0 - 60.0]	57.0 [48.0 - 66.0]	**0.008**
Elastography (kPa)	33.3 [21.8-40.6]	39.7 [22.5-42.6]	39.6 [32.4 - 55.5]	49.0 [36.9 - 73.0]	64.3 [45.6 - 83.0]	**0.039**
Distal Hand, n.	15	37	12	3	1	
Skin thickness (mm)	1.4 [1.2-1.5]	1.5 [1.3-1.7]	1.75 [1.2 – 2.0]	2.1 [1.6 – 2.1]	2.1 [-]	**0.037**
Echogenicity (gray scale)	55.0 [37-74]	46.0 [35.5-61.0]	41.0 [20.3 - 52.5]	46.0 [35.0 – 57.0]	62.0 [-]	0.234
Elastography (kPa)	27.0 [15.9-40.4]	36.6 [31.3-42.5]	42.5 [31.7-71.8]	45.5 [43.1 - 57.3]	73.7 [-]	**0.007**
Distal Forearm, n.	15	42	9	2	0	
Skin thickness (mm)	1.5 [1.3-1.7]	1.4 [1.2-1.5]	1.6 [1.5-2.1]	1.7 [1.6 – 1.8]	-	**0.012**
Echogenicity (gray scale)	64.0 [57-71]	74.5 [64.8-87.3]	68.0 [54.5 - 74.5]	69.5 [59.0 – 80.0]	-	**0.045**
Elastography (kPa)	27.9 [21.1-41.1]	35.1 [27.9-41.0]	39.3 [26.6 - 46.8]	71.6 [53.8 – 89.3]	-	0.062
Abdomen, n.	15	51	2	0	0	
Skin thickness (mm)	2.0 [1.9-2.5]	1.8 [1.5-2.0]	2.4 [2.2 – 2.6]	-	-	**0.008**
Echogenicity (gray scale)	62.0 [49-81]	69.0 [62.0-86.0]	62.5 [41.0 – 84.0]	-	-	0.208
Elastography (kPa)	15.8 [9.4-25.9]	25.9 [19.6-29.2]	51.5 [17.1 - 85.8]	-	-	**0.035**

Figure 6. 1 Objective HFUS assessment of skin thickness according to local mRSS.

Skin thickness at each region of interest ((A) finger, (B) hand, (C) forearm, (D) abdomen) had a linear relationship with local mRSS in the SSc group. Statistical significance illustrated by post-hoc Dunn test. Data are re-presentation of Table 6.3.

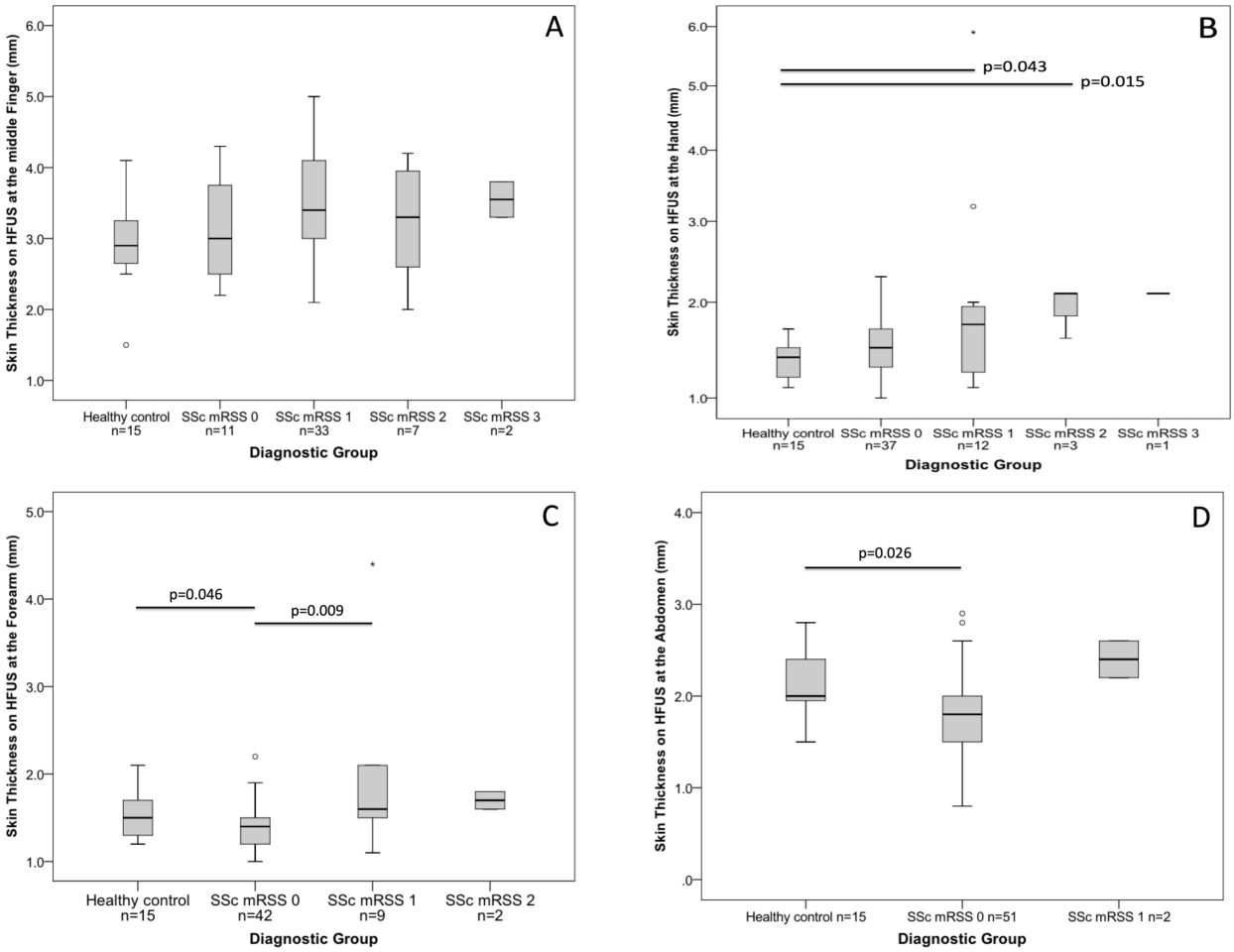

6.3.3 Relationship between ultrasound assessment of skin stiffness and clinical assessment using mRSS

There was a linear relationship between skin stiffness (using SWE) and local mRSS at the finger and hand (Figure 6.2). There was a similar trend at the forearm and abdomen (although numbers of patients with higher skin scores at these sites were low) (Figure 6.2). SWE values at both the abdomen (SSc 25.9KPa [19.6-29.2] versus HC 15.8KPa [9.4-25.9], p=0.026) and hand (SSc 36.6KPa [31.3-42.5] versus HC 27.0KPa [15.9-40.4], p=0.023) (Figure 6.2) were significantly higher in patients with SSc with a mRSS of 0 compared to HC. Furthermore, when skin thickness was objectively normal on HFUS

(Figure 6.3) there was still evidence of increased SWE at both the finger (71.2KPa [49.0-80.8] versus 33.3KPa [21.8-40.6], p<0.001) and hand (36.2KPa [30.7-42.5] versus 27.0KPa [15.9-40.4], p=0.042) compared to HC. Taken together, these findings indicate HFUS is capable of identifying aberrant tissue remodeling, even when the dermis is objectively normal thickness and clinically normal to palpation.

Figure 6. 2 HFUS assessment of skin quality according to local mRSS.

Echogenicity (white) and SWE (grey) are shown for each region of interest: finger (A), hand (B), forearm (C) and abdomen (D) demonstrating linear trends for skin stiffness to increase with increasing mRSS. In contrast echogenicity did not demonstrate a linear progression across mRSS grading but did show significant reduction (increased oedema) at the finger. Statistical significance illustrated using post-hoc Dunn test. Data are re-presentation of Table 6.3.

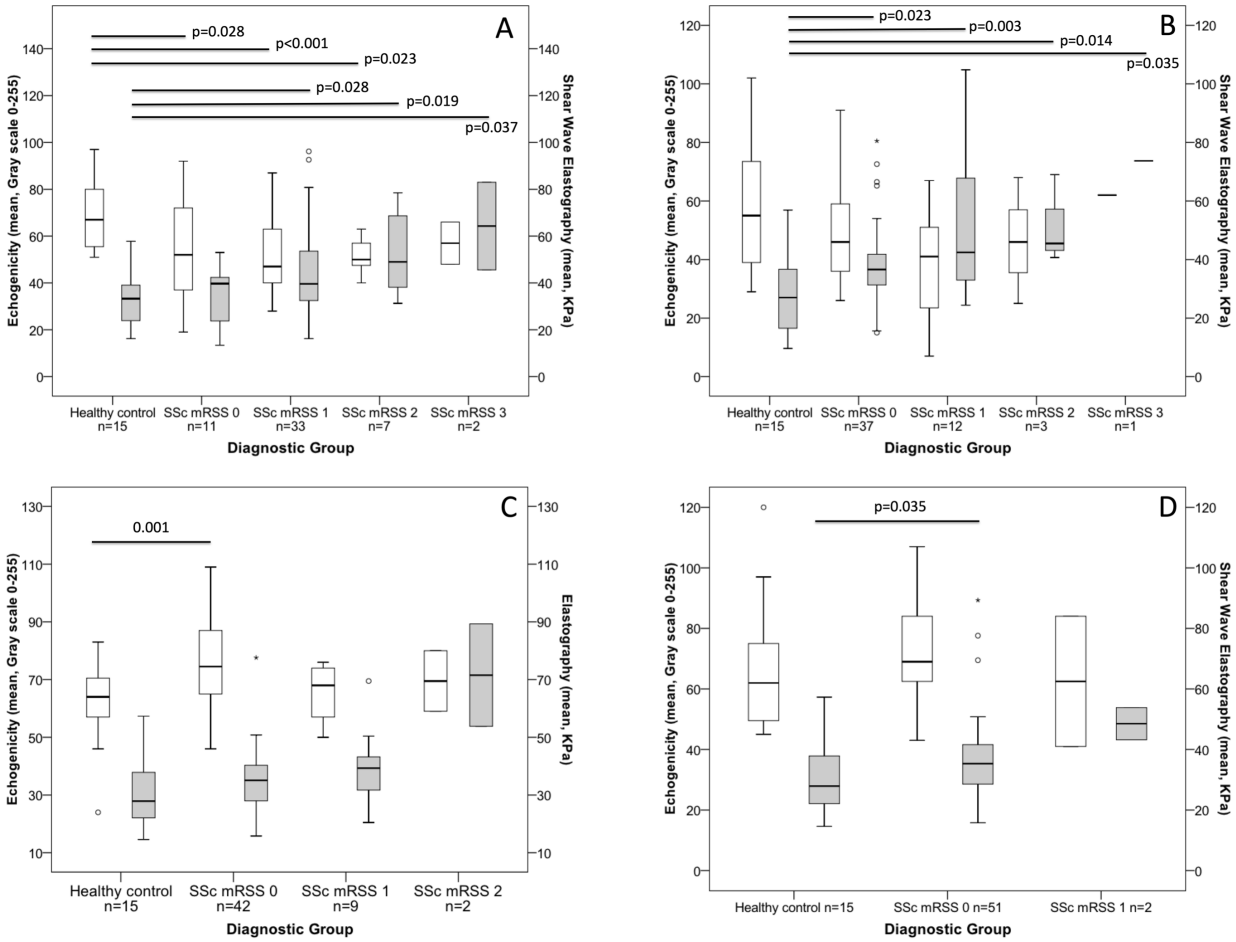

Figure 6. 3 HFUS assessment of skin quality according to objective skin thickness.

HFUS demonstrated changes in skin quality with echogenicity (white) and SWE (grey) in SSc compared to controls. There was a trend for progressive reduction in echogenicity (increasing oedema) from controls to SSc with objectively thickened skin at the distal regions ((A) finger and (B) hand). Similarly, a trend for increasing SWE was noted at (B) hand, (C) forearm and (D) abdomen. HFUS successfully identified changes in skin qualities compared to controls even when SSc skin was objectively of normal thickness, statistically significant at SWE at the finger, hand and abdomen. Significance illustrated using post-hoc Dunn test.

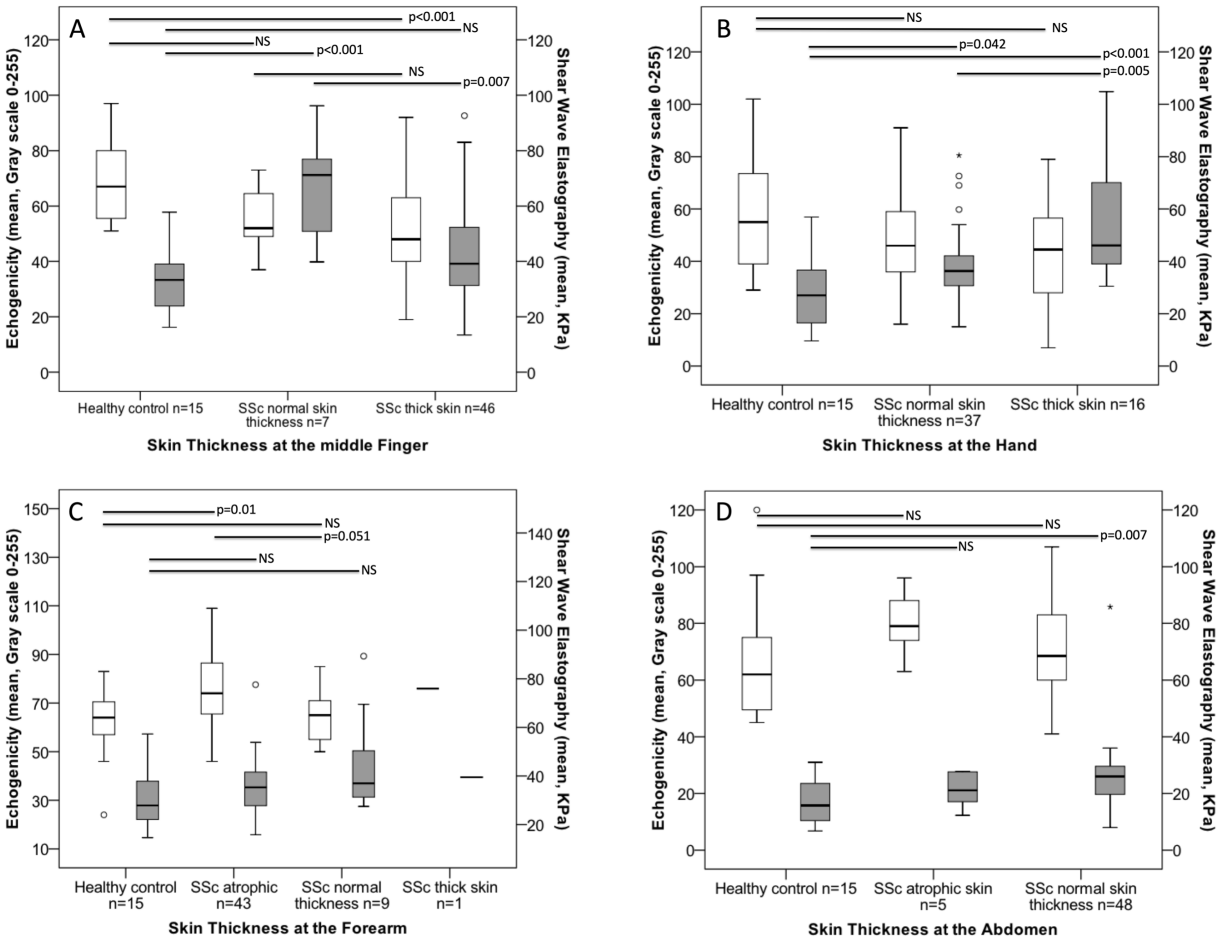

6.3.4 Relationship between HFUS assessment of dermal echogenicity and clinical assessment using mRSS

Unlike ST and SWE, there was not a linear relationship between echogenicity and local mRSS at any ROI. Echogenicity was, however, significantly lower at the finger in SSc with mRSS of 0 (52.0 [33.0-73.0], p=0.028), mRSS of 1 (47.0 [40.0-63.5], p<0.001) or mRSS of 2 (50.0 [46.0-60.0], p=0.023) compared to HC (67.0 [55.0-81.0]) reflecting more oedema (Figure 6.2).

Echogenicity was significantly increased at the forearm in SSc with mRSS of 0 compared to HC (74.5 [64.8-87.3] versus 64 [57.0-71.0], p=0.001) reflecting tissue fibrosis. Furthermore, there was a trend towards reduced echogenicity in SSc when ST was objectively normal on HFUS at the finger (52.0 [48.0-69.0] versus 67.0 [55.0-81.0], p=0.087) (Figure 6.3). Taken together, these findings suggest HFUS is able to demonstrate changes in skin oedema and fibrosis through tissue echogenicity, when skin thickness is otherwise objectively and clinically normal.

6.3.5 Application of HFUS in systemic sclerosis subgroups

6.3.5.1 HFUS assessment of early versus late SSc

Contrary to expectations, there were no significant differences between echogenicity or SWE between early and late SSc or correlation with disease duration (data not shown). This may be due to a combination of small numbers in the early subgroup and few treatment naïve participants (both vasodilator and DMARDs).

6.3.5.2 HFUS assessment in limited versus diffuse SSc

There was no significant difference in skin thickness or echogenicity between lcSSc and dcSSc at any anatomical site (Figure 6.4). SWE at the forearm was significantly higher in dcSSc than lcSSc (Figure 6.4) and similarly SWE at the hand approached significance (Figure 6.4) suggesting a greater burden of fibrotic disease in dcSSc, as expected (Figure 6.4).

The abdominal site (epigastrium) was chosen for assessment as it was felt that this would be the most likely anatomical area to examine non-lesional skin in SSc for the benefit of analysis in future chapters and as such the mRSS was equal to 0 in 51/53 SSc patients. It is therefore not surprising that HFUS parameters at the abdomen were not significantly different between

lcSSc and dcSSc. However, coupled with a significant increase in SWE and significantly thinner skin in lcSSc compared to controls (Figure 6.4), this suggests that lcSSc may in fact develop subclinical proximal skin involvement that in our cohort had reached the atrophic stage.

Figure 6. 4 High frequency ultrasound in SSc subgroups.

Box plots from left to right reflect finger (stripe), hand (white), forearm (spot), abdomen (grey). Notably few significant differences in HFUS parameters are observed between lcSSc and dcSSc ((A) skin thickness, (B) echogenicity, (C) SWE). SWE was significantly higher at the forearm in dcSSc and approached significance at the hand (C) compared to lcSSc demonstrating the greater burden of fibrotic disease that is typical of the dcSSc phenotype. Of interest, lcSSc demonstrated significant differences in skin thickness and SWE at the abdomen compared to controls and lack of difference with dcSSc that suggests lcSSc develop proximal scleroderma. Statistical analysis by Mann-Whitney U. Data are sub-analysis of overall cohort.

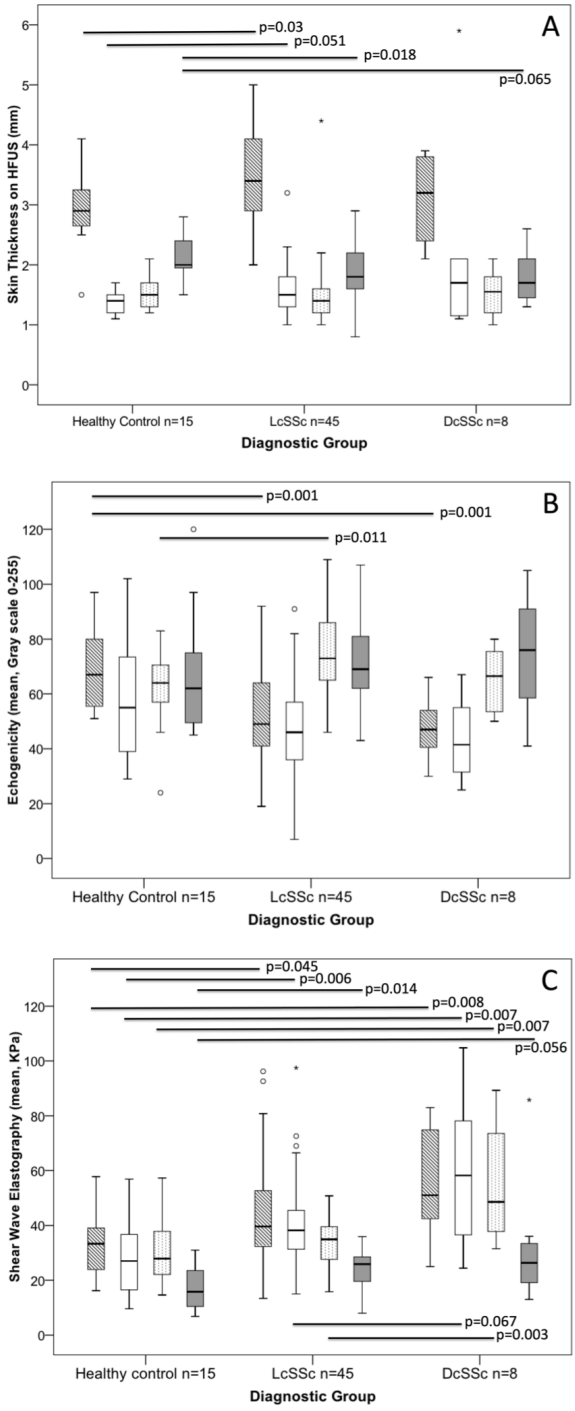

6.3.6 Inter-relationship between ultrasound parameters

There was no correlation between echogenicity and either SWE or skin thickness. Only a small number of weak correlations between skin thickness and SWE were identified (at the hand Spearman's ρ=+0.454, p=0.001 and at the finger ρ=-0.366, p=0.007), although this may have been a consequence of multiple testing and were not considered relevant. The general lack of consistent relationship between the 3 parameters likely reflects the complex and non-linear evolution of SSc skin pathology. For example, an area of normal ST in SSc may reflect uninvolved skin, early oedematous change prior to thickening or regression of fibrotic skin.

6.3.7 Histological validation of HFUS for assessing skin fibrosis

Skin biopsy was performed on 10 HC and 10 SSc participants at the distal forearm at the same site of HFUS assessment.

There were strong correlations between objective measurement of skin thickness on HFUS with each of the area, integrated density and sum of the gray scale for collagen staining for both the overall cohort and SSc alone (Table 6.4). The same patterns of strong correlations were observed between SWE and collagen staining for SSc participants (Table 6.4 and Figure 6.5). Of note, these associations were not carried through to the overall cohort (although p values approached significance p=0.056). There was no relationship between echogenicity and collagen content at the forearm suggesting that increased echogenicity may reflect other features of skin fibrosis.

Multiple linear regression analysis confirmed skin thickness and SWE at the forearm as significant predictors of local collagen deposition (integrated

density) in SSc $R^2 = 0.876$. The model was less strong when considering the cohort overall (SSc + HC), $R^2 = 0.518$.

Table 6. 4 Correlation between dermal collagen content at the distal forearm and HFUS parameters across the overall cohort.

p<0.05* and p≤0.001 using Spearman's rank correlation coefficient, ρ.

	Skin thickness (mm)	Echogenicity (mean, gray scale)	Elastography (mean, kPa)
Overall cohort (systemic sclerosis, n=10 + healthy controls, n=10)			
Area	**+0.697****	-0.064	+0.307
Mean Intensity	+0.046	-0.007	+0.182
Integrated Density	**+0.735****	-0.136	+0.433 (p=0.056)
Sum of gray scale	**+0.735****	-0.136	+0.433 (p=0.056)
Systemic sclerosis, n=10			
Area	**+0.669***	-0.098	**+0.717***
Mean Intensity	+0.215	-0.128	+0.73
Integrated Density	**+0.697***	-0.255	**+0.709***
Sum of gray scale	**+0.697***	-0.255	**+0.709***

Figure 6. 5 Assessment of skin fibrosis by Masson's trichrome and HFUS SWE.

Histological collagen content (blue) of forearm skin biopsies are shown by Masson's Trichrome staining (A, B) with paired HFUS SWE assessment at the same site for respective participants (C, D respectively) demonstrating skin stiffness. A healthy control representative of the control group mean for integrated density of collagen staining (A) has low skin stiffness on HFUS (C). SSc participant with the maximum integrated density of collagen staining for the SSc group, shows visibly increased collagen staining in the dermis (B) with increased skin stiffness (D). Scales: trichrome scale bar, 500μm. HFUS colour scale, stiff (red) to soft (blue). HFUS white numeric scale, depth (cm).

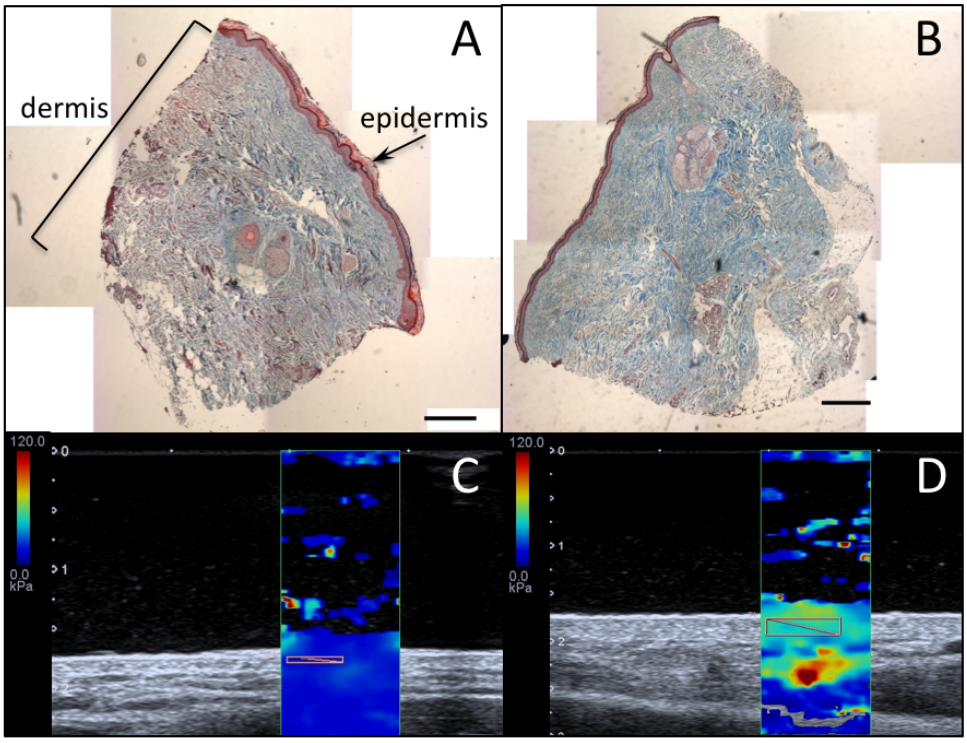

6.3.8 Reproducibility of high frequency ultrasound for skin assessment

Overall, reproducibility was very good, with very strong correlation between paired measurements for skin thickness (Intra-class correlation coefficient, ICC 0.946-0.978) and SWE (ICC 0.953-0.973) and strong correlation for echogenicity (ICC 0.648-0.865) (Table 6.5).

Table 6. 5 Intra-class correlation coefficient for HFUS parameters demonstrating intra-observer variability.

ROI	Intra-class correlation coefficient (95% CI)		
	Skin thickness (mm)	Echogenicity (mean, gray scale)	SWE (mean, kPa)
Proximal middle finger	0.946 (0.913-0.967)	0.782 (0.642-0.866)	0.954 (0.926-0.972)
Dorsal hand	0.970 (0.952-0.982)	0.744 (0.586-0.842)	0.953 (0.923-0.971)
Distal forearm	0.978 (0.965-0.987)	0.648 (0.432-0.783	0.964 (0.941-0.978)
Abdomen	0.963 (0.940-0.977)	0.865 (0.781-0.917)	0.973 (0.955-0.983)

6.4 Discussion

We have demonstrated for the first time that skin thickness and SWE on ultrasound correlate with dermal collagen deposition, which provides significant convergent validation for its use in SSc skin assessment. Additionally, the excellent reproducibility that we have demonstrated like others before (122, 165, 172-176) deems it reliable for such an application with appropriate training. Only one previous HFUS study has also taken anatomically paired skin biopsies which reported binary normal or abnormal skin based on thickening of collagen bundles (359), but made no direct correlation with HFUS data. Another study examined expression of ECM markers in patients examined by HFUS, but histological analysis was not performed (383). This work reported a strong positive correlation between the rate of increase in HFUS skin thickness and echogenicity with fibroblast proteoglycan production (383). The lack of correlation between echogenicity and collagen staining in our data suggests that increased echogenicity may reflect other dermal components of fibrotic skin, such as perhaps fibrillin and elastin rather than collagen alone.

Whitfield et al., (384) have reported on 4 gene expression profiles in SSc skin pertaining in part to the inflammatory and fibroproliferative phases. Our data suggests that HFUS may be able to differentiate between such gene profiles, through examination of ST, SWE and echogenicity. Whilst the technology for efficient machine learning is advancing (384), gene expression profiling relies on invasive tissue sampling and is not practical to repeat throughout the disease course. We have provided histological validation of the ability of ultrasound to reflect collagen deposition that occurs predominantly in the fibrotic phase. Paired study of gene profiling and ultrasound analysis may

further advance the application of the latter as a non-invasive virtual biopsy to aid personalized precision medicine of the future.

We have demonstrated that changes in SSc skin quality can be detected by ultrasound when ST is either clinically or objectively normal. Previous studies have demonstrated similar findings with skin thickness (141, 359, 385), although we are the first to demonstrate such abnormalities using dermal echogenicity and SWE. There are two likely explanations for the disparity between detection of skin pathology by ultrasound and mRSS. The first is that ultrasound is able to identify sub-clinical skin pathology, clinically felt to be uninvolved by the observer. The second is that mobile atrophic skin was scored as mRSS = 0 due to the lack of provision by the mRSS grading to document skin atrophy. Whatever the exact contribution of these 2 inter-related explanations, ultrasound appears to provide superior objective data regarding dermal pathology to the mRSS alone, with potentially important implications for SSc clinical trials. The incorporation of HFUS as a surrogate endpoint for skin involvement in SSc clinical trials may overcome issues around subjectivity and poor inter-rater reliability, potentially allowing treatment efficacy to be demonstrated more successfully in smaller single-blinded studies. HFUS is unlikely to surpass the mRSS in daily clinical practice, given the labour-intensive approach required for HFUS assessment at multiple sites.

Notably, neither SWE nor echogenicity consistently demonstrated significant changes in skin quality when skin thickness was normal. The lack of correlation between ultrasound parameters across the ROIs in our data, supports that one modality cannot substitute for another. This is in contrast to data from Hesselstrand et al., reporting a relationship between

echogenicity and skin thickness (383), which may be due to shorter disease duration in their cohort. We therefore consider that all 3 ultrasound parameters provide complementary data. Elastography may be additionally supportive by confirming the dermal interfaces and improving the accuracy and reproducibility of skin thickness measurement (174). Larger multicenter longitudinal studies may be of benefit in further understanding the inter-relationship and clinical relevance of the different ultrasound parameters.

Notably the SSc group in our study had a statistically significantly older mean age, which could be considered to influence skin thickness and elasticity. However, normal values for skin thickness according to age has been described using 20MHz HFUS and shown only 0.04-0.09mm difference between 50-59 and 60-69 year olds at our ROIs (386). We therefore concluded that whilst our SSc cohort was statistically significantly older than controls, the age difference was not felt to be clinically significant.

The lack of variation in echogenicity or SWE between early and late SSc in our cohort was contrary to expectations as we had anticipated that echogenicity may increase over time reflecting resolution of oedema towards the fibrotic phase. This has not been reported in the literature previously for comparison, but the lack of significant finding may suggest skin lesions do not progress in a unidirectional manner or (more likely) that our cohort contained a high proportion of late disease where the early oedematous phase had already resolve by the time of assessment.

The ability of HFUS to differentiate lcSSc from dcSSc appears inconsistent in the literature. We noted no difference in skin thickness at any site between SSc subgroups, which is in contrast to previous reports (141, 172, 366).

These studies, however, do conflict on the anatomical site at which significance is noted and again reflects the heterogeneity of populations. With similar confliction to our data, two studies by the same authors (172, 383) demonstrated lower echogenicity i.e. more oedema in dcSSc than lcSSc. Both study cohorts had relatively short disease duration, which may explain the variation from our findings. We did however, note increased skin stiffness at the forearm in dcSSc versus lcSSc, which has also been reported by others at the palmar finger (387).

The presence of stiffer atrophic abdominal skin in our lcSSc group that largely consists of patients with late disease, suggests that lcSSc do develop proximal skin changes but that they are sub-clinical in nature. Previous studies have reported that gene expression profiles in SSc skin globally reflect the phase of skin pathology regardless of whether sampling occurs at clinically lesional or non-lesional skin (166, 384, 388). The limitations of the mRSS in these studies preclude differentiation of truly uninvolved versus sub-clinical skin pathology. Addition of HFUS to identify subclinical pathology in the study designs may aid data interpretation and therefore greater understanding of SSc pathology.

There are some limitations to our study. We have demonstrated excellent intra-rater reproducibility in a single assessor to demonstrate the reliability of our data, but have not made a broader assessment of repeatability across or within multiple assessor, as this was not the primary aim of the study. We have assessed HFUS in a comparatively large number of SSc subjects compared to previous studies but SSc is a heterogeneous disease and larger studies would allow greater between-group comparisons to be made. Our study was cross-sectional in nature and larger multicenter longitudinal studies

(including treatment naive early patients) shall be important in defining HFUS parameter evolution in SSc skin disease.

At 18MHz, the dermo-subcutis junction at the proximal finger was not easily distinguishable in some SSc patients which we hypothesised may be due to a combination of sclerodermatous changes in the dermis creating a similar echo to the hypodermis thus reducing the echo interface, as well as pathological subcutaneous fat atrophy in the disease group at a site which naturally has little fatty tissue even in healthy subjects. This is a feature also observed in other studies on OCT with reduced clarity of the dermo-epidermal junction and papillary-reticular dermis interface in the scleroderma disease state (146). This is further reflected by previous reports of increased inter-observer variability in HFUS dermal thickness measurement at the finger compared to other anatomical sites (172). It has been suggested that higher frequencies of HFUS may provide better skin assessment than those in the lower end of the 'high frequency' range and particularly that they may have better sensitivity to identifying proximal skin thickening in lcSSc (385). Whilst this seems logical, there are few studies to affirm it and therefore further studies are required to determine the optimum frequency for this application whilst balancing against the limited accessibility of very high frequency machines (>50MHz).

Subjectively, we also noted that in SSc with high local skin scores at the finger, it was often difficult to obtain an accurate SWE reading on the first attempt. Iagnocco et al., reported similar problems for finger elastography in all participants and thus concluded this may be due to interference from the closely underlying bone (175). In our study, this practical difficulty did not occur with controls or lower local mRSS and thus we conclude that it

occurred due to the severity of pathology within the soft tissues rather than bony interference. Despite this, overall we still obtained good quality reproducible data by this technique.

6.4.1 Concluding remarks

In conclusion, we have demonstrated excellent repeatability of HFUS and reported analyses of the convergent validity of different HFUS parameters with both clinical assessment using the mRSS and dermal collagen content that suggests HFUS may have potential as a non-invasive virtual biopsy for the assessment of SSc-related skin pathology. We have demonstrated changes in the qualities of SSc skin at both clinically apparent lesional and non-lesional skin. Skin thickness and SWE stand out as highly reproducible parameters that reflect local collagen burden. Future studies comparing HFUS parameters with novel molecular subsets defined by paired gene profile signatures may help to support the use of HFUS in clinical trials, as well as personalizing medical interventions in SSc.

Chapter 7. The relationship between vasculopathy and skin pathology in systemic sclerosis

7.1 Introduction

In previous chapters (chapter 3-6), we have provided objective evidence of vasculopathy and skin pathology in SSc. While these features may appear to be distinct pathologies, it has long been suspected that these pathological events are inter-linked. LeRoy's vascular hypothesis (38) (discussed in detail in chapter 1.4.1) broadly alludes to such through the initial immune mediate attack resulting in endothelial disruption, tissue ischaemia and subsequent aberrant tissue remodelling. If confirmed, this would suggest fibrosis in skin (and other tissues) may be prevented with vasoactive therapies that prevent tissue ischaemia. There already exists within the literature a number of features which suggest a link between vasculopathy and skin pathology, most commonly with respect to structural capillary changes at the nailfold. A 20-year prospective study following the evolution of patients with RP noted transition on NC from giant capillaries to capillary loss occurring in close temporal relationship to the onset of definite SSc (usually defined by the emergence of cutaneous fibrosis) (46). A number of studies have also identified a positive and progressive association between the severity of microangiopathy on NC and extent of skin fibrosis (108, 113, 118, 122-124). It has also been noted that early NC changes are more frequently identified in lcSSc (23, 108) and late changes more prevalent in dcSSc (5, 113).

The expression and rate of progression of NC features also varies according to autoantibody specificities. SSc patients carrying RNAPIII (typically

associated with dcSSc) have been noted to develop enlarged capillaries significantly earlier (4 vs. 15 years) than patients with ACA (typically associated with lcSSc) with similar differences reported for capillary loss (46). Similarly, Scl-70 positive SSc are more likely to exhibit SSc-specific NC patterns (113) with an OR 6.4 for late NC pattern (95). ANA negative patients, who are typically considered to have a milder disease phenotype, appear to progress through NC patterns more slowly (95).

There has been a flurry of academic interest in the predictive value of NC in recent years. Patients with SSc-specific NC changes identified at a single assessment have an increased frequency of organ manifestations such as ILD compared to SSc patients with normal or non-specific NC changes (126). Similar findings are reported for ILD and PAH with more advanced NC patterns (108, 113, 114). Although there is mixed reporting on the association of individual NC parameters such as capillary loss with ILD and PAH (123, 128, 389).

A number of longitudinal studies have reported progressively increasing risk of developing new and severe SSc related organ involvement with advancing capillaroscopic patterns (110, 111, 115, 116) or capillary loss (110) including cardiopulmonary disease (110, 111, 115). Similarly, others have reported an association with mortality (117, 118).

Taken together, these in vivo observations suggest the extent and severity of vasculopathy may be an important factor dictating not only vascular sequelae but also fibrosis and therefore SSc clinical phenotype. However, despite the numerous references to the potential predictive value of NC in SSc, it should be noted that the varied nature and quality of some studies

with lack of adequate consideration of confounding, limits the detailed interpretation and translational potential (119).

The literature examining the relationship between skin perfusion and fibrosis (and potential vascular-fibrotic inter-relationship) is smaller. One study reported a negative correlation between finger perfusion and skin thickness at the same site, both on HFUS and mRSS (366). Others have also used HFUS as an objective measure of skin thickness to report links with vascular features (122, 390), with one paper examining skin stiffness (387). These all again suggest that there is a relationship between SSc vascular and skin pathology. Whilst use of objective measures of skin fibrosis using HFUS represents progress towards understanding the vascular-fibrotic inter-relationship, studies are few in number and have not previously assessed quantification of the inflammatory skin phase (illustrated by echogenicity) or patient-reported outcomes of digital vascular severity.

7.1.1 Chapter hypothesis, aims and objectives

We hypothesised that there is a relationship between vasculopathy and skin pathology in SSc. The aim of this chapter was therefore to provide further evidence of this relationship. The specific objectives were to correlate objective measure of SSc vasculopathy using LSCI, NC and HFUS with:

1. subjective assessment of skin pathology using traditional assessment by mRSS.
2. objective HFUS assessment of all 3 features of SSc skin pathology (skin thickness, echogenicity and SWE).

7.2 Methods

7.2.1 Study population

Healthy controls and SSc participants were recruited as described previously (chapter 2.1).

7.2.2 Study procedures

Objective measures of vasculopathy and skin pathology were performed on SSc participants as described in chapter 2. For the purposes of focused analysis, parameters from select regions of interest have been chosen from each assessment modality based on significant findings from these previous chapters. Specifically, data from RP diary (chapter 2.3), LSCI baseline perfusion and reperfusion gradient (as an average across the distal fingers 2-5, chapter 2.5), DVVi on HFUS (chapter 2.7 and 5.3.1) and overall NC classification and ICD (chapter 2.6) were used for quantification of vasculopathy. For skin pathology, data from HFUS echogenicity, skin thickness and elastography at the proximal middle finger (chapter 2.8) were used. Image and PROM analysis is described in respective methods chapters.

7.2.3 Statistical Analysis

Statistical analysis was performed using non-parametric tests in SPSS including Spearman's rank correlation coefficient and Kruskal-Wallis.

7.3 Results

SSc participant demographics are as described previously in chapter 3.3.1. Data were available for SSc participants as previously described for PROMs

(chapter 4.3.1), LSCI and NC (chapter 4.3.1), HFUS cSMI (chapter 5.3) and HUFS skin pathology (chapter 6.3).

7.3.1 The relationship between vasculopathy and cutaneous inflammation in early systemic sclerosis

Several interesting relationships were noted with echogenicity that demonstrate the paired temporal relationship of vasculopathy and skin progression. Echogenicity at the proximal phalanx showed a weak negative correlation with the reperfusion gradient on LSCI in the SSc group (Spearman's ρ = -0.31, p=0.03, Table 7.1), which improved to a strong association in early SSc (Spearman's ρ = -0.70, p=0.02). These findings suggest early SSc, where peripheral vascular function is less impaired, is associated with lower echogenicity (increased cutaneous oedema/inflammation and vascular leak), which resolves as vascular dysfunction progresses. Additionally, echogenicity correlated strongly with the ICD in early SSc (Spearman's ρ = +0.62, p=0.04), demonstrating that early inflammatory skin lesions are associated with less capillary loss. Furthermore, there was a non-significant trend for those with early NC changes to have lower echogenicity (more oedema/inflammation) on HFUS (Table 7.2).

Finger echogenicity in early SSc showed strong negative correlations with RCS and daily duration of RP (Spearman's ρ = -0.76, p=0.03 and -0.81, p=0.02 respectively) (Table 7.1). These findings suggest the patient experience of RP is worse in the presence of increased oedema. This may reflect poorer coping strategies and fewer opportunities to optimise vasodilator therapy in early disease. In contrast, in late SSc, echogenicity and RCS correlated positive (Spearman's ρ = +0.42, p=0.01), which was

more in line with expectations and suggests more severe Raynaud's symptoms (and tissue ischaemia) are associated with more advanced skin fibrosis in established disease.

7.3.2 Relationship between vasculopathy and skin thickness

In early SSc, there was a very strong positive correlation between baseline finger perfusion and finger skin thickness on HFUS (Spearman's ρ = +0.90, p<0.001, Table 7.1). These findings are consistent with the relationship between echogenicity and reperfusion gradient described above and suggest early disease is associated with less pronounced microangiopathy but higher levels of cutaneous oedema (puffy fingers). The reported correlations suggest a strong temporal relationship between vasculopathy and early skin pathology.

Furthermore, total mRSS in the overall SSc group had a weak negative correlation with the reperfusion gradient on LSCI (Spearman's ρ = -0.37, p=0.009, Table 7.1), which suggests that with a greater burden of skin disease, there is greater vascular impairment and reflecting the evolution of both vasculopathy and fibrosis in SSc. This association was stronger in lcSSc (Spearman's ρ = -0.42, p=0.006) and late disease (Spearman's ρ = -0.41, p=0.01).

Consistent with these findings (and those of earlier work), the ICD positively correlated with total mRSS (Spearman's ρ = +0.33, p=0.02) in SSc, which again showed stronger associations in late disease and lcSSc (Spearman's ρ = +0.38, p=0.01 and +0.42, p=0.006 respectively) (Table 7.1). A non-significant trend was also seen for an increased total mRSS across advancing SSc-specific NC classifications (p=0.053) (Table 7.2). This trend

was still apparent in sub-groups for lcSSc, dcSSc and early disease (data not shown). Similarly, there was a trend for skin thickness on HFUS to increase from early to active NC followed by a degree of thinning secondary to atrophy when late changes were present on nailfold capillaroscopy (Table 7.2).

Table 7. 1 Correlation of functional and structural parameters of digital vasculopathy with skin pathology at the finger in systemic sclerosis.

p<0.05* and p≤0.01** using Spearman's rank correlation coefficient. Abbreviations: AUC, area under the reperfusion curve; DVVi, dorsovolar vascularity Index; ECHO, echogenicity; HFUS, high frequency ultrasound; ICD, inter-capillary distance; LSCI, laser speckle contrast imaging; mRSS, modified Rodnan skin score; NC, Nailfold capillaroscopy; RCS, Raynaud's condition score; RP, Raynaud's phenomenon; ST, skin thickness; SWE, shear wave elastography.

	Systemic sclerosis				**Early SSc**				**Late SSc**				**LcSSc**				**DcSSc**			
	mRSS	ST	Echo	SWE	mRSS	ST	Echo	SWE	mRSS	ST	Echo	SWE	mRSS	ST	Echo	SWE	mRSS	ST	Echo	SWE
RP Diary, n.	44				8				36				38				6			
RCS	+0.09	+0.03	+0.190	+0.02	-0.06	+0.19	**-0.76***	+0.27	+0.11	+0.01	**+0.42****	-0.02	+0.10	+0.02	+0.25	+0.04	+0.43	+0.17	-0.32	-0.37
Daily frequency	+0.03	+0.08	+0.18	-0.06	-0.01	+0.37	-0.52	+0.16	+0.04	+0.07	+0.29	-0.05	-0.00	+0.06	+0.22	-0.11	+0.31	+0.20	-0.06	+0.09
Daily duration	-0.07	+0.08	+0.18	-0.06	-0.11	+0.03	**-0.81***	+0.32	-0.06	+0.09	+0.33	-0.06	-0.09	+0.05	+0.23	-0.06	+0.43	+0.17	-0.32	-0.37
LSCI, n.	52				11				41				44				8			
Baseline perfusion	+0.16	+0.20	-0.04	+0.09	-0.30	**+0.90****	+0.22	+0.12	+0.27	+0.03	-0.45	+0.06	+0.30 p=0.052	+0.22	-0.01	+0.06	-0.43	-0.05	-0.11	+0.45
LSCI, n.	49				10				39				41				8			
Reperfusion gradient	**-0.37****	-0.05	**-0.31***	-0.20	-0.33	-0.32	**-0.70***	+0.02	**-0.41****	+0.16	-0.24	-0.25	**-0.42****	+0.13	-0.28	-0.16	-0.20	-0.42	-0.60	-0.50
HFUS, n.	53				11				42				45				8			
DVVi	+0.13	+0.15	+0.02	+0.07	+0.49	+0.25	-0.04	+0.04	+0.00	+0.12	+0.05	+0.01	+0.04	+0.18	+0.02	+0.04	-0.36	+0.60	+0.18	-0.19
Nailfold capillaroscopy, n.	53				11				42				45				8			
ICD	**+0.33***	-0.09	+0.44	+0.17	+0.12	-0.02	**+0.62***	+0.01	**+0.42****	-0.07	-0.10	+0.22	**+0.38****	-0.14	-0.06	+0.13	+045	-0.12	+0.35	+0.48

Table 7. 2 Evaluation of skin pathology at the proximal finger according to systemic sclerosis specific nailfold capillaroscopy changes.

Statistical analysis across NC classifications using Kruskal-Wallis, for mRSS p=0.053 and for SWE p=0.027 (p<0.05* and p<0.01** using post-hoc Dunn compared to active NC).

Nailfold capillaroscopy classification (overall)	**n**	**Total mRSS (Scale 0-51) (median (IQR; min-max))**	**Skin thickness (mm, median (IQR))**	**Echogenicity (0-255, median (IQR))**	**Shear wave elastography (KPa, median (IQR))**
Non-specific	7	2 (0-6; 0-29)	3.1 (3.0-3.8)	41.0 (35.0-55.0)	39.4 (26.2-42.1)
Early	8	1.5 (0-2; 0-4)	2.6 (2.4-4.8)	40.5 (37.5-48.75)	**47.5 (35.4-66.6)***
Active	13	2 (0-6; 0-26)	3.7 (3.2-4.1)	52.0 (45.0-72.0)	**36.2 (21.1-39.7)**
Late	23	5 (2-11; 0-37)	3.3 (2.4-4.0)	50.0 (43.0-63.0)	**50.4 (32.5-73.0)****

7.3.3 The relationship between vasculopathy and skin stiffness

Skin at the proximal phalanx was significantly stiffer in those classified as having overall early and late NC changes compared to active (Table 7.1). This would suggest that skin may be stiff early in disease, followed by a period of softening and then stiffen again. The non-significant trend for lower echogenicity in those with early NC changes suggests that skin stiffness at this stage may in part be due to cutaneous oedema. Presumed resolution of such may then explain an apparent softening of skin followed by increased stiffness as scleroderma progresses to the established fibrosis.

7.4 Discussion

We have demonstrated several significant relationships between objective measures of vasculopathy and features of SSc skin pathology. These appear strongest and most numerous in early SSc. Certainly, both the baseline finger perfusion and the rate of recovery after an ischaemic stimulus appear to be less severe in early stages associated with the inflammatory phase of skin disease, and worse as skin thickening and oedema resolution. During the latter period of undertaking our study, an Italian group published data comparing *baseline* LSCI perfusion with objective measures of dermal thickness by HFUS (366). With some variation from our methodology, Ruaro et al., (366) demonstrated a moderate negative correlation between local baseline skin perfusion over the middle phalanx on LSCI and thickness at the finger by both HFUS and local finger mRSS in SSc. The same group have previously demonstrated similar findings by an alternative laser-based application using LDF (122). Our alternative positive relationship between baseline LSCI with HFUS finger skin thickness specifically in *early* SSc,

reinforces that skin pathology is a dynamic pathology and varies over the disease course.

The negative correlation between echogenicity and digital reperfusion after an ischaemic challenge builds on this story and is novel, and sheds new insight into the temporal relationship between vascular injury, vascular leak and aberrant tissue remodelling. To our knowledge, we are the first to report the relationship between echogenicity and ICD in early SSc, which supports the evolutionary nature of the vasculopathy and inter-relationship with tissue remodelling in the skin.

There were few associations between HFUS skin thickness and vasculopathy. However, others have reported an improvement in skin thickness on HFUS with the use of ERA therapy (391). Whilst small numbers and the lack of RCT design limit specific conclusions from this single study, this may be cautiously extrapolated to our cohort where the use of vasodilators (including ERA therapy) was high and may explain the isolated correlation between HFUS skin thickness and LSCI found in early SSc.

Others have reported a progressive increase in dermal thickness on HFUS with advancing NC patterns on a number of occasions (122, 366, 390). In contrast, we found a non-significant trend for HFUS finger skin thickness to increase and then atrophy (alongside late changes on NC). Differences in methodology and the large number of late SSc with atrophic skin may account for differences in our cohort. We did identify a strong trend for total mRSS (both the median and range) to increase across the SSc-specific NC patterns, in line with recent work (390). This paper also described a complementary increase in the plicometer skin test across NC patterns (390).

We have additionally reported a positive relationship between total mRSS and ICD, which to our knowledge is the first report of such.

Some have reported that the presence of normal or non-specific NC changes in SSc is associated with a lower burden of skin disease (124) which was not apparent in our cohort. As the majority of SSc (>86%) have specific NC changes (113), larger scale studies are required to accurately report on associations within this minority group.

Only one previous study has examined an association between elastography and late NC pattern by multiple regression analysis (387). We report a similar increase in SWE in late compared to early NC classification. We additionally demonstrated an increase in SWE in early NC compared to active, with an additional trend for increased oedema in this group. As those with early NC patterns tend to have low disease duration, these observations suggest a relationship between early microvascular change and changes in skin texture due to inflammatory oedema. This reinforces the limitations of skin assessment by mRSS in clinical trials (discussed previously, chapter 6) and also supports the combined application of multiple HFUS parameters in future studies where relationships with skin pathology are compared.

To our knowledge associations between the RP diary and HFUS skin pathology have not previously been reported. The strong negative association of the RP diary parameters with echogenicity in early SSc were surprising. This may in fact represent the patient learning curve associated with management of RP in early disease rather than a pathological relationship. Given that there has been an overall lack of associations between any clinical parameter and the RP diary across all chapters thus far,

as well as the mixed quality of the RP diary data due to seasonal variations, the latter should be interpreted with caution.

7.4.1 Concluding remarks

This works supports the available literature whilst also providing new insight into the inter-relationship between vasculopathy and tissue remodelling in the skin of people with SSc. Our findings support the general premise of the vascular hypothesis (38). In particular, we have identified novel relationships with the early inflammatory features of skin pathology and vasculopathy on LSCI and NC in early disease as well as increased SWE in those with early NC that likely relates to the oedematous phase. Due to the evolving nature of SSc pathology, further longitudinal study is required to examine this relationship in more detail.

Chapter 8 Circulating vascular biomarkers in systemic sclerosis related vasculopathy and fibrosis

8.1 Introduction

Circulating biomarkers are a valuable tool for disease activity and damage assessments across many health conditions. In the rheumatic disease, circulating inflammatory acute phase proteins form an integral part of disease activity scores in rheumatoid arthritis and have helped revolutionise our approach to management through treat-to-target approaches (392). Similarly, the management of gout is now largely based on circulating uric acid levels as a target for therapy (393). There has been a paucity of biomarkers in SSc. In recent years, circulating biomarkers such as urate and NT-proBNP have been applied in the field of PAH to support clinical decision-making around the need for right heart catheterisation (394, 395). At present, there are no validated biomarkers for skin or peripheral vascular disease although there has been interest in a number of potential biomarkers (chapter 1.8). Amongst these, there has been significant interest in VEGF-A molecular pathways (chapter 1.9). VEGF-A isoforms with divergent vasculogenic roles and fibrotic potential have been of particular interest, as are the interplay of angiopoietins whose actions are dependent upon the presence of VEGF-A signalling (discussed in detail chapter 1.9.6.1). Whilst the body of evidence for the role of these biomarkers in SSc pathology is growing steadily, rarely has there been correlation with objective measures of vascular and skin pathology, which therefore may limit our interpretation of these results.

8.1.1. Chapter hypothesis, aims and objectives

We hypothesised that expression of differential VEGF-A isoforms and angiopoietins are drivers of SSc vascular and skin pathology. The aims of this chapter were therefore to investigate the relationship between circulating vascular biomarkers and SSc vasculopathy and skin pathology. The specific objectives were:

1. To compare levels of plasma biomarkers in SSc versus controls.
2. To compare levels of plasma biomarkers with evidence of SSc vasculopathy on LSCI, NC and HFUS.
3. To compare levels of plasma biomarkers with evidence of SSc skin pathology on HFUS and mRSS.
4. To investigate platelets as a potential source of vascular biomarkers in SSc by comparing levels in platelet poor plasma and activate platelet releasate.

8.2 Methods

8.2.1 Study population

Healthy controls and SSc participants were recruited as described previously (chapter 2.1).

8.2.2 Study procedures

8.2.2.1 Microvascular imaging and analysis

Quantification of microvasculopathy by LSCI (chapter 2.5), NC (chapter 2.6) and HFUS cSMI (chapter 2.7) was performed as previously described. LSCI data described in this chapter represents the mean of values for 2-5th fingers. NC patterns described in this chapter represent the overall NC pattern (the worst pattern represented across the 3 examined digits). Similarly, individual

NC parameters such as ICD are reported as an overall value (a mean number across the 3 examined digits). HFUS cSMI data was determined as a vascularity index as previously described (chapter 5.3).

8.2.2.2 Clinical assessment of skin pathology

Skin pathology was assessed as previously described by HFUS (chapter 2.8) and mRSS (chapter 2.2.1).

8.2.2.3 Vascular biomarker detection by ELISA

Plasma and platelet releasate samples were prepared as per the methodology description in chapter 2.9. Vascular biomarkers were quantified in plasma by ELISA according to the manufacturers' instructions for panVEGF-A, sVEGFR1 and sTie-2 (K15190D Multiplex, Mesoscale discovery), VEGF-A_{165}b (DY3045 duoset, R&D Systems), angiopoietin-1 (DANG10 quantikine, R&D Systems) and angiopoietin-2 (DANG20 quantikine, R&D Systems) (chapter 2.9.2). Activated platelet releasate samples were also analysed by the same assays for panVEGF-A, VEGF-A_{165}b and angiopoietin-1. Ang-2 was not quantified in platelet releasate due to evidence that Ang-2 is not stored by platelets (307). All ELISAs were performed by the same investigator (VF).

8.2.3 Statistical analysis

Independent t-test and Pearson's Chi squared were used to compare demographic data. Non-parametric statistical tests were used to compare data from clinical assessments and plasma biomarkers including Mann-Whitney U and Kruskal-Wallis. Where the latter identified a significant difference between 2 or more groups, a post-hoc Dunn test was applied to report comparisons between individual pairs. Non-parametric comparisons

are presented as median [IQR]. Data displayed as box plots show median (horizontal line), interquartile ranges (box plot) and range (whiskers) with group outliers shown as asterisks and circles.

8.3 Results

8.3.1 Cohort demographic data

All healthy controls donated plasma samples (EDTA and citrate). Plasma could not be obtained from 2 SSc participants due to poor venous access. Three additional SSc participants had citrate samples only. Demographic data across the cohort was similar to that described previously (chapter 3.3.1). Specifically, that there was a significantly older age in the SSc groups compared to controls and that the former had a higher use of vasodilators as expected (Table 8.1 for plasma citrate donors and 8.2 for plasma EDTA donors). There was no difference between groups in smoking status.

Table 8. 1 Demographics of the study cohort for plasma citrate donors.

p<0.05* and p≤0.01** using Independent t-test for age compared and Pearson's Chi squared for vasodilator use compared to controls. Abbreviations: DU, digital ulcers; PAH, pulmonary arterial hypertension.

	Plasma citrate					
	HC	SSc	LcSSc	DcSSc	Early SSc	Late SSc
n.	15	51	44	7	11	40
Age, mean yrs (s.d.)	49.6 (8.9)	**61.9 (11.4)****	**62.0 (11.2)****	**61.7 (13.1)***	**62.0 (13.6)****	**61.9 (10.9)****
Smoking status, n. (%)						
Current	1 (7)	6 (12)	4 (9)	2 (29)	2 (18)	4 (10)
Ex-smoker	3 (20)	11 (22)	10 (23)	1 (14)	1 (9)	10 (25)
Vasodilator use, n. (%)	2 (13)	**33 (65)****	**28 (64)****	**5 (71)****	**8 (73)****	**25 (63)****
DU history n. (%)	-	15 (29.4)	14 (31.8)	1 (14.3)	1 (9.1)	14 (35)
PAH	-	3 (5.9)	3 (6.8)	0 (0)	0 (0)	3 (27.3)

Table 8. 2 Demographics of the study cohort for plasma EDTA donors.

p<0.05* and p≤0.01** using Independent t-test for continuous age data and Pearson's Chi squared for vasodilator use. Abbreviations: DU, digital ulcers; PAH, pulmonary arterial hypertension.

	Plasma EDTA					
	HC	SSc	LcSSc	DcSSc	Early SSc	Late SSc
n.	15	48	41	7	11	37
Age, mean yrs (s.d.)	49.6 (8.9)	**61.4 (11.4)****	**61.3 (11.3)****	**61.7 (13.1)***	**62.0 (13.6)****	**61.2 (10.9)****
Smoking status, n. (%)						
Current	1 (6.7)	6 (12.5)	4 (9.8)	2 (28.6)	2 (18.2)	4 (10.8)
Ex-smoker	3 (20)	10 (20.8)	9 (22)	1 (14.3)	1 (9.1)	9 (24.3)
Vasodilator use, n. (%)	2 (13)	**31 (65)****	**26 (63)****	**5 (71)****	**8 (73)****	**23 (62)****
DU history n. (%)	-	14 (29.2)	13 (31.7)	1 (14.2)	1(9.1)	13 (35.1)
PAH	-	3 (6.3)	3 (7.3)	0 (0)	0 (0)	3 (8.1)

8.3.2 Vascular biomarkers in systemic sclerosis

Across all investigated vascular biomarkers and soluble receptors, significantly increased median plasma levels were only identified for angiopoietin-2 in SSc compared to healthy controls (median 548pg/ml [458-780] versus 445 [348-616] respectively, p=0.012) (Figure 8.1 and Table 8.3). Whilst significant differences were not noted for VEGF-A biomarkers between groups, the upper range of plasma panVEGF-A and VEGF-A_{165}b were notably higher in SSc than controls. Indeed only 3/15 healthy controls had plasma VEGF-A_{165}b greater than the lower limit of detection by ELISA, with a maximum recorded plasma level of 46pg/mL. In comparison, n=16/51 SSc had positive VEGF-A_{165}b with a peak level of >4000pg/mL. Lack of statistical significance was due to a large number of participants with undetectable VEGF-A_{165}b resulting in both groups having a median = 0pg/mL. The limit of detection for VEGF-A_{165}b assay (DY3045, R&D Systems) was investigated by extending the standard curve and determined to be between 0 – 8.06 pg/mL (Appendix 4).

Similarly, we were not able to demonstrate a significant difference when VEGF-A_{165}b was divided into ordinal groups of successive plasma level (Table 8.4) again due to the low number of positive values.

Figure 8. 1 Vascular plasma biomarkers in systemic sclerosis.

Higher median plasma levels of angiopoietin-2 are higher in SSc than controls (E). Due to the large number of control and SSc with undetectable VEGF-A_{165}b, the median values for both groups =0pg/mL and therefore did not show significant differences. However, a notable greater range of plasma VEGF-A_{165}b is shown (B) in SSc with maximum levels >4000pg/mL in 2 SSc participants. A trend towards increase panVEGF-A in SSc was noted (A), and reduction in sVEGFR1 (C) and angiopoietin-1 (D). No difference was noted between groups for sTie-2 (F). Statistical analysis illustrated using Mann Whitney-U.

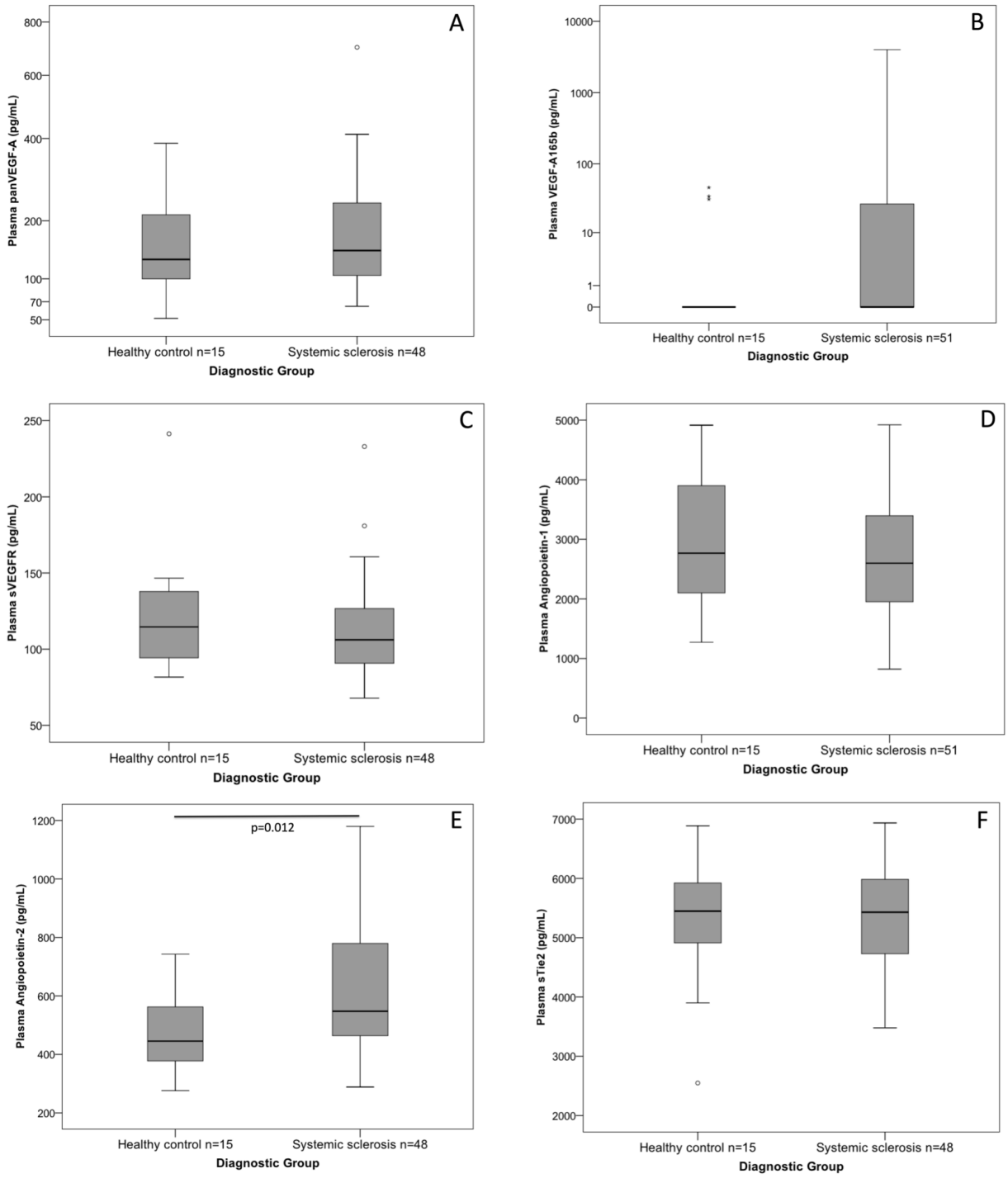

Table 8. 3 Plasma vascular biomarkers in systemic sclerosis and healthy controls.

p<0.05π and p≤0.01ø by Mann Whitney-U. Data are re-presentation of Figure 8.1.

	panVEGF-A	**VEGF-A_{165}b**	**panVEGF-A/ -A_{165}b ratio**	**sVEGFR1**	**Ang-1**	**Ang-2**	**Ang-1/-2 ratio**	**Tie-2**
n.	15	15	15	15	15	15	15	15
Healthy control, median pg/mL, (IQR; range)	130 (91-219; 51-387)	0 (0-0; 0-46)	12961 (5141-21852; 2-38664)	115 (89-138; 82-241)	2767 (1959-4054; 1272-4915)	**445 (348-616; 276-743)**	**6.2 (4.4-8.6; 2.6-11.0)**	5448 (4891-5970; 2548-6888)
n.	48	51	48	48	51	48	48	48
SSc, median pg/mL, (IQR; range)	144 (105-240; 65-702)	0 (0-33; 0->4000.0)	10485 (4-17972; 0-70167)	106 (91-129; 68-233)	2600 (1928-3422; 823-4921)	**548 (458-780; 288-1180) ø**	**4.4 (2.8-6.2; 1.5-10.6)π**	5430 (4717-5985; 3479-6936)

Table 8. 4 Distribution of detectable plasma VEGF-A_{165}b in SSc and controls.

Healthy control mean plasma VEGF-A_{165}b + 2 S.D. = 38.8pg/mL. Statistical analysis using Chi squared, p=0.589. Data are sub-analysis from Table 8.3.

Plasma VEGF-A_{165}b level	Healthy control, n. (%)	Systemic sclerosis, n. (%)
Subgroup total, n.	15	51
Undetectable	12 (80)	35 (69)
Very low (<39pg/mL, mean + 2 S.D. of healthy control group)	2 (13.3)	4 (7.8)
Low (39 - 50pg/mL)	1 (6.7)	2 (3.9)
Low/moderate (51-100pg/mL)	0 (0)	6 (11.8)
Moderate (101-300pg/mL)	0 (0)	1 (2)
High (301-1000pg/mL)	0 (0)	0 (0)
Very high (1001-4000pg/mL)	0 (0)	3(5.9)

There were no significant differences in clinical features between SSc with and without detectable VEGF-A_{165}b (data not shown, Chi squared). There were no significant differences between lcSSc versus dcSSc or early versus late SSc or with respect to DU history for any plasma vascular biomarker or soluble receptor (data not shown).

Given the competitive binding to VEGFR2, it was considered that the ratio, rather than the absolute level of panVEGF-A/VEGF-A_{165}b may be relevant. There was, however, no significant difference in the panVEGF-A/-A_{165}b ratio between HC and SSc (Table 8.3), lcSSc and dcSSc, early and late SSc or according to DU history (data not shown).

Similarly, we investigated the ratio of angiopoietin-1/-2 across the cohort. There was a significantly reduced ratio in SSc compared to controls (median

4.4 [2.8-6.2] versus 6.2 [4.4-8.6], p=0.018) demonstrating there is proportionally more Ang-2 in SSc (Table 8.3 and Figure 8.2) with the potential for an anti-angiogenic environment. No difference in Ang-1/-2 ratio was seen between SSc subgroups or DU history (data not shown).

Figure 8. 2 Reduced angiopoietin ratio in systemic sclerosis compared to controls suggests an anti-angiogenic environment.

The median group ratio of Ang-1/-2 in SSc is significantly less than that of controls. As such the relative proportion of Ang-2 with anti-angiogenic potential is greater in the disease group. Significance illustrated using Mann-Whitney U. Data are re-presentation from Table 8.3.

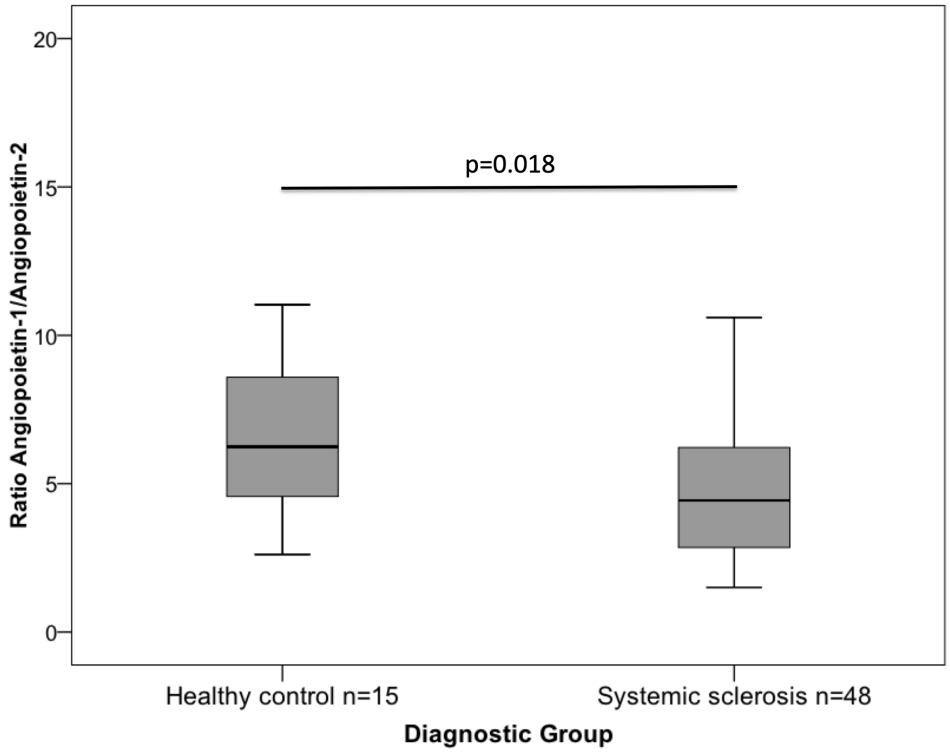

8.3.3 The relationship between plasma vascular biomarkers and objective clinical assessment of vasculopathy in systemic sclerosis

8.3.3.1 Relationship between vascular biomarkers and HFUS assessment of digital perfusion.

In healthy controls there was no significant difference in the DVVi regardless of whether circulating levels of VEGF-A_{165}b were detectable or not (Figure 8.3). Similarly, neither the absolute VEGF-A_{165}b level nor the ratio of panVEGF-A/-A_{165}b correlated with DVVi in healthy controls (Spearman's Rho = +0.220, p0.432 and -0.200, p=0.475 respectively), suggesting that low levels of the isoform are not detrimental to peripheral vasculature in otherwise healthy individuals.

Figure 8. 3 Finger Vascularity on HFUS in the presence of VEGF-A_{165}b.

Healthy controls show no significant difference in DVVi irrespective of detectable VEGF-A_{165}b levels. In contrast, SSc showed a significantly lower DVVi in the presence of detectable VEGF-A_{165}b than SSc without it. The DVVi in SSc with undetectable VEGF-A_{165}b was still lower than healthy participants with a detectable (p=0.047) and undetectable (non-significant) VEGF-A_{165}b. Statistical analysis illustrated using post-hoc Dunn test.

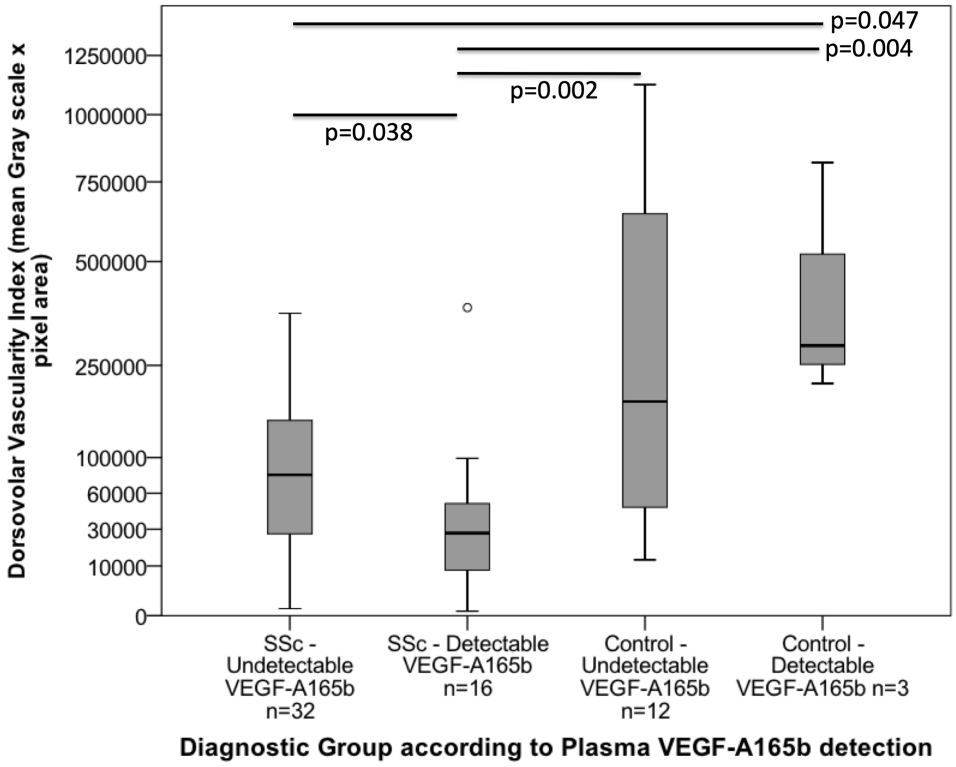

In contrast, DVVi in systemic sclerosis had a weak negative correlation with plasma VEGF-A_{165}b (Spearman's Rho = -0.289, p=0.039) (Table 8.5), which supports the anti-angiogenic nature of this isoform in SSc pathology. The correlation strengthened in late SSc (-0.336 p=0.034) as well as a notable absence of correlation in early SSc, which both reflects the progressive nature of SSc vasculopathy with time and implicates VEGF-A_{165}b with such. No significant correlation was noted in SSc-DU (data not shown), possibly due to treatment effect.

Additionally, SSc with detectable VEGF-A_{165}b in plasma had significantly lower DVVi than SSc without it (Figure 8.3), again demonstrating a

pathological link of the inhibitory isoform in SSc. However, the median DVVi for SSc was lower than controls even when VEGF-A_{165}b was undetectable. This may suggest that plasma VEGF-A_{165}b is dynamic over time and quantification of peripheral vasculopathy at a single time point (as undertaken in this study) reflects the consequence of historical VEGF-A_{165}b exposure. It is also likely that other biomarkers are involved to explain these findings.

8.3.3.2 Relationship between vascular biomarkers and LSCI assessment of digital perfusion.

Ang-2 had a weak negative correlation with the reperfusion gradient after ischaemic challenge in SSc (Table 8.5).

Table 8. 5 Correlation between objective measures of microvasculopathy in systemic sclerosis and vascular biomarkers.

p<0.05* and ≤0.01** using Spearman's rank correlation coefficient.

	panVEGF-A	VEGF-A_{165}b	panVEGF-A/ -A_{165}b ratio	sVEGFR1	Ang-1	Ang-2	Ang-1/-2 Ratio	sTie-2
n.	44	47	44	44	47	44	44	44
LSCI reperfusion gradient	+0.118	+0.043	-0.054	-0.290 (p=0.056)	+0.094	**-0.356 ***	-0.175	**+0.325 ***
n.	48	51	48	48	51	48	48	48
HFUS DVVi	-0.169	**-0.289 ***	+0.162	-0.083	-0.083	-0.021	-0.075	-0.059
n.	48	51	48	48	51	48	48	48
NC ICD	+0.01	+0.0106	+0.023	+0.019	-0.04	+0.284	+0.2	-0.233

8.3.3.3 Relationship between vascular biomarkers and Nailfold capillaroscopy assessment.

Ang-2 did not demonstrate any significant correlation with ICD in SSc (Table 8.5). Whilst there was no association between Ang-1/-2 ratio and ICD in SSc overall, there was a strong negative correlation with overall mean ICD in early SSc (-0.609, p=0.047), again suggesting an anti-angiogenic environment with a greater proportion of circulating Ang-2. This relationship was not observed in late SSc suggesting that angiopoietins may influence early vascular pathology. There were no significant correlations in SSc-DU for angiopoietins (data not shown).

When considering the overall NC pattern, there was a non-significant trend for panVEGF-A to reduce with advancing NC pattern in SSc. Similarly, there was a non-significant trend for Ang-2 to increase. Median angiopoietin-2 levels in SSc with late NC pattern were higher ($p<0.001$) compared to healthy controls (Figure 8.4 and Table 8.6). There was no significant difference identified between the median values for plasma VEGF-A_{165}b according to overall NC pattern in SSc, again due to the high number of samples where it was undetectable resulting in a median of 0. However, the mean and upper range of VEGF-A_{165}b was notably higher in those exhibiting the active pattern and lowest in those with late capillaroscopy. This suggests that circulating levels rise at the point of initial capillary loss and implicates VEGF-A_{165}b in NC progression.

Figure 8. 4 Expression of vascular biomarkers with nailfold capillary progression.

A trend for (A) panVEGF-A to decrease and (B) angiopoietin-2 to increase across advancing SSc NC patterns (Kruskal-Wallis). Angiopoietin-2 was significantly higher in SSc with late NC pattern than controls (post-hoc analysis using Dunn test).

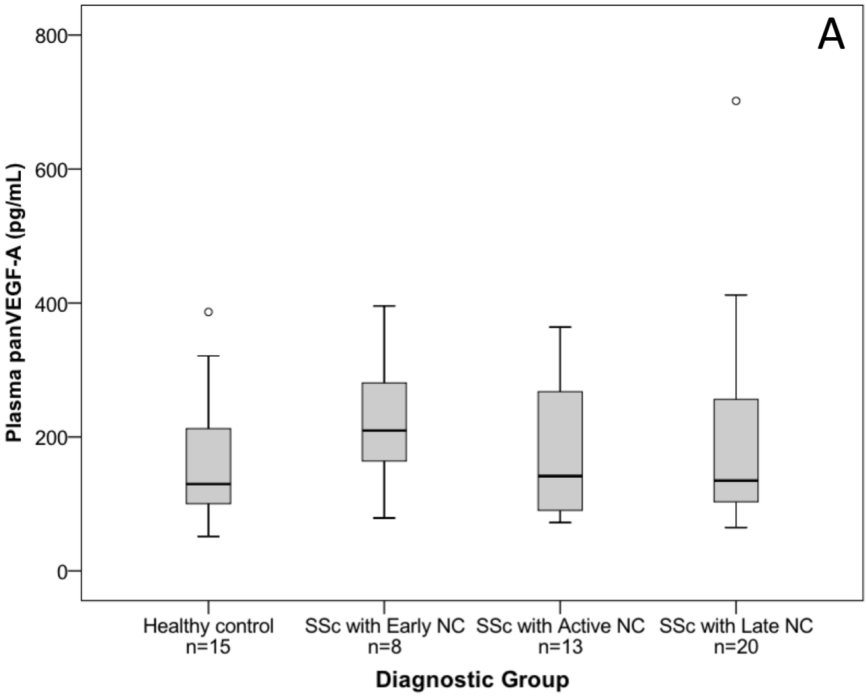

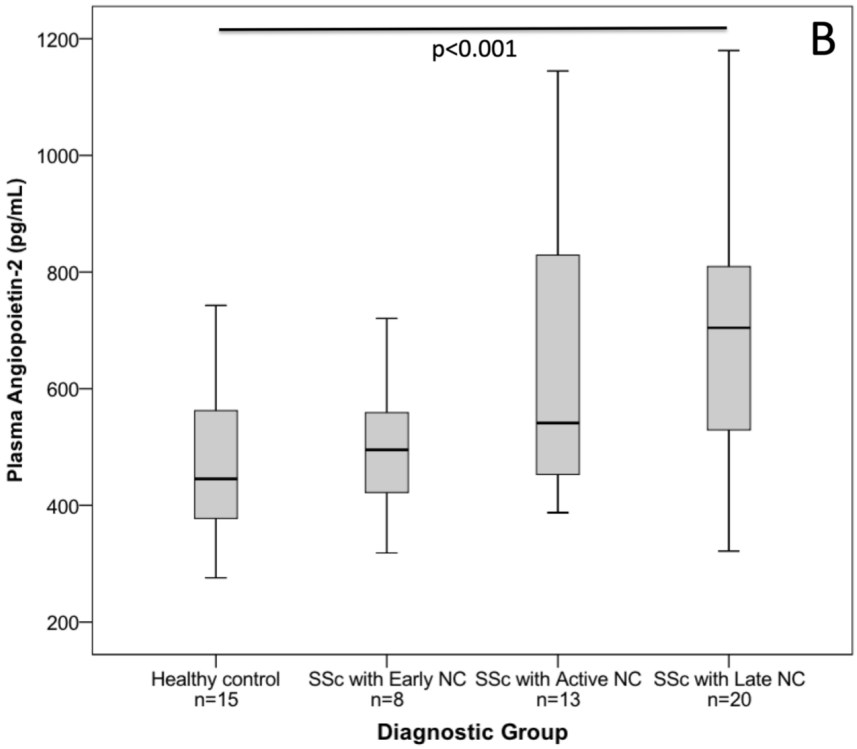

Table 8. 6 Circulating VEGF-A levels according to overall nailfold capillaroscopy pattern in systemic sclerosis.

Statistical comparison between SSc and controls (Mann-Whitney U) is shown as previously demonstrated in Table 8.3. Statistical comparison between controls and all SSc NC patterns is illustrated using Kruskal-Wallis. p≤0.01¥ for paired comparisons between individual NC patterns and controls using post-hoc Dunn test. Data are re-presentation of Figure 8.4.

	Biomarker median pg/mL (mean; IQR, range)		
	Pan-VEGF-A	**VEGF-A_{165}b**	**Ang-2 median**
n.	15	15	15
Healthy controls	130 (169; 91-219, 51-387)	0.0 (7.5; 0-0, 0-46)	445 (476; 348-616, 276-743)
n.	48	51	48
SSc group overall	144 (187; 105-240, 65-702)	0.0 (217; 0-33, 0->4000)	**548 (630; 458-780, 288-1180)**
p value (MWU)	0.628	0.279	**0.012**
SSc Early (n=8)	210 (223; 158-300, 79-396)	0.0 (112; 0-30, 0-844)	495 (499; 419-565, 318-721)
SSc Active (n=13)	141 (176; 89-270, 72-364)	0.0 (625; 0.0-62, 0-4000)	541 (639; 422-830, 388-1145)
SSc Late (n=20)	135 (199; 102-268, 65-702)	0.00 (27; 0-40, 0-176)	**704 (708; 529-824, 322-1180)¥**
p value (Kruskal-Wallis)	0.547	0.607	**0.004**

8.3.4 The relationship between circulating vascular biomarkers and systemic sclerosis related skin disease

Contrary to our hypothesis, there was no relationship seen between VEGF-A isoforms and skin disease measured on HFUS at the proximal finger in SSc (Table 8.7). However, angiopoietins demonstrated a weak correlation with HFUS skin parameters such that Ang-1 and Ang-2 increase with resolution of cutaneous oedema and Ang-2 increases with skin stiffness suggesting increasing fibrosis (Table 8.7).

There were no significant correlations between vascular biomarkers and ex vivo forearm collagen staining in SSc (data not shown). However, plasma VEGF-A_{165}b in HC strongly correlated with forearm collagen (Spearman's $\rho = -0.701$, $p=0.024$), which mirrored a significant reduction in forearm collagen in HC where VEGF-A_{165}b was detectable (n=2) versus undetectable (n=8) (integrated density = 1289 [1188-] versus 4691 [4329-6064] respectively, $p= 0.044$), noting however, that numbers were small in the former.

Table 8. 7 Correlation between vascular plasma biomarkers and skin disease at the proximal finger on HFUS in systemic sclerosis.

p<0.05* and ≤0.01** using Spearman's Rank Correlation coefficient.

	Biomarker							
	panVEGF-A	**VEGF-A_{165}b**	**panVEGF-A/-A_{165}b ratio**	**sVEGFR1**	**Ang-1**	**Ang-2**	**Ang-1/-2 ratio**	**sTie-2**
n.	48	51	48	48	51	48	48	48
Total mRSS	-0.192	-0.077	0.042	+0.034	-0.129	0.255	-0.246	0.114
n.	48	51	48	48	51	48	48	48
Skin thickness	0.003	0.056	-0.099	+0.024	-0.035	-0.235	0.185	-0.014
n.	48	51	48	48	51	48	48	48
Echogenicity	-0.018	-0.154	0.115	+0.222	**+0.381 ****	**+0.330 ***	0.083	0.146
n.	48	51	48	48	51	48	48	48
SWE	0.045	-0.189	0.13	-0.158	0.069	**+0.348 ****	-0.228	0.005

8.3.5 What is the source of VEGF-A isoforms?

As expected, the median panVEGF-A level in activated P-RP was significantly higher than in P-PP alone in both SSc and controls demonstrating that VEGF-A is stored and released by activated circulating platelets (Table 8.8 and Figure 8.5). Additionally, the increase in platelet versus plasma panVEGF-A in SSc achieved greater significance (Wilcoxon Rank test, $p<0.001$) than controls ($p=0.036$) (Table 8.8).

There was no significant difference in levels of VEGF-A_{165}b in activated P-RP compared to P-PP potentially due to the low number of detectable results resulting in the median result = 0. When considering only cases where VEGF-A_{165}b was detectable in P-PP (and excluding those taking anti-platelets or NSAIDs, n=15) there was still no significant difference between median P-PP and P-RP VEGF-A_{165}b levels (88 [37-686], range 22-4000 versus 80 [33-197], range 0.0-4444 respectively, $p=0.865$).

Angiopoietin-1 was significantly higher in activated P-RP than P-PP again suggesting Ang-1 is released by activated platelets.

There was no significant difference in the median level of vascular biomarkers in activated platelet releasate in SSc compared to controls, lcSSc versus dcSSc or early versus late SSc. However, SSc P-RP had non-significantly lower Ang-1 than controls demonstrating the potential for an anti-angiogenic environment.

Table 8. 8 Vascular biomarkers in activated platelet releasate across the study cohort.

p<0.05Ω and p≤0.001Δ using Wilcoxon rank test for paired PPP/PRP samples. There were no significant differences between any biomarker in activated platelet releasate in SSc versus controls using Mann-Whitney U. There was a trend (n.s.) for lower Ang-1 in activated PRP in SSc than controls using Mann-Whitney U.

	Whole study cohort (SSc+HC)			**Healthy controls**			**Systemic sclerosis**		
	panVEGF-A	**VEGF-A_{165}b**	**Ang-1**	**panVEGF-A**	**VEGF-A_{165}b**	**Ang-1**	**panVEGF-A**	**VEGF-A_{165}b**	**Ang-1**
n.	63	66	66	15	15	15	48	51	51
Platelet poor plasma, median (IQR; range)	144 (105-233; 51-702	0.0 (0-24; 0-4000)	2618 (1951-3688; 823-4921)	130 (91-219; 51-387)	0.0 (0-0; 0-46)	2767 (1959-4054; 1272-4915)	144 (105-240; 65-702)	0.0 (0-33; 0-4000)	2600 (1928-3422; 823-4921)
n.	63	63	**63**	**15**	**15**	**15**	**48**	**48**	**48**
Activated Platelet releasate, median (IQR; range)	**357 (121-620; 42-1406)**Δ	0.0 (0-20; 0-4444)	**19319 (14087-27665; 1502-40107)**Δ	**357 (98-620; 42-993)Ω**	0.00 (0.00-0.00; 0.00-35.1)	**23985 (15260-28047; 2597-39454)**Δ	**360 (132-623; 63-1406)**Δ	0.0 (0-24; 0-4444)	**18519 (13713-25873; 1502-40107)**Δ

Figure 8. 5 Release of vascular biomarkers following platelet activation.

From left to right, paired levels of panVEGF-A, VEGF-A_{165}b and angiopoietin-1 in plasma (white) and activated platelet releasate (grey) are shown. Significantly increased levels of panVEGF-A and angiopoietin-1 are seen in both systemic sclerosis and healthy controls after platelet activation. No significant difference is seen in VEGF-A_{165}b levels after platelet activation. No significant difference is seen in the biomarker levels of platelet releasate between SSc and controls. Statistical significance illustrated using Wilcoxon rank test. Data are re-presentation of Table 8.8.

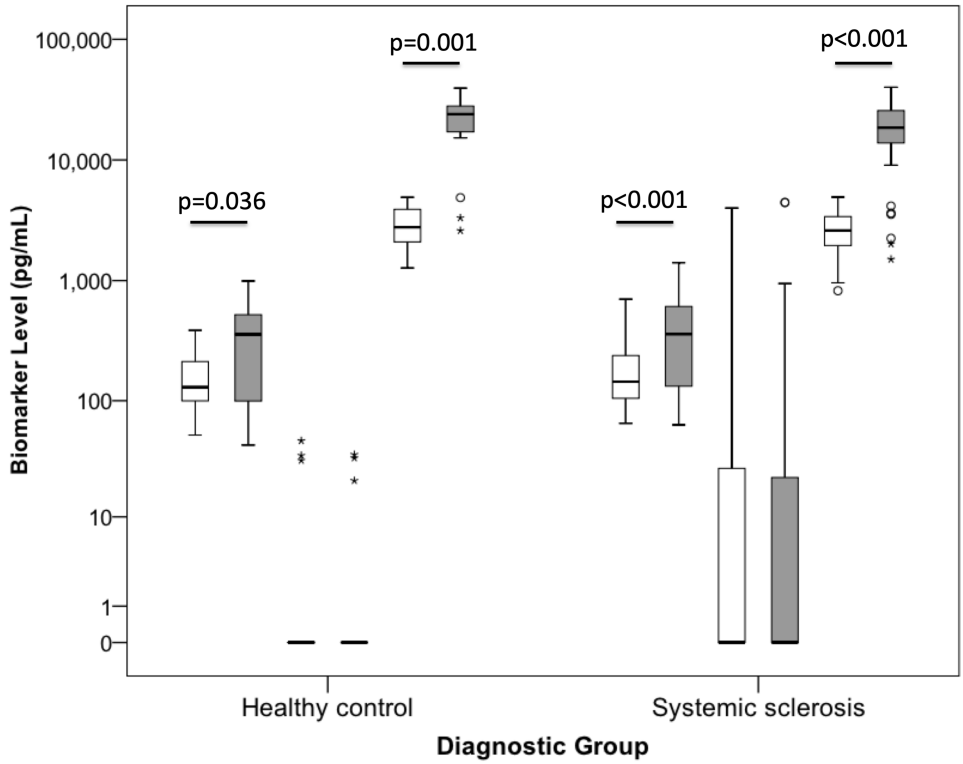

8.4 Discussion

8.4.1 Vascular biomarkers are increased in systemic sclerosis in favour of vascular inhibition

The first reports of increased levels of inhibitory VEGF-A_{165}b isoform in SSc (280, 302) generated great interest in their potential as a future vascular biomarker. In striking contrast to that, we have not found a statistically significant difference in plasma levels between our SSc cohort and controls due to a high number of undetectable results in both groups. One explanation for the disparity in the findings of our work with earlier studies is that a minimum 10-15 day washout of vasodilators and DMARDs was protocolled

in previous work (302). Indeed, similar to the documented effects of Iloprost on panVEGF-A (396), we hypothesise there may be a therapeutic effect of vasodilators on VEGF-A_{165}b levels. We did, however, observe a notable difference in the percentage of SSc participants with detectable VEGF-A_{165}b in plasma as well as a remarkably higher maximum level in line with Manetti et al., (who reported VEGF-A_{165}b 56 - 1056pg/mL in SSc versus 0 – 350pg/mL in controls) (302). This again suggests that this inhibitory isoform contributes to the anti-angiogenic milieu in SSc and is further reflected in our novel finding of reduced finger perfusion on HFUS associated with VEGF-A_{165}b in plasma. The correlation between HFUS vascularity and VEGF-A_{165}b in late but not early SSc supports the hypothesis that the impact of inhibitory isoforms may evolve over time. Somewhat surprisingly, despite the significantly lower vascularity indices in SSc-DU (discussed in chapter 5), there was no correlation between vascularity and VEGF-A_{165}b in SSc-DU group, which again may be due to use of vasodilators. Similarly, (and in line with previous reports), we did not find any difference in plasma VEGF-A_{165}b between lcSSc and dcSSc (280, 302) or early versus late (302).

We expected to find a progressive increase in VEGF-A_{165}b across NC patterns with progressive vascular loss, as demonstrated by Manetti et al., (280). The observed peak of mean VEGF-A_{165}b in our cohort actually occurred in relation to active NC changes when capillary drop out is first featured. Levels were also higher in early NC phase than late NC, which suggests that VEGF-A_{165}b may precede structural vascular loss. Variations in study results across the literature with respect to this relationship may again be due to a therapeutic effect or alternatively be dependent on the temporal sampling window as patients transition from one NC phase to the

next. Indeed, we noted a trend for SSc with late NC changes to have higher vasodilator use and significantly higher PDE-5 inhibitor use (chapter 4.3.3 Table 4.1). Longitudinal studies with serial plasma and NC analysis are required to fully elucidate the implications of VEGF-A_{165}b in structural vasculopathy and therapeutic interventions on both.

We have previously described the divergent nature of Ang-1 and -2 in the presence of panVEGF-A (chapter 1.9.6.1). Our parallel findings of increased Ang-2 (299, 304, 316, 317, 319, 397, 398) and a reduced Ang-1/-2 ratio (299, 316, 319, 398) as well as a trend for an increase in panVEGF-A (123, 145, 270, 277, 278, 299, 302, 304, 319, 398-400) in SSc are in line with previous reports and further demonstrate the anti-angiogenic milieu that occurs in SSc. To our knowledge, we are the first to identify a negative relationship between Ang-2 and reperfusion gradient on LSCI which suggests an inhibitory actions of Ang-2 influence vasoactive capacity. In similar regard we have shown Ang-2 increases with advancing NC patterns that has been reported elsewhere (299, 317, 398). Of interest, we noted a strong negative correlation between Ang-1/-2 ratio and ICD in early but not late disease suggesting that the relative ratio of angiopoietins may be relevant early in the pathological processes but that vascular regression continues as Ang-2 increases towards late NC patterns.

PanVEGF-A levels did not significantly differ with disease duration in our cohort, which corresponds with some previous reports (270, 277, 299, 302, 401), whilst others have described increased panVEGF-A in early SSc (145). We hypothesize that such variability in the literature may again be due to treatment effect across different study populations.

There are a number of other conflicting observations across both the published literature and our data with respect to angiopoietins, sTie-2 and panVEGF-A in relation to NC parameters (270, 277, 278, 318, 319, 398), SSc subtypes (145, 270, 277, 299, 302, 304), autoantibody profile (270, 299, 303) and SSc-DU (145, 270, 272, 299). These would benefit from large-scale longitudinal study with repeated sampling pre and post-treatment initiation.

8.4.2 The relationship between angiopoietins and evolving skin pathology

We have demonstrated for the first time that there is a relationship between angiopoietins and in vivo skin pathology such that Ang-1 and -2 increase as oedema resolves towards the fibrotic phase and that parallel increases in Ang-2 also relate to increasing skin stiffness. There is disagreement between the few studies that examined a relationship between Ang-2 and mRSS (299, 317), for which we again consider the potential influence of medication in those cohorts. Whilst two previous cross-sectional studies have not demonstrated any relationship between Ang-2 and drug treatment (299, 304), one longitudinal study has demonstrated a reduction in Ang-2 with successive Cyclophosphamide therapy, which also related to improvements in pulmonary fibrosis post treatment (402). Indeed, the relationship with Ang-2 and fibrosis may therefore be stronger in early treatment naïve patients and warrants further study.

Other angiogenic signalling factors that share structural properties with angiopoietins such as angiopoietin-like protein 3 [Angptl-3] are also significantly raised in SSc related vasculopathy and skin thickening (403,

404), as well as dermatomyositis (404) (another autoimmune rheumatic disease frequently overlaps with SSc features). With similar regard, anti-angiogenic endostatin correlates with and both mRSS and histopathological skin fibrosis in previous reports (145). These parallel observations within the wider literature support the truly complex nature of SSc pathology.

We did not demonstrate a relationship between circulating VEGF-A and skin pathology, which is contrary to our hypothesis and may be due to a limitation of the study having a mixed cohort of early and late, lcSSc and dcSSc patients as well as lack of therapeutic naïve numbers. The published literature is also conflicting such that one study has shown a strong correlation between serum VEGF-A and mRSS (277) whilst others have not (145, 299).

There appeared to be a significant negative relationship between VEGF-A_{165}b in HC and collagen content of forearm skin that was not apparent in SSc. This may suggest that VEGF-A_{165}b does discourage fibrotic pathways in healthy individuals. We cautiously speculate that in other factors in SSc overcome the anti-fibrotic actions of VEGF-A_{165}b or that the relationship is negated by the effect of vasodilator use on VEGF-A_{165}b levels. For further consideration, circulating levels of vascular biomarkers may not be reflective of organ specific expression.

8.4.3 Platelets are a source of anti-angiogenic vascular biomarkers in systemic sclerosis

We have confirmed that platelets are a source of panVEGF-A and Ang-1 in both SSc and HC as expected. We did not however, show a significant

difference in platelet expression between diagnostic groups despite the increase in platelet panVEGF-A previously reported in SSc (307). The lack of significance applicable to platelet Ang-1 was also reported in this study (307), although we noted a trend for SSc platelets to store less Ang-1, which may translate to lesser vasculogenic potential compared to controls. The lack of a significant difference in both PPP and PRP Ang-1 may again be attributable to the therapeutic effect of vasodilators. Indeed, platelets are also a source of increased Ang-1 and panVEGF-A in hypertension in otherwise healthy individuals and a reduction by therapeutic anti-hypertensive agents has been previously reported (405).

Whilst there is only one previous study to formally report the platelet expression of Ang-1 in SSc, those reporting circulating levels in serum versus plasma are also relevant to this discussion. Platelet activation is inherent in serum samples due to the methodology in sample processing. Conversely, platelet aggregation is largely inhibited in plasma due to addition of citrate or EDTA buffers to the phlebotomy conduits and may only occur in the presence of high centrifugal forces during sample preparation (discussed in chapter 2.9). As such, some previous studies utilising serum have shown reduced circulating Ang-1 in both pre-SSc (316) and established disease (316, 317, 398) compared to controls. In contrast, another study demonstrated higher *plasma* Ang-1 in SSc (319). We in turn, found comparable levels in platelet poor plasma but also noted a non-significant reduction in Ang-1 in platelet releasate compared to controls. This not only demonstrates that platelet biomarker expression may contribute to pathology in SSc but also may explain variations in published reports.

Just prior to completing sample collection for our study, Hirigoyen et al. (308) published results demonstrating release of low but detectable levels of VEGF-A_{165}b from SSc platelets by an alternative methodology involving isolating, washing and activating SSc platelets. As our methods compared PPP to activated PRP, we are unlikely to detect significantly different VEGF-A_{165}b in PRP as the platelet contribution in plasma appeared to be very small in Hirigoyen's data. We did not have the facilities to follow this procedure. Furthermore, the majority of our samples had already been subject to our described methodology when this work was published (chapter 2.9).

In contrast to the haemopoietic lineage of platelets, other studies have demonstrated increased panVEGF-A and VEGFR2 expression by cultured mesenchymal stem cells from SSc donors (406). Additional increase in panVEGF-A and VEGFR2 were observed in co-culture with SSc endothelial cells suggesting there is pathological function of individual cells with additional amplification by paracrine interactions (406). This reflects the truly systemic nature of SSc at a biological and clinical level.

8.4.4 Concluding remarks

The evidence for an altered profile of vascular biomarker in SSc is ever increasing and not only supports the vascular basis of this disease but also implicated these biomarkers in fibrosis and skin pathology. We have demonstrated that expression of circulating vascular biomarkers in SSc are altered to the detriment of vascular health. In particular we report for the first time that peripheral vasculopathy is worse in SSc in the presence of VEGF-A_{165}b and increased Ang-2. We have further demonstrated for the first time that there is a relationship between angiopoietins and skin pathology which

builds on the principles of the Vascular hypothesis. Our data highlights these signalling molecules as potential future biomarkers for clinical application and therapeutic targets in SSc vasculopathy and skin disease.

Future studies should consider the influence of medication on their study design and aim to include treatment naïve patients where possible in order to understand the relevance of vascular biomarkers on SSc pathology and disease course.

Chapter 9. Altered expression of hypoxia inducible factor and VEGF-A isoforms in systemic sclerosis skin

9.1 Introduction

9.1.1 Vascular biomarkers in SSc skin disease

We have demonstrated an altered expression of vascular biomarkers such as VEGF-A_{165}b and Ang-2 in SSc plasma in favour of an anti-angiogenic environment (chapters 1.9 and 8). Both VEGF-A and angiopoietins have been implicated in both SSc vasculopathy (277, 280, 299, 302, 304, 316, 317, 319) and skin pathology (39, 277, 284, 300, 302, 317) (discussed in detail in chapters 1.9 and 8). The available data from these sources most commonly reports on either pre-clinical models or circulating biomarkers. Whilst circulating levels may broadly represent the systemic exposure of signalling factors, the tissue specific expression may be more relevant in determining pathology and clinical phenotype. There are minimal reports of inhibitory vascular biomarker expression (including VEGF-A_{165}b (302) and Ang-2 (316)) in human ex vivo SSc skin. Report of dermal Ang-2 expression has also been limited to the vasculature (316). Further study of tissue specific data in other SSc cohorts is required to make firm conclusions about the respective roles of these vascular biomarkers in tissue fibrosis.

9.1.2 Hypoxia inducible factor

As discussed in detail in chapter 1.4.1, SSc lesional skin is notably hypoxic (39) and as such previous investigators have considered the role of HIF1α in SSc pathogenesis as part of the vascular hypothesis (38). Whilst there has been relatively little study of HIF in SSc, there is evidence of particular single

nucleotide polymorphisms of the HIF1A gene (341) as well as increased serum levels of HIF1α in SSc (407). It is also hypothesised that HIF1α with downstream VEGF-A and angiopoietin-like proteins have a role in activation of osteoclasts at the distal phalanx of ischaemic fingertips resulting in bony resorption in SSc patients (408). *In vitro* experiments have demonstrated upregulation of HIF1α dependent CTGF and collagen in dermal fibroblasts in response to hypoxic stimulus (301, 409). Whilst this suggests that hypoxia induced HIF1α pathways may play a role in SSc fibrogenesis, there has been little *ex vivo* work investigating the expression of HIF paralogs in SSc whole skin. Those few who have reported it, show notable lack of consensus between them (39, 300, 409). Distler et al., first described a surprising reduction in HIF1α in the skin of SSc despite tissues being objectively hypoxic (39). Ioannou et al., subsequently described increased HIF1α in SSc skin (300). Most recently Zhou et al., (409) reported comparable HIF1α staining in the epidermis of SSc and controls but increased expression in dermal cells of the disease group. These conflicting reports have therefore unfortunately failed to add further explanation to the potential role of hypoxia induced HIF1α dependent pathways in SSc pathology. Additionally, this existing data are limited to the expression of HIF1α and other HIFα paralogs including HIF2α have not been studied in SSc to date.

Outside of SSc-specific research, previous studies in rodent models and human single cell cultures have demonstrated differential expression of HIFα paralogs dependent on the pattern of hypoxic exposure. Specifically, HIF1α is preferentially expressed following intermittent periods of hypoxia versus HIF2α with chronic continuous hypoxia (241, 245, 247, 337-340, 410-413) (discussed in detail in chapter 1.9.7). Extrapolating from these studies, there

is potential for HIFα paralog expression in hypoxic SSc tissues to be dynamic in response to the evolving vasculopathy. The expression of HIF2α in SSc skin at different stages of disease is therefore of interest and as of yet unreported in the literature. Both VEGF-A (240, 249) and angiopoietins (414) are downstream targets of HIF and thus the relationship between their respective expression in SSc skin warrants further exploration.

9.1.3 Histological assessment of pathological skin

In SSc research, the particular focus of study is often directed in dermis due to the overactive dermal fibroblasts and collagen deposition forming a prominent and notorious feature of the disease. Limited attention has been paid to alterations in the epidermis in SSc research, but those who have chosen to study it have revealed abnormal maturation of keratinocytes in both involved and uninvolved skin (415). Interestingly, SSc keratinocytes drive aberrant fibroblast stimulation (415) suggesting that the epithelium is a key initiator of skin fibrosis. Endothelin (an endothelium derived vasoconstrictor) is implicated in this cell-cell interaction (415). The specific *epidermal* expression of other vascular biomarkers including VEGF-A_{165}b is therefore of interest, given the potential for signal translation to the dermis and the possible anti-fibrotic implications of this isoform (256). Indeed, there have been recent clinical trials investigating the therapeutic response of SSc skin disease to vasodilator therapies either as primary or secondary outcome objectives (162, 237). Figure 9.1 demonstrates usual skin histology for appreciation of the close histological relationship of cutaneous structures.

Figure 9. 1 Example skin histology.

Haematoxylin and eosin (H&E) staining of skin tissue sections demonstrate usual skin histology including: (A) e epidermis, d dermis, sc stratum corneum, *basal epidermal keratinocytes in the basal/deepest layer of the epidermis. (B) h hair follicles and follicular keratinocytes, se sebaceous gland. (C) p papillary muscle. (D) sw sweat gland. Scale bars represent 200μm. H&E sections were performed by the Pathology department (RUH) and imaged at the university of Bath (VF). Figure created by VF using own images.

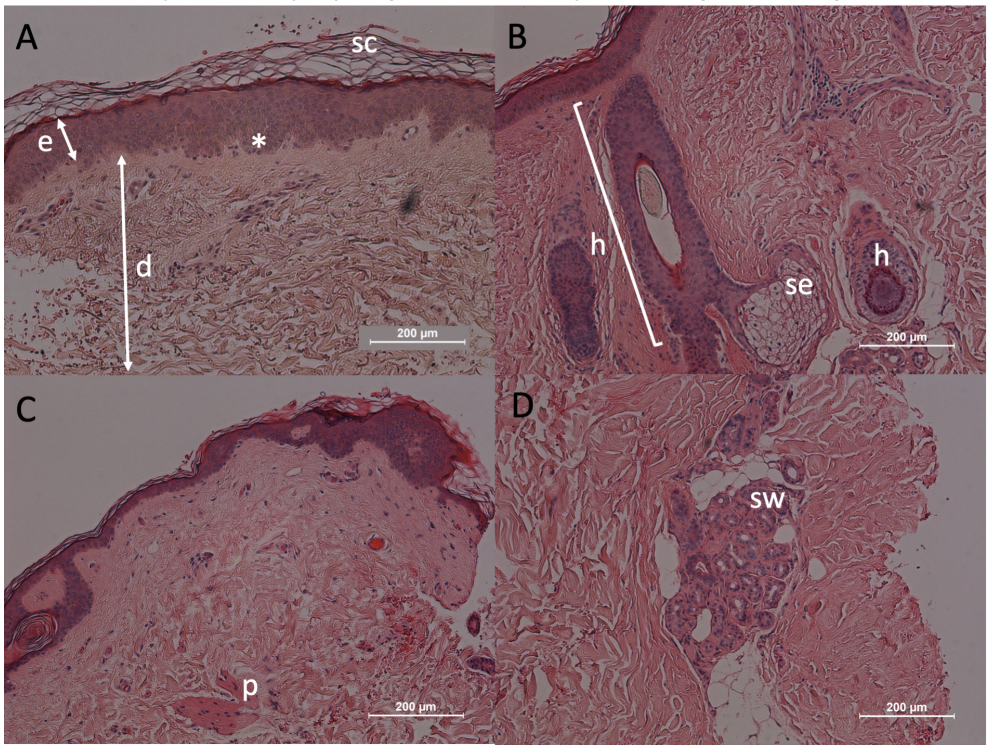

9.1.4 Chapter hypothesis, aims and objectives

We hypothesised that VEGF-A isoforms and angiopoietins, influenced by HIFα paralog expression, are drivers of in SSc skin pathology and relate to the burden on vasculopathy. The aim of this chapter was therefore to investigate the expression of these vascular biomarkers in SSc skin. The specific objectives were to:

- Explore the expression of HIF1α, HIF2α, panVEGF-A, VEGF-A_{165}b and angiopoietins in lesional SSc skin compared to non-lesional skin and healthy controls.

- Explore the inter-relationship between epidermal expression of HIF1α, HIF2α, panVEGF-A, VEGF-A_{165}b in SSc and clinical features of vasculopathy and skin pathology.

9.2 Methods

9.2.1 Study population

Healthy controls and SSc participants were recruited as described previously (chapter 2.1). A proportion of participants underwent skin biopsy as previously described (chapter 2.10.1) which was utilised for investigation in this chapter.

9.2.2 Immunofluorescent staining of HIFα paralogs and VEGF-A isoforms

Immunohistochemical staining of biomarkers by indirect immunofluorescence (IHC-IF) (chapter 2.11.2) and image acquisition (chapter 2.11.2.1) were undertaken as described previously.

9.2.1.1 Immunofluorescent image analysis

Post-acquisition image processing and epidermal quantification was performed using Zen blue lite software version 2.3 (Zeiss, U.K.). Linear unmixing was performed on a sample of images for HIFα and VEGF-A stains and confirmed no significant spectral overlap between the assigned laser wavelengths. Histological location of staining was noted for each donor and graded on a 5-point scale according to absent, weak, moderate, strong or very strong. Where staining occurred in the epidermis, semi-quantification was performed using sum of the pixel intensity across the field of view (expressed as arbitrary units) by drawing a ROI to encompass the whole depth and width of the epidermis (using Zen blue lite software version 2.3,

Zeiss, U.K.*)*. Mean intensity was not utilised as it did not appear to be representative of the visible stain due to the black background in the unstained tissue negating the quantified specific staining.

9.2.3 Masson's trichrome

Immunohistochemical staining of dermal collagen in serial sections of skin samples was undertaken using Masson's trichrome as described previously (chapter 2.11.1). Collagen staining was quantified as described previously (chapter 6.2.3).

9.2.4 Clinical assessments

9.2.4.1 Microvascular imaging

Clinical assessments for nailfold capillaroscopy to report overall inter-capillary distance (ICD) (chapter 2.6), finger perfusion on laser speckle imaging (LSCI, average across distal 2-5th fingers) (chapter 2.5) and HFUS cSMI for DVVi (chapter 2.7) were performed as described previously.

9.2.4.2 Skin assessment

SSc participants underwent mRSS assessment at the site of forearm and abdominal skin biopsies as previously described (chapter 2.2.1). Skin thickness, echogenicity and SWE were assessed at the same sites as skin biopsy as previously described (chapter 2.8).

9.2.4.3 Circulating biomarkers

Plasma biomarkers were quantified as described previously (chapter 2.9) for panVEGF-A and VEGF-A_{165}b.

9.2.5 Statistical analysis

Demographic data was analysed as previously described (chapter 3.3.6). Qualitative histological distribution of tissue staining was described for respective groups without statistical analysis. The semi-quantified epidermal expression of HIF1α, HIF2α, panVEGF-A and VEGF-A_{165}b was also described as a ratio (x-fold increase) in SSc compared to the health control group mean. Epidermal HIF1α, HIF2α, panVEGF-A and VEGF-A_{165}b for healthy controls was set a reference ratio of 1.0. Statistical comparisons for x-fold HIF1α, HIF2α, panVEGF-A and VEGF-A_{165}b utilized non-parametric tests to compare group medians using Mann-Whitney U. Correlation of semi-quantified epidermal expression of HIF1α, HIF2α, panVEGF-A and VEGF-A_{165}b (as the sum of pixel intensity) was undertaken using Spearman's rank correlation coefficient (Rho, ρ).

9.3 Results

9.3.1 Tissue samples and demographics

IF staining was performed on forearm samples from 10 SSc (5 early and 5 late) and 5 HC. Demographic data for tissue donors for IHC-IF is reported in detail in chapter 3.3.6. In brief, SSc and HC donors for IHC-IF were age and sex matched. HC donors consisted of 4 non-smokers and 1 ex-smoker. Two SSc donors were current smokers (Pearson's Chi squared, χ^2 p=0.223). SSc donors had a significantly higher use of vasodilators (n=7/10) compared to HC (n=0/5) as expected (χ^2 p=0.01, chapter 3.3.6 Table 3.8). DcSSc had a higher rate of vasodilator use than lcSSc (2/5 versus 5/5, χ^2 p=0.038). There was no significant difference in vasodilator use in early versus late SSc (3/5 versus 4/5, χ^2 p=0.490).

Clinical features of skin donors are shown in Table 9.1. All SSc participants who underwent skin biopsy at the forearm had lesional skin at the biopsy site judged by mRSS and/or HFUS parameters. Four SSc who donated skin biopsies had mRSS = 0 at the forearm (Table 9.1) but were deemed to have atrophic skin on HFUS (data not shown). IHC-IF staining was also performed on skin sections from the abdomen of 3 SSc donors at an area of clinically uninvolved skin (mRSS=0). One of the SSc abdominal skin donors (VIF27) had atrophic skin according to HFUS and 2 had normal skin thickness (data not shown). Echogenicity and SWE at the abdomen for these 3 SSc donors were within the mean +/- 2 S.D. of healthy controls.

Table 9. 1 Clinical features of skin donors.

Abbreviations: ACA, anti-centromere antibody; ANA, anti-nuclear antibody; dcSSc, diffuse cutaneous systemic sclerosis; DU, digital ulcers; GORD, gastroesophageal reflux disease; ILD, interstitial lung disease; lcSSc, limited cutaneous systemic sclerosis; mRSS, modified Rodnan skin score; Nor-90, anti-nucleolus-organising regions antibody; Scl-70, anti-topoisomerase antibody; RNAPIII, anti-RNA-polymerase III antibody; U1RNP, anti-U1RNP antibody. Overall nailfold capillaroscopy classification described is the most advanced pattern represented across 3 fingers.

VIF Study number	Diagnostic group	Age (yrs), gender	Years since first non-RP symptom	Autoantibody status	SSc specific clinical features	Local mRSS	Nailfold capillary classification	Current vasodilator use	DMARD ever
04	HC	56 female	-	-	-	-	normal	N	-
07	HC	58 female	-	-	-	-	normal	N	-
13	HC	40 male	-	-	-	-	normal	N	-
22	HC	59 female	-	-	-	-	non-specific	N	-
38	HC	66 male	-	-	-	-	normal	N	-
36	Early lcSSc	74 female	2.9	ANA (non-specific)	Scleroderma	0	early	N	N
61	Early lcSSc	55 male	0.7	Pm-Scl, Ro	GORD, scleroderma, telangectasia, synovitis, ILD	1	late	N	Y
21	Early dcSSc	81 female	2.9	Nor-90	GORD, scleroderma, ILD	1	late	Y	Y
30	Early dcSSc	74 female	0.8	RNAPIII	GORD, scleroderma	2	non-specific	Y	Y
48	Early dcSSc	61 male	1.8	RNAPIII	Telangectasia, scleroderma	1	active	Y	Y
23	Late lcSSc	56 female	12.2	Scl-70	GORD, scleroderma, DU, telangectasia, calcinosis, synovitis, ILD	0	active	Y	Y
25	Late lcSSc	66 female	40.8	ACA	GORD, scleroderma, DU, telangectasia, calcinosis	0	late	N	N
27	Late lcSSc	77 female	59.9	Scl-70	GORD, scleroderma, DU, telangectasia, calcinosis, ILD	1	late	Y	N
12	Late dcSSc	53 female	7.6	Scl-70	GORD, scleroderma, DU, telangectasia, ILD	2	late	Y	Y
18	Late dcSSc	56 female	9.2	Scl-70, U1RNP	GORD, scleroderma, telangectasia, ILD	0	non-specific	Y	Y

9.3.2 Expression of HIF and vascular biomarkers are upregulated in lesional SSc skin compared to controls

Examples of immunofluorescent staining are shown in Figure 9.2. Histological description of immunoreactivity for each biomarker is illustrated in Tables 9.2-9.4. Semi-quantified epidermal expression of biomarkers is represented in Figures 9.3 and 9.4.

Figure 9. 2 Immunofluorescent detection of vascular biomarkers in systemic sclerosis skin.

Strong panVEGF-A immunoreactivity is seen in the superficial epidermis as well as some basal epidermal keratinocytes (asterisk) at the forearm of an early lcSSc patient (VIF61) (B-C). In the same patient, VEGF-A_{165}b is seen in dermal fibroblast (arrow) (A+C). Ang-2 was expressed in the epidermis (G), dermal blood vessels (arrows, G) and strongly in sweat glands (H) of the same patient. In comparison lesser intensity of Ang-2 staining was seen in sweat glands (I) and panVEGF-A in the superficial epidermis (D-F) of healthy controls. Some basal epidermal keratinocytes expressed panVEGF-A (asterisk, E-F) in controls. Minimal VEGF-A_{165}b is expressed in dermal blood vessels in a control (arrows, D+F). Co-localisation of weak HIF1α and strong HIF2α is seen in follicular keratinocytes of an early dcSSc (VIF48) (J-L). Serial sections from the same donor show strong panVEGF-A (N-O) co-localised with HIF2α (K-L) in a hair follicle but without significant VEGF-A_{165}b expression (M-O). Tie-2 expression is seen in papillary muscle (strong), hair follicle (weak), sweat gland (weak) (P) and dermal blood vessels (Q (arrow) & R) is shown for a late lcSSc (VIF25). Images for individual channels are shown for VEGF-A_{165}b (A, D, M), panVEGF-A (B, E, N), HIF1α (J) and HIF2α (K) as well as overlay image with DAPI nuclear stain (C, F, O for VEGF-A and L for HIF). Scale bars indicate 50μm (A-Q) and 20μm (R).

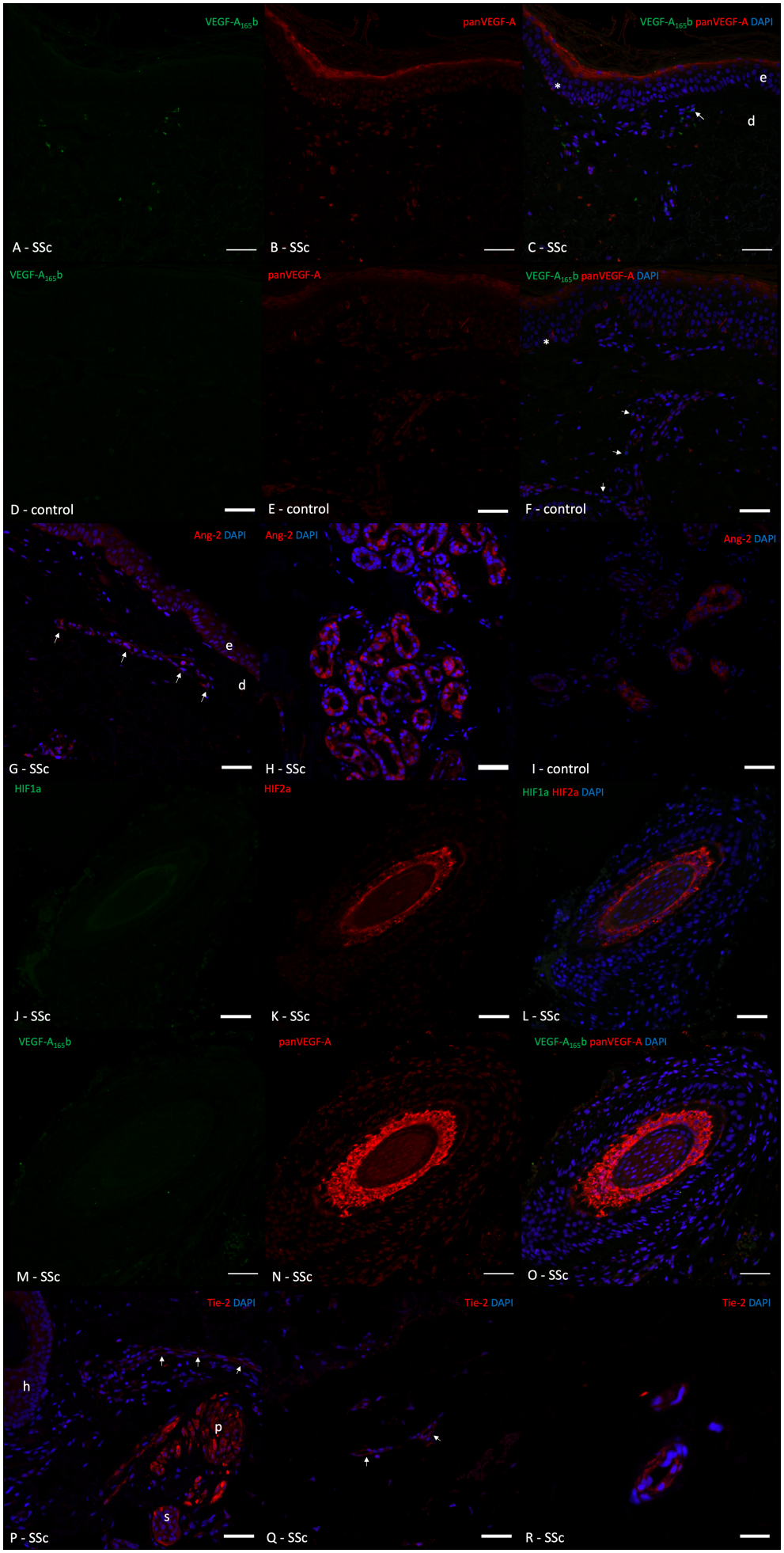
VEGF-A165b
panVEGF-A
VEGF-A165b panVEGF-A DAPI
e
d
A - SSc
B - SSc
C - SSc
VEGF-A165b
panVEGF-A
VEGF-A165b panVEGF-A DAPI
D - control
E - control
F - control
Ang-2 DAPI
Ang-2 DAPI
Ang-2 DAPI
e
d
G - SSc
H - SSc
I - control
HIF1a
HIF2a
HIF1a HIF2a DAPI
J - SSc
K - SSc
L - SSc
VEGF-A165b
panVEGF-A
VEGF-A165b panVEGF-A DAPI
M - SSc
N - SSc
O - SSc
Tie-2 DAPI
Tie-2 DAPI
Tie-2 DAPI
h
p
s
P - SSc
Q - SSc
R - SSc

9.3.2.1 Increased HIF1α and HIF2α expression in SSc skin

In healthy controls immunoreactivity for HIF1α and HIF2α was rarely seen in the epidermis or dermis and weakly so when it was observed. In contrast and as expected, HIF1α and HIF2α immunoreactivity was more commonly observed in SSc patients (Table 9.2). HIF1α immunoreactivity was present in some but not all SSc in the superficial epidermis, follicular keratinocytes, sweat glands and dermal blood vessel (Table 9.2). HIF1α epidermal expression in SSc was generally weak, but semi-quantification showed significantly increased immunoreactivity compared to healthy controls in both lcSSc (median 1.5 x-fold increase compared to HC, p=0.008) and dcSSc (median 1.6 x-fold increase compared to HC, p=0.008) (Figure 9.3). Similarly, HIF1α was significantly increased in early SSc (median 1.5 x-fold increase compared to HC, p=0.008) and late SSc (median 1.7 x-fold increase compared to HC, p=0.008). There was a non-significant trend for increased median HIF1α in dcSSc versus lcSSc (1.6 versus 1.5 x-fold increase, p=0.690) and late versus early SSc (1.7 versus 1.5 x-fold increase, p=0.421) (Figure 9.3).

HIF2α was notably the more commonly expressed HIF paralog in the SSc patients compared to HIF1α and appeared with overall stronger immunoreactivity (Table 9.2). HIF2α was expressed in the majority of SSc in the superficial epidermis ranging from weak to strong immunoreactivity (Table 9.2). SSc showed significantly greater semi-quantified epidermal HIF2α than HC in both lcSSc (median 1.9 x-fold increase compared to HC, p=0.008) and dcSSc patients (median 2.2 x-fold increase compared to HC, p=0.008) (Figure 9.3). Similarly, early SSc (median 2.0 x-fold increase compared to HC, p=0.008) and late SSc (median 1.9 x-fold increase

compared to HC, p=0.008) showed increased HIF2α compared to controls (Figure 9.3). Additionally, there was a trend for early and dcSSc patients to express more epidermal HIF2α compared to their counterparts (dcSSc 2.2 versus lcSSc 1.9 x-fold increase, p=0.222; early 2.0 versus late 1.9 x-fold increase, p=0.841) (Figure 9.3). The strongest subjective HIF2α epidermal expression was observed in 3 early dcSSc specifically (Table 9.2). HIF2α was also present in follicular keratinocytes, sweat ducts and dermal blood vessels (Table 9.2). Among the 8 out of 10 SSc patients who exhibited HIF2α in follicular keratinocytes, the strongest staining was again amongst early compared to late SSc for both lcSSc and dcSSc groups. The early lcSSc patient (VIF061) with strong follicular staining of HIF2α had low total mRSS but had systemic disease in the form of ILD (Table 9.1). When HIF1α and HIF2α were both detected in the epidermis or hair follicles of SSc patients, they were co-localised (Figure 9.2).

Surprisingly, IHC-IF staining of HIF1α and HIF2α were predominantly cytoplasmic and only observed as nuclear reactivity for HIF2α in 2 dcSSc in the basal epidermal keratinocytes. These 2 patients also showed HIF2α cytoplasmic staining in the superficial epidermis. It may be that the confocal microscope gain settings that were chosen to prevent saturation of the strongest immunoreactivity, prevented lower level detection in the nucleus and does not influence our onward conclusions.

Table 9. 2 Expression of HIF1α and HIF2α by immunofluorescence in systemic sclerosis and healthy skin.

*1 HC & 2 SSc did not exhibit hair follicles within the tissue section for reference/comment.

Biomarker	Positive immunoreactivity: Healthy control	Positive immunoreactivity: Systemic sclerosis	Immunoreactivity description
n.	5	10	
HIF1α			
Epidermal keratinocytes	1 out of 5	4 out of 10	• Weak cytoplasmic stain in superficial epidermis in SSc & HC
Follicular keratinocytes	1 out of 4*	3 out of 8*	• Weak cytoplasmic stain in 1 HC only • No HIF1α staining was observed in any lcSSc patient • 3 dcSSc (1 early, 2 late) had weak follicular HIF1α
Sweat glands/ducts	0 out of 5	2 out of 10	• No HIF1α immunoreactivity in HC sweat glands. • 2 late lcSSc had weak cytoplasmic HIF1α staining.
Endothelial cells	0 out of 5	2 out of 10	• No HC dermal bv expressed HIF1α. • 2 dcSSc (1 early, 1 late) showed HIF1α immunoreactivity in dermal blood vessels.
HIF2α			
Epidermal keratinocytes	1 out of 5	8 out of 10	• Weak superficial cytoplasmic HIF2α in 1 HC only. • 1 early lcSSc showed moderate HIF2α in superficial epidermis. • 2 late lcSSc showed weak cytoplasmic HIF2α in the superficial epidermis. • 2 lcSSc showed no epidermal HIF2α (1 early, 1 late lcSSc) • 2 late dcSSc showed weak cytoplasmic staining in superficial epidermis plus some nuclear reactivity in 1/2 patient. • 2 early dcSSc showed moderate cytoplasmic HIF2α in the superficial epidermis and 1/2 some nuclear stain in basal epidermal keratinocytes. • 1 early dcSSc showed strong cytoplasmic stain through all suprabasal epidermis
Follicular keratinocytes	2 out of 4*	7 out of 8*	• 2 HC had weak cytoplasmic HIF2α. • 3 late lcSSc had weak to moderate cytoplasmic HIF2α staining. • 1 early lcSSc (with ILD) had strong cytoplasmic HIF2α staining. • 1 late dcSSc had moderate staining • 2 early dcSSc had strong to very strong immunoreactivity.
Sweat glands/ducts	1 out of 5	6 out of 10	• 1 HC had weak nuclear HIF2α staining • 3 late lcSSc had weak to moderate cytoplasmic staining for HIF2α. • 1 early lcSSc had weak nuclear HIF2α staining. • 2 dcSSc (1 early, 1 late) had moderate cytoplasmic/perinuclear staining.
Endothelial cells	0 out of 5	3 out of 10	• 3 SSc (1 lcSSc, 2 dcSSc) demonstrated HIF2α immunoreactivity in dermal blood vasculature.

Figure 9. 3 Semi-quantification of epidermal HIF expression in forearm skin.

Increased epidermal expression of HIF1α (A&C) and HIF2α (B&D) is seen in all SSc subgroups (lcSSc n=5, dcSSc n=5, early SSc n=5 and late SSc n=5) compared to controls (n=5). p=0.008 for all subgroup comparisons versus healthy controls (comparison of group median, Mann-Whitney U). Non-significant trends are seen for increased expression of HIF1α in dcSSc (A) and late SSc (C) as well as HIF2α in dcSSc (B) and early SSc (D) patients versus their subgroup counterparts. Data represents the x-fold increase in the sum of the pixel intensity across the epidermis referenced to the healthy control group mean. Controls were assigned a reference of 1.0. Horizontal line represents group median.

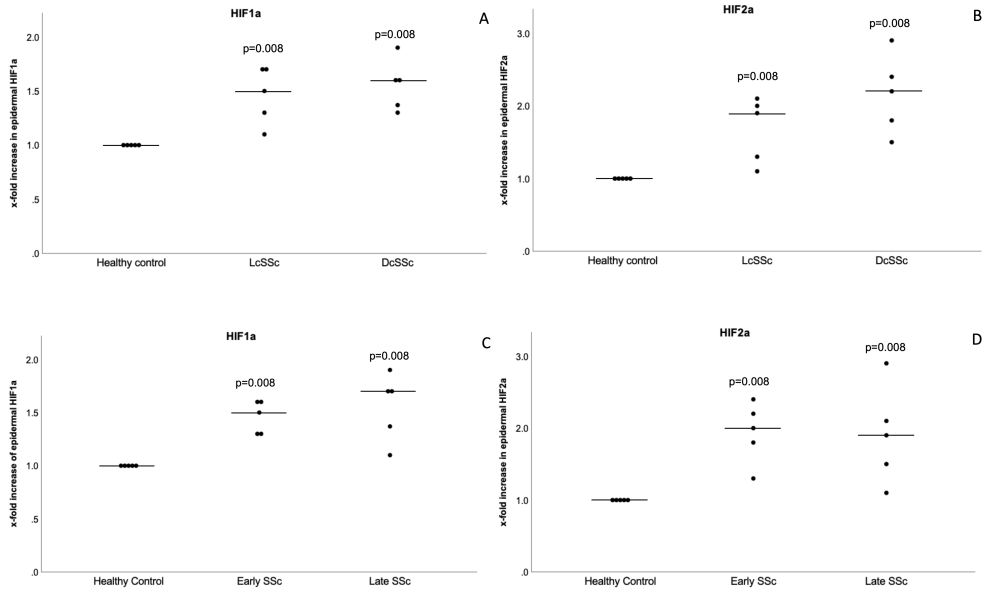

9.3.2.2 panVEGF-A and VEGF-A$_{165}$b are over-expressed in SSc

PanVEGF-A immunoreactivity was present in the superficial epidermis of all HC and SSc donors but was subjectively noted to be strong in proportionally more SSc patients (Table 9.3). Semi-quantification of epidermal panVEGF-A expression demonstrated a significant difference between controls and dcSSc (1.2 x-fold increase, p=0.032), but not between controls and any other sub-group (Figure 9.4). There was no significant difference in objective epidermal panVEGF-A between lcSSc and dcSSc (1.1 and 1.2 x-fold increase, p=0.548) or early SSc and late SSc (1.1 versus 1.2 x-fold increase, p=0.421) (Figure 9.4).

PanVEGF-A was also seen in basal epidermal keratinocytes in some HC and SSc donors (Table 9.3). PanVEGF-A was expressed in follicular keratinocytes in most HC and all SSc and was particularly strong in early SSc patients (Table 9.3). When HIF2α was expressed in follicular keratinocytes of SSc patients, panVEGF-A immunoreactivity co-localised (by comparison of serial tissue sections). PanVEGF-A was also expressed in half of SSc patients in dermal fibroblasts as well as endothelial cells in all SSc. In contrast, few HC had detectable endothelial panVEGF-A immunoreactivity and none in HC dermal fibroblasts.

The anti-angiogenic isoform VEGF-A_{165}b was expressed in the epidermis in just over half of the HC donors but with weak immunoreactivity and often in just one basal keratinocyte across the whole field of view. In the majority of controls, VEGF-A_{165}b was also weakly expressed in dermal blood vessels. In contrast, superficial epidermal VEGF-A_{165}b was expressed in most SSc patients, although it was again with weak immunoreactivity. Semi-quantification of VEGF-A_{165}b demonstrated a trend for increased epidermal expression in dcSSc versus lcSSc (1.0 versus 0.9 x-fold increase, p=0.421) suggesting a greater anti-angiogenic influence in the former (Figure 9.4). There was also a non-significant trend for increased VEGF-A_{165}b in late SSc versus early (1.1 versus 0.9 x-fold increase, p=0.310) (Figure 9.4).

VEGF-A_{165}b was universally expressed in endothelial cells in SSc patients to varying strengths of immunoreactivity and strongly so in one early lcSSc with ILD (VIF61). VEGF-A_{165}b was also expressed in dermal fibroblasts in 4 SSc patients (3 dcSSc and 1 lcSSc), 3 of whom were early in their disease course. One of these early SSc patients (VIF61) showed particularly strong

expression of VEGF-A_{165}b in fibroblasts and was phenotypically lcSSc but also had systemic disease in the form of ILD. VEGF-A_{165}b was only seen in follicular keratinocytes in 1 early dcSSc.

Figure 9. 4 Semi-quantification of epidermal VEGF-A expression in forearm skin.

Significantly increased epidermal expression of panVEGF-A is seen in dcSSc (n=5) (A) with a trend towards increased expression in late SSc (n=5) (C). No significant difference in epidermal VEGF-A_{165}b is seen compared to healthy controls (B&D). P values illustrated demonstrate comparison to healthy controls (Mann-Whitney U). Data represents the x-fold increase in the sum of the pixel intensity across the epidermis referenced to the healthy control group mean. Controls were assigned a reference of 1.0. Horizontal line represents group median.

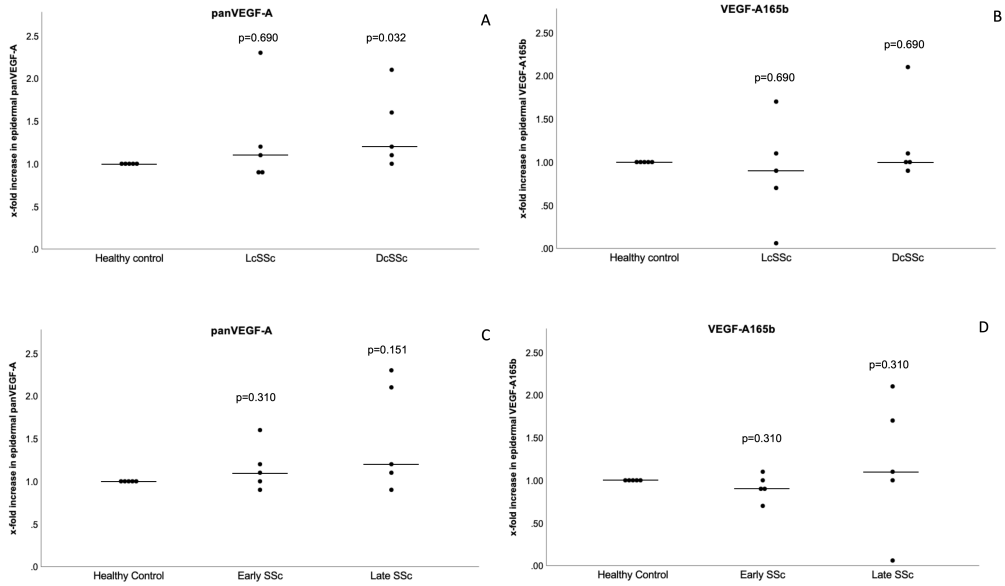

Table 9. 3 Expression of panVEGF-A and VEGF-A_{165}b by immunofluorescence in systemic sclerosis and healthy skin.

*1 HC & 2 SSc did not exhibit hair follicles within the tissue section for reference/comment.

Biomarker	Positive immunoreactivity		Immunoreactivity description
	Healthy control	Systemic sclerosis	
n.	5	10	
panVEGF-A			
Epidermal keratinocytes	5 out of 5	10 out of 10	• All HC displayed panVEGF-A staining in superficial epidermis (predominantly moderate strength) and some basal keratinocytes. • SSc showed similar histological distribution of staining to HC but with proportionally more patients with stronger staining (SSc: 10% weak, 50% moderate, 40% strong versus HC: 20% weak, 60% moderate, 20% strong). • No notable difference between early/late or limited/diffuse SSc.
Follicular keratinocytes	3 out of 4*	8 out of 8*	• 3 HC showed varying intensities of panVEGF-A immunoreactivity (weak-strong). • 4 lcSSc (1 early, 3 late) showed immunoreactivity in hair follicles. The early lcSSc was very strong and moderate-strong in late lcSSc patients. • 4 dcSSc showed some immunoreactivity in hair follicles. 2 early dcSSc showed very strong staining compared to weak or moderate in late dcSSc.
Endothelial cells	3 out of 5	10 out of 10	• 3 HC showed immunoreactivity in dermal blood vessels. • All SSc showed positive staining in dermal blood vessels.
Fibroblasts	0 out of 5	5 out of 10	• 1 lcSSc did not show VEGF-A_{165}b immunoreactivity in fibroblasts, did have panVEGF-A staining.
VEGF-A_{165}b			
Epidermal keratinocytes	3 out of 5	7 out of 10	• HC showed weak epidermal VEGF-A_{165}b in small areas of some donors. 1 HC displaying weak immunoreactivity in the superficial epidermis and a single basal keratinocyte. 2 other HCs showed immunoreactivity in a single basal keratinocyte only. • 4 lcSSc (2 early, 2 late) showed weak superficial epidermis immunoreactivity. • 3 dcSSc (1 early, 2 late) showed weak superficial epidermis immunoreactivity.
Follicular keratinocytes	0 out of 4*	1 out of 8*	• Minimal staining for VEGF-A_{165}b was noted in 1 early dcSSc only.
Endothelial cells	4 out of 5	10 out of 10	• 4 HC showed weak immunoreactivity in a few endothelial cells only. • All SSc showed endothelial expression of VEGF-A_{165}b. • 4 lcSSc (1 early, 3 late) showed weak immunoreactivity in dermal vasculature. 1 other early lcSSc showed strong staining in vessels surround sebaceous glands. • 5 dcSSc showed weak endothelial cell expression.
Dermal fibroblasts	0 out of 5	4 out of 10	• 3 dcSSc (2 early, 1 late) demonstrated immunoreactivity in fibroblasts for VEGF-A_{165}b. • 1 early lcSSc (with ILD) had strong staining of several fibroblasts in the dermis.

9.3.2.3 Angiopoietin-2 and Tie-2 are more frequently expressed in vasculature in SSc

Immunofluorescent staining for angiopoietin-1 (Fisher MA5-23884) did not show any positive immunoreactivity despite attempts at optimisation. As such it was abandoned and is therefore not reported further herein.

Dermal staining of Ang-2 was present in sweat glands of all HC and SSc without any notable disparity in the overall strength of immunoreactivity between SSc versus HC or lcSSc versus dcSSc. However, early SSc tended to have stronger subjective sweat gland Ang-2 immunoreactivity compared to late SSc. Ang-2 expression in the dermal blood vessels was common in SSc compared to less frequent weak staining in HC. The strongest vascular staining for Ang-2 occurred in dcSSc patients and one early lcSSc patient (VIF61) the latter of whom had systemic involvement with ILD. Expression of Ang-2 was infrequent in both SSc and HC in the epidermis, but when it did occur it was with stronger immunoreactivity in SSc than HC. Ang-2 was also expressed (rarely) in follicular keratinocytes, papillary muscles and leukocytes in both SSc and HC.

Weak immunoreactivity to Tie-2 was present in papillary muscles of all HC and lcSSc compared to moderate-strong staining in dcSSc. Tie-2 was expressed with similar intensity of immunoreactivity between groups in sweat glands and dermal vasculature, however, expression was notably more common in SSc than HC. Tie-2 was rarely seen in either HC or SSc in epidermal or follicular keratinocytes.

Table 9. 4 Expression of angiopoietins and Tie-2 by immunofluorescence in systemic sclerosis and healthy skin.

**3 SSc did not exhibit papillary muscle within tissue sections for reference/comment.

Biomarker	Positive immunoreactivity		Immunoreactivity description
	Healthy control	Systemic sclerosis	
n.	5	10	
Angiopoietin-2			
Epidermal keratinocytes	1 out of 5	3 out of 10	• Epidermal staining was found in 3 SSc (predominantly moderate intensity) versus 1 HC (weak immunoreactivity)
Follicular keratinocytes	1 out of 5	1 out of 10	• Ang-2 was found infrequently in follicular keratinocytes in both SSc and HC.
Papillary muscle	1 out of 5	1 out of 10	• 1 HC & 1 SSc (both also demonstrated Ang-2 in dermal leukocytes) exhibited immunoreactivity in papillary muscles.
Sweat glands	5 out of 5	10 out of 10	• All HC and SSc had Ang-2 expressed in sweat glands. • Intensity of staining varied from weak to strong in HC. • Early SSc had proportionally more donors with strong staining (1 dcSSc weak, 2 lcSSc strong, 2 dcSSc strong). • Late SSc tended to have weaker staining (2 lcSSc & 1 dcSSc weak, 1 lcSSc & 1 dcSSc moderate).
Endothelial cells	2 out of 5	8 out of 10	• Few HC showed immunoreactivity for Ang-2 in dermal vasculature. • 3 lcSSc (1 early, 2 late) had weak immunoreactivity for Ang-2 and 1 early lcSSc (with ILD) had strong staining. • 4 dcSSc demonstrated Ang-2 immunoreactivity in the dermal vasculature, 3 of which were moderate-strong.
Dermal cells	1 out of 5	1 out of 10	• 1 SSc & 1 HC expressed Ang-2 in dermal leukocytes.
Tie-2			
Epidermal keratinocytes	1 out of 5	1 out of 10	• There was rare and weak immunoreactivity in epidermal keratinocytes.
Follicular keratinocytes	2 out of 5	2 out of 10	• There was rare and weak immunoreactivity in follicular keratinocytes.
Papillary muscle	5 out of 5	7 Out of 7**	• 4 HC showed weak staining. 1 HC showed strong staining • LcSSc predominantly showed weak immunoreactivity. DcSSc tended to show moderate immunoreactivity.
Sweat glands	3 out of 5	10 out of 10	• 3 HC showed weak immunoreactivity in sweat glands. • All SSc showed weak(-moderate) immunoreactivity in sweat glands.
Endothelial cells	3 out of 5	9 out of 10	• 3 HC showed Tie-2 staining in dermal vasculature. • 9 SSc showed Tie-2 staining in dermal vasculature with similar intensity to HC.

9.3.3 Epidermal expression of HIFs correlate with VEGF-A in lesional SSc skin

Epidermal HIF1α correlated strongly with both epidermal panVEGF-A and VEGF-A_{165}b in the SSc group (all patients) (Table 9.5), suggesting that both may be induced by the presence of HIF1α. In contrast, HIF2α demonstrated a significant strong relationship with VEGF-A_{165}b (all patients) but only a moderate relationship with panVEGF-A the latter of which did not reach significance, possibly due to small numbers.

The positive relationship between both HIF1α and 2α paralogs with VEGF-A_{165}b strengthened in late SSc (+1.0 p=0.01, and +0.9 p=0.037 respectively), but lost significance in early SSc (data not shown). Additionally, the relationship between HIF1α and panVEGF-A lost significance in late SSc (data not shown).

Table 9. 5 Correlation between epidermal HIFα and VEGF-A in SSc.

Statistical analysis by Spearman's rank correlation coefficient, n=10.

Biomarker	panVEGF-A	VEGF-A_{165}b
HIF1α	**+0.758**	**+0.903**
p value	**0.011**	**<0.001**
HIF2α	+0.552	**+0.709**
p value	0.098	**0.022**

9.3.4 Epidermal expression of hypoxia induced biomarkers correlate with clinical measures of vasculopathy and fibrosis

9.3.4.1 Epidermal HIFα and panVEGF-A correlate with peripheral vasculopathy

Amongst the combined group of participants (SSc+HC), epidermal expression of HIF1α and HIF2α at the forearm had moderate positive relationships with mean inter-capillary distance, although due to small numbers did not achieve significance (+0.482 p=0.069 and +0.489 p=0.064 respectively, n=15). This suggests that as microvascular loss progresses tissue hypoxia worsens. In further support of this, in the SSc group, HIF2α correlated with vascularity index at the nailfold (NVi) although did not achieve significance due to small numbers (-0.588 p=0.074, n=10).

The epidermal expression of VEGF-A isoforms at the forearm appeared less relevant to peripheral vasculopathy. There was no significant correlation between VEGF-A isoforms and ICD or NVi in the combined or SSc only group (data not shown). There was no correlation between ex vivo epidermal pan- or VEGF-A_{165}b at the forearm and baseline perfusion or peak PORH on LSCI in the combined cohort. However, amongst the SSc group (n=10) there

was a positive relationship between baseline peripheral perfusion on LSCI and epidermal panVEGF-A expression, but again did not achieve significance (+0.624 p=0.054). The overall lack of relationship between VEGF-A isoforms in skin and peripheral vasculopathy may suggest that systemic exposure (in plasma) is more relevant to the occurrence of vascular sequelae.

9.3.4.2 Epidermal VEGF-A_{165}b correlates with skin pathology

There was a strong negative relationship between epidermal expression of VEGF-A_{165}b and forearm skin thickness on HFUS (-0.672 p=0.006) in the combined cohort (SSc+HC), which was also apparent in the SSc only group (-0.612 p=0.06), although just failing to achieve significance in the latter due to small numbers.

There was no correlation between any epidermal biomarkers with either SWE, echogenicity or collagen quantification for either the combined cohort or SSc group only. Similarly, there was no relationship with total or local mRSS.

9.3.4.3 Relationship between biomarker expression in the skin and plasma

There was no correlation between ex vivo epidermal biomarkers and plasma panVEGF-A and VEGF-A_{165}b for either SSc only or the combined cohort, which suggests that the localised tissue expression and systemic exposure to these signalling factors is not directly related.

9.3.5 HIF and VEGF-A_{165}b isoform are expressed in clinically uninvolved skin

HIF paralogs and vascular biomarkers were investigated in 3 patients who had also donated clinically uninvolved skin from the abdomen where the local mRSS=0. Comparative staining for paired tissue samples from lesional forearm skin and clinically uninvolved skin from the abdomen is shown in Table 9.6.

Table 9. 6 Expression of HIF paralogs and VEGF-A in clinically involved and uninvolved SSc skin.

*VIF27 (late lcSSc) had a clinically uninvolved skin at the abdomen based on a local mRSS scoring =0, but actually had atrophic skin on HFUS at that site suggesting the abdominal skin was not truly unaffected. **Hair follicles were not represented in the abdominal skin biopsy for VIF27 for comparison.

	Description of immunoreactivity					
SSc donor	**VIF12 (late dcSSc)**		**VIF27 (late lcSSc)**		**VIF61 (early lcSSc)**	
Anatomical site of biopsy	**Forearm**	**Abdomen**	**Forearm**	**Abdomen**	**Forearm**	**Abdomen**
Local mRSS score (0-3)	2	0	1	0*	1	0
Biomarker						
HIF1α						
Epidermal keratinocytes	weak	nil	nil	nil	weak	weak
Follicular keratinocytes	weak	weak	nil	**	nil	nil
Endothelial cells	nil	nil	nil	nil	nil	positive
HIF2α						
Epidermal keratinocytes	weak	nil	nil	nil	moderate	Weak
Follicular keratinocytes	moderate	Very strong	moderate	**	strong	nil
Sweat glands/ducts	nil	nil	positive	nil	nil	nil
Endothelial cells	nil	nil	nil	nil	nil	nil
panVEGF-A						
Epidermal keratinocytes	moderate	nil	strong	weak	strong	weak
Follicular keratinocytes	weak	Very strong	strong	**	Very strong	weak
Endothelial cells	positive	positive	positive	positive	positive	positive
VEGF-A_{165}b						
Epidermal keratinocytes	weak	nil	nil	nil	weak	weak
Follicular keratinocytes	nil	weak	weak	**	weak	nil
Endothelial cells	positive	positive	positive	positive	positive	positive
Fibroblast	positive	nil	nil	nil	positive	nil

The subtleties of HIF paralogs and VEGF-A isoform expression in clinically uninvolved skin varied with each SSc donor. Our general observation is that in clinically uninvolved proximal skin of lcSSc patients there was reduced HIF paralog expression compared to sclerodermatous skin. In contrast, there was increased HIF2α expression in uninvolved skin in the dcSSc patient suggesting increased hypoxic drive in the more severe phenotype and predating clinically apparent skin pathology.

PanVEGF-A expression in lesional SSc forearm skin was increased compared to clinically uninvolved proximal skin in all 3 patients. The level of panVEGF-A expression in clinically uninvolved skin was subjectively comparable to that seen in healthy control forearm skin.

There was no particular pattern of VEGF-A_{165}b expression in clinically uninvolved skin. However, it was noted to be expressed in each sample at various histological locations and subjectively felt to be expressed more widely than in healthy control forearm skin demonstrating that anti-angiogenic drivers are expressed prior to the onset of clinically apparent skin pathology.

There was no notable difference in Ang-2 or Tie-2 expression between biopsy sites in any of the 3 donors (data not shown).

9.4 Discussion

We have demonstrated for the first time that HIF2α is over-expressed in SSc lesional skin and correlates with downstream panVEGF-A and VEGF-A_{165}b suggesting VEGF-A isoforms in SSc are driven by HIFα dependent pathways. This supports the convention that lesional SSc skin is a hypoxic

environment (39). The positive relationship between epidermal HIFα paralog expression and both ICD and NVi implicates vasculopathy as a contributing factor and collectively supports the Vascular hypothesis (38). In idiopathic PAH, HIF2α drives endothelial-mesenchymal transition in pulmonary vascular endothelium leading to vascular wall remodelling and obliterative vasculopathy (245). We therefore consider that the hypoxic upregulation of HIF2α in SSc skin may feedforward to perpetuate the obliterative evolving vasculopathy seen in SSc over time (107). When coupled with anti-angiogenic actions of VEGF-A_{165}b upregulation, hypoxia in SSc skin may further worsen. Interestingly, previous data has reported a specific lack of relationship between cutaneous HIF1α expression and nailfold capillaroscopy classification in a cohort of treatment naïve patients (300), which may suggest that this relationship is specific to the HIF2α paralog. Alternatively, our novel finding of predominant HIF2α over HIF1α expression in our cohort may explain these opposing relationships as well as conflicting reports of cutaneous HIF1α expression in previous studies (39, 300, 409).

In our cohort, there is a tendency for increased HIF1α, HIF2α, panVEGF-A and VEGF-A_{165}b in those with more severe fibrotic phenotypes (namely dcSSc patients and one lcSSc with ILD) despite increased use of vasodilators in dcSSc subgroup, which suggests that the burden of fibrotic disease directly relates to the magnitude of hypoxic exposure. This is further evidenced by the disparity between HIFα paralog expression in non-lesional skin of dcSSc versus lcSSc. The stronger correlation between HIF2α and VEGF-A_{165}b compared with that of panVEGF-A, suggests that the HIF2α paralog has more specific influence over the former. This is in line with our original hypothesis that differential expression of HIFα paralogs may dictate

downstream VEGF-A splicing. Further longitudinal study may be beneficial to confirm if these relationships are dynamic over the course of disease.

We report for the first time a negative relationship between the VEGF-A_{165}b isoform and objective skin thickness on HFUS suggesting VEGF-A_{165}b is inhibitory of SSc skin pathology. This is also reported in murine models of idiopathic pulmonary fibrosis (another fibrotic disease)(256). Increased fibroblast VEGF-A_{165}b in our patients may therefore represent a biological attempt to correct excessive fibrosis in those with the worst phenotype. This data sheds light on the pathogenesis of evolving SSc skin disease and presents VEGF-A_{165}b as a potential therapeutic target for skin fibrosis. Its use would, however, be markedly complicated by the negative implications of such therapy on vasculopathy.

The trend for augmented HIF2α expression in early versus late SSc suggests a temporal relationship between early hypoxia and skin pathology which reinforces the vascular hypothesis (38). However, based on previous literature of HIFα paralog expression in both murine models and human cell culture (241, 245, 247, 337-340, 410-413), our original hypothesis had predicted HIF1α to be induced by intermittent patterns of hypoxia in early disease versus HIF2α induction by chronic continuous hypoxic exposure in late disease which is directly contrary to our findings. There was no difference in vasodilator use between early and late SSc in this cohort and therefore therapeutic exposure is not likely to be responsible for the alternative results. The early and predominant representation of HIF2α in SSc skin suggests that *persistent* vasculopathy and chronic continuous hypoxia occurs earlier in SSc pathology. Indeed, the unpublished opinion of some SSc experts is that the classification of early versus late disease should

be based on the time from the first RP symptom rather than the first non-RP (SSc specific) symptom as the hypoxic exposure from RP symptoms may predate clinical SSc onset by many years (41-43, 47).

Of further interest, is the finding that HIF2α expression was increased in non-lesional skin of a dcSSc patient. Whilst caution is applied when interpreting results from a single donor, this reinforces the hypothesis that hypoxia predates skin pathology. An alternative explanation for increase HIF2α expression in non-lesional skin may be an inherent reduction of PHD2 and thus a default reduction in HIF2α degradation rather than a hypoxic driven stabilization. This is a feature seen in lung vascular endothelium of idiopathic PAH patients (245) and may explain upregulation of downstream targets such as panVEGF-A in non-lesional normoxic skin (39). Indeed, we noted increased co-localised panVEGF-A and HIF2α in non-lesional skin of one dcSSc patient. Additionally, the presence of VEGF-A_{165}b in clinically uninvolved abdominal samples from lcSSc donors without co-expression of HIFα paralogs, suggesting that HIF *independent* pathways may also regulate the inhibitory isoform in clinically uninvolved skin. Further specific study of cutaneous pO_2 and HIFα degradation pathways in SSc would be of interest.

In our cohort of concurrently treated patients, VEGF-A_{165}b tended to have greater epidermal expression in late SSc which conflicts with the early disease association reported previously (302). An important differentiation between this Italian cohort and our own is the protocolled washout of drug therapies prior to study entry which may influence results.

The strong positive relationship between epidermal panVEGF-A expression and baseline finger perfusion on LSCI suggests panVEGF-A expression in

skin is beneficial in reducing the burden of SSc vasculopathy, as expected. VEGF-A_{165}b isoform expression in the epidermis did not however correlate with other aspects of peripheral vasculopathy (NC and HFUS cSMI) which may suggest the *vascular* expression of VEGF-A isoforms may be more relevant to the outcome of vascular sequelae, which is practically difficult to accurately quantify for direct comparison, due to the variations in histological orientation of vasculature in tissue sections. Indeed, we previously demonstrated a relationship between the inhibitory isoform VEGF-A_{165}b in plasma and DVVi (discussed in chapter 8). The lack of correlation between circulating and epidermal biomarker expression confirms that plasma sampling does not reflect skin specific expression (at least in a treated cohort) and may limit the clinical value of plasma biomarker sampling in relation to skin disease specifically.

In line with previous reports (316), we noted that Ang-2 expression in dermal vasculature was more common in SSc compared to control skin, reflecting an anti-angiogenic environment in the disease state. In contrast to this previous study (316), however, cutaneous expression of Ang-2 and Tie-2 in our cohort was particularly strong in those with a greater burden of fibrotic disease which may suggest a causative relationship. This is paralleled by our previous results demonstrating a correlation between plasma Ang-2 with both skin echogenicity and SWE (discussed in chapter 8) and suggests that Ang-2 is a potential therapeutic target for both vasculopathy and skin fibrosis. Further longitudinal studies including VEDOSS patients would be of benefit to further understand this relationship and whether Ang-2 drives skin fibrosis through vasculopathy and subsequent hypoxia or whether it has direct pro-fibrotic potential.

In some SSc patients, clinical features may overlap with other connective tissue diseases (CTD) including inflammatory myositis, most typically occurring in those with Pm-Scl autoantibodies. Given the close clinical association between these 2 CTD diagnoses, it is interesting to note that there is a trend towards increased expression of cutaneous panVEGF-A mRNA in patients with dermatomyositis (314), as well as significantly increased skeletal muscle panVEGF-A and VEGF-A_{165}b (416). Skeletal muscle expression of VEGF-A_{165}b correlates with TGFβ in myositis (416). This is in line with parallel reports that TGFβ encourages distal splicing in favour of VEGF-A_{165}b in podocytes (326) and cultured microvascular endothelial cells in SSc (302). TGFβ also correlates with VEGF-A_{165}b in lesional SSc skin (302). One early Pm-Scl+ SSc patient in our cohort (VIF61) stands out as having strong immunoreactivity to VEGF-A_{165}b in fibroblasts as well as cutaneous HIF2α and Ang-2. Further investigation of TGFβ and its relationship with HIF2α and Ang-2 in our cohort would be of interest.

9.4.1 Concluding remarks

We have demonstrated that HIFα paralogs, inhibitory VEGF-A_{165}b and Ang-2 are implicated in SSc skin pathology. We report the novel finding that HIF2α predominates in lesional skin and relates to both vasculopathy and fibrosis. HIFα and downstream panVEGF-A and VEGF-A_{165}b are potentiated especially in those with higher fibrotic burden suggesting a pathogenic link between hypoxia and aberrant tissue remodelling. VEGF-A_{165}b appears to have dual inhibitory associations with vasculopathy and fibrosis, the latter of which may represent a biological attempt to reverse excessive fibrosis. Further longitudinal studies are needed to understand temporal relationships between these biomarkers and skin disease in order to unlock the potential

for targeted therapies through these signalling pathways to treat SSc skin fibrosis.

Chapter 10. Influence of hypoxia on HIFα paralog and VEGF-A isoform expression in fibroblasts in systemic sclerosis

10.1 Introduction

We have demonstrated the link between hypoxia and SSc skin pathology through the upregulation of HIF2α, panVEGF-A and inhibitory VEGF-A_{165}b in lesional skin (chapter 9). Fibroblasts are considered to be central to SSc pathogenesis both as an effector cell of collagen production and aberrant tissue remodelling but also as a source of panVEGF-A (314) and inhibitory VEGF-A_{165}b isoform (39, 302) (and chapter 9) with potential paracrine and autocrine influence. The question of hypoxic influence on fibroblast expression of these biomarkers is relevant to SSc pathogenesis. Indeed, hypoxic exposure increases HIF1α and panVEGF-A in healthy and SSc fibroblasts (39, 301, 329) with no predilection for either donor group despite notable increases in VEGF-A mRNA in the diseased fibroblasts (301). This may suggest that the environment rather than the inherent cell phenotype is dictating expression, at least in single cell culture. The hypoxic regulation of VEGF-A_{165}b in cultured fibroblasts has not been reported to date. Given our data (chapter 9) demonstrating a relationship between dermal fibroblast expression of VEGF-A_{165}b and fibrotic burden this warrants investigation to further understand SSc pathogenesis.

Based on the differential influence of chronic intermittent hypoxia (CIH) versus chronic continuous hypoxia (CCH) on HIFα paralog expression demonstrated in rodent models (337-340) (discussed in detail chapter 1.9.7),

we considered the parallel patterns of hypoxic stimuli that occur in SSc and the potential influence on biomarker expression. Specifically, we hypothesised that intermittent hypoxia occurring in the earlier stages of vasculopathy (chapter 1.5), through more distinct RP attacks may translate to upregulation of HIF1α in SSc skin. Evolution of vasculopathy towards continuous hypoperfusion (90) may stimulate transition to HIF2α paralog upregulation. Such a transition may influence the relative expression of VEGF-A isoforms (Figure 10.1).

Figure 10. 1 Proposed pathway of VEGF-A isoform upregulation in response to hypoxia and influence on vasculopathy and fibrosis.

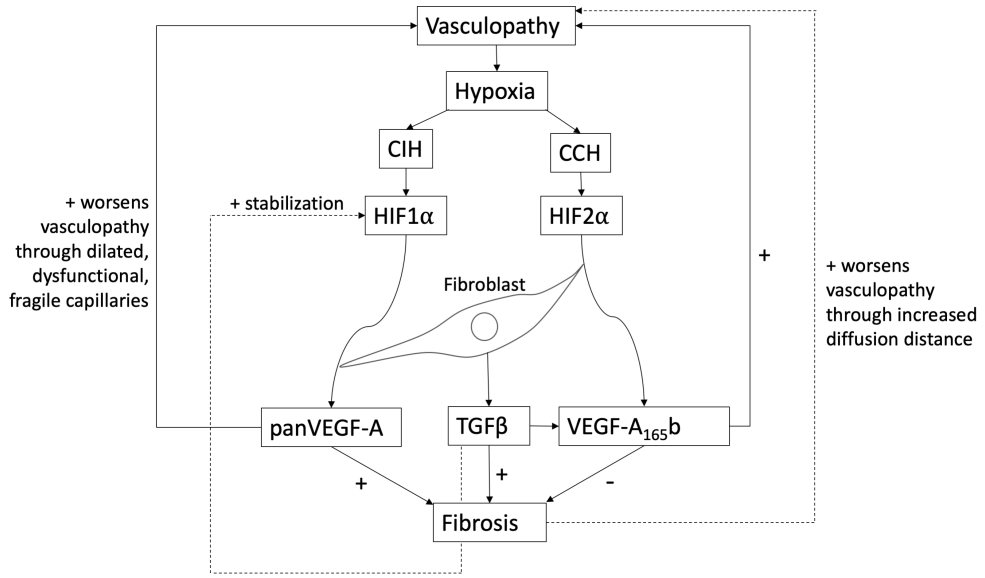

Over expression of TGFβ has been strongly demonstrated as a driver of fibrosis in SSc (322, 323, 417-421). Chronic hypoxic exposure of SSc fibroblasts increases downstream expression of TGFβ (301). TGFβ appears to drive increased panVEGF-A and collagen expression in SSc fibroblasts (314) in addition to stabilising HIF (301, 325) and thus HIF dependent pathways (discussed in detail chapter 1.9.6.4). Furthermore, TGFβ promotes distal splicing of VEGF-A exon 8 via p38 MAPK signalling (326) thus

increasing VEGF-A_{165}b production in cultured SSc-MVEC (302) (discussed in detail in chapter 1.9.6.4). There is therefore potential for hypoxia driven HIF and TGFβ to have collective responsibility for upregulation of panVEGF-A and VEGF-A_{165}b in SSc skin.

10.1.1 Chapter hypothesis, aims and objectives

Given the potential role of HIFα paralogs, VEGF-A isoforms and TGFβ to drive skin fibrosis through hypoxic stimulus, we hypothesised that differential patterns of hypoxic exposure alter the expression of HIF1α and HIF2α and in turn VEGF-A isoform production in SSc fibroblasts.

The aims of this chapter were to investigate the influence of different patterns of hypoxic exposure on fibroblast expression of these signalling factors. Our specific objectives were to:

- Explore the expression of HIF1α, HIF2α, panVEGF-A, VEGF-A_{165}b, TGFβ and Pro-Col I from SSc fibroblasts cultured under CIH and CCH compared to control fibroblasts.
- Explore the relative influence of HIF1α versus HIF2α on downstream VEGF-A isoform and TGFβ expression and subsequent Pro-Col I.
- Explore the specific influence of TGFβ on VEGF-A_{165}b expression under hypoxic conditions.

10.2 Methods

10.2.1 Fibroblast cell culture

Fibroblasts were cultured from human skin biopsies as per methodology (chapter 2.11.1) (by VF). Fibroblasts were exposed to different patterns of hypoxia and experimental stimuli as described previously (chapter 2.11.2) (by VF). Cell culture supernatant and lysates were prepared as previously

described (chapter 2.11.2.4) (by VF). Fibroblast phenotype was assessed as described previously (chapter 2.13.4).

10.2.2 Protein assays

Protein assays for HIF1α (VF), HIF2α (VF), panVEGF-A (masters students MS & TW), VEGF-A_{165}b (MS & TW), TGFβ (MS & TW) and Pro-Col I (MS & TW) were performed as previously described (chapter 2.11.3). Total protein quantification was confirmed using a Biorad protein assay (as previously described, chapter 2.11.3) (MS).

10.2.3 Statistical analysis

Statistical analysis was performed by VF. Demographic data of cell culture donors utilised appropriate parametric tests including Independent t-test. Protein assay results were analysed by non-parametric statistical tests including Kruskal-Wallis.

10.3 Results

10.3.1 Fibroblast cell culture donors

Cells were cultured from 3 early dcSSc patients and 3 age and sex matched non-smoker controls from forearm biopsies.

10.3.2 Protein quantification

Biorad protein assay on cell lysate confirmed approximately equal levels of total protein in each sample, implying that cell numbers were alike in each well (data not shown).

HIF1α and 2α were not detectable in cell culture lysates which we hypothesise may be due to a combination of the instability of HIFα even at -

80°C as well as the necessary protocolled dilutions of samples in order to reduce the urea in the cell lysis buffer to appropriate levels for the HIFα assays. HIF1α and HIF2α ELISA example standard curves are shown in Appendix 4.

PanVEGF-A, VEGF-A_{165}b, TGFβ and Pro-Col I were detectable in fibroblast cell cultures. However, data was not reproducible and so is not presented further in this thesis.

10.4 Discussion

Methodology for this chapter is presented in this thesis despite the lack of reliable data, to demonstrate the additional skills learnt for fibroblast explant culture, cell passage and hypoxic stimulation using the hypoxic chamber facilities.

Our hypothesis that alternative patterns of hypoxic stimuli influence the relative expression of HIFα paralogs and VEGF-A isoforms remains of interest and may be further investigated with the use of larger cell culture samples and alternative methodology such as western-blot to improve detection of HIFα paralogs.

11. Final conclusions

11.1 Introduction

Detailed discussion of our data with respect to the pertinent literature has been reviewed within respective chapters. This chapter will not duplicate those discussions but will summarize the most notable findings from each chapter, highlighting our contribution to the SSc literature, its translational potential and areas on ongoing unmet research need.

11.2 Vasculopathy

The vascular hypothesis (38) designated SSc as primarily an autoimmune vascular disease from which the consequences include inflammation and fibrosis. The vasculopathy of SSc is both structural and functional (chapter 1.5), but can result in profound tissue ischaemia that can lead to tissue damage such as digital ulceration.

11.2.1 Limitations of patient-reported outcome measures

The challenge for recent clinical trials targeting vascular sequelae in SSc (201) has been an inadequacy of the patient-reported outcome measures in reflecting the patient experience of SSc-RP. Indeed, since planning our study, patients themselves have vocalised that the RP diary is subjective and that documenting and defining ‘a single attack’ can be challenging (376). We have highlighted the poor convergent validity of patient-reported outcome measures (the RCS diary and SHAQ) with non-invasive objective measures of vasculopathy in SSc (chapter 4 and 5). Work is underway to develop and validate novel PROMs. Objective non-invasive microvascular tools such as LSCI and HFUS cSMI could greatly support drug development for digital vascular complications of SSc. Our findings provide additional evidence for

the use of LSCI in demonstrating vascular dysfunction in SSc and we have undertaken one of earliest studies of the novel HFUS application to quantify digital vasculopathy in SSc.

11.2.2 LSCI and PORH testing demonstrate SSc vascular dysfunction

We have demonstrated vascular dysfunction using sensitive LSCI, providing evidence that SSc patients have abnormal vascular kinetics following an ischaemic PORH challenge (chapter 4). Novel findings include demonstration that SSc is associated with impaired recovery after a period of ischaemia (reperfusion gradient). These data suggest endothelial-dependent vasodilatory potential of the microvasculature is impaired in SSc.

11.2.3 SSc vasculopathy is dynamic and progressive

We have highlighted the dynamic and progressive nature of structural microvascular changes at the nailfold with reduced capillary density and worsening NC classification associated with longer disease duration (chapter 4).

11.2.4 Novel application of HFUS cSMI for SSc vascular imaging

We have demonstrated the novel use of HFUS cSMI imaging to document the reduced peripheral vascularity seen in SSc even at ambient temperatures.

11.2.5 Severe vasculopathy results in tissue damage

We have demonstrated that those with the worst vasculopathy are vulnerable to tissue damage in the form of SSc-DU. We have demonstrated for the first time that LSCI with PORH challenge identified a reduced capacity to maximally vasodilate (peak PORH), an impaired rate of vascular recovery

(reperfusion gradient) and DDD at peak PORH in subjects with a history of SSc-DU. Furthermore, in this severe SSc-DU group, the ICD on NC is increased and vascularity on HFUS reduced reflecting the significant vasculopathy in those with tissue loss. The collective potential clinical application of these imaging techniques is to identify those most at risk of SSc-DU and escalate therapy appropriately.

11.2.6 Convergent validity of three microvascular imaging techniques in SSc

Nailfold capillaroscopy is a well-established technique in SSc research (422), but its use has been restricted by the availability of equipment, labour intensive image acquisition and challenges around qualitative and/or semi-quantitative image analysis. We have demonstrated the relationship between impaired microvascular perfusion on LSCI and structural microvascular loss at the nailfold with increasing ICD and dysfunctional giant capillaries (chapter 4.3.4) (Figure 11.1), which collectively suggests that quantifiable methods such as LSCI provide indirect reflections of structural vascular changes. This relationship also suggests that progressive capillary loss secondary to the obliterative microangiopathy of SSc results in a notable reduction in the vasodilatory potential of the microvasculature, making tissues particularly vulnerable to ischaemic injury.

Whilst LSCI is sensitive and applicable (chapter 4) its use is currently limited to specialist centres of which there are a small number across the U.K. The addition of provocation tests to perfusion imaging can be uncomfortable and increases image acquisition times, but does appear to provide additional information beyond baseline imaging (and is a distinct advantage over nailfold capillaroscopy which focuses on capillary morphology rather than

function). Additional work is required to establish the optimal microvascular imaging protocol (and imaging modalities) that provides the maximum information on microvascular structure and function in SSc. Whether this may be achieved using a single imaging modality (such as LSCI) or whether we shall remain reliant upon multiple techniques has yet to be established. In the meantime, the present work and other efforts in this field are providing valuable mechanistic insight into the exact nature of microangiopathy in SSc.

In chapter 5, I have presented data demonstrating that HFUS cSMI may have potential practical superiority over functional testing using LSCI given that the former differentiated between disease groups even at baseline and despite concurrent use of vasodilators. HFUS data also correlated with peak PORH on LSCI (with particular strength at the fingertip) suggesting that baseline HFUS vascularity also indirectly reflects the patient's capacity to vasodilate during perfusion recovery. HFUS cSMI imaging was practically faster to perform and potentially more accessible, which presents it as a more useful outcome measure for baseline data in clinical trials. The potential limitation of HFUS cSMI is the lack of correlation with other functional LSCI PORH parameters meaning that data that may document therapeutic response may be missed using HFUS.

11.2.7 Future research

We remain some way off being able to apply novel techniques such as cSMI in clinical trials of SSc-related digital vasculopathy. Future work is required to assess the repeatability of cSMI under stable conditions and the sensitivity of HFUS cSMI to change following administration of vasodilators. Future studies could also examine the potential additive benefit of a function challenges over basal perfusion in isolation.

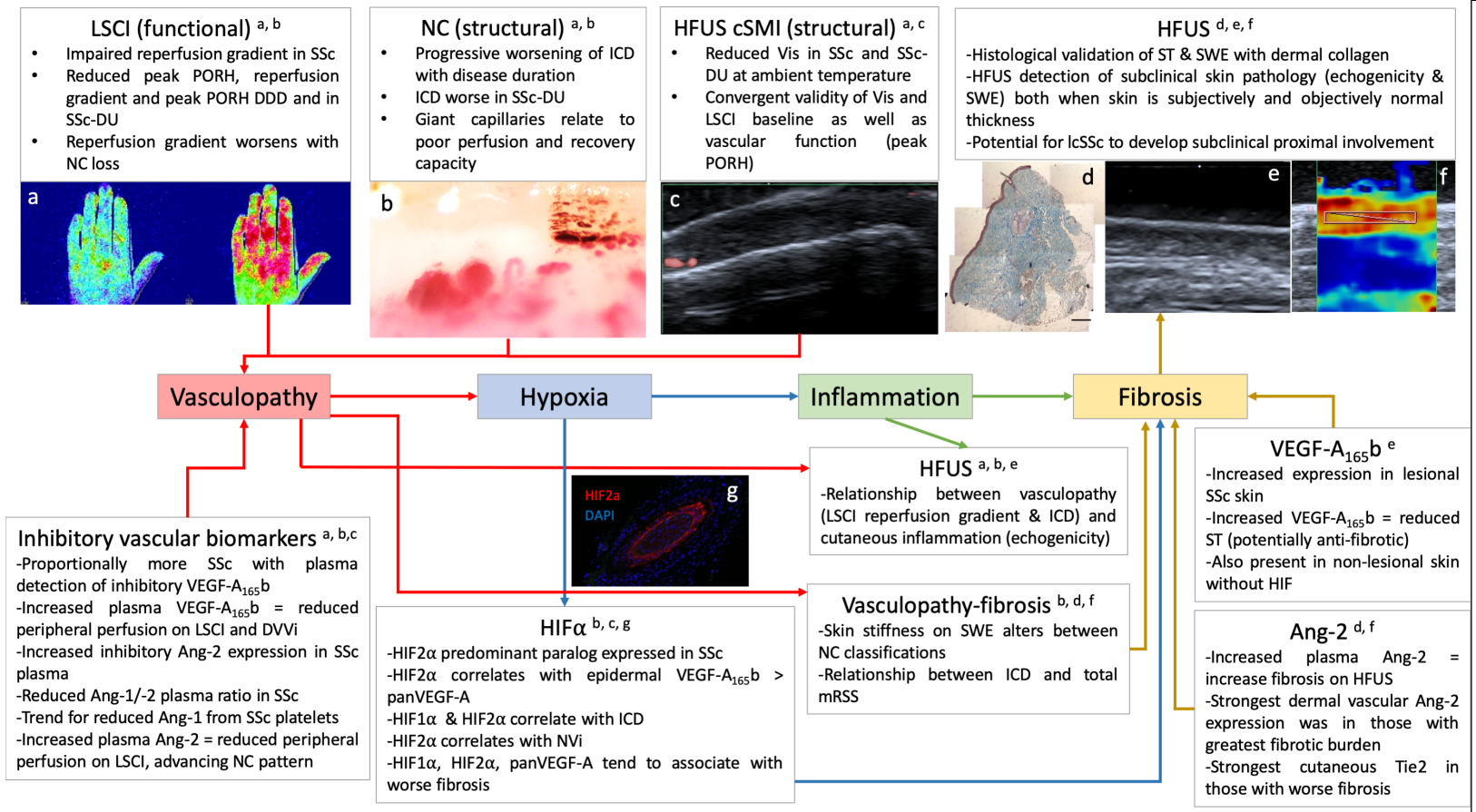

Figure 11. 1 Summary of study conclusions demonstrating the inter-relationship between vasculopathy, inflammation and fibrosis.

(a) LSCI demonstrating reduced baseline hand perfusion and reduced hyperaemia response following an ischaemic challenge. **(b)** Nailfold capillaroscopy (x22 magnification) demonstrating an active pattern with giant capillaries, microhaemorrhage and reduce capillary number. **(c)** HFUS cSMI demonstrating markedly reduce peripheral vascularity in an SSc patient at the distal middle finger. **(d)** Masson's Trichrome stain demonstrating increased collagen (blue) deposition in a SSc patient. **(e)** HFUS assessment of echogenicity and skin thickness. **(f)** SWE demonstrating stiff skin in SSc. **(g)** Staining of HIF2α in SSc lesional skin. Figure created by VF using own images.

11.3 Cutaneous fibrosis

The data presented in chapter 6 supports the use of HFUS as an objective measure of skin pathology and has highlighted potential with clinical advantages of HFUS over clinician assessment using the mRSS alone. We have undertaken much needed assessment of the convergent validity of HFUS with dermal collagen in SSc. We have added to the available data to reinforce the reproducibility of HFUS for skin application. We have also demonstrated that HFUS SWE and echogenicity can identify subclinical changes in skin quality when skin thickness is both subjectively and objectively normal. Similarly, we have also reported the potential for lcSSc to develop subclinical proximal skin involvement which again demonstrates superiority of HFUS over the mRSS alone. In recent years, there have been several clinical trials of promising therapeutic agents in dcSSc that have failed to achieve statistical significance when examining the net benefits of active treatment over placebo therapy alone (230, 234, 237). HFUS may provide a reliable quantitative surrogate assessment of skin pathology that could help support drug development in this field.

11.3.1 Future research

Longitudinal studies are required to assess the sensitivity of HFUS to change over time as well as triangulate HFUS data, gene expression profile of SSc skin and histology in order to complete its validation as a virtual biopsy for use in both routine clinical practice and clinical trials of SSc.

11.4 Evidence for inter-relationship between vasculopathy, inflammation and fibrosis in SSc

SSc is a heterogeneous disease with a complex and poorly understood pathogenesis. The heterogeneous clinical phenotype and large number of putative biomarkers highlights the challenges in identifying unifying common pathways and therapeutic targets in SSc. I have examined the inter-relationship between tissue hypoxia and fibrosis through non-invasive in vivo assessments of digital vasculopathy and cutaneous fibrosis with circulating biomarkers associated with the VEGF-A pathways in SSc.

11.4.1 Clinical evidence of the link between vasculopathy, inflammation and fibrosis

In chapter 7 we provided evidence for the pathogenic link between vasculopathy and skin pathology which furthers our understanding of SSc disease mechanisms. Specifically, the strong correlation between cutaneous echogenicity and both the post ischaemic reperfusion gradient and ICD on NC, provide novel evidence of the relationship between vasculopathy and skin oedema in early SSc (chapter 7). The weakening of these associations in late SSc demonstrates the complex and dynamic pathology in SSc. The apparent dynamic relationship between microvascular changes on NC classification and HFUS SWE would suggest a relationship between skin quality and vasculopathy in line with the vascular hypothesis (38). The complex inter-woven relationship between vasculopathy, inflammation and fibrosis is presented in Figure 11.1.

11.4.2 Clinical correlation of novel vascular biomarkers in SSc vasculopathy

Our literature review (chapter 1.9 and chapter 8 and 9) has explored the pathogenic inter-relationship between vasculopathy, skin fibrosis and vascular biomarkers including HIF, downstream VEGF-A isoforms and angiopoietins.

We have demonstrated that inhibitory vascular growth factors (VEGF-A_{165}b and Ang-2) are upregulated in SSc plasma (chapter 8) and lesional SSc skin (chapter 9), favouring an anti-angiogenic environment and capillary loss (Figure 11.1). Specifically, we have demonstrated for the first time that increased plasma levels of VEGF-A_{165}b are associated with reduced peripheral digital perfusion on both LSCI and HFUS cSMI. We have also shown for the first time that increased plasma Ang-2 translates to impaired peripheral perfusion on LSCI as well as advancing NC patterns (Figure 11.1).

Furthermore, we have shown that vasculopathy relates to cutaneous hypoxia reflected in the novel relationship between HIF1α and 2α with ICD as well as NVi with the latter. The striking over-expression of HIF2α in lesional SSc skin particularly in early disease suggests a temporal relationship and further supports the pathogenic link with vasculopathy and hypoxia (chapter 9). PanVEGF-A and VEGF-A_{165}b are considered downstream effectors of HIFα. However, we also report expression of the latter in non-lesional skin which appears to be non-HIF dependent.

11.4.3 Evidence for the role of vascular biomarkers in SSc skin pathology

We have also provided extended evidence of the vascular-fibrotic link through the profibrotic relationship of angiogenic biomarkers with skin pathology. Epidermal expression of HIF1α, HIF2α, panVEGF-A and VEGF-A_{165}b in lesional skin is associated with more severe skin involvement. Additionally, Ang-2 (evidenced through both plasma association with SWE and echogenicity, and cutaneous vascular expression in dcSSc) and Tie2 (with increased cutaneous expression in dcSSc) are also implicated. Amongst these vascular biomarkers, we have reported a novel relationship between epidermal VEGF-A_{165}b expression and objective HFUS skin thickness that may explain the natural regression in mRSS that occurs over the natural course of disease. Our data marks this isoform as both a potential biomarker of disease activity and therapeutic target for skin disease (as paralleled with biomarkers for therapeutic response in colon cancer (267)). These potential therapeutic implications are tempered by the potential negative consequence of iatrogenic VEGF-A_{165}b upregulation on the vasculopathy of SSc. This could have therapeutic implications for novel treatments in SSc such as Nintedinib which target VEGF signalling pathways (237). Targeting Ang-2 however, may both provide pro-angiogenic and reduce anti-fibrotic stimuli. Further work is however needed to understand Ang-2 exact role in skin pathology in SSc.

11.4.4 Further research

Further study is needed to explore:

- Longitudinal studies to map HIF paralog, VEGF-A_{165}b and Ang-2 expression in relation to the onset and evolution of both vasculopathy and skin pathology.
- The influence of differential patterns of hypoxia on HIF paralog determination and downstream VEGF-A_{165}b and Ang-2.
- The likely early non-HIF dependent drivers of VEGF-A_{165}b in SSc skin.

11.5 Limitations of our study:

Concurrent administration of vasodilators during the study may have reduced the number of statistically significant differences with regard to vascular imaging particularly with respect to LSCI baseline parameters. We felt that protocolled washout of vasodilators could adversely influence enrolment, enriching the cohort to those with early and less severe disease. Mandating a washout period would have been challenging and potentially harmful for patients. Longitudinal studies to capture data before initiation of vasodilators would be most beneficial with follow up data to observe response. Additionally, we consider the impact of vasodilators and DMARDs on biomarker detection in ex vivo skin and skin pathology assessed by HFUS as previously discussed (chapter 6 and 9).

A second factor for consideration is that our cohort consisted of a mixed cohort (early, late SSc and limited and diffuse) with large numbers of late lcSSc. Future studies may benefit from enrolling more homogeneous patient cohorts.

11.6 Final considerations and personal reflection

Collectively, the data presented in this thesis has provided further support of the inter-relationship between vasculopathy, inflammation and fibrosis in SSc pathology through the combined considerations of non-invasive imaging techniques and original reports of vascular biomarkers that likely drive vascular-fibrotic paradigms. We have provided novel, practically useful and translational data for the use of HFUS in assessment of SSc skin pathology. We have additionally examined its potential as an objective assessment of SSc vasculopathy.

The SRUK fellowship that supported this period of research has also enabled me to develop a large number of new skills, many of which are transferable to my clinical practice as a Rheumatologist. These include skills in microvascular imaging (including image acquisition and analysis of NC images), HFUS, skin biopsy collection and laboratory techniques including ELISA, IHC and cell culture. I have learnt a great deal about research governance and the ethical frameworks governing research in human subjects. I have also developed skills in study methodology and the critical appraisal of the existing literature. Finally, this work has enabled me to develop my skills as a doctor managing people living with SSc and hope this period of research will form a platform for me to develop my skills as a clinician and investigator in the field of SSc in the future.

References

1. Flower VA, Barratt SL, Ward S, Pauling JD. The role of vascular endothelial growth factor in systemic sclerosis. Curr Rheumatol Rev. 2019;15(2):99-109.
2. Barratt SL, Flower VA, Pauling JD, Millar AB. VEGF (vascular endothelial growth factor) and fibrotic lung disease. Int J Mol Sci. 2018;19(5).
3. Nikpour M, Stevens WM, Herrick AL, Proudman SM. Epidemiology of systemic sclerosis. Best Pract Res Clin Rheumatol. 2010;24(6):857-69.
4. Steen VD, Oddis CV, Conte CG, Janoski J, Casterline GZ, Medsger TA, Jr. Incidence of systemic sclerosis in Allegheny County, Pennsylvania. A twenty-year study of hospital-diagnosed cases, 1963-1982. Arthritis Rheum. 1997;40(3):441-5.
5. Meier FM, Frommer KW, Dinser R, Walker UA, Czirjak L, Denton CP, et al. Update on the profile of the EUSTAR cohort: An analysis of the EULAR Scleroderma trials and research group database. Ann Rheum Dis. 2012;71(8):1355-60.
6. Le Guern V, Mahr A, Mouthon L, Jeanneret D, Carzon M, Guillevin L. Prevalence of systemic sclerosis in a French multi-ethnic county. Rheumatology (Oxford). 2004;43(9):1129-37.
7. Jaeger VK, Tikly M, Xu D, Siegert E, Hachulla E, Airo P, et al. Racial differences in systemic sclerosis disease presentation: A European Scleroderma trials and research group study. Rheumatology (Oxford). 2020;59(7):1684-94.
8. Magnant J, de Monte M, Guilmot JL, Lasfargues G, Diot P, Asquier E, et al. Relationship between occupational risk factors and severity markers of systemic sclerosis. J Rheumatol. 2005;32(9):1713-8.
9. Conrad K, Mehlhorn J. Diagnostic and prognostic relevance of autoantibodies in uranium miners. Int Arch Allergy Immunol. 2000;123(1):77-91.
10. Zuo X, Zhang L, Luo H, Li Y, Zhu H. Systematic approach to understanding the pathogenesis of systemic sclerosis. Clin Genet. 2017;92(4):365-71.
11. Pattanaik D, Brown M, Postlethwaite BC, Postlethwaite AE. Pathogenesis of systemic sclerosis. Front Immunol. 2015;6:272.
12. Zhou X, Tan FK, Wang N, Xiong M, Maghidman S, Reveille JD, et al. Genome-wide association study for regions of systemic sclerosis susceptibility in a Choctaw indian population with high disease prevalence. Arthritis Rheum. 2003;48(9):2585-92.
13. Valenzi E, Bulik M, Tabib T, Morse C, Sembrat J, Trejo Bittar H, et al. Single-cell analysis reveals fibroblast heterogeneity and myofibroblasts in systemic sclerosis-associated interstitial lung disease. Ann Rheum Dis. 2019;78(10):1379-87.
14. Arnett FC, Cho M, Chatterjee S, Aguilar MB, Reveille JD, Mayes MD. Familial occurrence frequencies and relative risks for systemic sclerosis (scleroderma) in three United States cohorts. Arthritis Rheum. 2001;44(6):1359-62.
15. Feghali-Bostwick C, Medsger TA, Jr., Wright TM. Analysis of systemic sclerosis in twins reveals low concordance for disease and high

concordance for the presence of antinuclear antibodies. Arthritis Rheum. 2003;48(7):1956-63.
16. Aslani S, Sobhani S, Gharibdoost F, Jamshidi A, Mahmoudi M. Epigenetics and pathogenesis of systemic sclerosis; the ins and outs. Hum Immunol. 2018;79(3):178-87.
17. Wang Y, Fan PS, Kahaleh B. Association between enhanced type i collagen expression and epigenetic repression of the fli1 gene in scleroderma fibroblasts. Arthritis Rheum. 2006;54(7):2271-9.
18. Henderson J, Brown M, Horsburgh S, Duffy L, Wilkinson S, Worrell J, et al. Methyl cap binding protein 2: A key epigenetic protein in systemic sclerosis. Rheumatology (Oxford). 2019;58(3):527-35.
19. Sing T, Jinnin M, Yamane K, Honda N, Makino K, Kajihara I, et al. Microrna-92a expression in the sera and dermal fibroblasts increases in patients with scleroderma. Rheumatology (Oxford). 2012;51(9):1550-6.
20. Kuwana M. Circulating anti-nuclear antibodies in systemic sclerosis: Utility in diagnosis and disease subsetting. J Nippon Med Sch. 2017;84(2):56-63.
21. Steen VD. Autoantibodies in systemic sclerosis. Semin Arthritis Rheum. 2005;35(1):35-42.
22. Ostojic P, Damjanov N, Pavlov-Dolijanovic S, Radunovic G. Peripheral vasculopathy in patients with systemic sclerosis: Difference in limited and diffuse subset of disease. Clin Hemorheol Microcirc. 2004;31(4):281-5.
23. Ostojic P, Damjanov N. Different clinical features in patients with limited and diffuse cutaneous systemic sclerosis. Clin Rheumatol. 2006;25(4):453-7.
24. Muangchan C, Canadian Scleroderma Research G, Baron M, Pope J. The 15% rule in scleroderma: The frequency of severe organ complications in systemic sclerosis. A systematic review. J Rheumatol. 2013;40(9):1545-56.
25. Priora M, Manetta T, Scarati M, Parisi S, Lagana A, Peroni CL, et al. Serological and clinical profile of systemic sclerosis: Analysis in a cohort of patients from a single center in northern Italy. G Ital Dermatol Venereol. 2018;153(1):33-8.
26. Rozman B, Cucnik S, Sodin-Semrl S, Czirjak L, Varju C, Distler O, et al. Prevalence and clinical associations of anti-ku antibodies in patients with systemic sclerosis: A European EUSTAR-initiated multi-centre case-control study. Ann Rheum Dis. 2008;67(9):1282-6.
27. Young A, Namas R, Dodge C, Khanna D. Hand impairment in systemic sclerosis: Various manifestations and currently available treatment. Curr Treatm Opt Rheumatol. 2016;2(3):252-69.
28. Nihtyanova SI, Sari A, Harvey JC, Leslie A, Derrett-Smith EC, Fonseca C, et al. Using autoantibodies and cutaneous subset to develop outcome-based disease classification in systemic sclerosis. Arthritis Rheumatol. 2020;72(3):465-76.
29. Committee SfSCotARADaTc. Preliminary criteria for the classification of systemic sclerosis (scleroderma). Subcommittee for scleroderma criteria of the American rheumatism association diagnostic and therapeutic criteria committee. Arthritis Rheum. 1980;23(5):581-90.
30. LeRoy EC, Medsger TA, Jr. Criteria for the classification of early systemic sclerosis. J Rheumatol. 2001;28(7):1573-6.
31. van den Hoogen F, Khanna D, Fransen J, Johnson SR, Baron M, Tyndall A, et al. 2013 classification criteria for systemic sclerosis: An American college of rheumatology/European league against rheumatism collaborative initiative. Ann Rheum Dis. 2013;72(11):1747-55.

32. Jordan S, Maurer B, Toniolo M, Michel B, Distler O. Performance of the new acr/eular classification criteria for systemic sclerosis in clinical practice. Rheumatology (Oxford). 2015;54(8):1454-8.
33. Alhajeri H, Hudson M, Fritzler M, Pope J, Tatibouet S, Markland J, et al. 2013 American college of rheumatology/European league against rheumatism classification criteria for systemic sclerosis outperform the 1980 criteria: Data from the Canadian scleroderma research group. Arthritis Care Res (Hoboken). 2015;67(4):582-7.
34. Herrick AL, Peytrignet S, Lunt M, Pan X, Hesselstrand R, Mouthon L, et al. Patterns and predictors of skin score change in early diffuse systemic sclerosis from the European scleroderma observational study. Ann Rheum Dis. 2018;77(4):563-70.
35. Wu PC, Huang MN, Kuo YM, Hsieh SC, Yu CL. Clinical applicability of quantitative nailfold capillaroscopy in differential diagnosis of connective tissue diseases with Raynaud's phenomenon. J Formos Med Assoc. 2013;112(8):482-8.
36. Avouac J, Fransen J, Walker UA, Riccieri V, Smith V, Muller C, et al. Preliminary criteria for the very early diagnosis of systemic sclerosis: Results of a delphi consensus study from EULAR scleroderma trials and research group. Ann Rheum Dis. 2011;70(3):476-81.
37. Minier T, Guiducci S, Bellando-Randone S, Bruni C, Lepri G, Czirjak L, et al. Preliminary analysis of the very early diagnosis of systemic sclerosis (VEDOSS) EUSTAR multicentre study: Evidence for puffy fingers as a pivotal sign for suspicion of systemic sclerosis. Ann Rheum Dis. 2014;73(12):2087-93.
38. Campbell PM, LeRoy EC. Pathogenesis of systemic sclerosis: A vascular hypothesis. Semin Arthritis Rheum. 1975;4(4):351-68.
39. Distler O, Distler JH, Scheid A, Acker T, Hirth A, Rethage J, et al. Uncontrolled expression of vascular endothelial growth factor and its receptors leads to insufficient skin angiogenesis in patients with systemic sclerosis. Circ Res. 2004;95(1):109-16.
40. Cracowski JL, Kom GD, Salvat-Melis M, Renversez JC, McCord G, Boignard A, et al. Postocclusive reactive hyperemia inversely correlates with urinary 15-f2t-isoprostane levels in systemic sclerosis. Free Radic Biol Med. 2006;40(10):1732-7.
41. Freemont AJ, Hoyland J, Fielding P, Hodson N, Jayson MI. Studies of the microvascular endothelium in uninvolved skin of patients with systemic sclerosis: Direct evidence for a generalized microangiopathy. Br J Dermatol. 1992;126(6):561-8.
42. Prescott RJ, Freemont AJ, Jones CJ, Hoyland J, Fielding P. Sequential dermal microvascular and perivascular changes in the development of scleroderma. J Pathol. 1992;166(3):255-63.
43. Roumm AD, Whiteside TL, Medsger TA, Jr., Rodnan GP. Lymphocytes in the skin of patients with progressive systemic sclerosis. Quantification, subtyping, and clinical correlations. Arthritis Rheum. 1984;27(6):645-53.
44. Camargo CZ, Sekiyama JY, Arismendi MI, Kayser C. Microvascular abnormalities in patients with early systemic sclerosis: Less severe morphological changes than in patients with definite disease. Scand J Rheumatol. 2015;44(1):48-55.
45. Vasile M, Avouac J, Sciarra I, Stefanantoni K, Iannace N, Cravotto E, et al. From VEDOSS to established systemic sclerosis diagnosis according to ACR/EULAR 2013 classification criteria: A French-Italian capillaroscopic survey. Clin Exp Rheumatol. 2018;36 Suppl 113(4):82-7.
46. Koenig M, Joyal F, Fritzler MJ, Roussin A, Abrahamowicz M, Boire G, et al. Autoantibodies and microvascular damage are independent

predictive factors for the progression of Raynaud's phenomenon to systemic sclerosis: A twenty-year prospective study of 586 patients, with validation of proposed criteria for early systemic sclerosis. Arthritis Rheum. 2008;58(12):3902-12.
47. Broz P, Aschwanden M, Partovi S, Schulte AC, Benz D, Takes M, et al. Assessment of cutaneous microcirculation in unaffected skin regions by transcutaneous oxygen saturation monitoring and laser doppler flowmetry in systemic sclerosis. Clin Hemorheol Microcirc. 2015;60(3):263-71.
48. Raschi E, Chighizola CB, Cesana L, Privitera D, Ingegnoli F, Mastaglio C, et al. Immune complexes containing scleroderma-specific autoantibodies induce a profibrotic and proinflammatory phenotype in skin fibroblasts. Arthritis Res Ther. 2018;20(1):187.
49. Salojin KV, Le Tonqueze M, Saraux A, Nassonov EL, Dueymes M, Piette JC, et al. Antiendothelial cell antibodies: Useful markers of systemic sclerosis. Am J Med. 1997;102(2):178-85.
50. Florey OJ, Johns M, Esho OO, Mason JC, Haskard DO. Antiendothelial cell antibodies mediate enhanced leukocyte adhesion to cytokine-activated endothelial cells through a novel mechanism requiring cooperation between fc{gamma}riia and cxcr1/2. Blood. 2007;109(9):3881-9.
51. Herrick AL. Pathogenesis of Raynaud's phenomenon. Rheumatology (Oxford). 2005;44(5):587-96.
52. Olsen N, Nielsen SL. Prevalence of primary Raynaud phenomena in young females. Scand J Clin Lab Invest. 1978;38(8):761-4.
53. De Angelis R, Salaffi F, Grassi W. Raynaud's phenomenon: Prevalence in an italian population sample. Clin Rheumatol. 2006;25(4):506-10.
54. Sunderkotter C, Riemekasten G. Pathophysiology and clinical consequences of Raynaud's phenomenon related to systemic sclerosis. Rheumatology (Oxford). 2006;45 Suppl 3:iii33-5.
55. Bakst R, Merola JF, Franks AG, Jr., Sanchez M. Raynaud's phenomenon: Pathogenesis and management. J Am Acad Dermatol. 2008;59(4):633-53.
56. Minson CT, Berry LT, Joyner MJ. Nitric oxide and neurally mediated regulation of skin blood flow during local heating. J Appl Physiol (1985). 2001;91(4):1619-26.
57. Mosdosi B, Bolcskei K, Helyes Z. Impairment of microcirculation and vascular responsiveness in adolescents with primary raynaud phenomenon. Pediatr Rheumatol Online J. 2018;16(1):20.
58. Maga P, Henry BM, Kmiotek EK, Gregorczyk-Maga I, Kaczmarczyk P, Tomaszewski KA, et al. Postocclusive hyperemia measured with laser doppler flowmetry and transcutaneous oxygen tension in the diagnosis of primary raynaud's phenomenon: A prospective, controlled study. Biomed Res Int. 2016;2016:9645705.
59. Stoyneva Z. Postocclusive reactive hyperemia in hand-arm vibration syndrome. Int J Occup Med Environ Health. 2016;29(4):659-66.
60. Herrick AL. Vascular function in systemic sclerosis. Curr Opin Rheumatol. 2000;12(6):527-33.
61. Gaillard-Bigot F, Roustit M, Blaise S, Gabin M, Cracowski C, Seinturier C, et al. Abnormal amplitude and kinetics of digital postocclusive reactive hyperemia in systemic sclerosis. Microvasc Res. 2014;94:90-5.
62. Ruaro B, Sulli A, Alessandri E, Pizzorni C, Ferrari G, Cutolo M. Laser speckle contrast analysis: A new method to evaluate peripheral blood perfusion in systemic sclerosis patients. Ann Rheum Dis. 2014;73(6):1181-5.

63. Sulli A, Ruaro B, Cutolo M. Evaluation of blood perfusion by laser speckle contrast analysis in different areas of hands and face in patients with systemic sclerosis. Ann Rheum Dis. 2014;73(11):2059-61.
64. Rosato E, Rossi C, Molinaro I, Giovannetti A, Pisarri S, Salsano F. Laser doppler perfusion imaging in systemic sclerosis impaired response to cold stimulation involves digits and hand dorsum. Rheumatology (Oxford). 2011;50(9):1654-8.
65. Keberle M, Tony HP, Jahns R, Hau M, Haerten R, Jenett M. Assessment of microvascular changes in Raynaud's phenomenon and connective tissue disease using colour doppler ultrasound. Rheumatology (Oxford). 2000;39(11):1206-13.
66. Rajagopalan S, Pfenninger D, Kehrer C, Chakrabarti A, Somers E, Pavlic R, et al. Increased asymmetric dimethylarginine and endothelin 1 levels in secondary Raynaud's phenomenon: Implications for vascular dysfunction and progression of disease. Arthritis Rheum. 2003;48(7):1992-2000.
67. Blaise S, Maas R, Trocme C, Kom GD, Roustit M, Carpentier PH, et al. Correlation of biomarkers of endothelium dysfunction and matrix remodeling in patients with systemic sclerosis. J Rheumatol. 2009;36(5):984-8.
68. Dooley A, Gao B, Bradley N, Abraham DJ, Black CM, Jacobs M, et al. Abnormal nitric oxide metabolism in systemic sclerosis: Increased levels of nitrated proteins and asymmetric dimethylarginine. Rheumatology (Oxford). 2006;45(6):676-84.
69. Pauling JD, Saketkoo LA, Matucci-Cerinic M, Ingegnoli F, Khanna D. The patient experience of raynaud's phenomenon in systemic sclerosis. Rheumatology (Oxford). 2019;58(1):18-26.
70. Pauling JD, Domsic RT, Saketkoo LA, Almeida C, Withey J, Jay H, et al. Multinational qualitative research study exploring the patient experience of Raynaud's phenomenon in systemic sclerosis. Arthritis Care Res (Hoboken). 2018;70(9):1373-84.
71. Steen V, Denton CP, Pope JE, Matucci-Cerinic M. Digital ulcers: Overt vascular disease in systemic sclerosis. Rheumatology (Oxford). 2009;48 Suppl 3:iii19-24.
72. Steen VD, Medsger TA, Jr. The value of the health assessment questionnaire and special patient-generated scales to demonstrate change in systemic sclerosis patients over time. Arthritis Rheum. 1997;40(11):1984-91.
73. Merkel PA, Herlyn K, Martin RW, Anderson JJ, Mayes MD, Bell P, et al. Measuring disease activity and functional status in patients with scleroderma and raynaud's phenomenon. Arthritis Rheum. 2002;46(9):2410-20.
74. Khanna D, Lovell DJ, Giannini E, Clements PJ, Merkel PA, Seibold JR, et al. Development of a provisional core set of response measures for clinical trials of systemic sclerosis. Ann Rheum Dis. 2008;67(5):703-9.
75. Wilkinson JD, Leggett SA, Marjanovic EJ, Moore TL, Allen J, Anderson ME, et al. A multicenter study of the validity and reliability of responses to hand cold challenge as measured by laser speckle contrast imaging and thermography: Outcome measures for systemic sclerosis-related Raynaud's phenomenon. Arthritis Rheumatol. 2018;70(6):903-11.
76. Hughes M, Moore T, Manning J, Wilkinson J, Dinsdale G, Roberts C, et al. Reduced perfusion in systemic sclerosis digital ulcers (both fingertip and extensor) can be increased by topical application of glyceryl trinitrate. Microvasc Res. 2017;111:32-6.

77. Wigley FM, Wise RA, Mikdashi J, Schaefer S, Spence RJ. The post-occlusive hyperemic response in patients with systemic sclerosis. Arthritis Rheum. 1990;33(11):1620-5.
78. Vayssairat M, Blaison N, Baudot N, Evenou P, Gilard M, Mathieu JF. Action of nifedipine on the post-ischemic cold hyperemia reaction in Raynaud's phenomenon. J Mal Vasc. 1989;14(4):299-302.
79. Gunawardena H, Harris ND, Carmichael C, McHugh NJ. Maximum blood flow and microvascular regulatory responses in systemic sclerosis. Rheumatology (Oxford). 2007;46(7):1079-82.
80. Boignard A, Salvat-Melis M, Carpentier PH, Minson CT, Grange L, Duc C, et al. Local hyperemia to heating is impaired in secondary Raynaud's phenomenon. Arthritis Res Ther. 2005;7(5):R1103-12.
81. Cracowski JL, Roustit M. Current methods to assess human cutaneous blood flow: An updated focus on laser-based-techniques. Microcirculation. 2016;23(5):337-44.
82. Wollersheim H, Reyenga J, Thien T. Postocclusive reactive hyperemia of fingertips, monitored by laser doppler velocimetry in the diagnosis of Raynaud's phenomenon. Microvasc Res. 1989;38(3):286-95.
83. Salvat-Melis M, Carpentier PH, Minson CT, Boignard A, McCord GR, Paris A, et al. Digital thermal hyperaemia impairment does not relate to skin fibrosis or macrovascular disease in systemic sclerosis. Rheumatology (Oxford). 2006;45(12):1490-6.
84. Roustit M, Simmons GH, Baguet JP, Carpentier P, Cracowski JL. Discrepancy between simultaneous digital skin microvascular and brachial artery macrovascular post-occlusive hyperemia in systemic sclerosis. J Rheumatol. 2008;35(8):1576-83.
85. Grattagliano V, Iannone F, Praino E, De Zio A, Riccardi MT, Carrozzo N, et al. Digital laser doppler flowmetry may discriminate "limited" from "diffuse" systemic sclerosis. Microvasc Res. 2010;80(2):221-6.
86. Rossi M, Bazzichi L, Ghiadoni L, Mencaroni I, Franzoni F, Bombardieri S. Increased finger skin vasoreactivity and stimulated vasomotion associated with simvastatin therapy in systemic sclerosis hypercholesterolemic patients. Rheumatol Int. 2012;32(12):3715-21.
87. Waszczykowska A, Gos R, Waszczykowska E, Dziankowska-Bartkowiak B, Jurowski P. Assessment of skin microcirculation by laser doppler flowmetry in systemic sclerosis patients. Postepy Dermatol Alergol. 2014;31(1):6-11.
88. Della Rossa A, Cazzato M, d'Ascanio A, Tavoni A, Bencivelli W, Pepe P, et al. Alteration of microcirculation is a hallmark of very early systemic sclerosis patients: A laser speckle contrast analysis. Clin Exp Rheumatol. 2013;31(2 Suppl 76):109-14.
89. Domsic RT, Dezfulian C, Shoushtari A, Ivanco D, Kenny E, Kwoh CK, et al. Endothelial dysfunction is present only in the microvasculature and microcirculation of early diffuse systemic sclerosis patients. Clin Exp Rheumatol. 2014;32(6 Suppl 86):S-154-60.
90. Della Rossa A, D'Ascanio A, Barsotti S, Stagnaro C, Mosca M. Post-occlusive reactive hyperaemia (pohr) in systemic sclerosis: Very early disease (VEDOSS) represents a separate entity compared to established disease. Scand J Rheumatol. 2016;45(5):408-11.
91. Kwiatkowska M, Rakowska A, Walecka I, Rudnicka L. The diagnostic value of trichoscopy in systemic sclerosis. J Dermatol Case Rep. 2016;10(2):21-5.
92. Carrai V, Miniati I, Guiducci S, Capaccioli G, Alterini R, Saccardi R, et al. Evidence for reduced angiogenesis in bone marrow in ssc: Immunohistochemistry and multiparametric computerized imaging analysis. Rheumatology (Oxford). 2012;51(6):1042-8.

93. Cutolo M, Sulli A, Smith V. Assessing microvascular changes in systemic sclerosis diagnosis and management. Nat Rev Rheumatol. 2010;6(10):578-87.
94. Cutolo M, Pizzorni C, Tuccio M, Burroni A, Craviotto C, Basso M, et al. Nailfold videocapillaroscopic patterns and serum autoantibodies in systemic sclerosis. Rheumatology (Oxford). 2004;43(6):719-26.
95. Sulli A, Ruaro B, Smith V, Pizzorni C, Zampogna G, Gallo M, et al. Progression of nailfold microvascular damage and antinuclear antibody pattern in systemic sclerosis. J Rheumatol. 2013;40(5):634-9.
96. Nagy Z, Czirjak L. Nailfold digital capillaroscopy in 447 patients with connective tissue disease and Raynaud's disease. J Eur Acad Dermatol Venereol. 2004;18(1):62-8.
97. Sag S, Sag MS, Tekeoglu I, Kamanli A, Nas K, Aydin Y. Nailfold videocapillaroscopy results in patients with rheumatoid arthritis. Clin Rheumatol. 2017;36(9):1969-74.
98. Bissell LA, Abignano G, Emery P, Del Galdo F, Buch MH. Absence of scleroderma pattern at nail fold capillaroscopy valuable in the exclusion of scleroderma in unselected patients with raynaud's phenomenon. BMC Musculoskelet Disord. 2016;17(1):342.
99. Smith V, Vanhaecke A, Herrick AL, Distler O, Guerra MG, Denton CP, et al. Fast track algorithm: How to differentiate a "scleroderma pattern" from a "non-scleroderma pattern". Autoimmun Rev. 2019;18(11):102394.
100. Chora I, Romano E, Manetti M, Mazzotta C, Costa R, Machado V, et al. Evidence for a derangement of the microvascular system in patients with a very early diagnosis of systemic sclerosis. J Rheumatol. 2017;44(8):1190-7.
101. Dinsdale G, Moore T, O'Leary N, Berks M, Roberts C, Manning J, et al. Quantitative outcome measures for systemic sclerosis-related microangiopathy - reliability of image acquisition in nailfold capillaroscopy. Microvasc Res. 2017;113:56-9.
102. Ingegnoli F, Ughi N, Dinsdale G, Orenti A, Boracchi P, Allanore Y, et al. An international survey on non-invasive techniques to assess the microcirculation in patients with Raynaud's phenomenon (sunshine survey). Rheumatol Int. 2017;37(11):1879-90.
103. Chung CP, Avalos I, Stein CM. Oxidative stress, microvascular dysfunction, and scleroderma: An association with potential therapeutic implications, a commentary on "postocclusive reactive hyperemia inversely correlates with urinary 15-f2t-isoprostane levels in systemic sclerosis". Free Radic Biol Med. 2006;40(10):1698-9.
104. Abignano G, Daniel A, Green L, Eng S, Del Galdo F. Microvascular flow assessed by dynamic optical coherence tomography: First non-invasive quantitative outcome measure of microvascular disease in systemic sclerosis. J Scleroderma Relat Disord2017. p. S3.
105. Ruaro B, Sulli A, Pizzorni C, Paolino S, Smith V, Cutolo M. Correlations between skin blood perfusion values and nailfold capillaroscopy scores in systemic sclerosis patients. Microvasc Res. 2016;105:119-24.
106. Murray AK, Moore TL, Manning JB, Taylor C, Griffiths CE, Herrick AL. Noninvasive imaging techniques in the assessment of scleroderma spectrum disorders. Arthritis Rheum. 2009;61(8):1103-11.
107. Cutolo M, Herrick AL, Distler O, Becker MO, Beltran E, Carpentier P, et al. Nailfold videocapillaroscopic features and other clinical risk factors for digital ulcers in systemic sclerosis: A multicenter, prospective cohort study. Arthritis Rheumatol. 2016;68(10):2527-39.
108. Caramaschi P, Canestrini S, Martinelli N, Volpe A, Pieropan S, Ferrari M, et al. Scleroderma patients nailfold videocapillaroscopic patterns are

associated with disease subset and disease severity. Rheumatology (Oxford). 2007;46(10):1566-9.
109. Herrick AL, Moore TL, Murray AK, Whidby N, Manning JB, Bhushan M, et al. Nail-fold capillary abnormalities are associated with anti-centromere antibody and severity of digital ischaemia. Rheumatology (Oxford). 2010;49(9):1776-82.
110. Avouac J, Lepri G, Smith V, Toniolo E, Hurabielle C, Vallet A, et al. Sequential nailfold videocapillaroscopy examinations have responsiveness to detect organ progression in systemic sclerosis. Semin Arthritis Rheum. 2017;47(1):86-94.
111. Smith V, Decuman S, Sulli A, Bonroy C, Piettte Y, Deschepper E, et al. Do worsening scleroderma capillaroscopic patterns predict future severe organ involvement? A pilot study. Ann Rheum Dis. 2012;71(10):1636-9.
112. Sebastiani M, Manfredi A, Colaci M, D'Amico R, Malagoli V, Giuggioli D, et al. Capillaroscopic skin ulcer risk index: A new prognostic tool for digital skin ulcer development in systemic sclerosis patients. Arthritis Rheum. 2009;61(5):688-94.
113. Ingegnoli F, Ardoino I, Boracchi P, Cutolo M, co-authors E. Nailfold capillaroscopy in systemic sclerosis: Data from the eular scleroderma trials and research (eustar) database. Microvasc Res. 2013;89:122-8.
114. Riccieri V, Vasile M, Iannace N, Stefanantoni K, Sciarra I, Vizza CD, et al. Systemic sclerosis patients with and without pulmonary arterial hypertension: A nailfold capillaroscopy study. Rheumatology (Oxford). 2013;52(8):1525-8.
115. Smith V, Riccieri V, Pizzorni C, Decuman S, Deschepper E, Bonroy C, et al. Nailfold capillaroscopy for prediction of novel future severe organ involvement in systemic sclerosis. J Rheumatol. 2013;40(12):2023-8.
116. Sulli A, Pizzorni C, Smith V, Zampogna G, Ravera F, Cutolo M. Timing of transition between capillaroscopic patterns in systemic sclerosis. Arthritis Rheum. 2012;64(3):821-5.
117. Pavan TR, Bredemeier M, Hax V, Capobianco KG, da Silva Mendonca Chakr R, Xavier RM. Capillary loss on nailfold capillary microscopy is associated with mortality in systemic sclerosis. Clin Rheumatol. 2018;37(2):475-81.
118. Tieu J, Hakendorf P, Woodman RJ, Patterson K, Walker J, Roberts-Thomson P. The role of nailfold capillary dropout on mortality in systemic sclerosis. Intern Med J. 2018;48(5):517-23.
119. Paxton D, Pauling JD. Does nailfold capillaroscopy help predict future outcomes in systemic sclerosis? A systematic literature review. Semin Arthritis Rheum. 2018;48(3):482-94.
120. Pauling JD. Could nailfold videocapillaroscopy usher in a new era of preventative disease-modifying therapeutic intervention in systemic sclerosis? Rheumatology (Oxford). 2017;56(7):1053-5.
121. Pauling JD, Reilly E, Smith T, Frech TM. Evolving symptom characteristics of Raynaud's phenomenon in systemic sclerosis and their association with physician and patient-reported assessments of disease severity. Arthritis Care Res (Hoboken). 2019;71(8):1119-26.
122. Sulli A, Ruaro B, Alessandri E, Pizzorni C, Cimmino MA, Zampogna G, et al. Correlations between nailfold microangiopathy severity, finger dermal thickness and fingertip blood perfusion in systemic sclerosis patients. Ann Rheum Dis. 2014;73(1):247-51.
123. De Santis M, Ceribelli A, Cavaciocchi F, Crotti C, Massarotti M, Belloli L, et al. Nailfold videocapillaroscopy and serum VEGF levels in scleroderma are associated with internal organ involvement. Auto Immun Highlights. 2016;7(1):5.

124. Fichel F, Baudot N, Gaitz JP, Trad S, Barbe C, Frances C, et al. Systemic sclerosis with normal or nonspecific nailfold capillaroscopy. Dermatology. 2014;228(4):360-7.
125. Tolosa-Vilella C, Morera-Morales ML, Simeon-Aznar CP, Mari-Alfonso B, Colunga-Arguelles D, Callejas Rubio JL, et al. Digital ulcers and cutaneous subsets of systemic sclerosis: Clinical, immunological, nailfold capillaroscopy, and survival differences in the spanish rescle registry. Semin Arthritis Rheum. 2016;46(2):200-8.
126. Ghizzoni C, Sebastiani M, Manfredi A, Campomori F, Colaci M, Giuggioli D, et al. Prevalence and evolution of scleroderma pattern at nailfold videocapillaroscopy in systemic sclerosis patients: Clinical and prognostic implications. Microvasc Res. 2015;99:92-5.
127. Soulaidopoulos S, Triantafyllidou E, Garyfallos A, Kitas GD, Dimitroulas T. The role of nailfold capillaroscopy in the assessment of internal organ involvement in systemic sclerosis: A critical review. Autoimmun Rev. 2017;16(8):787-95.
128. Castellvi I, Simeon-Aznar CP, Sarmiento M, Fortuna A, Mayos M, Geli C, et al. Association between nailfold capillaroscopy findings and pulmonary function tests in patients with systemic sclerosis. J Rheumatol. 2015;42(2):222-7.
129. Saba L, Yuan C, Hatsukami TS, Balu N, Qiao Y, DeMarco JK, et al. Carotid artery wall imaging: Perspective and guidelines from the asnr vessel wall imaging study group and expert consensus recommendations of the american society of neuroradiology. AJNR Am J Neuroradiol. 2018;39(2):E9-E31.
130. Lescoat A, Yelnik CM, Coiffier G, Wargny M, Lamotte C, Cazalets C, et al. Ulnar artery occlusion and severity markers of vasculopathy in systemic sclerosis: A multicenter cross-sectional study. Arthritis Rheumatol. 2019;71(6):983-90.
131. Schioppo T, Orenti A, Boracchi P, De Lucia O, Murgo A, Ingegnoli F. Evidence of macro- and micro-angiopathy in scleroderma: An integrated approach combining 22-mhz power doppler ultrasonography and video-capillaroscopy. Microvasc Res. 2019;122:125-30.
132. Rosato E, Gigante A, Barbano B, Cianci R, Molinaro I, Pisarri S, et al. In systemic sclerosis macrovascular damage of hands digital arteries correlates with microvascular damage. Microvasc Res. 2011;82(3):410-5.
133. Luders S, Friedrich S, Ohrndorf S, Glimm AM, Burmester GR, Riemekasten G, et al. Detection of severe digital vasculopathy in systemic sclerosis by colour doppler sonography is associated with digital ulcers. Rheumatology (Oxford). 2017;56(11):1865-73.
134. Jagasia MH, Greinix HT, Arora M, Williams KM, Wolff D, Cowen EW, et al. National institutes of health consensus development project on criteria for clinical trials in chronic graft-versus-host disease: I. The 2014 diagnosis and staging working group report. Biol Blood Marrow Transplant. 2015;21(3):389-401 e1.
135. He A, Kwatra SG, Zampella JG, Loss MJ. Nephrogenic systemic fibrosis: Fibrotic plaques and contracture following exposure to gadolinium-based contrast media. BMJ Case Rep. 2016;2016.
136. Sharma A. Scleroderma-like disorders. Curr Rheumatol Rev. 2018;14(1):22-7.
137. Azevedo VF, Serafini SZ, Werner B, Muller CS, Franchini CF, Morais RL. Stiff skin syndrome versus scleroderma: A report of two cases. Clin Rheumatol. 2009;28(9):1107-11.
138. Aoki M, Matsushita S, Kawai K, Kanekura T. Scleromyxedema clinically resembling to scleroderma. Indian J Dermatol. 2016;61(1):127.

139. Khanna D, Furst DE, Clements PJ, Allanore Y, Baron M, Czirjak L, et al. Standardization of the modified rodnan skin score for use in clinical trials of systemic sclerosis. J Scleroderma Relat Disord. 2017;2(1):11-8.
140. Rodnan GP, Lipinski E, Luksick J. Skin thickness and collagen content in progressive systemic sclerosis and localized scleroderma. Arthritis Rheum. 1979;22(2):130-40.
141. Hesselstrand R, Scheja A, Wildt M, Akesson A. High-frequency ultrasound of skin involvement in systemic sclerosis reflects oedema, extension and severity in early disease. Rheumatology (Oxford). 2008;47(1):84-7.
142. Hesselstrand R, Carlestam J, Wildt M, Sandqvist G, Andreasson K. High frequency ultrasound of skin involvement in systemic sclerosis - a follow-up study. Arthritis Res Ther. 2015;17:329.
143. Hayes RL, Rodnan GP. The ultrastructure of skin in progressive systemic sclerosis (scleroderma). I. Dermal collagen fibers. Am J Pathol. 1971;63(3):433-42.
144. Aden N, Shiwen X, Aden D, Black C, Nuttall A, Denton CP, et al. Proteomic analysis of scleroderma lesional skin reveals activated wound healing phenotype of epidermal cell layer. Rheumatolog. 2008;47(12):1754-60.
145. Farouk HM, Hamza SH, El Bakry SA, Youssef SS, Aly IM, Moustafa AA, et al. Dysregulation of angiogenic homeostasis in systemic sclerosis. Int J Rheum Dis. 2013;16(4):448-54.
146. Abignano G, Aydin SZ, Castillo-Gallego C, Liakouli V, Woods D, Meekings A, et al. Virtual skin biopsy by optical coherence tomography: The first quantitative imaging biomarker for scleroderma. Ann Rheum Dis. 2013;72(11):1845-51.
147. Valanciene G, Jasaitiene D, Valiukeviciene S. Pathogenesis and treatment modalities of localized scleroderma. Medicina (Kaunas). 2010;46(10):649-56.
148. Razykov I, Levis B, Hudson M, Baron M, Thombs BD, Canadian Scleroderma Research G. Prevalence and clinical correlates of pruritus in patients with systemic sclerosis: An updated analysis of 959 patients. Rheumatology (Oxford). 2013;52(11):2056-61.
149. Johnson ME, Franks JM, Cai G, Mehta BK, Wood TA, Archambault K, et al. Microbiome dysbiosis is associated with disease duration and increased inflammatory gene expression in systemic sclerosis skin. Arthritis Res Ther. 2019;21(1):49.
150. Clements PJ, Wong WK, Hurwitz EL, Furst DE, Mayes M, White B, et al. Correlates of the disability index of the health assessment questionnaire: A measure of functional impairment in systemic sclerosis. Arthritis Rheum. 1999;42(11):2372-80.
151. Jewett LR, Hudson M, Malcarne VL, Baron M, Thombs BD, Canadian Scleroderma Research G. Sociodemographic and disease correlates of body image distress among patients with systemic sclerosis. PLoS One. 2012;7(3):e33281.
152. Clements PJ, Lachenbruch PA, Ng SC, Simmons M, Sterz M, Furst DE. Skin score. A semiquantitative measure of cutaneous involvement that improves prediction of prognosis in systemic sclerosis. Arthritis Rheum. 1990;33(8):1256-63.
153. Domsic RT, Rodriguez-Reyna T, Lucas M, Fertig N, Medsger TA, Jr. Skin thickness progression rate: A predictor of mortality and early internal organ involvement in diffuse scleroderma. Ann Rheum Dis. 2011;70(1):104-9.
154. Shand L, Lunt M, Nihtyanova S, Hoseini M, Silman A, Black CM, et al. Relationship between change in skin score and disease outcome in

diffuse cutaneous systemic sclerosis: Application of a latent linear trajectory model. Arthritis Rheum. 2007;56(7):2422-31.
155. Steen VD, Medsger TA, Jr. Improvement in skin thickening in systemic sclerosis associated with improved survival. Arthritis Rheum. 2001;44(12):2828-35.
156. Steen VD, Medsger TA, Jr., Rodnan GP. D-penicillamine therapy in progressive systemic sclerosis (scleroderma): A retrospective analysis. Ann Intern Med. 1982;97(5):652-9.
157. Brennan P, Silman A, Black C, Bernstein R, Coppock J, Maddison P, et al. Reliability of skin involvement measures in scleroderma. The UK Scleroderma study group. Br J Rheumatol. 1992;31(7):457-60.
158. Verrecchia F, Laboureau J, Verola O, Roos N, Porcher R, Bruneval P, et al. Skin involvement in scleroderma--where histological and clinical scores meet. Rheumatology (Oxford). 2007;46(5):833-41.
159. Clements P, Lachenbruch P, Siebold J, White B, Weiner S, Martin R, et al. Inter and intraobserver variability of total skin thickness score (modified rodnan tss) in systemic sclerosis. J Rheumatol. 1995;22(7):1281-5.
160. Clements PJ, Lachenbruch PA, Seibold JR, Zee B, Steen VD, Brennan P, et al. Skin thickness score in systemic sclerosis: An assessment of interobserver variability in 3 independent studies. J Rheumatol. 1993;20(11):1892-6.
161. Khanna D, Denton CP, Lin CJF, van Laar JM, Frech TM, Anderson ME, et al. Safety and efficacy of subcutaneous tocilizumab in systemic sclerosis: Results from the open-label period of a phase ii randomised controlled trial (fasscinate). Ann Rheum Dis. 2018;77(2):212-20.
162. Distler O, Pope J, Denton C, Allanore Y, Matucci-Cerinic M, de Oliveira Pena J, et al. Rise-ssc: Riociguat in diffuse cutaneous systemic sclerosis. Respir Med. 2017;122 Suppl 1:S14-S7.
163. Khanna D, Spino C, Johnson S, Chung L, Whitfield ML, Denton CP, et al. Abatacept in early diffuse cutaneous systemic sclerosis: Results of a phase ii investigator-initiated, multicenter, double-blind, randomized, placebo-controlled trial. Arthritis Rheumatol. 2020;72(1):125-36.
164. Denton CP. Challenges in systemic sclerosis trial design. Semin Arthritis Rheum. 2019;49(3S):S3-S7.
165. Kaloudi O, Bandinelli F, Filippucci E, Conforti ML, Miniati I, Guiducci S, et al. High frequency ultrasound measurement of digital dermal thickness in systemic sclerosis. Ann Rheum Dis. 2010;69(6):1140-3.
166. Hinchcliff M, Huang CC, Wood TA, Matthew Mahoney J, Martyanov V, Bhattacharyya S, et al. Molecular signatures in skin associated with clinical improvement during mycophenolate treatment in systemic sclerosis. J Invest Dermatol. 2013;133(8):1979-89.
167. Moon KW, Song R, Kim JH, Lee EY, Lee EB, Song YW. The correlation between durometer score and modified rodnan skin score in systemic sclerosis. Rheumatol Int. 2012;32(8):2465-70.
168. Kuwahara Y, Shima Y, Shirayama D, Kawai M, Hagihara K, Hirano T, et al. Quantification of hardness, elasticity and viscosity of the skin of patients with systemic sclerosis using a novel sensing device (vesmeter): A proposal for a new outcome measurement procedure. Rheumatology (Oxford). 2008;47(7):1018-24.
169. Enomoto DN, Mekkes JR, Bossuyt PM, Hoekzema R, Bos JD. Quantification of cutaneous sclerosis with a skin elasticity meter in patients with generalized scleroderma. J Am Acad Dermatol. 1996;35(3 Pt 1):381-7.
170. Babalola O, Mamalis A, Lev-Tov H, Jagdeo J. Optical coherence tomography (oct) of collagen in normal skin and skin fibrosis. Arch Dermatol Res. 2014;306(1):1-9.

171. Sedky MM, Fawzy SM, El Baki NA, El Eishi NH, El Bohy Ael M. Systemic sclerosis: An ultrasonographic study of skin and subcutaneous tissue in relation to clinical findings. Skin Res Technol. 2013;19(1):e78-84.
172. Akesson A, Hesselstrand R, Scheja A, Wildt M. Longitudinal development of skin involvement and reliability of high frequency ultrasound in systemic sclerosis. Ann Rheum Dis. 2004;63(7):791-6.
173. Scheja A, Akesson A. Comparison of high frequency (20 mhz) ultrasound and palpation for the assessment of skin involvement in systemic sclerosis (scleroderma). Clin Exp Rheumatol. 1997;15(3):283-8.
174. Di Geso L, Filippucci E, Girolimetti R, Tardella M, Gutierrez M, De Angelis R, et al. Reliability of ultrasound measurements of dermal thickness at digits in systemic sclerosis: Role of elastosonography. Clin Exp Rheumatol. 2011;29(6):926-32.
175. Iagnocco A, Kaloudi O, Perella C, Bandinelli F, Riccieri V, Vasile M, et al. Ultrasound elastography assessment of skin involvement in systemic sclerosis: Lights and shadows. J Rheumatol. 2010;37(8):1688-91.
176. Cannao PM, Vinci V, Caviggioli F, Klinger M, Orlandi D, Sardanelli F, et al. Technical feasibility of real-time elastography to assess the peri-oral region in patients affected by systemic sclerosis. J Ultrasound. 2014;17(4):265-9.
177. Alexander H, Miller DL. Determining skin thickness with pulsed ultra sound. J Invest Dermatol. 1979;72(1):17-9.
178. Fornage BD, McGavran MH, Duvic M, Waldron CA. Imaging of the skin with 20-mhz us. Radiology. 1993;189(1):69-76.
179. Mlosek RK, Malinowska S. Ultrasound image of the skin, apparatus and imaging basics. J Ultrason. 2013;13(53):212-21.
180. Nessi R, Blanc M, Bosco M, Dameno S, Venegoni A, Betti R, et al. Skin ultrasound in dermatologic surgical planning. J Dermatol Surg Oncol. 1991;17(1):38-43.
181. Jasaitiene D, Valiukeviciene S, Linkeviciute G, Raisutis R, Jasiuniene E, Kazys R. Principles of high-frequency ultrasonography for investigation of skin pathology. J Eur Acad Dermatol Venereol. 2011;25(4):375-82.
182. Schmid-Wendtner MH, Dill-Muller D. Ultrasound technology in dermatology. Semin Cutan Med Surg. 2008;27(1):44-51.
183. Tedeschini E, Pingani L, Simoni E, Ferrari D, Giubbarelli C, Giuggioli D, et al. Correlation of articular involvement, skin disfigurement and unemployment with depressive symptoms in patients with systemic sclerosis: A hospital sample. Int J Rheum Dis. 2014;17(2):186-94.
184. Sariyildiz MA, Batmaz I, Budulgan M, Bozkurt M, Yazmalar L, Inanir A, et al. Sleep quality in patients with systemic sclerosis: Relationship between the clinical variables, depressive symptoms, functional status, and the quality of life. Rheumatol Int. 2013;33(8):1973-9.
185. Sandqvist G, Hesselstrand R, Petersson IF, Kristensen LE. Work disability in early systemic sclerosis: A longitudinal population-based cohort study. J Rheumatol. 2015;42(10):1794-800.
186. Domsic RT, Nihtyanova SI, Wisniewski SR, Fine MJ, Lucas M, Kwoh CK, et al. Derivation and external validation of a prediction rule for five-year mortality in patients with early diffuse cutaneous systemic sclerosis. Arthritis Rheumatol. 2016;68(4):993-1003.
187. Hao Y, Hudson M, Baron M, Carreira P, Stevens W, Rabusa C, et al. Early mortality in a multinational systemic sclerosis inception cohort. Arthritis Rheumatol. 2017;69(5):1067-77.
188. Tyndall AJ, Bannert B, Vonk M, Airo P, Cozzi F, Carreira PE, et al. Causes and risk factors for death in systemic sclerosis: A study from the EULAR Scleroderma trials and research (EUSTAR) database. Ann Rheum Dis. 2010;69(10):1809-15.

189. Denton CP, Hughes M, Gak N, Vila J, Buch MH, Chakravarty K, et al. BSR and BHPR guideline for the treatment of systemic sclerosis. Rheumatology (Oxford). 2016;55(10):1906-10.
190. Kowal-Bielecka O, Fransen J, Avouac J, Becker M, Kulak A, Allanore Y, et al. Update of EULAR recommendations for the treatment of systemic sclerosis. Ann Rheum Dis. 2017;76(8):1327-39.
191. Nihtyanova SI, Ong VH, Denton CP. Current management strategies for systemic sclerosis. Clin Exp Rheumatol. 2014;32(2 Suppl 81):156-64.
192. Rirash F, Tingey PC, Harding SE, Maxwell LJ, Tanjong Ghogomu E, Wells GA, et al. Calcium channel blockers for primary and secondary Raynaud's phenomenon. Cochrane Database Syst Rev. 2017;12:CD000467.
193. Tingey T, Shu J, Smuczek J, Pope J. Meta-analysis of healing and prevention of digital ulcers in systemic sclerosis. Arthritis Care Res (Hoboken). 2013;65(9):1460-71.
194. Lekakis J, Mavrikakis M, Papamichael C, Papazoglou S, Economou O, Scotiniotis I, et al. Short-term estrogen administration improves abnormal endothelial function in women with systemic sclerosis and raynaud's phenomenon. Am Heart J. 1998;136(5):905-12.
195. Terregino CA, Seibold JR. Influence of the menstrual cycle on Raynaud's phenomenon and on cold tolerance in normal women. Angiology. 1985;36(2):88-95.
196. Parikh V, Bhardwaj A, Nair A. Pharmacotherapy for pulmonary arterial hypertension. J Thorac Dis. 2019;11(Suppl 14):S1767-S81.
197. Humbert M, Coghlan JG, Ghofrani HA, Grimminger F, He JG, Riemekasten G, et al. Riociguat for the treatment of pulmonary arterial hypertension associated with connective tissue disease: Results from patent-1 and patent-2. Ann Rheum Dis. 2017;76(2):422-6.
198. Huntgeburth M, Kiessling J, Weimann G, Wilberg V, Saleh S, Hunzelmann N, et al. Riociguat for the treatment of Raynaud's phenomenon: A single-dose, double-blind, randomized, placebo-controlled cross-over pilot study (digit). Clin Drug Investig. 2018;38(11):1061-9.
199. Nagaraja V, Spino C, Bush E, Tsou PS, Domsic RT, Lafyatis R, et al. A multicenter randomized, double-blind, placebo-controlled pilot study to assess the efficacy and safety of riociguat in systemic sclerosis-associated digital ulcers. Arthritis Res Ther. 2019;21(1):202.
200. Khanna D, Allanore Y, Denton CP, Kuwana M, Matucci-Cerinic M, Pope JE, et al. The effects of riociguat on Raynaud’s phenomenon and digital ulcers in patients with diffuse systemic sclerosis: Results from phase IIb RISE-SSC study. ACR/ARP Annual Meeting; Atlanta, Georgia, USA.2019. p. 1-5420.
201. Denton CP, Hachulla E, Riemekasten G, Schwarting A, Frenoux JM, Frey A, et al. Efficacy and safety of selexipag in adults with Raynaud's phenomenon secondary to systemic sclerosis: A randomized, placebo-controlled, phase II study. Arthritis Rheumatol. 2017;69(12):2370-9.
202. Tashkin DP, Elashoff R, Clements PJ, Goldin J, Roth MD, Furst DE, et al. Cyclophosphamide versus placebo in scleroderma lung disease. N Engl J Med. 2006;354(25):2655-66.
203. Becker MO, Schohe A, Weinert K, Huscher D, Schneider U, Burmester GR, et al. Responders to cyclophosphamide: Results of a single-centre analysis among systemic sclerosis patients. Ann Rheum Dis. 2012;71(12):2061-2.
204. Tehlirian CV, Hummers LK, White B, Brodsky RA, Wigley FM. High-dose cyclophosphamide without stem cell rescue in scleroderma. Ann Rheum Dis. 2008;67(6):775-81.

205. Kowal-Bielecka O, Landewe R, Avouac J, Chwiesko S, Miniati I, Czirjak L, et al. EULAR recommendations for the treatment of systemic sclerosis: A report from the EULAR Scleroderma trials and research group (EUSTAR). Ann Rheum Dis. 2009;68(5):620-8.
206. van den Hoogen FH, Boerbooms AM, Swaak AJ, Rasker JJ, van Lier HJ, van de Putte LB. Comparison of methotrexate with placebo in the treatment of systemic sclerosis: A 24 week randomized double-blind trial, followed by a 24 week observational trial. Br J Rheumatol. 1996;35(4):364-72.
207. Pope JE, Bellamy N, Seibold JR, Baron M, Ellman M, Carette S, et al. A randomized, controlled trial of methotrexate versus placebo in early diffuse scleroderma. Arthritis Rheum. 2001;44(6):1351-8.
208. Stratton RJ, Wilson H, Black CM. Pilot study of anti-thymocyte globulin plus mycophenolate mofetil in recent-onset diffuse scleroderma. Rheumatology (Oxford). 2001;40(1):84-8.
209. Derk CT, Grace E, Shenin M, Naik M, Schulz S, Xiong W. A prospective open-label study of mycophenolate mofetil for the treatment of diffuse systemic sclerosis. Rheumatology (Oxford). 2009;48(12):1595-9.
210. Nihtyanova SI, Brough GM, Black CM, Denton CP. Mycophenolate mofetil in diffuse cutaneous systemic sclerosis-a retrospective analysis. Rheumatology (Oxford). 2007;46(3):442-5.
211. Mendoza FA, Nagle SJ, Lee JB, Jimenez SA. A prospective observational study of mycophenolate mofetil treatment in progressive diffuse cutaneous systemic sclerosis of recent onset. J Rheumatol. 2012;39(6):1241-7.
212. van Laar JM, Farge D, Tyndall A. Stem cell transplantation: A treatment option for severe systemic sclerosis? Ann Rheum Dis. 2008;67 Suppl 3:iii35-8.
213. Binks M, Passweg JR, Furst D, McSweeney P, Sullivan K, Besenthal C, et al. Phase i/ii trial of autologous stem cell transplantation in systemic sclerosis: Procedure related mortality and impact on skin disease. Ann Rheum Dis. 2001;60(6):577-84.
214. McSweeney PA, Nash RA, Sullivan KM, Storek J, Crofford LJ, Dansey R, et al. High-dose immunosuppressive therapy for severe systemic sclerosis: Initial outcomes. Blood. 2002;100(5):1602-10.
215. Farge D, Passweg J, van Laar JM, Marjanovic Z, Besenthal C, Finke J, et al. Autologous stem cell transplantation in the treatment of systemic sclerosis: Report from the EBMT/EULAR registry. Ann Rheum Dis. 2004;63(8):974-81.
216. Herrick AL, Pan X, Peytrignet S, Lunt M, Hesselstrand R, Mouthon L, et al. Treatment outcome in early diffuse cutaneous systemic sclerosis: The european scleroderma observational study (esos). Ann Rheum Dis. 2017;76(7):1207-18.
217. Farge D, Nash R, Laar JM. Autologous stem cell transplantation for systemic sclerosis. Autoimmunity. 2008;41(8):616-24.
218. Spiera RF, Gordon JK, Mersten JN, Magro CM, Mehta M, Wildman HF, et al. Imatinib mesylate (gleevec) in the treatment of diffuse cutaneous systemic sclerosis: Results of a 1-year, phase IIa, single-arm, open-label clinical trial. Ann Rheum Dis. 2011;70(6):1003-9.
219. Distler O, Distler, Jorg H. W., Varga, John, Denton, Christopher P., Lafyatis, Robert A., Wigley, Fredrick M., et al. A multi-center, open-label, proof of concept study of imatinib mesylate demonstrates no benefit for the treatment of fibrosis in patients with early, diffuse systemic sclerosis. . Arthritis Rheum2010. p. 1.
220. Pope J, McBain D, Petrlich L, Watson S, Vanderhoek L, de Leon F, et al. Imatinib in active diffuse cutaneous systemic sclerosis: Results of a six-

month, randomized, double-blind, placebo-controlled, proof-of-concept pilot study at a single center. Arthritis Rheum. 2011;63(11):3547-51.
221. Prey S, Ezzedine K, Doussau A, Grandoulier AS, Barcat D, Chatelus E, et al. Imatinib mesylate in scleroderma-associated diffuse skin fibrosis: A phase ii multicentre randomized double-blinded controlled trial. Br J Dermatol. 2012;167(5):1138-44.
222. Phumethum V, Jamal S, Johnson SR. Biologic therapy for systemic sclerosis: A systematic review. J Rheumatol. 2011;38(2):289-96.
223. Denton CP, Engelhart M, Tvede N, Wilson H, Khan K, Shiwen X, et al. An open-label pilot study of infliximab therapy in diffuse cutaneous systemic sclerosis. Ann Rheum Dis. 2009;68(9):1433-9.
224. Poelman CL, Hummers LK, Wigley FM, Anderson C, Boin F, Shah AA. Intravenous immunoglobulin may be an effective therapy for refractory, active diffuse cutaneous systemic sclerosis. J Rheumatol. 2015;42(2):236-42.
225. Khanna D, Bush E, Nagaraja V, Koenig A, Khanna P, Young A, et al. Tofacitinib in early diffuse cutaneous systemic sclerosis— results of phase I/II investigator-initiated, double-blind randomized placebo-controlled trial. ACR/ARP Annual Meeting; 2019; Atlanta, Georgia, USA2019. p. 1-5420.
226. Jordan S, Distler JH, Maurer B, Huscher D, van Laar JM, Allanore Y, et al. Effects and safety of rituximab in systemic sclerosis: An analysis from the European Scleroderma trial and research (EUSTAR) group. Ann Rheum Dis. 2015;74(6):1188-94.
227. Daoussis D, Liossis SN, Tsamandas AC, Kalogeropoulou C, Kazantzi A, Sirinian C, et al. Experience with rituximab in scleroderma: Results from a 1-year, proof-of-principle study. Rheumatology (Oxford). 2010;49(2):271-80.
228. Daoussis D, Liossis SN, Tsamandas AC, Kalogeropoulou C, Paliogianni F, Sirinian C, et al. Effect of long-term treatment with rituximab on pulmonary function and skin fibrosis in patients with diffuse systemic sclerosis. Clin Exp Rheumatol. 2012;30(2 Suppl 71):S17-22.
229. Saunders P, Tsipouri V, Keir GJ, Ashby D, Flather MD, Parfrey H, et al. Rituximab versus cyclophosphamide for the treatment of connective tissue disease-associated interstitial lung disease (recital): Study protocol for a randomised controlled trial. Trials. 2017;18(1):275.
230. Khanna D, Denton CP, Jahreis A, van Laar JM, Frech TM, Anderson ME, et al. Safety and efficacy of subcutaneous tocilizumab in adults with systemic sclerosis (fasscinate): A phase 2, randomised, controlled trial. Lancet. 2016;387(10038):2630-40.
231. Shima Y, Kawaguchi Y, Kuwana M. Add-on tocilizumab versus conventional treatment for systemic sclerosis, and cytokine analysis to identify an endotype to tocilizumab therapy. Mod Rheumatol. 2019;29(1):134-9.
232. Khanna D, Lin CJF, Kuwana M, Allanore Y, Batalov A, Butrimiene I, et al., editors. Efficacy and safety of tocilizumab for the treatment of systemic sclerosis: Results from a phase 3 randomized controlled trial. American College of Rheumatology; 2019; Atlanta, Georgia.
233. Dees C, Beyer C, Distler A, Soare A, Zhang Y, Palumbo-Zerr K, et al. Stimulators of soluble guanylate cyclase (sgc) inhibit experimental skin fibrosis of different aetiologies. Ann Rheum Dis. 2015;74(8):1621-5.
234. Distler O, Allanore Y, Denton CP, Kuwana M, Matucci- Cerinic M, Pope JE, et al. Riociguat in patients with early di. ACR/ARP Annual Meeting; 2019; Atlanta, Georgia, USA.2019. p. 1-5420.
235. Distler JH, Feghali-Bostwick C, Soare A, Asano Y, Distler O, Abraham DJ. Review: Frontiers of antifibrotic therapy in systemic sclerosis. Arthritis Rheumatol. 2017;69(2):257-67.

236. Atanelishvili I, Akter T, Noguchi A, Vuyiv O, Wollin L, Silver RM, et al. Antifibrotic efficacy of nintedanib in a cellular model of systemic sclerosis-associated interstitial lung disease. Clin Exp Rheumatol. 2019;37 Suppl 119(4):115-24.
237. Distler O, Highland KB, Gahlemann M, Azuma A, Fischer A, Mayes MD, et al. Nintedanib for systemic sclerosis-associated interstitial lung disease. N Engl J Med. 2019;380(26):2518-28.
238. Huang J, Beyer C, Palumbo-Zerr K, Zhang Y, Ramming A, Distler A, et al. Nintedanib inhibits fibroblast activation and ameliorates fibrosis in preclinical models of systemic sclerosis. Ann Rheum Dis. 2016;75(5):883-90.
239. Card PB, Erbel PJ, Gardner KH. Structural basis of arnt pas-b dimerization: Use of a common beta-sheet interface for hetero- and homodimerization. J Mol Biol. 2005;353(3):664-77.
240. Deng W, Feng X, Li X, Wang D, Sun L. Hypoxia-inducible factor 1 in autoimmune diseases. Cell Immunol. 2016;303:7-15.
241. Semenza GL. Hypoxia-inducible factors in physiology and medicine. Cell. 2012;148(3):399-408.
242. Doedens A, Johnson RS. Transgenic models to understand hypoxia-inducible factor function. Methods in enzymology. Oxygen biology and hypoxia. Volume 435: Academic Press; 2007. p. 87-105.
243. Zhou G, Dada LA, Wu M, Kelly A, Trejo H, Zhou Q, et al. Hypoxia-induced alveolar epithelial-mesenchymal transition requires mitochondrial ros and hypoxia-inducible factor 1. Am J Physiol Lung Cell Mol Physiol. 2009;297(6):L1120-30.
244. Lei W, He Y, Shui X, Li G, Yan G, Zhang Y, et al. Expression and analyses of the hif-1 pathway in the lungs of humans with pulmonary arterial hypertension. Mol Med Rep. 2016;14(5):4383-90.
245. Tang H, Babicheva A, McDermott KM, Gu Y, Ayon RJ, Song S, et al. Endothelial hif-2alpha contributes to severe pulmonary hypertension due to endothelial-to-mesenchymal transition. Am J Physiol Lung Cell Mol Physiol. 2018;314(2):L256-L75.
246. Johns RA, Takimoto E, Meuchel LW, Elsaigh E, Zhang A, Heller NM, et al. Hypoxia-inducible factor 1alpha is a critical downstream mediator for hypoxia-induced mitogenic factor (fizz1/relmalpha)-induced pulmonary hypertension. Arterioscler Thromb Vasc Biol. 2016;36(1):134-44.
247. Bartoszewski R, Moszynska A, Serocki M, Cabaj A, Polten A, Ochocka R, et al. Primary endothelial cell-specific regulation of hypoxia-inducible factor (HIF)-1 and HIF-2 and their target gene expression profiles during hypoxia. FASEB J. 2019;33(7):7929-41.
248. Downes NL, Laham-Karam N, Kaikkonen MU, Yla-Herttuala S. Differential but complementary HIF1alpha and HIF2alpha transcriptional regulation. Mol Ther. 2018;26(7):1735-45.
249. Neufeld G, Cohen T, Gengrinovitch S, Poltorak Z. Vascular endothelial growth factor (VEGF) and its receptors. FASEB J. 1999;13(1):9-22.
250. Senger DR, Galli SJ, Dvorak AM, Perruzzi CA, Harvey VS, Dvorak HF. Tumor cells secrete a vascular permeability factor that promotes accumulation of ascites fluid. Science. 1983;219(4587):983-5.
251. Ferrara N, Henzel WJ. Pituitary follicular cells secrete a novel heparin-binding growth factor specific for vascular endothelial cells. 1989. Biochem Biophys Res Commun. 2012;425(3):540-7.
252. Leung DW, Cachianes G, Kuang WJ, Goeddel DV, Ferrara N. Vascular endothelial growth factor is a secreted angiogenic mitogen. Science. 1989;246(4935):1306-9.

253. Carmeliet P, Ferreira V, Breier G, Pollefeyt S, Kieckens L, Gertsenstein M, et al. Abnormal blood vessel development and lethality in embryos lacking a single vegf allele. Nature. 1996;380(6573):435-9.
254. Fong GH, Rossant J, Gertsenstein M, Breitman ML. Role of the flt-1 receptor tyrosine kinase in regulating the assembly of vascular endothelium. Nature. 1995;376(6535):66-70.
255. Hu K, Olsen BR. The roles of vascular endothelial growth factor in bone repair and regeneration. Bone. 2016;91:30-8.
256. Barratt SL, Blythe T, Jarrett C, Ourradi K, Shelley-Fraser G, Day MJ, et al. Differential expression of VEGF-Axxx isoforms is critical for development of pulmonary fibrosis. Am J Respir Crit Care Med. 2017;196(4):479-93.
257. Byrne AM, Bouchier-Hayes DJ, Harmey JH. Angiogenic and cell survival functions of vascular endothelial growth factor (VEGF). J Cell Mol Med. 2005;9(4):777-94.
258. Alvarez-Aznar A, Muhl L, Gaengel K. Vegf receptor tyrosine kinases: Key regulators of vascular function. Curr Top Dev Biol. 2017;123:433-82.
259. Hoeben A, Landuyt B, Highley MS, Wildiers H, Van Oosterom AT, De Bruijn EA. Vascular endothelial growth factor and angiogenesis. Pharmacol Rev. 2004;56(4):549-80.
260. Bates DO, Cui TG, Doughty JM, Winkler M, Sugiono M, Shields JD, et al. VEGF165b, an inhibitory splice variant of vascular endothelial growth factor, is down-regulated in renal cell carcinoma. Cancer Res. 2002;62(14):4123-31.
261. Delcombel R, Janssen L, Vassy R, Gammons M, Haddad O, Richard B, et al. New prospects in the roles of the c-terminal domains of VEGF-A and their cooperation for ligand binding, cellular signaling and vessels formation. Angiogenesis. 2013;16(2):353-71.
262. Eswarappa SM, Fox PL. Antiangiogenic vegf-ax: A new participant in tumor angiogenesis. Cancer Res. 2015;75(14):2765-9.
263. Manetti M, Guiducci S, Matucci-Cerinic M. The crowded crossroad to angiogenesis in systemic sclerosis: Where is the key to the problem? Arthritis Res Ther. 2016;18:36.
264. Ballmer-Hofer K, Andersson AE, Ratcliffe LE, Berger P. Neuropilin-1 promotes VEGFR-2 trafficking through rab11 vesicles thereby specifying signal output. Blood. 2011;118(3):816-26.
265. Bills VL, Varet J, Millar A, Harper SJ, Soothill PW, Bates DO. Failure to up-regulate VEGF165b in maternal plasma is a first trimester predictive marker for pre-eclampsia. Clin Sci (Lond). 2009;116(3):265-72.
266. Kikuchi R, Nakamura K, MacLauchlan S, Ngo DT, Shimizu I, Fuster JJ, et al. An antiangiogenic isoform of vegf-a contributes to impaired vascularization in peripheral artery disease. Nat Med. 2014;20(12):1464-71.
267. Bunni J, Shelley-Fraser G, Stevenson K, Oltean S, Salmon A, Harper SJ, et al. Circulating levels of anti-angiogenic VEGF-A isoform (VEGF-Axxxb) in colorectal cancer patients predicts tumour VEGF-A ratios. Am J Cancer Res. 2015;5(6):2083-9.
268. Ramakrishnan S, Anand V, Roy S. Vascular endothelial growth factor signaling in hypoxia and inflammation. J Neuroimmune Pharmacol. 2014;9(2):142-60.
269. Heinolainen K, Karaman S, D'Amico G, Tammela T, Sormunen R, Eklund L, et al. VEGFR3 modulates vascular permeability by controlling vegf/vegfr2 signaling. Circ Res. 2017;120(9):1414-25.
270. Distler O, Del Rosso A, Giacomelli R, Cipriani P, Conforti ML, Guiducci S, et al. Angiogenic and angiostatic factors in systemic sclerosis: Increased levels of vascular endothelial growth factor are a feature of the

earliest disease stages and are associated with the absence of fingertip ulcers. Arthritis Res. 2002;4(6):R11.
271. Avouac J, Wipff J, Goldman O, Ruiz B, Couraud PO, Chiocchia G, et al. Angiogenesis in systemic sclerosis: Impaired expression of vascular endothelial growth factor receptor 1 in endothelial progenitor-derived cells under hypoxic conditions. Arthritis Rheum. 2008;58(11):3550-61.
272. Silva I, Teixeira A, Oliveira J, Almeida I, Almeida R, Aguas A, et al. Endothelial dysfunction and nailfold videocapillaroscopy pattern as predictors of digital ulcers in systemic sclerosis: A cohort study and review of the literature. Clin Rev Allergy Immunol. 2015;49(2):240-52.
273. McMahan Z, Schoenhoff F, Van Eyk JE, Wigley FM, Hummers LK. Biomarkers of pulmonary hypertension in patients with scleroderma: A case-control study. Arthritis Res Ther. 2015;17:201.
274. Glodkowska-Mrowka E, Gorska E, Ciurzynski M, Stelmaszczyk-Emmel A, Bienias P, Irzyk K, et al. Pro- and antiangiogenic markers in patients with pulmonary complications of systemic scleroderma. Respir Physiol Neurobiol. 2015;209:69-75.
275. Gigante A, Navarini L, Margiotta D, Amoroso A, Barbano B, Cianci R, et al. Angiogenic and angiostatic factors in renal scleroderma-associated vasculopathy. Microvasc Res. 2017;114:41-5.
276. Rentka A, Harsfalvi J, Berta A, Koroskenyi K, Szekanecz Z, Szucs G, et al. Vascular endothelial growth factor in tear samples of patients with systemic sclerosis. Mediators Inflamm. 2015;2015:573681.
277. Choi JJ, Min DJ, Cho ML, Min SY, Kim SJ, Lee SS, et al. Elevated vascular endothelial growth factor in systemic sclerosis. J Rheumatol. 2003;30(7):1529-33.
278. Avouac J, Vallucci M, Smith V, Senet P, Ruiz B, Sulli A, et al. Correlations between angiogenic factors and capillaroscopic patterns in systemic sclerosis. Arthritis Res Ther. 2013;15(2):R55.
279. Kaner RJ, Crystal RG. Compartmentalization of vascular endothelial growth factor to the epithelial surface of the human lung. Mol Med. 2001;7(4):240-6.
280. Manetti M, Guiducci S, Romano E, Bellando-Randone S, Lepri G, Bruni C, et al. Increased plasma levels of the VEGF165b splice variant are associated with the severity of nailfold capillary loss in systemic sclerosis. Ann Rheum Dis. 2013;72(8):1425-7.
281. Jinnin M, Makino T, Kajihara I, Honda N, Makino K, Ogata A, et al. Serum levels of soluble vascular endothelial growth factor receptor-2 in patients with systemic sclerosis. Br J Dermatol. 2010;162(4):751-8.
282. Romano E, Chora I, Manetti M, Mazzotta C, Rosa I, Bellando-Randone S, et al. Decreased expression of neuropilin-1 as a novel key factor contributing to peripheral microvasculopathy and defective angiogenesis in systemic sclerosis. Ann Rheum Dis. 2016;75(8):1541-9.
283. Higashi-Kuwata N, Makino T, Inoue Y, Ihn H. Expression pattern of VEGFR-1, -2, -3 and d2-40 protein in the skin of patients with systemic sclerosis. Eur J Dermatol. 2011;21(4):490-4.
284. Maurer B, Distler A, Suliman YA, Gay RE, Michel BA, Gay S, et al. Vascular endothelial growth factor aggravates fibrosis and vasculopathy in experimental models of systemic sclerosis. Ann Rheum Dis. 2014;73(10):1880-7.
285. Dor Y, Djonov V, Abramovitch R, Itin A, Fishman GI, Carmeliet P, et al. Conditional switching of vegf provides new insights into adult neovascularization and pro-angiogenic therapy. EMBO J. 2002;21(8):1939-47.

286. Manetti M, Milia AF, Guiducci S, Romano E, Matucci-Cerinic M, Ibba-Manneschi L. Progressive loss of lymphatic vessels in skin of patients with systemic sclerosis. J Rheumatol. 2011;38(2):297-301.
287. Honda N, Jinnin M, Kajihara I, Makino T, Fukushima S, Ihn H. Impaired lymphangiogenesis due to excess vascular endothelial growth factor-d/flt-4 signalling in the skin of patients with systemic sclerosis. Br J Dermatol. 2010;163(4):776-80.
288. Chitale S, Al-Mowallad AF, Wang Q, Kumar S, Herrick A. High circulating levels of VEGF-C suggest abnormal lymphangiogenesis in systemic sclerosis. Rheumatology (Oxford). 2008;47(11):1727-8.
289. Kylhammar D, Hesselstrand R, Nielsen S, Scheele C, Radegran G. Angiogenic and inflammatory biomarkers for screening and follow-up in patients with pulmonary arterial hypertension. Scand J Rheumatol. 2018;47(4):319-24.
290. Porkholm M, Bono P, Saarinen-Pihkala UM, Kivivuori SM. Higher angiopoietin-2 and VEGF levels predict shorter EFs and increased non-relapse mortality after pediatric hematopoietic sct. Bone Marrow Transplant. 2013;48(1):50-5.
291. Min CK, Kim SY, Lee MJ, Eom KS, Kim YJ, Kim HJ, et al. Vascular endothelial growth factor (VEGF) is associated with reduced severity of acute graft-versus-host disease and nonrelapse mortality after allogeneic stem cell transplantation. Bone Marrow Transplant. 2006;38(2):149-56.
292. Kim DH, Lee NY, Lee MH, Sohn SK. Vascular endothelial growth factor gene polymorphisms may predict the risk of acute graft-versus-host disease following allogeneic transplantation: Preventive effect of vascular endothelial growth factor gene on acute graft-versus-host disease. Biol Blood Marrow Transplant. 2008;14(12):1408-16.
293. Holtan SG, Verneris MR, Schultz KR, Newell LF, Meyers G, He F, et al. Circulating angiogenic factors associated with response and survival in patients with acute graft-versus-host disease: Results from blood and marrow transplant clinical trials network 0302 and 0802. Biol Blood Marrow Transplant. 2015;21(6):1029-36.
294. Yao Y, Wang L, Zhou J, Zhang X. HIF-1alpha inhibitor echinomycin reduces acute graft-versus-host disease and preserves graft-versus-leukemia effect. J Transl Med. 2017;15(1):28.
295. Wang J, Lu Z, Xu Z, Tian P, Miao H, Pan S, et al. Reduction of hepatic fibrosis by overexpression of von hippel-lindau protein in experimental models of chronic liver disease. Sci Rep. 2017;7:41038.
296. Tzouvelekis A, Harokopos V, Paparountas T, Oikonomou N, Chatziioannou A, Vilaras G, et al. Comparative expression profiling in pulmonary fibrosis suggests a role of hypoxia-inducible factor-1alpha in disease pathogenesis. Am J Respir Crit Care Med. 2007;176(11):1108-19.
297. Zhao ZM, Liu HL, Sun X, Guo T, Shen L, Tao YY, et al. Levistilide a inhibits angiogenesis in liver fibrosis via vascular endothelial growth factor signaling pathway. Exp Biol Med (Maywood). 2017;242(9):974-85.
298. Maurer B, Distler A, Suliman YA, Gay RE, Michel BA, Gay S, et al. Vascular endothelial growth factor aggravates fibrosis and vasculopathy in experimental models of systemic sclerosis. Ann Rheum Dis. 2013.
299. Riccieri V, Stefanantoni K, Vasile M, Macri V, Sciarra I, Iannace N, et al. Abnormal plasma levels of different angiogenic molecules are associated with different clinical manifestations in patients with systemic sclerosis. Clin Exp Rheumatol. 2011;29(2 Suppl 65):S46-52.
300. Ioannou M, Pyrpasopoulou A, Simos G, Paraskeva E, Nikolaidou C, Venizelos I, et al. Upregulation of VEGF expression is associated with accumulation of HIF-1alpha in the skin of naive scleroderma patients. Mod Rheumatol. 2013;23(6):1245-8.

301. Distler JH, Jungel A, Pileckyte M, Zwerina J, Michel BA, Gay RE, et al. Hypoxia-induced increase in the production of extracellular matrix proteins in systemic sclerosis. Arthritis Rheum. 2007;56(12):4203-15.
302. Manetti M, Guiducci S, Romano E, Ceccarelli C, Bellando-Randone S, Conforti ML, et al. Overexpression of VEGF165b, an inhibitory splice variant of vascular endothelial growth factor, leads to insufficient angiogenesis in patients with systemic sclerosis. Circ Res. 2011;109(3):e14-26.
303. Lauer BM, Baechler, E.C., Molitor, J.A., editor The anti-angiogenic VEGF-165b isoform is elevated in both anti-centromere and anti-topoisomerase positive systemic sclerosis patients. 13th International Workshop on Scleroderma Research; 2013 3rd August 2013; Boston University, Boston, Massachusetts.
304. Cossu M, Andracco R, Santaniello A, Marchini M, Severino A, Caronni M, et al. Serum levels of vascular dysfunction markers reflect disease severity and stage in systemic sclerosis patients. Rheumatology (Oxford). 2016;55(6):1112-6.
305. Bielecki M, Kowal K, Lapinska A, Chwiesko-Minarowska S, Chyczewski L, Kowal-Bielecka O. Peripheral blood mononuclear cells from patients with systemic sclerosis spontaneously secrete increased amounts of vascular endothelial growth factor (VEGF) already in the early stage of the disease. Adv Med Sci. 2011;56(2):255-63.
306. Corallo C, Cutolo M, Kahaleh B, Pecetti G, Montella A, Chirico C, et al. Bosentan and macitentan prevent the endothelial-to-mesenchymal transition (endomt) in systemic sclerosis: In vitro study. Arthritis Res Ther. 2016;18(1):228.
307. Solanilla A, Villeneuve J, Auguste P, Hugues M, Alioum A, Lepreux S, et al. The transport of high amounts of vascular endothelial growth factor by blood platelets underlines their potential contribution in systemic sclerosis angiogenesis. Rheumatology (Oxford). 2009;48(9):1036-44.
308. Hirigoyen D, Burgos PI, Mezzano V, Duran J, Barrientos M, Saez CG, et al. Inhibition of angiogenesis by platelets in systemic sclerosis patients. Arthritis Res Ther. 2015;17:332.
309. Sanchez-Elsner T, Botella LM, Velasco B, Corbi A, Attisano L, Bernabeu C. Synergistic cooperation between hypoxia and transforming growth factor-beta pathways on human vascular endothelial growth factor gene expression. J Biol Chem. 2001;276(42):38527-35.
310. Faller DV. Endothelial cell responses to hypoxic stress. Clin Exp Pharmacol Physiol. 1999;26(1):74-84.
311. Wu WK, Llewellyn OP, Bates DO, Nicholson LB, Dick AD. Il-10 regulation of macrophage VEGF production is dependent on macrophage polarisation and hypoxia. Immunobiology. 2010;215(9-10):796-803.
312. Cipriani P, Di Benedetto P, Capece D, Zazzeroni F, Liakouli V, Ruscitti P, et al. Impaired cav-1 expression in ssc mesenchymal cells upregulates vegf signaling: A link between vascular involvement and fibrosis. Fibrogenesis Tissue Repair. 2014;7:13.
313. Del Galdo F, Sotgia F, de Almeida CJ, Jasmin JF, Musick M, Lisanti MP, et al. Decreased expression of caveolin 1 in patients with systemic sclerosis: Crucial role in the pathogenesis of tissue fibrosis. Arthritis Rheum. 2008;58(9):2854-65.
314. Kajihara I, Jinnin M, Honda N, Makino K, Makino T, Masuguchi S, et al. Scleroderma dermal fibroblasts overexpress vascular endothelial growth factor due to autocrine transforming growth factor beta signaling. Mod Rheumatol. 2013;23(3):516-24.

315. Saito M, Hamasaki M, Shibuya M. Induction of tube formation by angiopoietin-1 in endothelial cell/fibroblast co-culture is dependent on endogenous vegf. Cancer Sci. 2003;94(9):782-90.
316. Moritz F, Schniering J, Distler JHW, Gay RE, Gay S, Distler O, et al. Tie2 as a novel key factor of microangiopathy in systemic sclerosis. Arthritis Res Ther. 2017;19(1):105.
317. Michalska-Jakubus M, Kowal-Bielecka O, Chodorowska G, Bielecki M, Krasowska D. Angiopoietins-1 and -2 are differentially expressed in the sera of patients with systemic sclerosis: High angiopoietin-2 levels are associated with greater severity and higher activity of the disease. Rheumatology (Oxford). 2011;50(4):746-55.
318. Noda S, Asano Y, Aozasa N, Akamata K, Yamada D, Masui Y, et al. Serum tie2 levels: Clinical association with microangiopathies in patients with systemic sclerosis. J Eur Acad Dermatol Venereol. 2011;25(12):1476-9.
319. Dunne JV, Keen KJ, Van Eeden SF. Circulating angiopoietin and tie-2 levels in systemic sclerosis. Rheumatol Int. 2013;33(2):475-84.
320. Tsou PS, Rabquer BJ, Ohara RA, Stinson WA, Campbell PL, Amin MA, et al. Scleroderma dermal microvascular endothelial cells exhibit defective response to pro-angiogenic chemokines. Rheumatology (Oxford). 2016;55(4):745-54.
321. Tsou PS, Amin MA, Campbell PL, Zakhem G, Balogh B, Edhayan G, et al. Activation of the thromboxane a2 receptor by 8-isoprostane inhibits the pro-angiogenic effect of vascular endothelial growth factor in scleroderma. J Invest Dermatol. 2015;135(12):3153-62.
322. Denton CP, Abraham DJ. Transforming growth factor-beta and connective tissue growth factor: Key cytokines in scleroderma pathogenesis. Curr Opin Rheumatol. 2001;13(6):505-11.
323. Dumoitier N, Chaigne B, Regent A, Lofek S, Mhibik M, Dorfmuller P, et al. Scleroderma peripheral b lymphocytes secrete interleukin-6 and transforming growth factor beta and activate fibroblasts. Arthritis Rheumatol. 2017;69(5):1078-89.
324. Yamane K, Ihn H, Kubo M, Tamaki K. Increased transcriptional activities of transforming growth factor beta receptors in scleroderma fibroblasts. Arthritis Rheum. 2002;46(9):2421-8.
325. McMahon S, Charbonneau M, Grandmont S, Richard DE, Dubois CM. Transforming growth factor beta1 induces hypoxia-inducible factor-1 stabilization through selective inhibition of PHD2 expression. J Biol Chem. 2006;281(34):24171-81.
326. Nowak DG, Woolard J, Amin EM, Konopatskaya O, Saleem MA, Churchill AJ, et al. Expression of pro- and anti-angiogenic isoforms of vegf is differentially regulated by splicing and growth factors. J Cell Sci. 2008;121(Pt 20):3487-95.
327. Wang D, Huang HJ, Kazlauskas A, Cavenee WK. Induction of vascular endothelial growth factor expression in endothelial cells by platelet-derived growth factor through the activation of phosphatidylinositol 3-kinase. Cancer Res. 1999;59(7):1464-72.
328. Trojanowska M. Role of pdgf in fibrotic diseases and systemic sclerosis. Rheumatology (Oxford). 2008;47 Suppl 5:v2-4.
329. Hong KH, Yoo SA, Kang SS, Choi JJ, Kim WU, Cho CS. Hypoxia induces expression of connective tissue growth factor in scleroderma skin fibroblasts. Clin Exp Immunol. 2006;146(2):362-70.
330. Sato S, Nagaoka T, Hasegawa M, Tamatani T, Nakanishi T, Takigawa M, et al. Serum levels of connective tissue growth factor are elevated in patients with systemic sclerosis: Association with extent of skin sclerosis and severity of pulmonary fibrosis. J Rheumatol. 2000;27(1):149-54.

331. Jasmin J-Fo. Caveolins and caveolae roles in signaling and disease mechanisms. Frank PG, Lisanti MP, editors. New York, NY: New York, NY : Springer US; 2012.
332. Di Guglielmo GM, Le Roy C, Goodfellow AF, Wrana JL. Distinct endocytic pathways regulate tgf-beta receptor signalling and turnover. Nat Cell Biol. 2003;5(5):410-21.
333. Castello-Cros R, Whitaker-Menezes D, Molchansky A, Purkins G, Soslowsky LJ, Beason DP, et al. Scleroderma-like properties of skin from caveolin-1-deficient mice: Implications for new treatment strategies in patients with fibrosis and systemic sclerosis. Cell Cycle. 2011;10(13):2140-50.
334. Xu Q, Briggs J, Park S, Niu G, Kortylewski M, Zhang S, et al. Targeting STAT3 blocks both HIF-1 and VEGF expression induced by multiple oncogenic growth signaling pathways. Oncogene. 2005;24(36):5552-60.
335. Zhang YJ, Zhang Q, Yang GJ, Tao JH, Wu GC, Huang XL, et al. Elevated serum levels of interleukin-1beta and interleukin-33 in patients with systemic sclerosis in chinese population. Z Rheumatol. 2018;77(2):151-9.
336. Antonelli A, Fallahi P, Ferrari SM, Giuggioli D, Colaci M, Di Domenicantonio A, et al. Systemic sclerosis fibroblasts show specific alterations of interferon-gamma and tumor necrosis factor-alpha-induced modulation of interleukin 6 and chemokine ligand 2. J Rheumatol. 2012;39(5):979-85.
337. Peng YJ, Yuan G, Ramakrishnan D, Sharma SD, Bosch-Marce M, Kumar GK, et al. Heterozygous HIF-1alpha deficiency impairs carotid body-mediated systemic responses and reactive oxygen species generation in mice exposed to intermittent hypoxia. J Physiol. 2006;577(Pt 2):705-16.
338. Peng YJ, Yuan G, Khan S, Nanduri J, Makarenko VV, Reddy VD, et al. Regulation of hypoxia-inducible factor-alpha isoforms and redox state by carotid body neural activity in rats. J Physiol. 2014;592(17):3841-58.
339. Li Y, Shi B, Huang L, Wang X, Yu X, Guo B, et al. Suppression of the expression of hypoxia-inducible factor-1alpha by RNA interference alleviates hypoxia-induced pulmonary hypertension in adult rats. Int J Mol Med. 2016;38(6):1786-94.
340. Brusselmans K, Compernolle V, Tjwa M, Wiesener MS, Maxwell PH, Collen D, et al. Heterozygous deficiency of hypoxia-inducible factor-2alpha protects mice against pulmonary hypertension and right ventricular dysfunction during prolonged hypoxia. J Clin Invest. 2003;111(10):1519-27.
341. Wipff J, Dieude P, Avouac J, Tiev K, Hachulla E, Granel B, et al. Association of hypoxia-inducible factor 1a (HIF1a) gene polymorphisms with systemic sclerosis in a French European caucasian population. Scand J Rheumatol. 2009;38(4):291-4.
342. Andrigueti FV, Ebbing PCC, Arismendi MI, Kayser C. Evaluation of the effect of sildenafil on the microvascular blood flow in patients with systemic sclerosis: A randomised, double-blind, placebo-controlled study. Clin Exp Rheumatol. 2017;35 Suppl 106(4):151-8.
343. Guiducci S, Bellando Randone S, Bruni C, Carnesecchi G, Maresta A, Iannone F, et al. Bosentan fosters microvascular de-remodelling in systemic sclerosis. Clin Rheumatol. 2012;31(12):1723-5.
344. Corrado A, Neve A, Costantino E, Palladino GP, Foschino Barbaro MP, Cantatore FP. Effect of endothelin inhibition on lung fibroblasts on patients with systemic sclerosis. Minerva Med. 2013;104(5):505-17.
345. Richeldi L, Cottin V, du Bois RM, Selman M, Kimura T, Bailes Z, et al. Nintedanib in patients with idiopathic pulmonary fibrosis: Combined evidence from the tomorrow and inpulsis((r)) trials. Respir Med. 2016;113:74-9.

346. van den Hoogen F, Khanna D, Fransen J, Johnson SR, Baron M, Tyndall A, et al. 2013 classification criteria for systemic sclerosis: An American college of rheumatology/Wuropean league against rheumatism collaborative initiative. Arthritis Rheum. 2013;65(11):2737-47.
347. Hughes M, Herrick AL. Digital ulcers in systemic sclerosis. Rheumatology (Oxford). 2017;56(1):14-25.
348. LeRoy EC, Black C, Fleischmajer R, Jablonska S, Krieg T, Medsger TA, Jr., et al. Scleroderma (systemic sclerosis): Classification, subsets and pathogenesis. J Rheumatol. 1988;15(2):202-5.
349. Poole JL, Steen VD. The use of the health assessment questionnaire (haq) to determine physical disability in systemic sclerosis. Arthritis Care Res. 1991;4(1):27-31.
350. Pauling JD, Shipley JA, Raper S, Watson ML, Ward SG, Harris ND, et al. Comparison of infrared thermography and laser speckle contrast imaging for the dynamic assessment of digital microvascular function. Microvasc Res. 2012;83(2):162-7.
351. Pauling JD, Shipley JA, Hart DJ, McGrogan A, McHugh NJ. Use of laser speckle contrast imaging to assess digital microvascular function in primary raynaud phenomenon and systemic sclerosis: A comparison using the Raynaud condition score diary. J Rheumatol. 2015;42(7):1163-8.
352. Briers D, Duncan DD, Hirst E, Kirkpatrick SJ, Larsson M, Steenbergen W, et al. Laser speckle contrast imaging: Theoretical and practical limitations. J Biomed Opt. 2013;18(6):066018.
353. Tew GA, Klonizakis M, Crank H, Briers JD, Hodges GJ. Comparison of laser speckle contrast imaging with laser doppler for assessing microvascular function. Microvasc Res. 2011;82(3):326-32.
354. Cutolo M, Vanhaecke A, Ruaro B, Deschepper E, Ickinger C, Melsens K, et al. Is laser speckle contrast analysis (LASCA) the new kid on the block in systemic sclerosis? A systematic literature review and pilot study to evaluate reliability of lasca to measure peripheral blood perfusion in scleroderma patients. Autoimmun Rev. 2018;17(8):775-80.
355. Lambrecht V, Cutolo M, De Keyser F, Decuman S, Ruaro B, Sulli A, et al. Reliability of the quantitative assessment of peripheral blood perfusion by laser speckle contrast analysis in a systemic sclerosis cohort. Ann Rheum Dis. 2016;75(6):1263-4.
356. Anderson ME, Moore TL, Lunt M, Herrick AL. The 'distal-dorsal difference': A thermographic parameter by which to differentiate between primary and secondary Raynaud's phenomenon. Rheumatology (Oxford). 2007;46(3):533-8.
357. Berks M, Tresadern P, Dinsdale G, Murray A, Moore T, Herrick A, et al. An automated system for detecting and measuring nailfold capillaries. Med Image Comput Comput Assist Interv. 2014;17(Pt 1):658-65.
358. Sousa-Neves J, Cerqueira M, Santos-Faria D, Afonso C, Teixeira F. Ultrasound assessment of skin thickness performed on fingers: A tool for estimating overall severity of skin disease in systemic sclerosis patients? Acta Reumatol Port. 2017;42(4):339-40.
359. Ihn H, Shimozuma M, Fujimoto M, Sato S, Kikuchi K, Igarashi A, et al. Ultrasound measurement of skin thickness in systemic sclerosis. Br J Rheumatol. 1995;34(6):535-8.
360. Cosgrove D, Piscaglia F, Bamber J, Bojunga J, Correas JM, Gilja OH, et al. EFSUMB guidelines and recommendations on the clinical use of ultrasound elastography. Part 2: Clinical applications. Ultraschall Med. 2013;34(3):238-53.
361. Bamber J, Cosgrove D, Dietrich CF, Fromageau J, Bojunga J, Calliada F, et al. EFSUMB guidelines and recommendations on the clinical

use of ultrasound elastography. Part 1: Basic principles and technology. Ultraschall Med. 2013;34(2):169-84.
362. Italiano JE, Jr., Richardson JL, Patel-Hett S, Battinelli E, Zaslavsky A, Short S, et al. Angiogenesis is regulated by a novel mechanism: Pro- and antiangiogenic proteins are organized into separate platelet alpha granules and differentially released. Blood. 2008;111(3):1227-33.
363. Denton C, Garcia P, Shiwen X. Eustar guidelines for preparation and storage of biologic samples in systemic sclerosis: Explant cultures of dermal fibroblasts [Available from: http://www.eustar.org/index.php?module=ContentExpress&func=display&ceid=75&bid=19&btitle=eustar&meid=59.
364. Poormoghim H, Moghadam AS, Moradi-Lakeh M, Jafarzadeh M, Asadifar B, Ghelman M, et al. Systemic sclerosis: Demographic, clinical and serological features in 100 iranian patients. Rheumatol Int. 2013;33(8):1943-50.
365. Hachulla E, Launay D. Diagnosis and classification of systemic sclerosis. Clin Rev Allergy Immunol. 2011;40(2):78-83.
366. Ruaro B, Sulli A, Pizzorni C, Paolino S, Smith V, Alessandri E, et al. Correlations between blood perfusion and dermal thickness in different skin areas of systemic sclerosis patients. Microvasc Res. 2018;115:28-33.
367. Clark S, Hollis S, Campbell F, Moore T, Jayson M, Herrick A. The "distal-dorsal difference" as a possible predictor of secondary raynaud's phenomenon. J Rheumatol. 1999;26(5):1125-8.
368. Walker UA, Jaeger VK, Bruppacher KM, Dobrota R, Arlettaz L, Banyai M, et al. Prospective evaluation of the capillaroscopic skin ulcer risk index in systemic sclerosis patients in clinical practice: A longitudinal, multicentre study. Arthritis Res Ther. 2018;20(1):239.
369. Ennis H, Moore T, Murray A, Vail A, Herrick AL. Further confirmation that digital ulcers are associated with the severity of abnormality on nailfold capillaroscopy in patients with systemic sclerosis. Rheumatology (Oxford). 2014;53(2):376-7.
370. Lovy M, MacCarter D, Steigerwald JC. Relationship between nailfold capillary abnormalities and organ involvement in systemic sclerosis. Arthritis Rheum. 1985;28(5):496-501.
371. Cutolo M, Zampogna G, Vremis L, Smith V, Pizzorni C, Sulli A. Longterm effects of endothelin receptor antagonism on microvascular damage evaluated by nailfold capillaroscopic analysis in systemic sclerosis. J Rheumatol. 2013;40(1):40-5.
372. Cestelli V, Manfredi A, Sebastiani M, Praino E, Cannarile F, Giuggioli D, et al. Effect of treatment with iloprost with or without bosentan on nailfold videocapillaroscopic alterations in patients with systemic sclerosis. Mod Rheumatol. 2017;27(1):110-4.
373. Rosato E, Molinaro I, Borghese F, Rossi C, Pisarri S, Salsano F. Bosentan improves skin perfusion of hands in patients with systemic sclerosis with pulmonary arterial hypertension. J Rheumatol. 2010;37(12):2531-9.
374. Motegi SI, Sekiguchi A, Saito S, Ishibuchi H, Kishi C, Yasuda M, et al. Successful treatment of Raynaud's phenomenon and digital ulcers in systemic sclerosis patients with botulinum toxin b injection: Assessment of peripheral vascular disorder by angiography and dermoscopic image of nail fold capillary. J Dermatol. 2018;45(3):349-52.
375. Gigante A, Navarini L, Margiotta D, Barbano B, Afeltra A, Rosato E. In systemic sclerosis, microvascular and hands digital arteries damage correlates with serum levels of endostatin. Microcirculation. 2018;25(4):e12449.

376. Pauling JD, Saketkoo LA, Domsic RT. Patient perceptions of the raynaud's condition score diary provide insight into its performance in clinical trials of Raynaud's phenomenon: Comment on the article by denton et al. Arthritis Rheumatol. 2018;70(6):973-4.
377. Karbalaie A, Emrani Z, Fatemi A, Etehadtavakol M, Erlandsson BE. Practical issues in assessing nailfold capillaroscopic images: A summary. Clin Rheumatol. 2019;38(9):2343-54.
378. Schmidt WA, Krause A, Schicke B, Wernicke D. Color doppler ultrasonography of hand and finger arteries to differentiate primary from secondary forms of Raynaud's phenomenon. J Rheumatol. 2008;35(8):1591-8.
379. Bregenzer N, Distler O, Meyringer R, Scholmerich J, Muller-Ladner U, Lock G. Doppler ultrasound identifies increased resistive indices in ssc. Ann Rheum Dis. 2004;63(1):109-10.
380. Blagojevic J, Piemonte G, Benelli L, Braschi F, Fiori G, Bartoli F, et al. Assessment, definition, and classification of lower limb ulcers in systemic sclerosis: A challenge for the rheumatologist. J Rheumatol. 2016;43(3):592-8.
381. Messineo D. Correlation doppler ultrasound index vascular on kidneys, penis, and digital arteries in patient with systemic sclerosis: What obstacles? Clin Ter. 2018;169(6):e272-e3.
382. Artul S, Nseir W, Armaly Z, Soudack M. Superb microvascular imaging: Added value and novel applications. J Clin Imaging Sci. 2017;7:45.
383. Hesselstrand R, Westergren-Thorsson G, Scheja A, Wildt M, Akesson A. The association between changes in skin echogenicity and the fibroblast production of biglycan and versican in systemic sclerosis. Clin Exp Rheumatol. 2002;20(3):301-8.
384. Franks JM, Martyanov V, Cai G, Wang Y, Li Z, Wood TA, et al. A machine learning classifier for assigning individual patients with systemic sclerosis to intrinsic molecular subsets. Arthritis Rheumatol. 2019;71(10):1701-10.
385. Ruaro B, Sulli A, Paolino S, Pizzorni C, Ghio M, Alessandri E, et al. Op0037 evaluation of skin involvement in systemic sclerosis patients by using two ultrasound transducers with different frequency. Annals of the Rheumatic Diseases. 2017;76(Suppl 2):66-7.
386. Nedelec B, Forget NJ, Hurtubise T, Cimino S, de Muszka F, Legault A, et al. Skin characteristics: Normative data for elasticity, erythema, melanin, and thickness at 16 different anatomical locations. Skin Res Technol. 2016;22(3):263-75.
387. Grembiale RD, Bruno C, Tripolino C, Ursini F, Calabria M, Naty S, et al. Correlation between elastosonography and nailfold microvascular alterations in systemic sclerosis patients. Clin Hemorheol Microcirc. 2016;62(1):71-8.
388. Milano A, Pendergrass SA, Sargent JL, George LK, McCalmont TH, Connolly MK, et al. Molecular subsets in the gene expression signatures of scleroderma skin. PLoS One. 2008;3(7):e2696.
389. Soulaidopoulos S, Triantafyllidou E, Garyfallos A, Kitas GD, Dimitroulas T. The role of nailfold capillaroscopy in the assessment of internal organ involvement in systemic sclerosis: A critical review. Autoimmun Rev. 2017.
390. Ruaro B, Pizzorni C, Paolino S, Smith V, Ghio M, Casabella A, et al. Correlations between nailfold microvascular damage and skin involvement in systemic sclerosis patients. Microvasc Res. 2019;125:103874.
391. Ruaro B, Sulli A, Pizzorni C, Ghio M, Smith V, Tomatis V, et al. Ab0738 improvement of dermal thickness in systemic sclerosis patients

treated with endothelin receptor antagonist: Long term study by high frequency ultrasound. Ann Rheum Dis. 2018;77(Suppl 2):1507-8.
392. Allaart CF, Breedveld FC, Dijkmans BA. Treatment of recent-onset rheumatoid arthritis: Lessons from the best study. J Rheumatol Suppl. 2007;80:25-33.
393. Hui M, Carr A, Cameron S, Davenport G, Doherty M, Forrester H, et al. The british society for rheumatology guideline for the management of gout. Rheumatology (Oxford). 2017;56(7):1246.
394. Coghlan JG, Denton CP, Grunig E, Bonderman D, Distler O, Khanna D, et al. Evidence-based detection of pulmonary arterial hypertension in systemic sclerosis: The detect study. Ann Rheum Dis. 2014;73(7):1340-9.
395. Hao Y, Thakkar V, Stevens W, Morrisroe K, Prior D, Rabusa C, et al. A comparison of the predictive accuracy of three screening models for pulmonary arterial hypertension in systemic sclerosis. Arthritis Res Ther. 2015;17:7.
396. Mittag M, Beckheinrich P, Haustein UF. Systemic sclerosis-related raynaud's phenomenon: Effects of iloprost infusion therapy on serum cytokine, growth factor and soluble adhesion molecule levels. Acta Derm Venereol. 2001;81(4):294-7.
397. Gerlicz Z, Dziankowska-Bartkowiak B, Dziankowska-Zaborszczyk E, Sysa-Jedrzejowska A. Disturbed balance between serum levels of receptor tyrosine kinases tie-1, tie-2 and angiopoietins in systemic sclerosis. Dermatology. 2014;228(3):233-9.
398. Michalska-Jakubus M, Cutolo M, Smith V, Krasowska D. Imbalanced serum levels of ang1, ang2 and vegf in systemic sclerosis: Integrated effects on microvascular reactivity. Microvasc Res. 2019;125:103881.
399. Kuryliszyn-Moskal A, Klimiuk PA, Sierakowski S. Soluble adhesion molecules (svcam-1, se-selectin), vascular endothelial growth factor (vegf) and endothelin-1 in patients with systemic sclerosis: Relationship to organ systemic involvement. Clin Rheumatol. 2005;24(2):111-6.
400. Kawashiri SY, Nishino A, Igawa T, Takatani A, Shimizu T, Umeda M, et al. Prediction of organ involvement in systemic sclerosis by serum biomarkers and peripheral endothelial function. Clin Exp Rheumatol. 2018;36 Suppl 113(4):102-8.
401. Mok MY, Yiu KH, Wong CY, Qiuwaxi J, Lai WH, Wong WS, et al. Low circulating level of CD133+KDR+ cells in patients with systemic sclerosis. Clin Exp Rheumatol. 2010;28(5 Suppl 62):S19-25.
402. Takahashi T, Asano Y, Akamata K, Aozasa N, Taniguchi T, Noda S, et al. Dynamics of serum angiopoietin-2 levels correlate with efficacy of intravenous pulse cyclophosphamide therapy for interstitial lung disease associated with systemic sclerosis. Mod Rheumatol. 2013;23(5):884-90.
403. Ichimura Y, Asano Y, Akamata K, Aozasa N, Noda S, Taniguchi T, et al. Serum angiopoietin-like protein 3 levels: Possible correlation with progressive skin sclerosis, digital ulcers and pulmonary vascular involvement in patients with systemic sclerosis. Acta Derm Venereol. 2014;94(2):157-62.
404. Hayashi Y, Jinnin M, Makino T, Kajihara I, Makino K, Honda N, et al. Serum angiopoietin-like protein 3 concentrations in rheumatic diseases. Eur J Dermatol. 2012;22(4):500-4.
405. Nadar SK, Blann AD, Lip GY. Plasma and platelet-derived vascular endothelial growth factor and angiopoietin-1 in hypertension: Effects of antihypertensive therapy. J Intern Med. 2004;256(4):331-7.
406. Cipriani P, Di Benedetto P, Ruscitti P, Campese AF, Liakouli V, Carubbi F, et al. Impaired endothelium-mesenchymal stem cells cross-talk in systemic sclerosis: A link between vascular and fibrotic features. Arthritis Res Ther. 2014;16(5):442.

407. Heger LA, Kerber M, Hortmann M, Robinson S, Mauler M, Stallmann D, et al. Expression of the oxygen-sensitive transcription factor subunit HIF-1alpha in patients suffering from secondary Raynaud syndrome. Acta Pharmacol Sin. 2019;40(4):500-6.
408. Siao-Pin S, Damian LO, Muntean LM, Rednic S. Acroosteolysis in systemic sclerosis: An insight into hypoxia-related pathogenesis. Exp Ther Med. 2016;12(5):3459-63.
409. Zhou X, Liu C, Lu J, Zhu L, Li M. 2-methoxyestradiol inhibits hypoxia-induced scleroderma fibroblast collagen synthesis by phosphatidylinositol 3-kinase/AKT/mTOR signalling. Rheumatology (Oxford). 2018;57(9):1675-84.
410. Cowburn AS, Crosby A, Macias D, Branco C, Colaco RD, Southwood M, et al. HIF2alpha-arginase axis is essential for the development of pulmonary hypertension. Proc Natl Acad Sci U S A. 2016;113(31):8801-6.
411. Hickey MM, Richardson T, Wang T, Mosqueira M, Arguiri E, Yu H, et al. The von hippel-lindau chuvash mutation promotes pulmonary hypertension and fibrosis in mice. J Clin Invest. 2010;120(3):827-39.
412. Yu AY, Shimoda LA, Iyer NV, Huso DL, Sun X, McWilliams R, et al. Impaired physiological responses to chronic hypoxia in mice partially deficient for hypoxia-inducible factor 1alpha. J Clin Invest. 1999;103(5):691-6.
413. Dai Z, Li M, Wharton J, Zhu MM, Zhao YY. Prolyl-4 hydroxylase 2 (phd2) deficiency in endothelial cells and hematopoietic cells induces obliterative vascular remodeling and severe pulmonary arterial hypertension in mice and humans through hypoxia-inducible factor-2alpha. Circulation. 2016;133(24):2447-58.
414. Kelly BD, Hackett SF, Hirota K, Oshima Y, Cai Z, Berg-Dixon S, et al. Cell type-specific regulation of angiogenic growth factor gene expression and induction of angiogenesis in nonischemic tissue by a constitutively active form of hypoxia-inducible factor 1. Circ Res. 2003;93(11):1074-81.
415. Aden N, Nuttall A, Shiwen X, de Winter P, Leask A, Black CM, et al. Epithelial cells promote fibroblast activation via il-1alpha in systemic sclerosis. J Invest Dermatol. 2010;130(9):2191-200.
416. Volpi N, Pecorelli A, Lorenzoni P, Di Lazzaro F, Belmonte G, Agliano M, et al. Antiangiogenic VEGF isoform in inflammatory myopathies. Mediators Inflamm. 2013;2013:219313.
417. Denton CP, Ong VH, Xu S, Chen-Harris H, Modrusan Z, Lafyatis R, et al. Therapeutic interleukin-6 blockade reverses transforming growth factor-beta pathway activation in dermal fibroblasts: Insights from the fasscinate clinical trial in systemic sclerosis. Ann Rheum Dis. 2018;77(9):1362-71.
418. Liang R, Sumova B, Cordazzo C, Mallano T, Zhang Y, Wohlfahrt T, et al. The transcription factor gli2 as a downstream mediator of transforming growth factor-beta-induced fibroblast activation in ssc. Ann Rheum Dis. 2017;76(4):756-64.
419. Derrett-Smith EC, Dooley A, Baliga R, Hobbs A, MacAllister R, Abraham D, et al. An exploration of pulmonary vascular vegf signalling in a tgf beta-dependent mouse model of systemic sclerosis. Rheumatology. 2011;50:134-5.
420. Jimenez SA, Castro SV, Piera-Velazquez S. Role of growth factors in the pathogenesis of tissue fibrosis in systemic sclerosis. Curr Rheumatol Rev. 2010;6(4):283-94.
421. Ihn H. The role of tgf-beta signaling in the pathogenesis of fibrosis in scleroderma. Arch Immunol Ther Exp (Warsz). 2002;50(5):325-31.
422. Boulon C, Devos S, Mangin M, Decamps-Le Chevoir J, Senet P, Lazareth I, et al. Reproducibility of capillaroscopic classifications of systemic

sclerosis: Results from the sclerocap study. Rheumatology (Oxford). 2017;56(10):1713-20.

Appendix 1. Clinical Imaging & Analysis

1.1 LSCI Imaging settings

Laser Speckle Contrast Imaging FLPI (Moor Instruments, Axminster, UK) Image acquisition settings	
Warm up	30 minutes minimum
Laser wavelength	775nm
Laser position	30 cm +/- 2cm from target
Laser angle	30°
Time constant	1.0 second
Exposure time	8.3 ms
Sample rate	25 Hz
Time interval for flux calculation	40 seconds
Review software time constant	1.0

FLPI LSCI Calibration settings	
Calibration frequency	Monthly (100% pass)
Warm up	30 minutes minimum
Laser position	25 cm from calibration block at 90°
Calibration block	MoorFLPI-CAL-2PFS, Moor Instruments Shake for 10 seconds, rest for 2 minutes

1.2 HFUS settings APLIO A500

HFUS Vascularity settings	
Transducer	PLT 1204 18L7 probe (18MHz)
Gain	87
Frame rate	55fps/FR2
DiffT	18M
DR	75
Precision	5
Mechanical index	1.2
Aplipure	7 Apure+
Colour map	4
Time smooth	4

HFUS Skin thickness & Echogenicity settings	
Transducer	PLT 1204 18L7 probe (18MHz)
Gain	74
Frame rate	52fps
DiffT	18MHz
DR	70
Precision	3
Mechanical index	1.3
Aplipure	7 Apure+

HFUS SWE settings	
Transducer	PLT1005BT 14L5 probe (14 MHz)
Frame rate	16fps
Diff	14
Diff pitch	2
DR	70
Precision	3
Mechanical index	1.5
Aplipure	6
Persistence	0
FR control	1
SF	1
Track frequency	1

Appendix 2. Immunohistochemistry and Immunofluorescent staining of skin tissue sections

2.1 Recipe

Antigen retrieval buffer - citric acid buffer recipe pH 6.0, 1 litre
Trisodium citrate dehydrate (W302600 Sigma) 2.94g
pH 6.0
0.5mL tween-20
mqH2O to total volume 1000mL

2.2 Optimisation of blocking buffer for immunohistochemical tissue staining

Optimisation was undertaken using different blocking buffers, at increasing concentrations and incubation times in order to minimize non-specific antigen-antibody binding. Consistent imaging settings (Confocal microscope, Zeiss, LSM-880) were used to semi-quantify the level of background fluorescence with each blocking buffer (Zen Blue Lite software, v2.3). Images were captured at consistent magnification (x20/0.8) and excitation wavelengths (Excitation wavelength 488, gain 580; excitation wavelength 568, gain 460). Table A2.1 demonstrates the mean intensity of the respective fluoroferes in the epidermis and dermis, showing optimal blocking using 5% normal goat serum. It was noted that a 2-hour incubation at room temperature did not notably reduce intensity of staining. Additionally, the blocking buffer was noted to be evaporating during the extended incubation time at room temperature despite sections being placed in a covered container. As this risked the sections drying out which itself may

increase background auto-fluorescence of the tissue, and there was no superior blocking by a longer incubation, it was decided to maintain a 1 hour incubation for blocking phase thereafter.

Table A2. 1 Optimisation of Immunohistochemical staining blocking.

Optimal blocking of non-specific antibody binding and thus reduced background fluorescence represented as the mean intensity of fluorescence (mean gray scale 0-255), using 5% normal goat serum (NGS) compared to increasing concentrations of bovine serum albumin (BSA). No additional benefit was gained by increasing incubation time.

Mean intensity (gray scale 0-255) of background fluourescence					
Excitation wavelength		**488**		**568**	
Incubation time	**Blocking buffer**	**Epidermis**	**Dermis**	**Epidermis**	**Dermis**
1 hour	1% BSA	4.8	1.1	1.3	0.1
	2.5% BSA	4.4	0.7	0.6	0.0
	5% BSA	2.1	0.3	0.5	0.0
	5% NGS	**1.149**	**0.5**	**0.4**	**0.1**
2 hours	1%	4.4	1.3	0.9	0.1
	2.5% BSA	4.4	1.1	0.9	0.1

2.3 Controls antibodies for Immunohistochemical staining

2.3.1 Immunofluorescence staining of tissue sections

Primary antibody control tissue sections were generated using non-target antibodies from mouse and rabbit. Due to limited time and resource of tissue sections, primary controls were performed once at the same concentration of the most concentrated target primary antibodies which was felt to be the most stringent approach (Table A2.2).

Table A2. 2 Primary and Secondary control antibody dilutions.

Primary non-target antibodies were used as control staining. Dilutions were chosen to match that of the most concentrated target primary antibody. Controls were imaged using the same microscope settings as each of the respective primary target antibodies. Secondary controls involved omission of the primary antibody at the relevant incubation step. Both primary and secondary controls were incubated with secondary antibodies at concentrations shown in table.

Antibody dilutions for IHC-IF controls			
Antibody	**Supplier**	**Dilution**	**Final concentration (μg/mL)**
Primary antibodies			
Mouse IgG control	Santa Cruz sc-2025	1:25	40
Rabbit IgG control	R&D AB105C	1:100	10
Secondary antibodies			
Goat anti-mouse (Alexa-488)	Invitrogen 15626746	1:200	10
Goat anti-rabbit (Alexa-568)	Invitrogen 10032302	1:200	10

Secondary controls were performed by incubation by omission of primary antibodies (incubation with NGS only at the point of protocoled primary antibody incubation) as a 'dummy' incubation step. Secondary antibody dilutions are shown in Table A2.2. Sections were then imaged using consistent microscope settings for each donor for respective primary antibodies (Table A2.3). Images were captured using *Confocal microscope (LSM-880, Zeiss, U.K),* x20/0.8 DCII objective and averaging 2, bit depth 8bit.

Table A2. 3 Zeiss microscope imaging settings.

For each tissue stain, all donor tissues were imaged at the same microscope settings to allow for semi-quantification and comparison. Primary control sections were imaged at each of these settings for reference of respective target antibody stains.

Imaging acquisition settings for Zeiss confocal microscope		
	Gain	
Primary antibody target	**Alexa 488 (green)**	**Alexa 568 (red)**
HIF1α	635	-
HIF2α	-	570
VEGF-A_{165}b	709	-
panVEGF-A	-	655
Ang-1	716	-
Ang-2	480	-
Tie-2	-	587
CD31	-	723

2.3.2 Immunohistochemical HRP methodology for tissue staining

Deparaffinisation, rehydration of skin sections and antigen retrieval was performed as per IHC-IF staining (chapter 2.11.2). Endogenous peroxidases were then blocked to prevent non-specific reaction of the chromagen in HRP using fresh 30% H_2O_2 (in the following ratios 1 part H_2O_2 (Sigma H1009): 1.8 part methanol (Sigma 322415): 7.2 parts mqH_2O) for 15 minutes. Sections were washed in mqH_2O 3 times for 2 minutes each. Sections were permeablized twice for 10 minutes each (1% NGS + 0.4% triton in PBS) followed by a wash in PBS (3 x 2 minutes). Sections were blocked for 1 hour at room temperature in 5% NGS and then incubated with the primary VEGF-A_{165}b antibody as for IHC-IF (chapter 2.11.2). Sections were washed the next day and incubated with a secondary antibody conjugated with HRP (1:200 in NGS, Sigma A2304) for 1 hour at room temperature and washed again in

PBS. Sections were finally incubated with novored (Vector labs SK-4800) made according to manufacturer protocol and terminated by washing in mqH_2O before counterstaining with Haematoxylin (Vector labs H-3401) and blueing with ammonium hydroxide (Sigma 221228). Sections were then washed in mqH_2O followed by running tap water and finally mqH_2O. Sections were then dehydrated in ethanol, mounted in media (Fisher 12667746) and cover-slipped. Image acquisition was performed on Leica microscope (CTR4000) with compatible software (Leica application suite LAS v4.3).

2.3.3 Example tissue staining controls

Figure A2.1 demonstrates representative primary and secondary controls. Secondary controls showed minimal background tissue autofluorescence which likely occurs due to the use of formalin to fix tissue sections. Primary control IgGs, however, demonstrated high levels of background autofluorescence (more so with mouse IgG) which may be due to a component of the antibody diluent. Additionally, primary control mouse IgG demonstrated specific nuclear staining in the epidermis which was present despite optimisation of the blocking buffer. This was present to a lesser extent depending on the confocal microscope gain settings applied and was not present in any of the samples stained with specific target primary antibodies. Immunohistochemical staining with HRP (Appendix A2.3.2) later confirmed nuclear binding by the mouse control IgG, demonstrating that the control antibody does in fact have some specific anti-human activity (Figure A2.1). Time limitations prevented procurement of further control primary antibodies. It was therefore decided that IF images for each primary target antibody would be interpreted such that only specific staining not matching the nuclear staining in primary control sections would be considered as positive results.

Figure A2. 1 Negative controls for Immunofluorescent tissue staining of human skin sections.

FFPE skin sections were incubated with non-immune normal mouse (A) and rabbit (C) IgG for primary controls with Alexa fluoro secondary antibodies for immunofluorescence (Alexa fluoro-488 and -568 respectively). (A) Mouse IgG primary control antibody is actually seen to have cross reactivity with human nucleic material (arrow) in the epidermis (e) and dermis (d) as well as some background cytoplasmic staining in the epidermis. (B) Similar nuclear staining (arrow) is seen by alternative IHC-HRP technique using the same mouse primary control antibody. (C) Only minor non-specific fluorescence is seen with normal rabbit IgG likely due to autofluorescence of formalin fixed tissue. Secondary controls were performed by omission of primary antibodies and incubation with secondary fluorescent antibodies only. No notable cross reactivity is seen for secondary antibodies: (D) goat anti-mouse antibody (Alexa fluoro-488) and (E) goat anti-rabbit (Alex fluoro-568). IHC-IF images obtained on Zeiss confocal microscope x20/0.8 DCII objective. IHC-HRP imaged on Leica microscope x20 objective. Scale bars indicate 50μm.

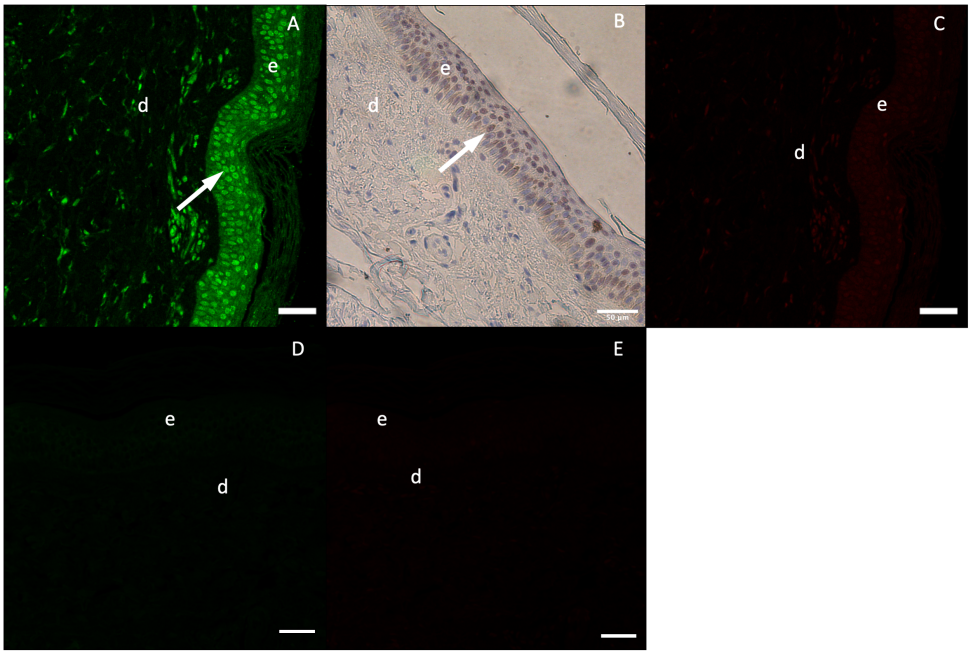

Appendix 3. Fibroblast cell culture

3.1 Cell culture medium

Culture media for skin biopsy whole tissue transport, fibroblast explant culture and passaging:

Fibroblast cell culture medium recipe		
Component	**Source**	**Recipe**
DMEM	Sigma D6429	450mL
Fetal bovine serum	Gibco 10500-064 Fisher 11550356	50mL
Penicillin-streptomycin 100U/mL	Gibco 15140122 Fisher 11548876	5mL
Gentamicin 50ug/mL	Sigma G1272	2.5mL
Amphotericin B 2.5ug/mL	Sigma A2942	5mL

3.2 Fibroblast freezer medium recipe

Fibroblast freezer medium recipe: DMEM supplemented with 20% FBS, 10% DMSO		
Component	**Source**	**Recipe**
DMEM + 10% FBS	Sigma D6429 (+ 10% FBS)	14mL
Neat FBS	Gibco 10500-064 Fisher 11550356	4mL
Sterile DMSO	Sigma D2650	2mL

3.3 Fibroblast cell lysis buffer recipe

Cell lysis buffer was sterile filtered and frozen at -20°C until use (made as per recipe from R&D Systems, compatible with HIF1α and 2α assay)

Fibroblast cell lysis buffer recipe		
Component	**Source**	**Recipe**
Sample diluent concentrate 1	R&D Systems	8mL
Urea	Sigma	14.416g
Sodium fluoride 0.5M	Sigma	0.4mL
Phosphostop		4 tablets
Complete mini protease inhibitor cocktail		
mqH2O	-	Made up to 40mL

3.4 SiRNA recipe for fibroblast experiments

SiRNA Recipe					
Step	**Reagent 1**	**Volume**	**Reagent 2**	**Volume**	**Final Reagent**
1	Opti-mem low serum medium	150uL	lipofectamine RNAiMAX reagent	9uL	Diluted lipofectamine reagent
2	Opti-mem low serum medium	150uL	SiRNA	3uL	30pmol SiRNA
3	SiRNA 30pmol	150uL	Diluted lipofectamine reagent	150uL	SiRNA – transfection reagent mix
4	SiRNA - transfection reagent	250uL	DMEM (+FBS +Abx)	1750uL	Terminal SiRNA 25pmol + 7.5uL lipofectamine

3.5 Fibroblast phenotyping

Fibroblasts were cultured and stained as described in chapter 2.12.4. Fibroblast cultures were confirmed by a spindle shaped morphology with the presence of mesenchymal marker vimentin and the absence of epithelial cell marker (cytokeratin-19). Positivity for αSMA in all control and SSc donor

cultures indicated cells were activated at the time of immunofluorescence (likely due to active cell division during culture).

Figure A3. 1 Fibroblast phenotyping by immunocytochemistry.

Fibroblast culture confirmed in all six donors with typical spindle shaped morphology, positivity to vimentin and αSMA and absence of reactivity to cytokeratin-19. No immuno-staining was seen with control antibody. Scale bar indicates 20μm.

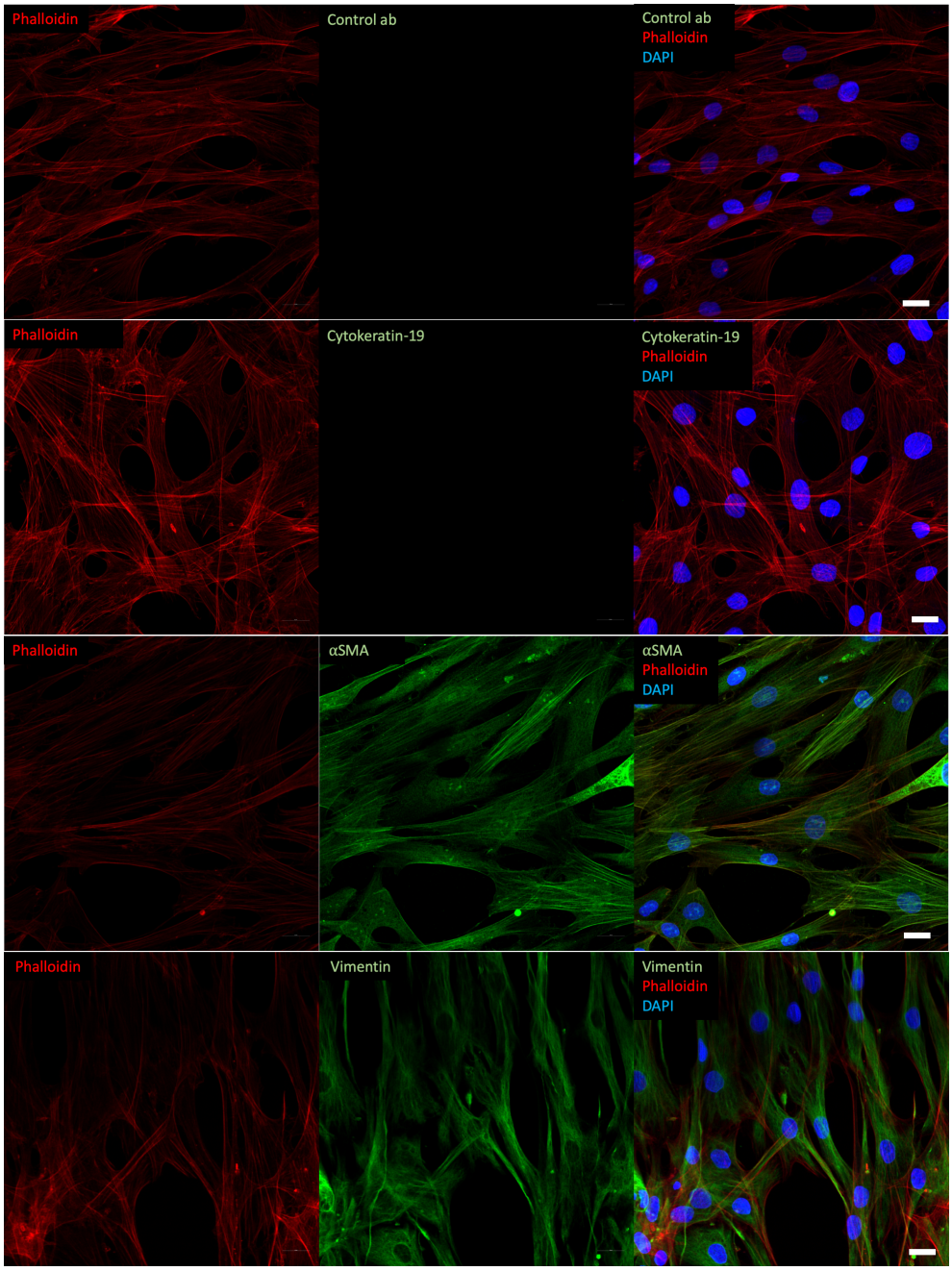

Appendix 4. Enzyme Linked Immunosorbent Assays

4.1 Plasma ELISAs

4.1.1 Limit of detection for VEGF-A_{165}b ELISA

The standard curve for VEGF-A_{165}b duoset ELISA (DY3045, R&D) used for plasma was extended and the limit of detection judged to be between 0-8.06 pg/mL.

Figure A4. 1 Example standard curve for VEGF-A_{165}b assay.

The limit of assay detection was determined by extending the standard curve and determined to be between 0-8.06 pg/mL (performed by VF).

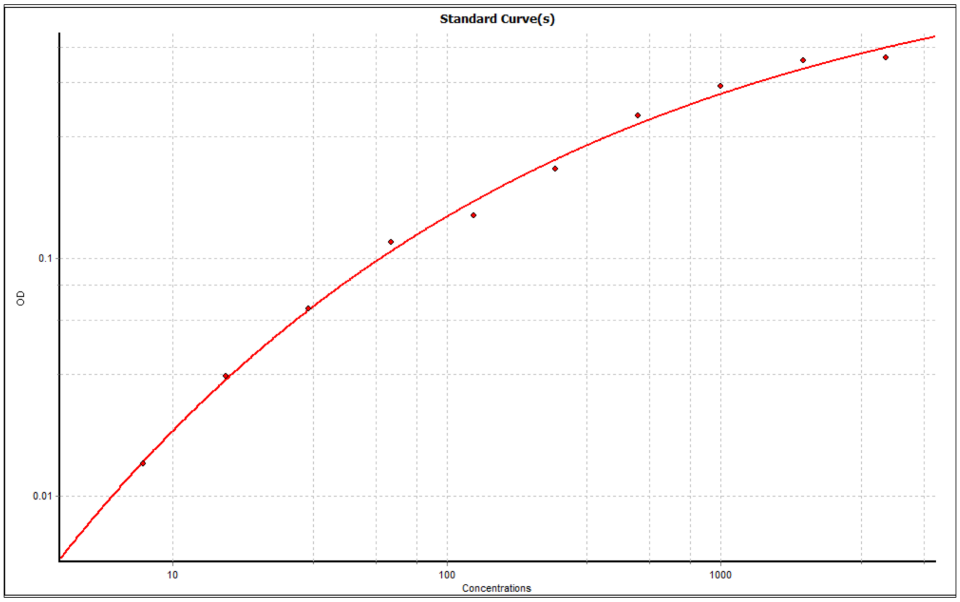

Table A4. 1 Intra class correlation coefficients (ICC) for plasma ELISAs.

ICCs demonstrate excellent reproducibility for pan-VEGF-A, VEGF-A_{165}b, sVEGFR1 and Ang-1 and -2 ELISAs for both intra and inter-plate repeats. ICC for Tie-2 also showed excellent intra-plate reproducibility. ICC for inter-plate reproducibility for Tie-2 were acceptable but less reliable than the other biomarkers on the MSD Cytokine panel. Significance illustrated as p<0.05* and p</=0.003** using ICC (2-way mixed analysis). ICC could not be calculated for inter-plate repeats for VEGF-A_{165}b ELISA as all samples (n = 8) had undetectable levels of VEGF-A_{165}b, however, all inter-plate repeats matched original results (***).

	Pan-VEGF-A	sVEGFR1	Tie-2	VEGF-A_{165}b	Ang-1	Ang-2
n.	8	8	8	8	8	5
Intra-plate reliability ICC (95% CI)	+0.999 (0.995-1.000)**	+0.926 (0.666-0.985)**	+0.950 (0.772-0.990)**	+0.979 (0.893-0.996)**	+0.946 (0.710-0.989)**	+0.995 (0.995-0.999)**
	10	10	10	8	11	3
Inter-plate reliability ICC (95% CI)	+0.926 (0.604-0.983)**	+0.918 (0.675-0.980)**	+0.696 (-0.150 – 0.923)*	***	+0.982 (0.936-0.995)**	+0.997 (0.948-1.000)**

4.2 ELISA for fibroblast cell culture

Example Standard curves for HIF1α and HIF2α are shown in Figure A4.2.

Figure A4. 2 Example standard curve for (A) HIF1α and (B) HIF2α.